Detection and Understanding of Wetting Mechanisms in Vacuum Membrane Distillation Applied to Desalination of Seawater

Paul Jacob

Université Fédérale
Toulouse Midi-Pyrénées

THÈSE

En vue de l'obtention du

DOCTORAT DE L'UNIVERSITÉ DE TOULOUSE

Délivré par :

L'Institut National des Sciences Appliquées de Toulouse

Présentée et soutenue par:

Paul Jacob

Le Mercredi 5 Décembre 2018

Détection et compréhension des mécanismes de mouillage en distillation membranaire sous vide appliquée au dessalement d'eau de mer

---

Ecole doctorale : **MEGEP - Mécanique, Energétique, Génie civil, Procédés**

Spécialité : **Génie des Procédés et de l'Environnement**

Unité de recherche

Laboratoire d'Ingénierie des Systèmes Biologiques et des Procédés (LISBP)

Thèse dirigée par

Prof. Corinne Cabassud et Dr. Stéphanie Laborie

Jury

Prof. Philippe Moulin, Rapporteur
Prof. Johannes S. Vrouwenvelder, Rapporteur
Prof. Rémi Lebrun, Président
Dr. Séréna Bandini, Examinatrice
Dr. Elodie Chabanon, Examinatrice
Dr. Jean-Pierre Mericq, Examinateur
Prof. Corinne Cabassud, Directrice de thèse
Dr. Stéphanie Laborie, Co-directrice de thèse

THÈSE

En vue de l'obtention du

DOCTORAT DE L'UNIVERSITE DE TOULOUSE

délivré par

INSTITUT NATIONAL DES SCIENCES APPLIQUEES de TOULOUSE

Spécialité : Génie des Procédés et de l'Environnement

par

Paul Jacob

Detection and Understanding of Wetting Mechanisms in Vacuum Membrane Distillation Applied to Desalination of Seawater

Soutenue le 5 Décembre 2018 devant le jury composé de

Prof. Philippe Moulin	Professeur - Université Aix-Marseille 3, France	Rapporteur
Prof. Johannes S. Vrouwenvelder	Professor - King Abdullah University of Science and Technology, Arabie Saoudite	Rapporteur
Prof. Remi Lebrun	Professeur - Université du Québec à Trois-Rivières, Canada	Président
Dr. Jean-Pierre Méricq	Maître de Conférences - Université Montpellier 2, France	Examinateur
Dr. Elodie Chabanon	Maître de Conférences - Université Lyon 1, France	Examinatrice
Dr. Séréna Bandini	Associate professor - Université de Bologne, Italie	Examinatrice
Prof. Corinne Cabassud	Professeure - INSA de Toulouse, France	Directrice
Dr. Stéphanie Laborie	Maître de Conférences - INSA de Toulouse, France	Co-directrice

Laboratoire d'Ingénierie des Systèmes Biologiques et des Procédés (LISBP)

LISBP, UMR5504 CNRS, UMR792 INRA, INSA Toulouse

Ecole Doctorale Mécanique, Energétique, Génie Civil et Procédés (MEGeP)

Abstract

With an ever-increasing population and the growing disparity in potable water resource, humanity has turned its attention to the oceans for its potable water needs. To overcome the current limitations in current desalination technologies, membrane distillation (MD) is actively being developed. The interest of MD for seawater desalination was established in the last decades but today the risk of membrane wetting is one of the major barrier for industrial implementation of MD. Under the framework of the ANR project "WETMEM", the issue of this thesis was to develop tools for better understanding wetting mechanisms in vacuum membrane distillation. Several fabricated (WETMEM partners) and commercial membranes were studied to understand the influences of membrane properties on wettability. Therefore, a definition and classification on wetting were formulated. After that two wetting indicators were developed using scanning electron microscopy and X-ray dispersion spectroscopy under a method called "Detection of Dissolved Tracer Intrusion". A proof of concept was provided with various wetting mechanisms visualized and interpreted. These *ex-situ* indicators were used with wettability tools (Contact Angle, Liquid Entry Pressure) to understand the influence of temperature (35-50°C), salinity (22-310 g/L NaCl sol.) and flow rate (400 – 4000 Re) on wetting and wettability of a PVDF membrane under vacuum membrane distillation. Indeed, it was found that salinity has a greater impact on wetting than the other operating parameters. Additionally, a proof of concept was provided for non-invasive *in-situ* optical method for visualizing wetting in membrane distillation. Progression of *in-situ* wetting visualization was validated at different scales for various saline solutions and seawaters.

Keywords: Membrane Distillation, Desalination, Wettability, Pore Wetting, Characterization Wetting Mechanisms, Wetting Indicators, Optical Tool, In-situ Wetting Detection

Résume

Avec une population toujours croissante et la pénurie de plus en plus importante des ressources en eau douce, l'humanité s'est tournée vers les océans pour ses besoins en eau potable. Afin de faire face aux limites des procédés conventionnels de dessalement d'eau de mer, la distillation membranaire (DM) connaît un intérêt croissant. Même si l'intérêt envers la DM pour le dessalement d'eau de mer est apparu au cours des dernières décennies, aujourd'hui le risque de mouillage des membranes est l'un des obstacles majeurs à son développement industriel. Dans le cadre du projet ANR « WETMEM », l'objectif de cette thèse est de développer des outils de compréhension des mécanismes de mouillage en distillation membranaire sous vide. Plusieurs membranes, fabriquées par des partenaires du projet WETMEM, et commerciales ont été étudiées afin de comprendre l'influence des propriétés des membranes sur les indicateurs de mouillabilité. De plus, une définition et une classification des mécanismes de mouillage ont été proposées. Par la suite, deux indicateurs de mouillage ont été développés à l'aide de la microscopie électronique à balayage et de la spectroscopie de dispersion de rayons X selon une méthode appelée « Détection d'intrusion de traceur dissous ». Une preuve de concept a été fournie, dans laquelle différents mécanismes de mouillage ont pu être visualisés et interprétés. Ces indicateurs ex situ ont alors été utilisés avec des indicateurs de mouillabilité (Angle de contact, Pression d'intrusion de liquide) afin de comprendre l'influence de la température (35-50 ° C), de la salinité (22-310 g / L de NaCl sol.) et du débit (400 - 4000 Re) sur le mouillage et la mouillabilité d'une membrane de PVDF en distillation membranaire sous vide. Il a alors été constaté que la salinité a l'impact le plus important sur le mouillage par rapport aux autres paramètres de fonctionnement. En outre, un outil optique in-situ non invasif a été développé. Il permet de visualiser le mouillage in-situ en distillation membranaire. La progression du mouillage in-situ a été observée à différentes échelles et pour différentes solutions salines et eaux de mer.

Mots Cles: *Distillation Membranaire, Dessalement, Mouillabilité, Mouillage Des Pores, Mécanismes De Caractérisation Du Mouillage, Indicateurs De Mouillage, Outil Optique, Détection Du Mouillage In Situ*

Scientific productions

Article

P. Jacob, S. Laborie, C. Cabassud, Visualizing and evaluating wetting in membrane distillation: New methodology and indicators based on Detection of Dissolved Tracer Intrusion (DDTI), Desalination. 443 (2018) 307–322. doi:10.1016/j.desal.2018.06.006.

Conference

P. Jacob, S. Laborie, C. Cabassud, Tools for visualizing and evaluating wetting in membrane distillation, in: Book Abstr., Czech Membrane Platform, Prague, Czech Republic, 2018: p. 113. https://www.melpro.cz/.

Contents

Introduction and thesis objectives

Our accessibility to the 3 % fresh water on earth is limited to 0.9 % underground, and 0.03 % surface waters only. With the advent industrial and agricultural sectors, over a billion people are without access to clean, fresh water making water scarcity a major concern globally. Nearly four in ten humans have no viable source of safe drinking water. Population growth and climate change have given rise to challenges in water security. The United Nations 2030 Agenda for Sustainable Development Goals (SDG) recognizes the importance of Goal 6 to ensure the availability and sustainable management of water. Rosegrant et al. (2002) project that for the *'first time in world history'* the demand for water in the non-agronomic sectors will surpass agricultural demands [1]. Thus, to fulfill our needs, humanity have turned to desalination. Today, brackish and seawater desalination appears as a significant alternative to produce drinking water in many countries, and in some areas, desalination is no longer a supplemental water resource but can be the major resource for both domestic and industrial demands. GWI (Global Water Intelligence) forecasts an annual growth rate of 8.62 % for the desalination market during the period 2018-2022 [2].

The first generations of desalination techniques were thermal based. They were soon followed by membrane-based technologies like Reverse Osmosis[3]. However, this technology is limited by the osmotic pressure[3]. To realize sustainable growth in the desalination sector issues like RO brine disposal [4] and improving water recovery need yet to be addressed. To overcome these limitations, the 3rd generation of desalination technologies, such as membrane distillation, forward osmosis[5], and capacitive deionization are actively being studied with emerging projects popping up all across the globe [6]. The interest of MD for seawater desalination was established in the last decade [7,8]. It is largely linked to the facts that MD can theoretically retain all non-volatiles and that the quality of the treated water does not depend on the quality of the saline water resource. With a possibility to increase water recovery and to reduce the volume of reverse osmosis brines [4] and the opportunity to couple the process with low grade heat from industrial waste heat [8,9], solar[10] or potentially even geothermal energy[11], MD is currently being viewed as a potential 3rd generation desalination technology for our future needs.

At its core, MD uses a hydrophobic microporous polymer with a partial pressure gradient across its opposing surfaces, allowing only low volatile compounds (such as water) to be selectively vaporized and transferred to the permeate side. With the sudden boom and relatively high potential application of this technology, many manufacturers are interested to develop[12], adapted [13] hydrophobic or create super hydrophobic membranes[14]. This technology performs well at controlled lab scales and

up to some extent at pilot scale levels and its potential interests are huge. To further this technology into a full-scale commercial application, one of the significant challenges it faces is for the membrane to remain dry during the process, which means that the liquid should not intrude inside pores. Indeed wetting may deteriorate permeate quality with time due to the transfer of salt with water (saline intrusion)[15]. Even if the risks of wetting occurrence and of the related process dysfunction are not well understood and qualified, membrane wetting has been regarded as one of the significant barriers for the industrial implementation of MD process [16,17] and has been cited as one of the main reasons MD is not being widely used at full-scale industrial level [18].

Ideally, membrane distillation assumes non-wetted pores at the beginning of the operation, but two other realistic conditions are prevalent, i.e. partially wetted and totally wetted pore. The current tools to evaluate pore wetting are unresponsive to the inherent position of the liquid-vapor interface during operation. At present, the tools and methodologies at our disposal to evaluate wetting only indicate the wetting potential of the membrane, and at best informs on total wetting in some pores. However, these techniques do not provide information pore scale or on the liquid-vapor interface and have distorted the understanding of the wetting phenomenon in membrane distillation, leading to confusion between wetting and wettability. The reality of the liquid-vapor interface being dynamic is not considered by state of the art due to a lack in adapted tools to characterize wetting. With a growing need for developing methods to evaluate wetting at a local scale and to push further our knowledge on the wetting phenomenon and its mechanisms, there is an acute need to develop better-adapted tools. Therefore, this thesis is a sincere effort for an in-depth assessment to characterize wetting using membrane contactors such as vacuum membrane distillation, by identifying and developing on our current stance and challenges at the fundamental level. A deeper understanding on wetting will advance this technology from various lab/pilot scale to establish membrane distillation as the 3rd generation of desalination technology. To push our knowledge further in understanding of the wetting phenomenon and its mechanisms, there is as acute need to develop better adapted tools.

Thus, the thesis begins with an attempt to understand and interpret wetting with the current state of the art (**Chapter 1**) as presented in the organizational flow chart below. During this process, an endeavor to definition pore wetting in membrane distillation is made while also characterizing various wetting mechanisms at the pore scale. Based on these definitions an exploration of several factors contributing towards wetting are considered. While summarizing various numerical models, experimental tools and protocols developed to assess, prevent and regenerate membranes from the wetting phenomenon. After discovering the lack of adequate tools in the current state of the art for assessing pore wetting, **Chapter 2** is dedicated to developing an innovative methodology to detect and

to evaluate wetting and to provide its proof of concept. Later on, **Chapter 3** utilizes the developed methodology to qualify and to quantify the influence of some operating parameters (such as temperature, flow rate, and salinity) on pore wetting. The influence on wettability is also checked by using the classical wettability indicators. Based on the gained knowledge, **Chapter 5** focuses on the development of an *in-situ* optical tool. It introduces theory and the proof of concept of a tool that was developed with the aim to visualize and interpret wetting propagation at both global and local scales. The tool's applicability is assessed using different feed solutions and validated by the wetting indicators previously developed. Finally, **Chapter 5** is dedicated to meet a WETMEM project objective that elaborates the efforts to select an appropriate spacer to measure permeance and performance for some commercial and fabricated membranes under vacuum membrane distillation (VMD). In this chapter, the physical and operating characteristics of membranes manufactured with different techniques and materials and having different average pore sizes, and thicknesses are assessed for their usability and performance in VMD.

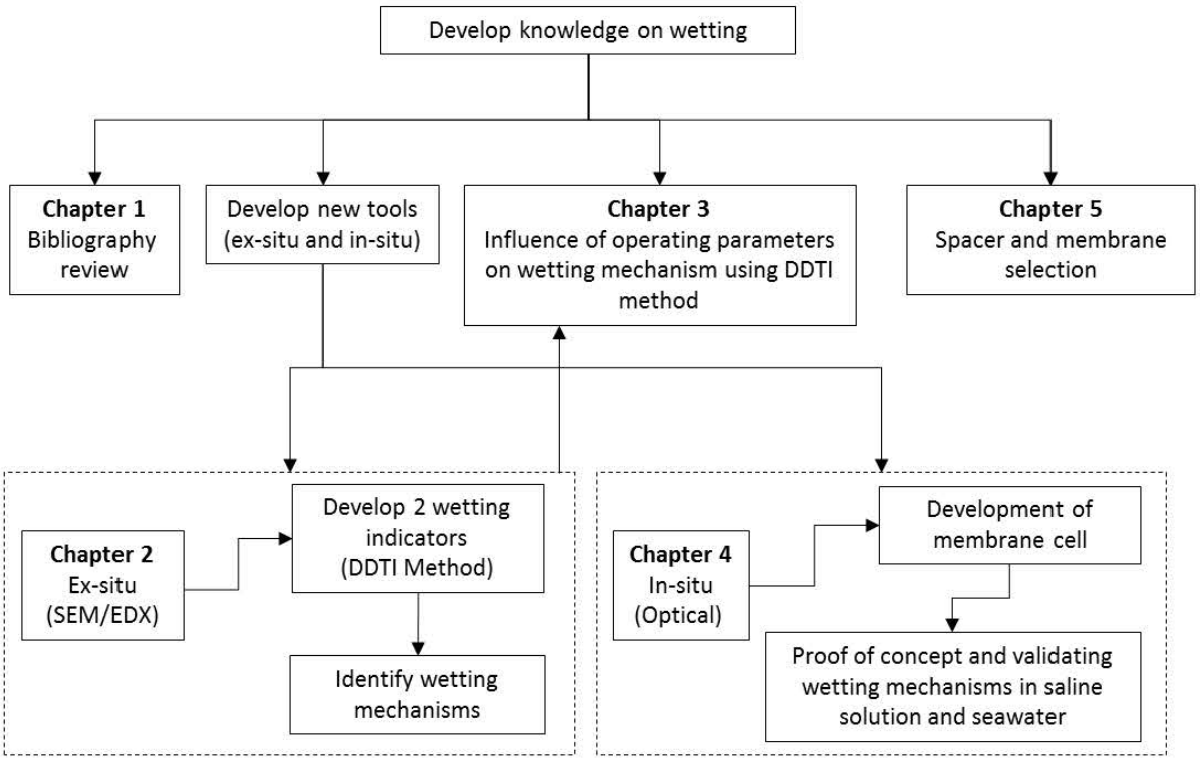

Organizational flowchart of the thesis

Summary of the thesis objectives (in English)

This thesis was conducted as part of the **ANR project (WETMEM)** with the ambitious scientific objectives to develop and explore new tools and methodologies to understand wetting in membrane

distillation. Thus, to address the problematic at the fundamental level, research has been conducted with the following objectives:

1. Producing a transversal and critical review on the state of art on the current knowledge on pore wetting and, on the methods, available to evaluate wetting.
2. Developing *ex-situ* tools and wetting indicators for visualizing, interpreting and evaluating wetting.
3. Using the developed wetting indicators for determining the effects of operating parameters on wetting and comparing them with wettability tools.
4. Developing an *in-situ* wetting detection tool and providing its proof of concept.
5. Characterizing membranes and spacers to be used in vacuum membrane distillation.

All chapters are written in English and the thesis manuscript is organized in the following manner:

- At the beginning of each thesis chapter (excluding the bibliography review), a preface with the organizational flowchart is given to better understand the context and position of the chapter in the thesis.
- Each thesis objective is assigned a dedicated chapter with its introduction, methods, results and conclusion.
- A summary of specific objectives in each chapter is provided in both English and French at the beginning of each chapter.
- Similarly, the conclusions are also written in English and French at the end of each chapter.

Résumé des objectifs de la thèse (en français)

*Cette thèse a été menée dans le cadre du projet **ANR (WETMEM)** avec des objectifs scientifiques ambitieux pour développer et explorer de nouveaux outils et méthodologies afin de comprendre le mouillage en distillation membranaire. Ainsi, pour répondre à cette problématique au niveau fondamental, des recherches ont été menées avec les objectifs suivants :*

1. *Faire un état de l'art critique des connaissances actuelles sur le mouillage des pores et sur les méthodes pour évaluer le mouillage.*
2. *Caractériser les membranes et les espaceurs à utiliser en distillation membranaire sous vide.*
3. *Développer des outils ex-situ et des indicateurs pour visualiser, interpréter et quantifier le mouillage.*

4. *Utiliser les indicateurs de mouillage mis au point pour déterminer les effets des paramètres de fonctionnement sur le mouillage – Comparer les tendances obtenues avec celles obtenues avec les indicateurs conventionnels de mouillabilité.*

5. *Développer un outil de détection de mouillage in situ et fournir la preuve de concept.*

Tous les chapitres sont écrits en anglais et le manuscrit de thèse est organisé de la manière suivante :

- *Au début de chaque chapitre de thèse (à l'exclusion de la revue de bibliographie), un organigramme de l'organisation est précédé d'une préface permettant de mieux comprendre le contexte et la position du chapitre dans la thèse.*

- *Chaque objectif de thèse fait l'objet d'un chapitre dédié avec une introduction, des méthodes avec leurs résultats et une conclusion.*

- *Un résumé des objectifs spécifiques de chaque chapitre est fourni en anglais et en français au début de chaque chapitre.*

- *De même, les conclusions sont également rédigées en anglais et en français à la fin de chaque chapitre.*

Chapter 1 : Wetting characterization and detection in membrane distillation: A review

Summary of objective (in English)

Nearly three decades of accelerated development in membrane distillation have potentially made it a cost-effective technology for both desalination and industrial use with and without coupling with alternative sources of heat and energy. This chapter explores the principal limitation for membrane distillation, i.e., wetting of the membrane, which may deteriorate the performance of the process. Wetting has gained more intense interest, and recent studies are trying to address this problem in their unique approaches. Thus, the goal of this chapter is to investigate wetting using published literature in membrane distillation. The originality of this chapter is to consider wetting at the pore scale with attention paid to liquid intrusion and re-discuss literature results with this viewpoint. The investigation includes describing pore wetting mechanisms, primary causes, and recent evolution of pore wetting models. The major part of the chapter concerns current methods to evaluate wettability in membrane distillation and emerging *ex-situ* and *in-situ* tools methods to detect wetting.

Résumé de l'objectif (en français)

Près de trois décennies de développement accéléré de la distillation membranaire en ont fait une technologie potentiellement rentable à la fois pour le dessalement et l'utilisation industrielle, avec et sans couplage à des sources alternatives de chaleur et d'énergie. Ce chapitre explore le risque principal de limitation de la distillation membranaire, le mouillage de la membrane, qui peut détériorer les performances du procédé. Le mouillage a suscité un intérêt de plus en plus intense et des études récentes tentent de résoudre ce problème dans une approche unique. Ainsi, le but de ce chapitre est d'étudier et de comprendre le mouillage en utilisant la littérature publiée sur la distillation membranaire. L'originalité de ce chapitre est de considérer le mouillage à l'échelle des pores avec une attention portée à l'intrusion de liquide et de réexaminer les résultats de la littérature avec ce point de vue. L'investigation comprend divers mécanismes de mouillage des pores, les principales causes de mouillage des pores, et l'évolution récente des modèles de mouillage des pores. La majeure partie du chapitre concerne les méthodes actuelles d'évaluation de la mouillabilité en distillation membranaire et les méthodes émergentes de détection du mouillage, y compris les outils ex situ et in situ.

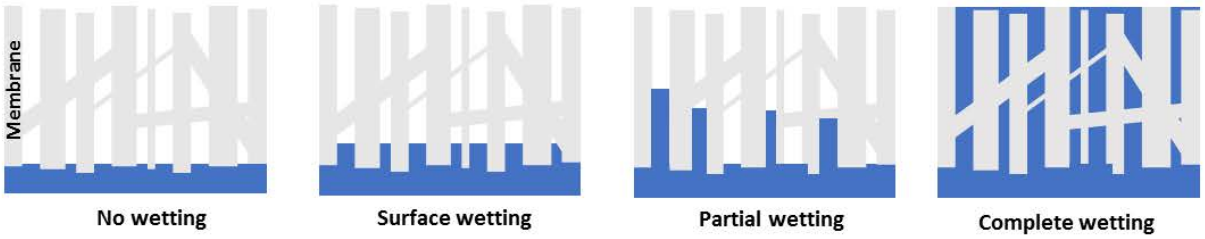

Graphical abstract

1.1. General introduction

The first scientific paper on membrane distillation (MD), titled "Vaporization through porous membranes," was published in 1967 by Findley (1967), and the first patent in 1968 by Bodell (1968). Detailed history and its future perspectives of this technology can be found elsewhere [6,21–23]. Based on the initial "Terminologies for Membrane Distillation" established in 1989 [24], MD can be defined as a "*process where only vapors are transported through a porous hydrophobic membrane which is in direct contact with the process liquid on one of its surface and the driving force is the partial pressure difference only*". The additional criteria are that the membrane should not have any influence on the vapor-liquid equilibrium of the liquids to be separated and, within the membrane, no capillary condensation should occur and the membrane itself should not get wetted by the process liquid.

In all its variants (MD configurations), the feed is heated and always circulated tangentially to the membrane surface. The differences in configurations mainly arise on the technique used for vapor to be condensed on the permeate side. Out of several configurations, six configurations are illustrated in **Figure 1.1.** When a liquid cooler than the feed is circulated directly on the surface of the membrane on the permeate side and the vapor generated inside the pore is directly condensed in the circulating liquid this configuration is known as Direct Contact Membrane Distillation (DCMD). This is the most common MD configuration studied at lab scale due to ease of setup. Instead, if a stagnant air gap is placed in the permeate compartment between the membrane surface and a condenser plate while allowing the permeated vapor to pass and condense on the condenser plate (cooled with a refrigerant or cold fluid in circulation), this configuration is termed as Air Gap Membrane Distillation (AGMD). In this configuration, there is a port at the bottom of the permeate side which collects the liquid condensed on the plate. When a stagnant liquid (which can be same as the distillate or an immiscible liquid to the vaporizing component from the feed) is introduced in the permeate side, this configuration is called Liquid Gap Membrane Distillation (LGMD) [25]. In LGMD, permeate is collected on the highest end of the module. When gas is tangentially flowing on the permeate side instead of a cold liquid, this configuration is called sweeping gas membrane distillation (SGMD). In this

configuration, condensation is achieved outside the membrane module in an external condenser. Thermostatic sweeping gas membrane distillation (TSGMD) is a combination of both AGMD and SGMD where a sweeping gas is the carrier of the vapor on the permeate side but a condenser plate cools the vapor which is collected, as in AGMD, at the bottom of the module [26]. Vacuum membrane distillation (VMD) configuration arises by applying reduced pressure (vacuum) on the permeate side, thus furthering the transmembrane partial pressure and thereby receiving the highest flux. Condensation occurs outside the membrane module in an external condenser. Several new configurations are being proposed in the literature in search of more energy efficient MD configurations/module design. For example, permeate gap membrane distillation (PGMD) [27], conductive gap membrane distillation (CGMD) [28], material gap membrane distillation (MGMD)[29].

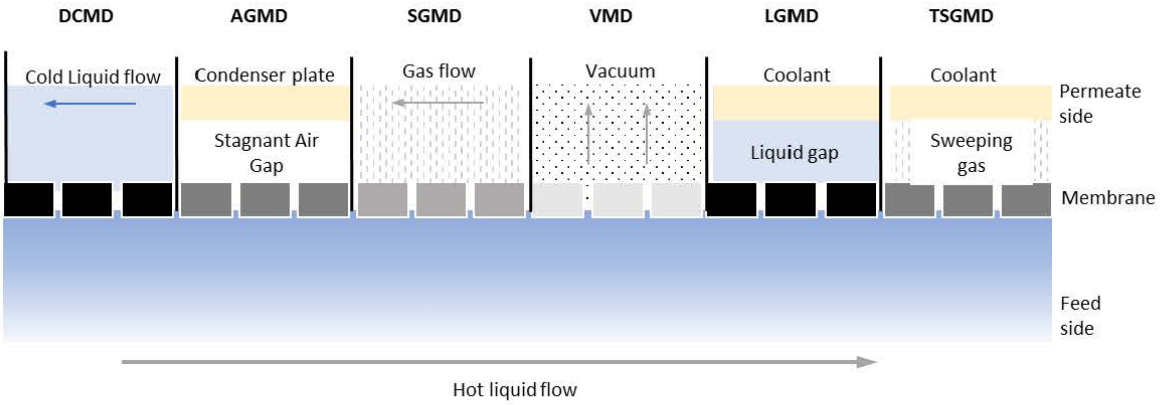

Figure 1.1: Membrane distillation configurations

Figure 1.2(a) presents the number of publications since the discovery of the process in 1967 based on Scopus database with the keyword "Membrane distillation – 2272 results". It should be noted that publications regarding membrane distillation are gaining high interest since the 1990s and 297 papers have been published in the year 2017. As presented in **Figure 1.2** (b), with the major subject of research in chemical engineering (23.7 %), chemistry (18.3 %), engineering (15 %), materials science (14.6 %), environmental science (13.4 %), energy (2.9 %) and other fields (12 %). The published papers on the DCMD configuration dominate, followed by VMD and AGMD. The other configurations are not well researched probably due to their novelty, complex operating conditions, and lack of dedicated systems to achieve the necessary process conditions.

Depending on the researched application for the process each configuration has its own advantages and limitations. For example, VMD configuration can be effectively used for collecting volatile compounds from the feed like in aroma recovery [30] but can also be used for desalination [31] purposes. SGMD is better suited for concentrating feed solution, where the low vapor pressure

components are of lesser interest e.g. as in applications like removing water from ethylene glycol or crystallization [32–34].

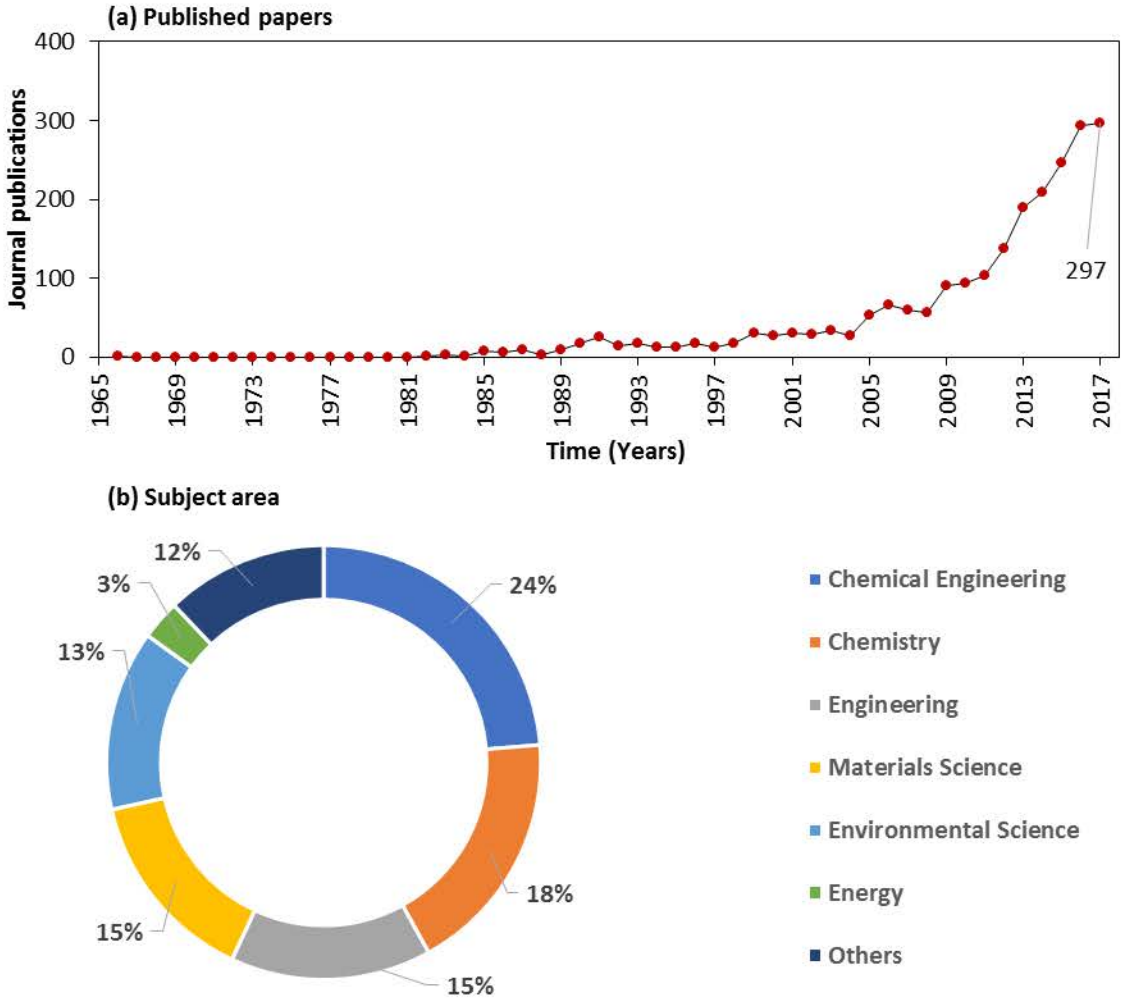

Figure 1.2: (a) Published papers and (b) disciplines on membrane distillation from 1967 till 2017 (Scopus)

Basically, in all configurations of membrane distillation, it should be noted that whatever is the carrier fluid on the permeate side and its condensation technique, simultaneous heat, and mass transfer from the feed side to the permeate side via a hydrophobic membrane is involved. The heat transfer occurs both through the membrane pores and the membrane material, but the mass transfer is assumed to only occur through the membrane pores as the material itself does not interact with the component transferred due to a very high void fraction and low surface energy. Like for pressure-driven membrane processes, fluid boundary layers exist both on the feed side for all configurations and on permeate side for the configurations using a liquid layer in the permeate side (excepted for VMD, AGMD, and SGMD). Liquid boundary layer results in temperature and concentration polarizations.

MD has received a lot of research interest in the past 30 years[35]. This technology is being studied today for conventional and emerging applications in the field of water treatment such as brine treatment [36], desalination [4], arsenic removal [37], pollutant removal [38], wastewater treatment [39], radioactive water decontamination [40] and process intensification issues [32,33]. The interest of MD for seawater desalination was established in the last decades and appears as an important motor for the evolution of the technology. It is largely linked to the facts that it can be coupled with renewable or waste energy resources [8,9] and that it can produce high quality treated water as it can theoretically retain ions, macromolecules, colloids, cells and all non-volatiles completely, without being limited by osmotic pressure, as for reverse osmosis. Moreover, the quality of the treated water does not depend on the quality of the saline water source that can be seawater or a hypersaline concentrates from RO [4] or geothermal [11] desalination. In the future, membrane distillation could be used as a direct process on seawater or coupled with other processes like solar powered reverse osmosis [41] and could then allow to be enhancing the global performance (recovery, productivity and low energy consumption). Some recent studies focused on the energetic and exegetic aspects of MD [42,43] and the economic analysis of desalination technologies in the context of carbon pricing or not [44] and confirmed that MD opportunities occur when heat is available at low cost, while extended recovery of RO brine is also viable. With a theoretical 100 % rejection and the opportunity to couple the process with low-grade heat from industrial waste heat, solar and geothermal energy, MD is currently being viewed as a potential 3rd generation desalination technology for our future needs [6]. With the sudden boom and relatively high potential application of this technology, many manufacturers are adapting existing membranes into more hydrophobic ones without deepening the knowledge of the fundamental aspects of this process. Evidently this technology performs both at lab scale [37], pilot scale (MEMSYS [45], Aquaver [46], Aquastill [47], SolarSpring[48], Scarab[9], Fraunhofer Institute for Solar Energy Systems (ISE) [49], Liqui-Cell [50], Convergence, Celgard Inc, etc.) and some industrial scale (AQUA-SEP, MEMSYS). However, unlike pressure driven processes, membrane distillation can potentially suffer from wetting depending on a variety of factors like operational conditions, feed properties and the membrane itself. Membrane wetting has been cited as one of the main reasons why MD is not being widely used at full-scale industrial level [18]. Most authors studying membrane distillation consider wetting at a global scale and determined by the effective passage of liquid through the membrane. To further this technology into a commercial application, one of the significant challenges it faces is for the membrane pores to remain dry during the process, as pore wetting deteriorates the performance with time (e.g. saline intrusion in the permeate, in case of desalination) [15]. Even if the risks of wetting occurrence and of the related

process dysfunction are not well understood and qualified, membrane wetting has been regarded as one of the major barriers for the industrial implementation of MD process [16,17].

As described earlier membrane distillation is receiving keen attention all over the world and both technological, and engineering aspects are currently being worked on and reviewed. Since early 2000, the principle focuses of review papers were on general technological potential [23,51,51–53], theoretical approaches in heat and mass transfer [17,54–57]. At present, the reviews are converging towards optimization [58], development of specific configurations, problems related crystallization[59], coupling different membrane technologies with renewable energies [60–63] and fouling/scaling [64–66]. There is an emerging focus on wetting issues, and an interest in wetting prevention, control and regeneration techniques [67].

However, it can be observed that in each article as well as in review papers, authors are using their own definition of wetting: there is a real need of a definition of wetting that could be used by the community. There is also a need of a method to detect wetting or its risk of occurrence i.e. wettability for the appropriate development of MD processes and as a help for the development of new membranes that could decrease the risk of wetting. The general objective of this chapter is to produce a helpful review of wetting detection and characterization tools in MD for researchers, membrane manufacturers, MD system developers, and producers.

Thus, to have a better understanding of wetting (at the fundamental level), the first aim of this chapter is to define pore wetting and then describe the various wetting mechanisms. In this chapter, wetting would be considered at the pore scale and as a localized phenomenon where pore wetting indicates the displacement of liquid-vapor interface inside the membrane pores. Later based on these definitions, the second aim is to introduce and to compare the different methods and indicators that are available to characterize or to detect pore wetting in membrane distillation. Both *ex-situ* and *in-situ* wetting detection methods will be considered.

1.2. Pore wetting

1.2.1. Definition and introductions

Membrane distillation exploits the natural or induced hydrophobicity of the polymer used as membranes. As rules of thumb, porous polymers with low surface energy are selected for MD as they are hydrophobic and ideally do not interact with the feed liquid. For example, polymers like PTFE/Teflon, PP and PVDF have been reported to be commonly used in MD [6]. However under adverse conditions the liquid might enter the membrane pores, and the membrane is then considered wet.

At its core, wetting is the ability of a liquid to maintain contact with a solid surface, resulting from intermolecular interactions when the two are brought together. It is thus more a definition of wettability (or wetting potential) than of wetting itself. Wettability is determined by a force balance between adhesive and cohesive forces. At present, there is no clear-cut definition on wetting in membrane pores or "pore wetting" in membrane distillation other than the guidelines set in 1989 describing the liquid entry pressure (LEP_w) as "wetting pressure" [24] and description of various researchers as per need. To better understand and describe this phenomenon in membrane distillation, it is proposed to consider wetting at the pore level and as a localized phenomenon: pore wetting indicates the displacement of the liquid vapor interface inside the membrane pores. Thus, the following definition of pore wetting is proposed here:

"Pore wetting can be defined as the phenomenon where a shift in equilibrium of the liquid/vapor interface promotes liquid intrusion into the hydrophobic pore, i.e., a displacement of the liquid/vapor interface inside the pore, due to the various forces acting upon it, via the interaction of fluid (feed or permeate) and the membrane material under a given operating condition". This definition is valid for all membrane distillation configurations.

The location of the liquid-vapor interface can be dynamic and depend on the process operating parameters and membrane material interactions which can significantly vary. So, this definition can be applied over the membrane lifetime and operation to characterize pore wetting at each stage of the membrane operating time.

Ideally, membrane distillation assumes non-wetted pores at least at the beginning of the operation, but due to the membrane properties, feed characteristics and operating conditions; three other realistic conditions can occur during membrane lifetime i.e. surface wetted, partially wetted, and fully wetted pore (see **Section 1.2.2**). In each case, when the pores get wet, there is a change in the mass transfer resistance. To maintain successful operation, the membrane should allow the passage of feed fluid in its vapor phase only, suggesting membrane should not get wet. However, it has been observed that membranes might become gradually less hydrophobic during operation, causing them to wet.

1.2.2. Mechanism of pore wetting

Literature considers wetting at the global scale not at the pore scale. Gryta, in the paper "*The influence of PP membrane surface porosity on the performance of membrane distillation process*" theorized different forms of membrane wetting in DCMD [68]. The potential mechanisms and the currently accepted forms of wetting in membrane distillation were proposed and it was suggested that, under

given operating conditions, a membrane can be submitted to four forms of wetting namely, non-wetted pores, surface wetting, partial wetting, and complete wetting, as illustrated in **Figure 1.3**. At pore scale, all forms of wetting can co-exist at different places of a membrane and might not occur sequentially. Wetting is a cumulative effect of the operating conditions and the intrinsic membrane properties on a localized point at the membrane surface during operation.

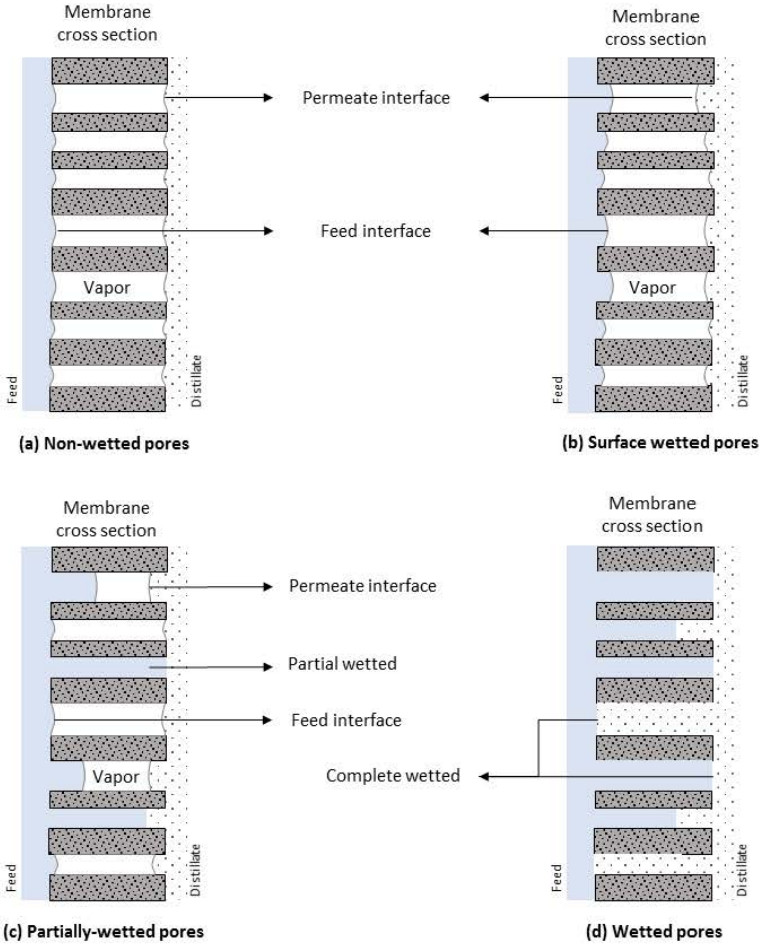

Figure 1.3 Schematic of various idealized forms of pore wetting (a) Non-wetted pores; (b) Surface wetted pores; (c) partially-wetted pores; (d) Totally-wetted pores- Adapted and redrawn from Gryta [68]

With this concern, we can propose to consider that the different mechanisms suggested by Gryta would be more precisely described by the following phrases:

a) Non- wetted pores
b) Partial intrusion of liquid in most pores
c) Total intrusion of liquid in some pores and partial intrusion of liquid in the others
d) Total intrusion of liquid in most pores

1.2.2.1. Non-wetted pores

At this stage, all the pores remain dry and the process is operating in its ideal conditions. Here the liquid/vapor interface is located on the feed side membrane surface and the membrane is performing as per the guidelines [24] (see **Figure 1.3 (a))**. Non-wetted pores are generally observed/assumed at the beginning of the process operation and are currently considered as a major assumption in most modeling approaches devoted to describing MD processes. Concerning operating time, short duration studies report no wetting observation and more extended studies (such as pilot and full-scale MD plants) have reported some form of wetting resulting from operating conditions, fouling, scaling on the membrane surface[69]. As an example, one of the notable publication [70], where a PP hollow fiber in DCMD using distilled water as feed was operated for 1100 h without any flux decline and detectable wetting but later when the feed was changed to tap water scaling developed on the membrane surface which leads to pore wetting.

1.2.2.2. Surface wetting = partial intrusion of liquid in most pores

Surface wetting results from an inward shift of the liquid/vapor interface (LVI) into the membrane pores but the LVI remains close to the feed surface (see **Figure 1.3** (b)). In this case, high purity distillate can still be produced, if the vapor gap inside the membrane pores is maintained. Surface wetting can be caused by degradation of the membrane material or scaling or fouling. Alternatively, surface wetting was also reported to have a positive effect on flux due to the reduced vapor diffusion path with larger pores inside the membrane surface to withhold the liquid/vapor interface [70].

1.2.2.3. Partial wetting = total intrusion of liquid in some pores

In this case, the membrane is performing below its ideal state with some pores completely wet. These wetted pores are now following filtration principles rather than membrane distillation principles (see **Figure 1.3** (c)). In desalination applications, partial wetting leads to a decline in permeate quality concerning conductivity, though the global flux and salt rejection rates may still be high. The MD operation can be continued if a majority of the pores are still dry, though a gradual decline of the distillate quality is typically observed. Researchers studying hydrophobic capillaries observed if a droplet is below the critical drop radius, spontaneous liquid intrusion in pores could occur [71]. This could explain a lot of *"random wetting"* observation in literature studying MD [72,73], indicating that under any given conditions there might be some pores which are already or spontaneously wet even at the beginning of the process. However the observations of liquid intrusion [71] were for a droplet isolated on a capillary and for now, liquid intrusion in pores has not been observed with a real

membrane distillation operation. The occurrence of partial wetting was discussed and detailed in a recent study on produced water [74]. Indeed, using molecular simulations to study oily wastewater in DCMD, it was found that solute molecules could get adsorb on the membrane surface with dissipative electrostatic forces and change the charge distribution of the membrane surface leading to partial wetting.

1.2.2.4. Complete wetting = total intrusion of liquid in most pores

Complete wetting is rarely reported in the literature as is associated with process failure. **Figure 1.3** (d) illustrates what could be this phenomenon. Under such conditions, there is no more liquid/vapor interface inside membrane pores, which are for most of them all filled with a liquid and pure Darcy's law-based filtration is occurring (with respect to the applied pressure) with a liquid bridge on most of the membrane cross-section. This would result in all solutes passing across the membrane cross-section, and thus in deteriorated permeate quality (indicated by an increase in TDS and conductivity).

1.3. Classifying wetting observations in literature

As wetting observations in the literature are subjective, most of the authors do not term wetting in its different forms. Thus, an effort was made to classify some wetting mechanisms observed in literature into the four categories namely: non-wetted pores (NW), surface wetting (SW), partial wetting (PW) and complete wetting (CW). Few examples of each wetting forms in literature are interpreted and summarized in **Table 1.1.** As deduced from the **Table**, all forms of wetting are prevalent in all membrane configurations regardless of the membrane material or the pore size.

Table 1.1: Categorized wetting observed in literature

Membrane Material / Pore (µm) / Type	Config	Feed / Operating conditions	Wetting type				Observation	Ref.
			NW	SW	PW	CW		
PVDF / 0.45 / FS	AGMD	Propanone in aqueous solutions / flow rate ~ Re 3500, Feed temp: 60 °C	-	-	-	●	At high propanone conc. and highest liquid flow rate was observed in the permeate	[75]
PP / 0.22 -0.55 / HF	DCMD	Distilled water / feed and permeate flow rate - 1.35 & 0.25 m/s, Feed Temp: 80°C, Permeate temp: 20°C	●	-	-	-	Operation for 1100h without evidence of wetting	[70]
PVDF + PAN Dual layer / 0.35 - 0.48 / HF	DCMD	3.5 wt % NaCl / Feed and permeate flow rate - 1.4 & 0.7 m/s, Feed Temp: 80°C, Permeate temp: 17 °C, duration 120 h	-	-	●	-	Permeate conductivity increases promoted wetting.	[76]
SMM /	DCMD	0.5 M NaCl / Feed Temp: 45 °C, Permeate temp: 35°C	●	-	-	-	MD with hydrophilic membranes 27 kg/m².h at 45°c without evidence of wetting	[77]
PP / 0.2 / HF	VMD	Synthetic inland brine / Vacuum pressure: −95 kPa, Feed temp:70°C, duration 15-800h	●	●	●	-	Severe wetting attested by conductivity variation in the permeate	[78]
PTFE With PP backing / 0.18 / FS	DCMD	10 g/L NaCl / feed and permeate flow rate - 0.26 m/s, Feed temp: 60°C, Permeate temp: ~24 °C, duration 2.5–5 h	-	-	-	●	Increased permeate flux and conductivity rise	[69]

Note: FS: Flat sheet, HF: Hollow fiber, NW: Non-wetted pores, SW: Surface wetting, PW: Partial wetting, CW: Complete wetting, ● reported

1.4. Pore wetting models

Although wetting is a fundamental aspect of membrane distillation, very little attention has been given towards the modeling pore wetting in membrane distillation. To the best of our knowledge, till 2018 there exist only three theoretical models (one conceived in 1993 and the other two in 2015) who independently derive the equations for liquid intrusion in pores or wetting. Peña et al. [79], devised a model in DCMD which identified the % of pore wetted during temperature and pressure driven steady states. Whereas Chua et al.[80] produced theoretical and experimental evidence that vacuum membrane distillation was achievable with pore intrusion using a hydrophilic membrane. Alternatively, Qtaishat and Matsuura [18] drew parallels between pervaporation and vacuum membrane distillation and theoretically derived the position of liquid inside a single pore by using mass balances. All the three models are introduced in the following sections.

1.4.1. Steady states in direct contact membrane distillation model

Peña et al. [79] developed a steady state model for DCMD which defined and evaluated wetting in a hydrophobic membrane. In their model and experiments, steady states were assessed via. balancing flux generated from wetted pores (non-isothermal flux) and non-wetted pores (non-isothermal vapor flux) simultaneously under a given operating condition. Once the steady state was achieved at time t, the % pores filled with water (α_i) was related to the ΔP_i^{st}(pressure difference at steady state) by Eq. 1.1.

$$\alpha_i = \frac{B'\Delta T_b}{A\Delta P_i^{st} - B'\Delta T_b} \qquad \text{Eq. 1.1}$$

Where: B' is the measured or apparent non-isothermal coefficient, ΔT_b is the temperature difference between the 2 sides of the membrane in the bulk phase ($\beta = B'\Delta T_b$), and A is the permeability coefficient. α_i cannot be directly calculated as A in unknown. Thus, J_i (flux) can be measured by either eliminating pressure difference between the two sides (where $\alpha_i = \left(1 - \frac{J_i}{B'\Delta T_b}\right)$) or by eliminating the temperature difference between the two sides ($\alpha_i = \left(\frac{J_i}{A\Delta P_i^{st}}\right)$). Finally, by using Eq. 1.1, flux (J_i) can be calculated using Eq. 1.2. Where the measured flux, J_i represents the contribution of non-isothermal and the isothermal hydraulic flux at the steady state:

$$J_i = \frac{B'\Delta T_b * A\Delta P_i^{st}}{B'\Delta T_b - A\Delta P_i^{st}} \qquad \text{Eq. 1.2}$$

Based on their model and experiments, membrane wetting was described by calculating temperature and flux at steady-state pressure differences.

For example, membrane TF-450 (PTFE, 0.45 μm) used in this study at feed and permeate temperatures of 313.15 and 303.15 K. Utilizing data from **Figure 1.4** and fitting this data using non-linear regression method (Eq. 1.2), to obtain A and β. The % of wetted pores was calculated at each steady-state pressure difference using Eq. 1.1, implying at steady state 17 - 23 % of the pores were wet with a pressure difference of 1.3 to 2 bar experienced by the DCMD system.

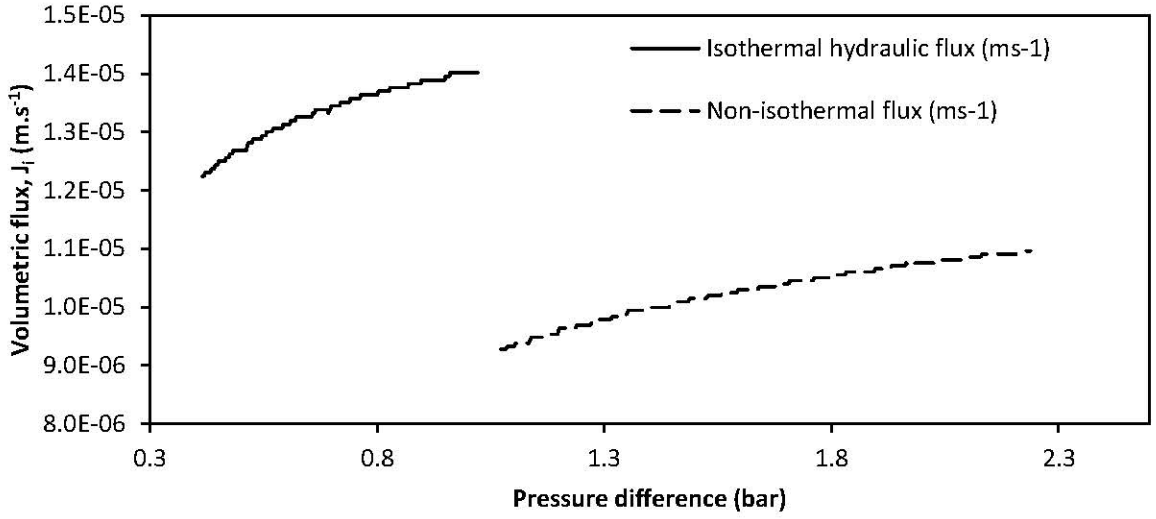

Figure 1.4: Isothermal and non-isothermal fluxes vs. the preceding steady-state pressure difference at ΔT_b 10 K for membrane TF-450. Data [79]

This model coupled with experiments may be used for understanding the impact on membrane wetting for a given membrane and feed solution at a set of temperature and pressure in DCMD configuration.

1.4.2. Pore intrusion model using hydrophilic membrane

Alternatively, Chua et al. [80] used nanoporous membranes coated with organosilica which showed a contact angle of 36°, thus making the surface hydrophilic. The authors presented experimentally and theoretically that vacuum membrane distillation without pore intrusion was possible in these hydrophilic membranes.

The following assumptions were made for developing the model:

- The system is in steady-state;
- Only heat conduction is considered at the feed side liquid boundary layer;
- Only heat conduction is considered across the membrane;
- Interconnectivity of pore channels is not considered.

Lucas Washburn's equation was used to identify the capillary forces on the membrane. Since the Lucas–Washburn equation has been proven to be applicable down to meso- and nano-scale [81,81]. Eq. 1.3 is used to express the capillary phenomena of water filling into the hydrophilic pore by defining the rise of liquid/vapor interface h(t) over time t [82].

$$h(t) = \left(\frac{\gamma_l r_p cos\theta}{2\eta_l}\right)^{1/2}\sqrt{t} \qquad \text{Eq. 1.3}$$

Where, γ_l is the liquid surface tension, r_p is the pore radius, θ is the contact angle between the liquid/vapor interface and the wall and η_l is the shear viscosity of liquid.

By solving the differential Eq. 1.3, volumetric flux can be obtained as Eq. 1.4, where h is the intrusion of water in a pore. **Figure 1.5** presents schematic to better visualizing the model.

$$J_{vol} = \frac{dh}{dt} = \frac{\gamma_l r_p cos\theta}{4h\eta_l} \qquad \text{Eq. 1.4}$$

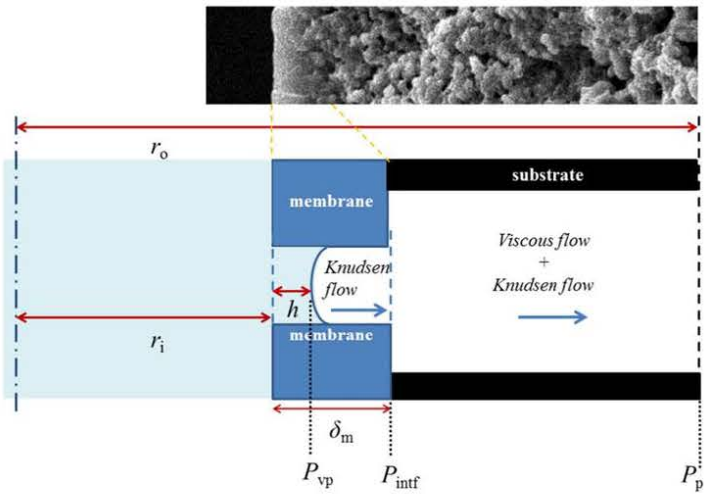

Figure 1.5 Schematic of the mass transfer within the nano pores across the membrane to its substrate. Original [80]

However, it should be noted that with their pore size at 2 nm (0.02µm) the membranes used in this study are in reality quite close of the dense membranes used in pervaporation, even if the authors do not consider them as pervaporation membranes. The applicability of this model for wetting intrusion is thus restrictive in classical membrane distillation as the membranes were not hydrophobic, to begin with, and pore size is not in the range of membranes used in MD.

1.4.3. Qtaishat and Matsuura model

This pore intrusion VMD model is based on a previous model developed for pervaporation (PV) by Okada & Matsuura (1991). The PV model describes the transport of the feed into the membrane pore and its evaporation at the liquid/vapor interface and the vapor transport to the permeate side. This model was used to derive the position liquid inside a single pore by using mass balances. In 2015, Qtaishat and Matsuura [18] proposed a similar model as Okada & Matsuura (1991) that was adapted for vacuum membrane distillation. This model was also based on the mass balance between liquid and vapor. The model assumptions and their justifications are presented in **Table 1.2.**

Table 1.2: Pore wetting model: equation assumptions and justifications for VMD

Model assumptions	Justifications
Single component isothermal system	VMD dealing with pure water only.
Single straight capillary of uniform diameter	Often used criteria in MD transport theory
Liquid transported by Poiseuille flow	Liquid transport 0.1 to 1 µm. Common for VMD
Vapor transportation by Knudsen flow	Referenced flow regime for VMD
Saturation vapor pressure is not affected by the meniscus formed at the interface	With regard to Kelvins equation $\frac{p}{p_0} = exp\left(-\frac{2\sigma V_m}{rRT}\right)$ Where p is the vapor pressure of the capillary of radius r and p_0 is the vapor pressure of flat liquid vapor interface, σ is the surface tension of the liquid, V_m is the molar volume of the liquid. Then p is only 0.4% of p_0

Qtaishat and Matsuura [18] VMD model was developed for a single capillary. **Figure 1.6** provides a visual representation of pore wetting in progress in a single capillary where p_f represents pressure at pore entrance, p_s is the pressure at liquid/vapor interface, p_c is the capillary pressure. The mass flow rate N_l (Kg/s) can be described as a function of the driving force as expressed in Eq. 1.5.

$$N_l = \frac{\pi \rho r^4}{8\eta\delta_l}\Delta p_l \qquad \text{Eq. 1.5}$$

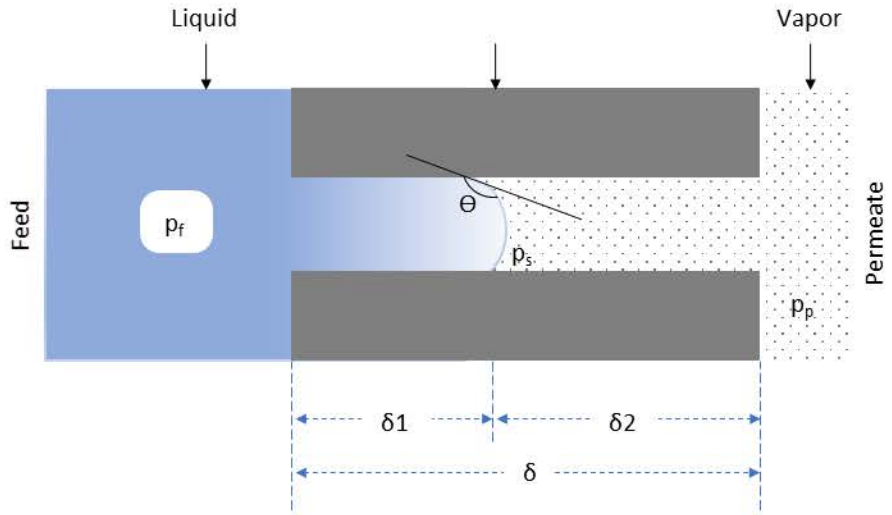

Figure 1.6: Pore wetting in progress in one capillary VMD pore. Redrawn from [18]

Where the density of the liquid is ρ (kg/m^3), r is the radius of the pore (m), η (Pa. s) viscosity of the liquid, δ (m) is total pore length and δ_l is the length the liquid penetrating inside the capillary. Δp_l is the driving force which is pressing liquid to move from feed side to the position δ_l. Δp_l is the pressure difference between feed (p_f) and the liquid/vapor interface (p_s) plus the capillary pressure (p_c) as presented in Eq. 1.6

$$\Delta p_l = p_f - p_s + p_c \qquad \text{Eq. 1.6}$$

The capillary pressure (p_c) can be denoted by the saturation vapor pressure of the liquid. Where σ the surface is tension (N/m) and θ is the contact angle.

$$p_c = \frac{2\sigma \cos\theta}{r} \qquad \text{Eq. 1.7}$$

After sequential derivation [18], the distance of the liquid intrusion in a single pore is derived as $\delta_l\ (m)$ and expressed as Eq. 1.8.

$$\partial_l = \frac{Ar\Delta p_l}{B\Delta p_v + Ar\Delta p_l}\partial \qquad \text{Eq. 1.8}$$

Where, $A = \pi\rho/8\eta$ and $B = \sqrt{(32\pi M/9RT)}$

The authors have provided some theoretical example cases; however, it should be noted that even if this model is not experimentally validated, it constitutes an interesting first step in addressing wetting and liquid intrusion in pores in MD. Experimental validation of this model and its further adaptation for other membrane distillation configurations would be the pressing needs to advance the theoretical aspect of wetting.

1.5. Parameters influencing pore wetting

Any entity that interacts with the membrane and causes a shift in the equilibrium of the liquid/vapor interface inducing liquid penetration into the hydrophobic pore can cause wetting. Based on the literature, the causes or parameters influencing pore wetting in membrane distillation can vary greatly. However, they can be broadly classified into four categories namely: membrane characteristics, fouling, operating parameters, and feed characteristics. As fouling and its different forms have been extensively discussed elsewhere [64,65,67], this parameter will not be discussed here.

1.5.1. Membrane characteristics

Intrinsic membrane characteristics such as pore size, porosity, thickness, tensile strength, contact angle, and surface free energy affect wetting. It is generally accepted that for membrane materials with low hydrophobicity (contact angle $\Theta \leq 90^0$) the risks of wetting are acute. Earlier studies using composite hydrophilic/hydrophobic layers [84] also confirmed it. However, recent studies with a dual layer [85], [86] and [77] have proven that improved flux can be obtained by attaching a hydrophilic layer and some have even used materials with contact angle < 90° to achieve membrane distillation [80]. Surface roughness is critical, as it affects many functional hydrophobic properties of the membrane including the membrane contact angle [87]. As the average roughness increases, the contact angle tends to increase due to the larger number of interactions between the crossing points of the fibers and the liquid [88]. This tendency, known in surface science as the lotus effect, is particularly enhanced for materials exhibiting contact angles >150° with the liquid [89,90]. Hydrophobicity of the membrane is a crucial part of membranes wetting resistance and arises due to the low surface energy of the polymer used to manufacture the membrane. Surface modifications on the base polymer were done by developing dual hydrophilic/hydrophobic membranes and by addition of particles to increase the surface hydrophobicity. The dual layer approach consists of forming a membrane which will exhibit both hydrophilicity and hydrophobicity simultaneously. This was done to achieve better flux and with an intention to prevent wetting. Typically, the two sides of the membranes present different water wetting behaviors. The incorporation of FSi particles into the outer layer

membrane elevated the membrane hydrophobicity. However, the authors noted that the hydrophobicity enhancement did not improve the membrane wetting resistance [76].

Most efforts on enhancing material properties of the MD membranes are made to have a higher flux and reduced incidence of wetting [88]. With an increase in pore size and porosity, there is an increase in permeance [88]. However, an increase in pore size can also lead to wetting, as the minimum pressure needed to wet the membrane, i.e., the liquid entry pressure (LEP), is significantly lowered. Shirazi et al. [91] while evaluating commercial membrane for DCMD found that the membrane with a large pore size (2 µm), resulted in feed penetration into the pores and caused pore wetting. Successful MD operation is normally observed in pore size ranging from 0.1 – 0.6 µm, however, literature cites up to 1 µm but rarely used due to very low liquid entry pressure. Researchers [92] have found thinner membrane with a smaller pore size and a cellular mixed-matrix structure underneath the membrane surface had a higher wetting resistance as compared to a thicker membrane with a larger pore size and a globular morphology.

Surface free energy (SFE) is a vital criterion for understanding the wetting potential of membranes used in MD. SFE is defined as the energy required to create a unit area of the surface of a material in a thermodynamically reversible manner [93]. The lower the surface energy, the lesser the material interacts with its environment. Typical polymers which exhibit low surface energies are listed in **Table 1.3**. The most common polymers that are used for membrane distillation are polytetrafluoroethylene (20 mN/m), polypropylene (30.1 mN/m) and polyvinylidene fluoride (30.3 mN/m). Polymers with low surface energy do not tend to interact with fluid that it comes in contact with, thus, are ideal for membranes used for membrane distillation.

Table 1.3: Surface energy of polymers as membranes or as coating for membranes used in membrane distillation (Data adapted from [94])

Name	Acronym	CAS No.	SFE at 20 °C (mN/m)
Polydimethylsiloxane	PDMS	9016-00-6	19.8
Polytetrafluoroethylene	PTFE / Teflon	9002-84-0	20.0
Polytrifluoroethylene	P3FEt/PTrFE	24980-67-4	23.9
Polyhexylmethacrylate	PHMA	25087-17-6	30.0
Polypropylene-isotactic	PP	25085-53-4	30.1
Polyvinylidene fluoride	PVDF	24937-79-9	30.3
Polyvinylacetate	PVA	9003-20-7	36.5

After extensive review, Eykens et al. [58] proposed the range of membrane properties which could be considered good for better performance including wetting resistance. Parameters reported in the literature and recommended by Eykens et al. [58] are presented in **Table 1.4.**

Table 1.4: Range of membrane properties for membrane distillation studied in literature and recommended by [58] to limit wetting risks

Parameters	**Range observed in literature** [17,23,95–97]	**Recommendation by** [58]
Pore diameter	0.012 - 1.2 µm	0.1 - 1 µm
Porosity (ϵ)	38-90%	80-90%
Thickness (δ)	10 - 200 µm	Low salinity: 30 - 60 µm, High salinity: 200 - 700 µm
Tensile strength	3.4 - 57.9 MP	As high as possible
Contact angle (θ)	80-160°	>105°, As high as possible
Water Liquid entry pressure (LEPw)	0.5 - 4.6	> 2.5 bar
Surface free energy	19.8-30.3	Low as possible

1.5.2. Operating conditions

1.5.2.1. Temperature

To make MD competitive to classical filtration techniques, several researchers have unitized high temperatures to achieve higher fluxes, as driving force in membrane distillation increases with temperature. It can be inferred that at high temperatures (50-90°C) the fluxes vary between 48 – 51 Kg/m².h in flat sheet membranes and 16 – 41 Kg/m².h for hollow fiber membranes under different MD configurations [98–101].

However, researchers [102] studying the effects of temperature (25-75°C) on PTFE membranes found that wettability significantly increased with an increase in temperature due to micro-evolution of the membrane material occurring at each temperature step. SEM images visualized this evolution (See **Figure 1.7** a, b, c and d) and quantified by the broadened pore size distribution and the increase in mean pore size (**Figure 1.7** e, f) at different temperatures (40-75°C). It can be concluded that the

evolution of some temperature dependent microstructures in the membrane can significantly impact wettability.

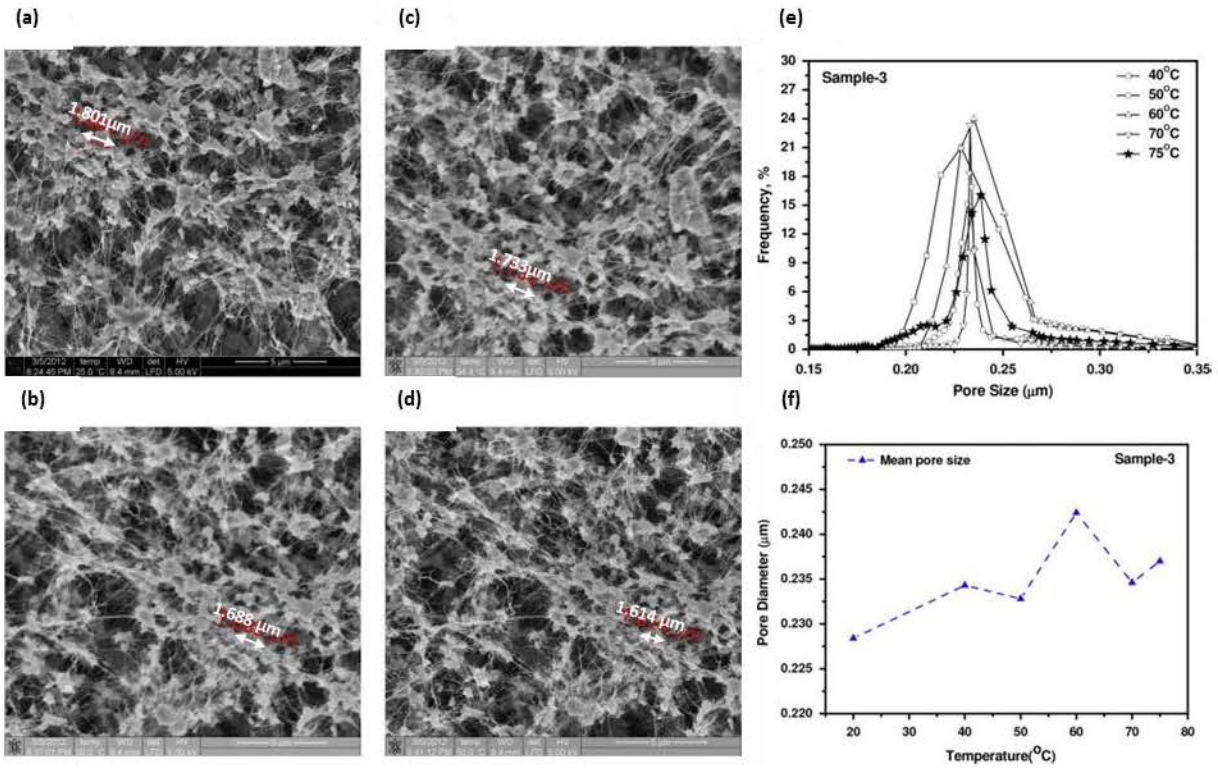

Figure 1.7: SEM images of microstructure evolution in expanded PTFE membrane at progressively increasing temperatures of (a) 25 °C, (b) 50 °C, (c) 35 °C and (d) at 50 °C after 5 min of heating. (e) Increasing pore size distribution and (f) pore diameter (μm) from 40-75°C (Adapted from [102])

Similarly, researchers [91] while studying PTFE membranes (0.22 - 2 μm) with NaCl solution (45 g/L) stated that by increasing the feed temperature to 80°C, the salt rejection for all membranes was 99.9 % except for membranes with biggest pores (2 μm). This membrane responded negatively to the temperature increase and, its pore size was cited as the cause of partial wetting. While others [92] using 264 g/L NaCl solution also reported wetting at higher feed temperatures (60 and 70 °C) that was observed by permeate conductivity measurements. In this study, pore wetting was easily observed due to salt saturation at the boundary layer. Several mechanisms might occur while increasing operating temperature. However, this also leads to higher salt concentration close to the membrane surface, which is known to induce scaling which is sometimes considered as a wetting promotor [64].

1.5.2.2. Pressure and re-circulation flow rates

It is well documented that liquid passes through the biggest membrane pores if the applied pressure exceeds the liquid entry pressure (LEP_w) on the membrane (see 5.1.2). Most studies have been done

under controlled conditions to understand wetting pressure, but information is overlooked during start-up of the MD system. In literature, it was reported that during process start-up a spike in conductivity is observed [103] [104] [105]. Few have noted that during pump start-up and shutdown there is an excess pressure which causes a spike in conductivity on the permeate side. **Figure 1.8** presents three studies, where conductivity spikes were reported at lab [103], pilot [104] and full scale [105].

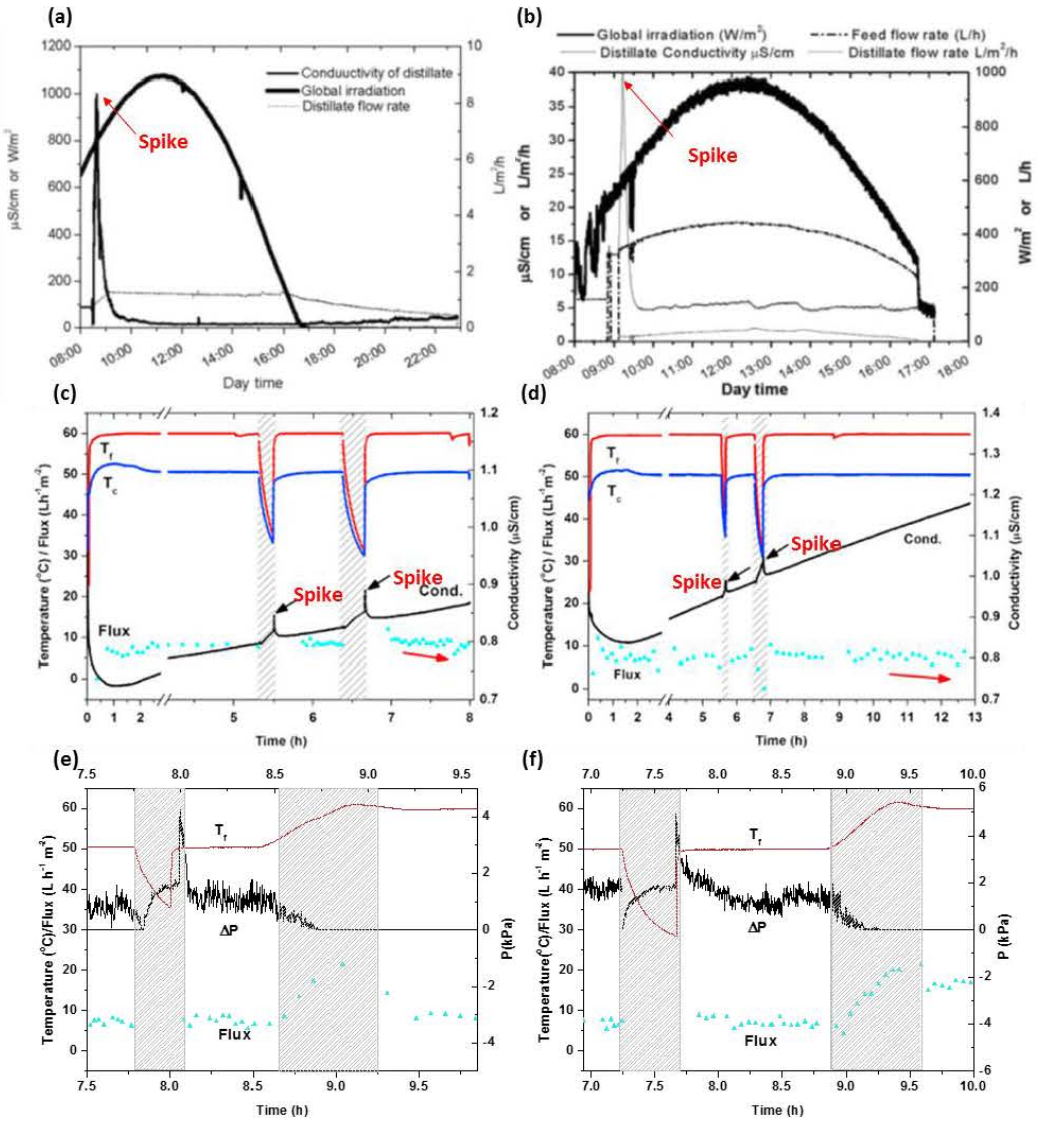

Figure 1.8: Conductivity spike during pump start up and pause in operations (a, b) AGMD small scale[104] (b) large scale AGMD [105] (c,d) Lab scale intermittent operation [103] (e,f) Absolute transmembrane pressure (black line), Tf (red line) and flux (blue dots) registered during MD operation [103]

This observation might indicate that during start-up some pores can get compromised/wet. Though the pressure build-up was below the LEP_w of the membrane, conductivity spikes were still observed (see **Figure 1.8 c, d**) [105]. Another study presents the absolute transmembrane pressure upon turning on and off the feed pumps (see **Figure 1.8 (e, f)**). During pump start-up, there is added pressure build-up at the beginning which may compromise the membrane pores as a progressive increase of the permeate conductivity was reported [103]. At lab scale, the membrane modules are small, and the pressure drop experienced by the membrane surface may not be significant. However, during scaling up, these pressure drops become significant as they can cause localized high-pressure zones and compromise the membranes at its biggest pores, which can explain the observed conductivity spikes during operation.

Additionally, in flat sheet MD cells, feed channels are designed to be narrow to achieve high Reynolds number and reduce concentration polarization and temperature polarization. Consequently, it also increases the pressure drop in the membrane module by increasing the re-circulation flowrate. Researchers [75] while studying propane separation at different operating conditions reported at high concentrations of propane and increasing the flow rate, though greater selectivity was achieved once the flowrate was maxed, however, wetting was observed soon after. Similarly, others studying DCMD concluded that at a high flow rate and elevated temperature facilitate wetting across the membrane [106]. Gryta [107] showed that hydrodynamic conditions influenced wetting and suggested that the hydraulic pressure should be maintained as low as possible to restrict wettability.

1.5.2.3. Support layer/Backing material

Support layer or backing material or spacers are regularly used in membrane distillation as they can provide additional mechanical strength, stability, and turbulence near the membrane surface. Researchers [108], studying the performance of the backing material in DCMD configuration found that the backing material reduces flux and thermal efficiency. The authors reported an increase in the vapor diffusion path and thermal resistances with the formation of a complex network with the addition of the backing material. Literature presents mix response to the use of support layer/backing material as it has been reported to both prevent and caused wetting. The compression of the membrane surface resulting from using backing material is presented in **Figure 1.9 (a, b, c)** before and after operation in membrane distillation. Guillen-Burrieza et al. [69], postulated that compaction by the backing material might have facilitated the wetting processes by allowing bridging of liquid water within the pores.

Additionally, **Figure 1.9 (d)** presents SEM images depression caused by backing material on the membrane surface, while **Figure 1.9 (e)** presents rupture of the membrane surface caused by the backing material. On the contrary, Eykens et al. [96] reported fracture on the membrane surface near the feed inlet (see **Figure 1.9 (f)**) when no backing material was used. Others have come to similar conclusions that thin membranes can undergo mechanical damage and become wet more easily [15,107,109]. Consequently, backing/spacers which should specifically be designed for MD and made in the appropriate material are needed even though they reduce flux by introducing additional thermal resistance, as the membranes used in MD are thin (30-120 μm) and fragile and need additional mechanical support for successful operation and wetting prevention.

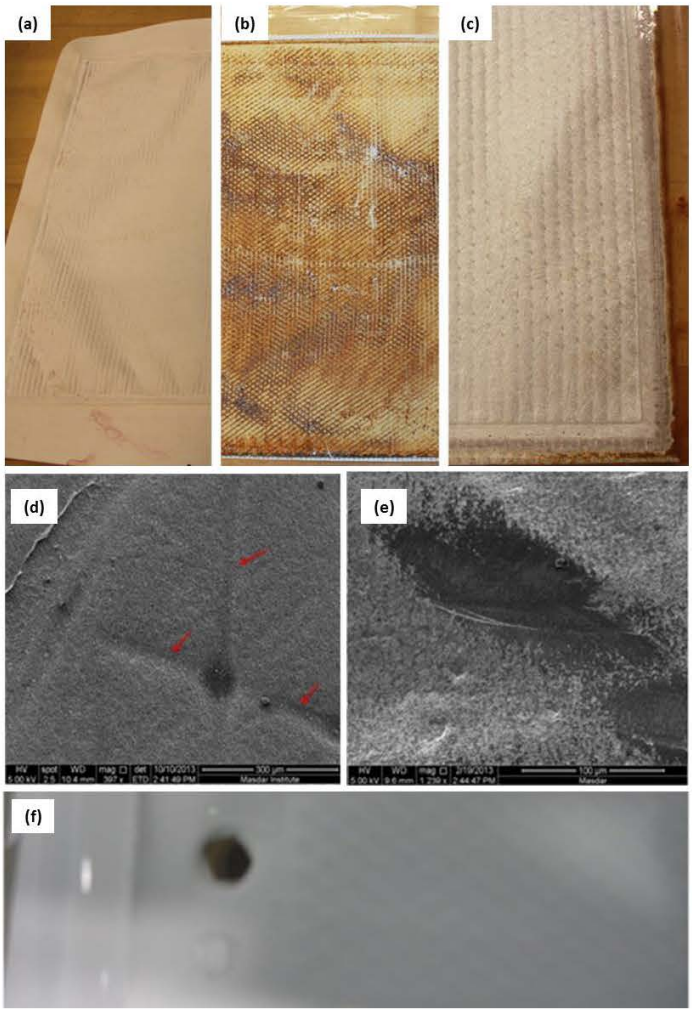

Figure 1.9: (a) Unused membrane (b) front side (c) back side of fouled membranes from Scarab MD modules (d) Representative SEM images of the back side of the fouled MD membranes (PP backer removed) PP backer imprint. (e) Partially destroyed membrane structure caused by the backer material. (f) fracture of the PP membrane at the feed inlet of the module without backing material.[96]

1.5.2.4. Intermittent operation

Several laboratory and pilot scale membrane distillation units are operated under intermittent operation. The justification is that the hydrophobic nature of the membrane, membrane pore size, and the low operating pressure are sufficient to prevent the feed solution from penetrating the membrane pores [110–113]. With some authors recommending "*Contrary to the continuous operation requirement for the reverse osmosis process, an intermittent operation of MD modules with dry periods is possible*" [49,111]. This was especially true for pilots working with solar power, where the MD was run during the day and shut down during the night (with and without draining the feed from the membrane module): for example, DCMD lab scale concentrating whey [110], VMD coupling with solar energy [113], PGMD coupled with solar [112], pilot scale DCMD using solar [114], pilot scale Solar Powered MD (SPMD) [104], large-scale SPMD [105]. To understand the effects of the intermittent operation, Guillen-Burrieza et al. [115] studied dry-out of the PVDF and PTFE membranes by simulating intermittent operation using seawater in membrane distillation. In their study, it was found that the membrane surface hydrophobicity reduced, and internal salt crystallization had occurred. Additionally, these observations were confirmed by in-depth analysis of the effects of the operation on solar-powered an intermitted pilot scale MD by the same authors [69], who recommends not to perform intermittent operation for membrane distillation because it may cause scaling and wetting.

1.5.2.5. Modification of membrane properties due to long term operation and storage

As progressively lab scale MD modules have led to pilot scale plants and eventually full-scale MD plants, with time the changes in intrinsic membrane properties will become an issue that will needs attention. There is an acute need to study membrane aging under real MD operating conditions and cleaning strategies to understand wetting impacts [69]. In literature, only a few studies with long-term operation [69,70,116–119] have reported on wetting in membrane distillation. Gryta et al. [117,118] further illustrated on the problem that storing membranes in distilled water, NaCl solution and even operating under MD crystallizer conditions led to degradation on the membrane surface. The permeability of a membrane soaked in a NaCl solution after 28 days was reduced by about 25–30 %, whereas the decline amounted to only 4–8 % when the membrane was soaked in distilled water [118]. While the membranes stored in the air had formed hydrophilic groups (hydroxyl or carboxyl groups) on its surface which also could lead to wetting. Guillen-Burrieza et al. [69] made similar observations, where membranes were found to be partially wet after keeping them for 21 days in a 35 g/L NaCl solution. A comparative analysis of virgin and aged membranes is presented in **Figure 1.10.**

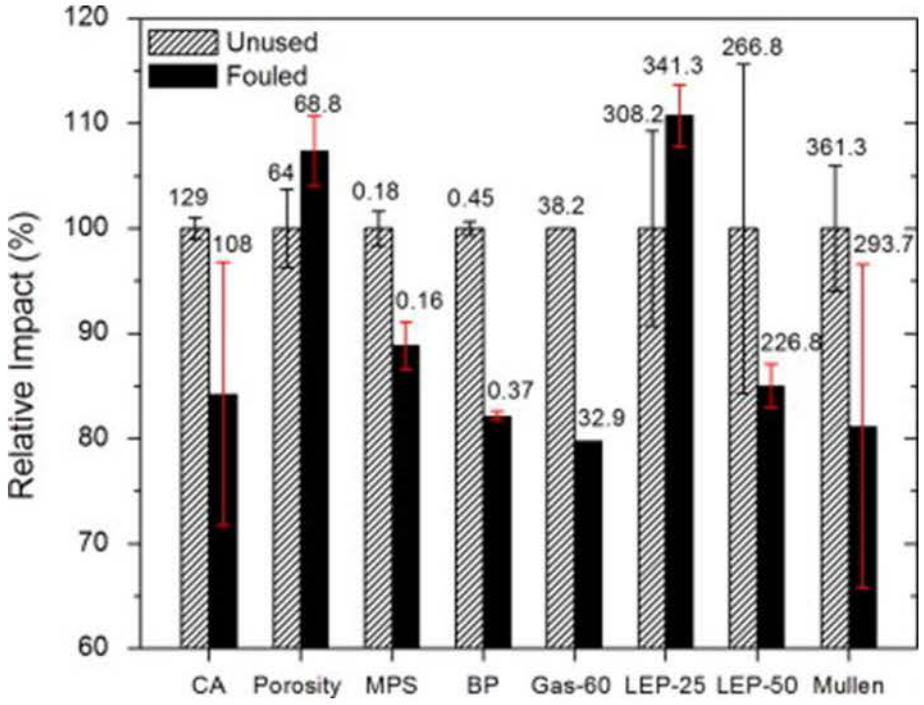

Figure 1.10: Relative impact (expressed as a percentage relative to the unused membranes results) of the long-term operation on the MD membranes used in the Scarab module at PSA (Spain). Absolute values are also depicted and are expressed in degrees (for CA test), percentage (for porosity), μm (for mean pore size (MPS) and bubble point (BP)), l min−1 cm−2 (for gas permeability) and kPa (for Mullen burst and LEP_w at 25 °C and 50 °C tests). Gas permeability values depicted were obtained at a pressure of 413.7 kPa (60 PSI) [69]

Here it can be seen that CA, MPS, BP, and gas permeability decreased after use, while porosity and LEPw increased, possibly due to temperature-dependent microstructure evolution and fouling. These parameters that define the membrane properties after extended use impacted its hydrophobicity and overall wetting resistance, thus raising concerns regarding membrane aging and its effects on wetting.

In a study it was presented that wetting had occurred on membranes after the operation; thus the membranes were studied using FTIR and showed polymer degradation had occurred and caused salt intrusion into the membrane pores [118]. Additionally, in the same paper after long-term storage and UV exposure, similar polymer degradation was observed, thus inferring the possibility of wetting. Later in 2016 using FTIR, the authors came to the same conclusion after testing membranes subjected to MD crystallizer [36]. Polymer degradation leads to wetting as it creates hydrophilic short chain monomers during both storage and operation resulting in the reduction in hydrophobicity on the membrane surface.

1.5.3. Feed characteristics

Due to the operating principles and its ability to achieve high concentrations at low pressures, MD is being applied to a variety of fields, which in turn exposes the process to a variety of feed sources. For example, Banat et al [116] while studying AGMD, using PVDF membrane (0.45 μm) reported an increase in flux and reduction in permeate quality when the feed solution was changed from tap water to seawater. This can be attributed to complete wetting.

Complete wetting can occur if the surface tension of the liquid is lower than or close to the surface energy of the membrane material used. For example, at 20°C, pure ethanol with a surface tension of 22.4 mN/m can readily wet PTFE with a surface energy 20 - 22 mN/m in environmental conditions, while water with its surface tension from 75 - 58 mN/m at 0.01-100°C would not be able to penetrate inside the membrane pores under normal atmospheric conditions. Thus, the suitability of the process to effectively treat a feed using MD can primarily be identified by the surface tension of the interacting feed and material under initial and final desired concentrations. However, many MD based process intensification applications depend on removing water/and or volatile compounds from a feed mixture. As the water transfers to the permeate side, feed fluid gets concentrated and may result in a change in surface tension at elevated temperatures leading to different mechanisms of wetting and ending up in complete wetting.

As membrane distillation is not affected by osmotic pressure during its process, many authors have utilized this property to develop membrane distillation crystallizers (MDCr). In MDCr, the feed is hypersaline solution intended for salt crystallization and precipitation in the bulk. It has been generally noted that salts above their saturation points tend to precipitate and some studies have shown that it can cause wetting on the membrane surface [117]. Thus, a higher risk of wetting might be prevalent when the intention of the process is the crystallization of salts as in MDCr. Also, some feed sources can reduce the surface tension of the solution or interacting membrane pores. Similarly, when volatile organic compounds, high organic content or surfactants are present in the aqueous feed solutions as in the case of wastewater treatment, there is a higher chance of pore wetting by lowering the surface tension of feed solution [120].

For example, Han et al [121], studying produced water in DCMD, found that a feed solution containing oil, sodium dodecyl sulfonate (SDS) and NaCl caused wetting. However, SDS, NaCl or oil alone did not significantly impact the flux, but the combination did it. While using SDS and oil only, no wetting was reported as SDS stabilized the oil emulsions resulting in an improvement in operation relative to oil alone. SDS and NaCl deteriorated MD performance even when oil was absent, and the authors

recommended separation of SDS and NaCl were needed as a pre-treatment before MD. To understand the dynamics of pore wetting observed by the previous authors, Velioğlu et al [74] used molecular simulations and found that the feed solution containing both SDS and NaCl interacted with the PVDF membranes : SDS strongly coupled with fluoride in PVDF and reduced the surface tension in the presence of NaCl, thus leading to severe pore wetting.

Gryta studied the effect of magnetized feed water on scale formation and wetting in membrane distillation in 2011 [122]. In this study, two 0.1 Tesla permanent magnets were attached to the feed port of the DCMD unit. While using the magnetic field, bigger crystallites with thinner and more porous deposits on the membrane surface were observed while compared to the untreated feed. Partial wetting was still prevalent on the membrane and the salt penetrated 40–50 μm deep into the membrane pores. Thus, it was concluded that the magnetic field applied on the feed piping had no influence on wettability for the studied membrane.

1.5.4. Summary on parameters influencing pore wetting

Wetting definitions taken by authors can greatly vary, as well as the tools and procedures that are used to detect wetting or its potential (wettability). Excepted for total wetting, the occurrence of wetting mechanisms is mainly an assumption that is taken, without evidence. This in turn makes it difficult to get a general trend on parameters influencing wetting, as wetting studies are scarce and the effects of operating conditions, membrane characteristics, and feed properties are not well understood. Thus, **Table 1.5** is a tentative to summarize the factors and their effects on what is commonly qualified as "wetting" in membrane distillation, in a generalized manner.

Table 1.5: Factors that affect wetting in various membrane distillation configurations

Parameters	Variables	Wetting impact
Feed side operating variables, effect of increasing	Temperature	↗↙↕
	Solute concentration	↗
	Flow rate	↗↔
	Pressure	↗
	Flux	↗
	Vapor pressure difference (VMD)	↗
Intermittent operation		↗
Membrane properties effect of increasing	Thickness	↙
	Pore size	↗
	Pore size distribution	↗
	Support layer	↗↙↕
	Surface roughness	↙

Parameters	Variables	Wetting impact
	Contact angle	↙
	Tensile strength	↙
Deposits on the membrane effect of increasing	Scaling	↗
	Fouling	↗
	Biological film	↗

Note: Increase ↗, Decrease ↙, Slight effect ↔, Not clear ↕

1.6. Common methods to evaluate wetting/wettability in membranes

The objective of evaluating wettability of membranes is to ensure that under normal operating conditions of the MD process, the feed fluid should not pass through the membrane in its liquid state resulting in disruption of the operating principles. At present, the standard methods for evaluating wettability of membrane is by assessing the liquid entry pressure (LEP_w) or "wetting pressure" [24] and membrane contact angle (CA). LEP_w and contact angle are mostly used to determine if the membrane would be potentially effective for membrane distillation. Primarily these methods are *ex-situ* and require sampling of membranes.

In the following section, techniques and tools currently being used for characterizing wettability of membrane in MD are elaborated and discussed. Potential wetting detection techniques can be broadly classified into *ex-situ* and *in-situ* methods. The following methods are used for characterizing wettability in membrane distillation but generally, this is done before and/or after the MD operation as these methods potentially destroy the membranes for further use as extensive sample preparation is required for most of them. Other than LEP_w and contact angle measurement, currently AFM, FTIR, and SEM/EDS are being also used to identify wetting. As LEP_w is the primary analysis done for any membrane used in membrane distillation, several models have been developed to estimate this value theoretically (such as Young Laplace Model, Franken Model, Kim and Harriott Model, Adapted Kim and Harriott Model, Modified Purcell LEP model) and are explained subsequently.

1.6.1. Contact angle

Contact angle (CA) is defined as an angle experimentally observed on the liquid side between the tangent to the solid surface and the tangent to the liquid–fluid interface at the contact line among the three phases[123]. If a contact angle between the surface and a drop of water is < 90° the material is considered hydrophilic and if a contact angle is observed to be > 90° the material is considered hydrophobic. This is one of the basic technics to qualify wetting ability in membrane distillation, as it helps to identify the degree of hydrophobicity in membranes. CA is an indicator towards the surface

energy of the polymer and a change in CA is a good indication towards understanding the change in hydrophobicity of the membrane.

With an improvement in material and polymer science, superhydrophobic membranes (surfaces > 150°) have been created with an intention to prevent wetting. In general, the surface energy is evaluated by contact angle measurement for membranes using water. As noted in **Table 1.3**, polymers with a lower surface free energy exhibit larger contact angle with water and therefore have less tendency for wetting. **Figure 1.11 (a, b, c)** presents three states of contact angles observed in MD membranes. Generally, MD membranes are hydrophobic and have a contact angle greater than 90 in their virgin state. However, the contact angle is not necessarily representative of hydrophobicity of the inner membrane pores. The surface energy of a membrane can change when exposed to operating conditions and feed including the time of exposure. It is worthy to note that only with an increase in the CA of the membranes, wetting cannot be prevented entirely but can be delayed [124]. By assessing the change in contact angle before and after use for membrane distillation with different feeds, it is often shown that membrane hydrophobicity has reduced, and wetting has occurred **(see Figure 1.11 (d, e)**).

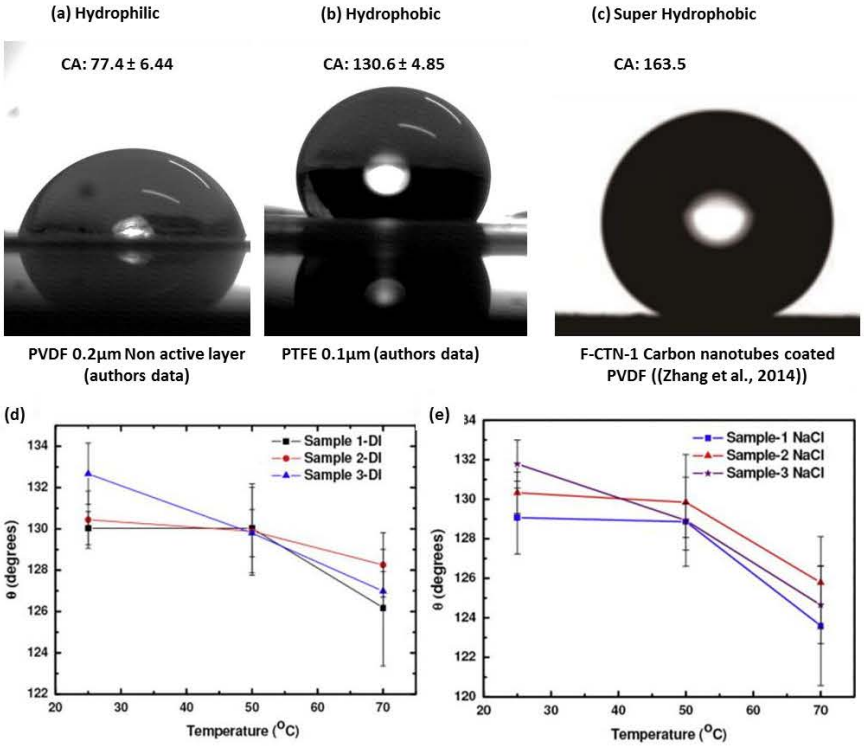

Figure 1.11: (a) Hydrophilic, (b) hydrophobic and (c) super-hydrophobic materials with their contact angles. CA variations with temperature for the three membrane samples using (d) DI water and (e) 3.5 wt% NaCl in DI water solution [102]

Table 1.6 presents the reduction in CA after being applied in the MD process [125–127] for desalination. After exposure to different feed solutions, CA for all membranes reduced significantly, and some surfaces were more in the hydrophilic range than hydrophobic, thus increasing the risks of wetting due to a reduction in surface energy. CA is one of the primary techniques to both characterize and evaluate potential wettability of membranes used or developed for membrane distillation.

Table 1.6: Contact angle of membranes before and after MD experiments

Feed source	Membrane material / pore size	Operating conditions	Contact angle (°)		Experimental duration (h)	Ref.
			Before	After		
3.5% NaCl	PVDF / 0.45 µm	DCMD	123.5	90.5	1	[127]
	F-CNT-1M		163.5	160.7		
	F-CNT-2M		157.4	154.5	2	
	F-CNT- 3M		142.8	118.5		
Seawater	PTFE / 0.22µm	DCMD	137.7	8.9	23	[126]
RO concentrate				23.9	23	
Saturated $CaSO_4$				8.9	16	
Seawater (Arabian Gulf)	PP / 0.22 µm,	DCMD	134.8	40.5	19	[125]
	PP / 0.45µm		133.2	36.1	30	
	PTFE / 0.22 µm		136.7	13.8	25	

Note : CTN : Carbon nanotubes composite PVDF membrane

1.6.2. Liquid entry pressure (LEP_w)

LEP_w is an important parameter and reported by nearly all publications using membrane distillation. LEP_w (also known as "Wetting pressure") is defined as the pressure that must be applied onto pure water before it penetrates by convection inside the pores of a non-wetted (dry) membrane and is observed in the permeate side. The first drop of water in the permeate side is observed when the biggest pore is completely wetted. Thus, to standardize the LEP_w measurement all the experiments are generally done using ultra-pure water (conductivity 18.2 MΩ.cm) at 25°C. As it is an indication towards the hydrophobicity and gives an overall idea of the operating pressure required for water to enter the largest pore of the membrane (r_{max}), at present, LEP_w is calculated using Franken model (Eq. 1.9)

$$LEP_w = \frac{-2B\gamma\cos\theta}{r_{max}} \qquad \text{Eq. 1.9}$$

Where: Θ is the CA (Contact angle between the wetting liquid and the hydrophobic membrane), r_{max} (m) being the maximum pore radius of the membrane and ϒ represents the surface tension. Factor B has to be rapidly defined (see paragraph 5.1.2.2).

An overview of the LEP_w of different types of the membrane is presented in **Table 1.7.** It can be noted that, as previously said, most membranes used are either PTFE or PVDF with a high porosity and relatively high LEP_w. Typically, in literature, membranes used in MD have a LEP_w of 0.5 - 4.6 bars and, as MD is operated at atmospheric pressures, these LEP_w values are considered high enough to prevent wetting. However, it should be noted that LEP_w is measured at STP and not at the operating temperatures and this value should be considered as only an indicator of partial wetting potential.

Table 1.7 Properties of some commercial membranes used for MD, including LEP_w

Membrane type	Manufacturer	Material	Average pore size, Rav (nm)	Thickness δ (µm)	LEP_w (bar)	Porosity, ε (%)	Ref.
PV22	Millipore	PVDF	220	126 ± 7	2.29 ± 0.03	62 ± 2	
PV45	Millipore	PVDF	245	116 ± 9	1.10 ± 0.04	66 ± 2	
PTS20	Gore	PTFE/PP	200	184 ± 8	4.63 ± 8	44 ± 6	[128]
PT20	Gore	PTFE/PP	200	64 ± 5	3.68 ± 0.01	90 ± 1	
PT45	Gore	PTFE/PP	450	77 ± 8	2.88 ± 0.01	89 ± 4	
Accurel® S6/2	AkzoNobel	PP	200	450	1.4	70	[53]
Fluoropore	Millipore	PTFE	220	175	4.2	40	[4]

With an increase in temperature, a reduction in LEP_w has been observed [69,102]. As presented in **Figure 1.12,** a 3-fold reduction in LEP (using NaCl sol. and DI water) was observed while the temperature increased from 25 to 70°C. It is a matter of concern as most MD pilots/plants are operated at 40-70°C, with an understanding that LEP is well above the operating pressure. Thus, operating pressure variations during start-up/shutdown might cause wetting to occur, due to a reduction in LEP. Also, it must be noted that as the process continues in time and depending on the feed characteristics, fouling/scaling and membrane degradation might occur thus further lowering the LEP and increasing the risks of membrane wetting.

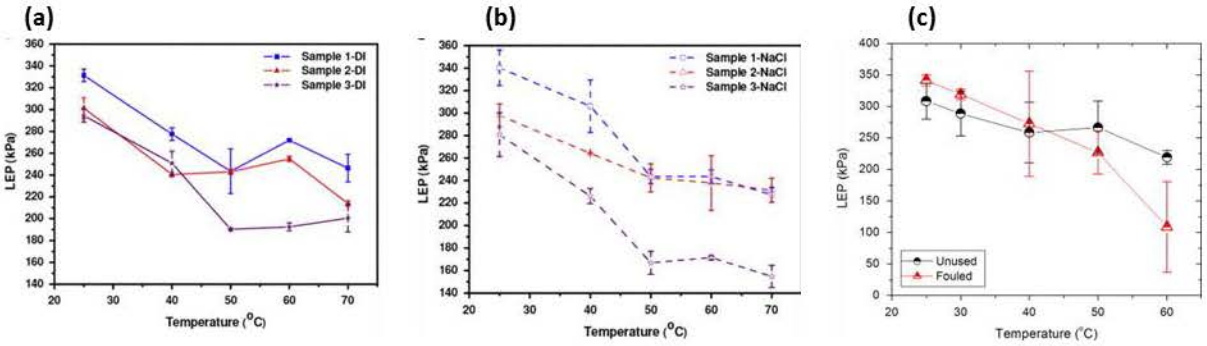

Figure 1.12: (a) LEP measurements as a function of temperature for the unused and fouled MD membranes used in the Scarab module at PSA (Spain). All measurements were done using a 35 g/L NaCl solution.[102] LEP variations with temperature for the three membrane samples using (b) DI water and (c) 3.5 wt% NaCl in DI water solution.[69]

As LEP_w is the primary technique used by most researchers for determining the feasibility of membrane for MD application, therefore, many models were conceived to describe LEP both experimentally and theoretically. LEP is developed based on the standard capillarity model developed by Young-Laplace in 1807. The history of liquid entry pressure (LEP) modeling, from this original concept to the more recent evolutions is presented in **Figure 1.13**. In this next sub-section some significant theoretical models developed are briefly introduced and discussed. For detailed derivations refer to the respective papers.

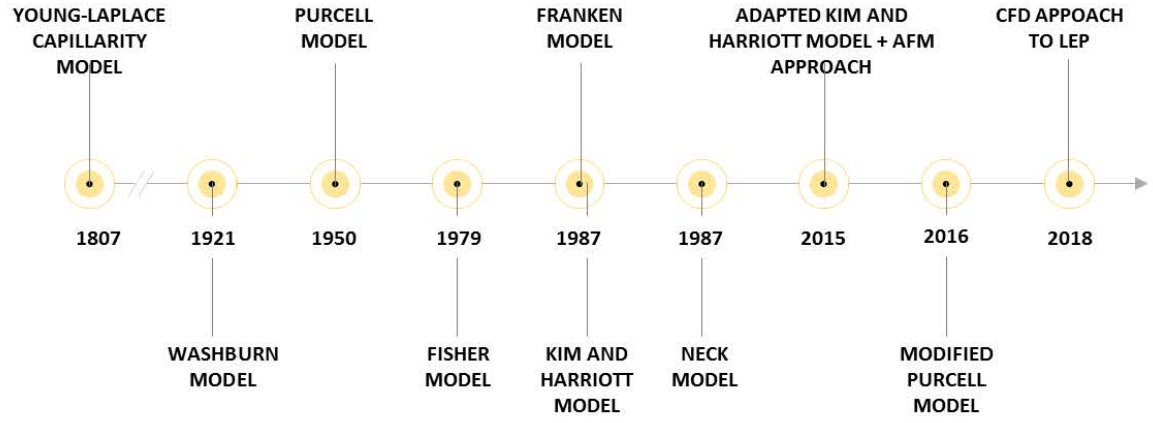

Figure 1.13: History and the evolution in LEP modelling

1.6.2.1. Young Laplace Model

Traditionally, standard model for capillarity is used for measuring LEP uses Young-Laplace (YL) equation [129] adapted subsequently [130,131] and is presented in Eq. 1.10.

$$LEP_w = \frac{-2\,\gamma \cos\theta}{r_{max}} \qquad \text{Eq. 1.10}$$

Where: Θ is the (contact angle (CA) between the wetting liquid and the hydrophobic membrane, r_{max} (m) is the maximum pore radius of the membrane and ϒ represents the surface tension of water.

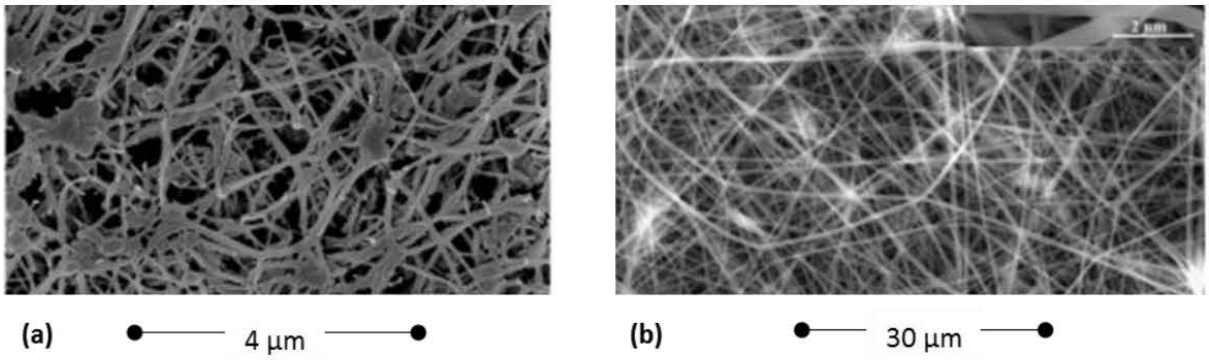

Figure 1.14: SEM images of (A) PTFE membrane (0.22 µm) (B) PVDF membrane (0.2 µm) Adapted from [132,133]

This model assumes uniform cylindrical pores and a constant radius of curvature, but it should be noted that most membranes do not have such a pore structure. For example, **Figure 1.14** presents PTFE and PVDF membranes which are commonly used in MD, and it can be seen that these structures are more like a matrix rather than uniform pores. Therefore, the capillary-based model using YL equation may

not be the most accurate model for predicting wetting. Researchers demonstrated that YL model could not be applied to stretched membranes like PTFE **(Figure 1.14 (a))** and had a tendency to over predicts LEP or wetting pressure [134].

1.6.2.2. Franken Model

Thus to account for the asymmetric non-circular pores in membranes, Franken et al. [120] introduced the pore geometry factor (B) to accommodate the irregularities in the YL model. In the newer model, the B value represents 1 for completely circular pore and between 1 and 0 for non- circular pore ones. (Eq. 1.11)

$$LEP_w = \frac{-2B\gamma\cos\theta}{r_{max}} \qquad \text{Eq. 1.11}$$

The authors [120] associated the B value with the curvature radius of the surface pores. Stretched membranes with non-circular pores (e.g., PTFE) and small curvature radius were assigned B values of 0.5–0.6. Concerning the Franken model, two membranes A (elliptical) and B (round pores) having similar contact angle and rmax, will have different LEP values and LEP_w will be greater for the one with round pores than the one with elliptical ones. At present, Franken model is being used to calculate wetting pressure in most reviewed literature theoretically. Though the Franken model could theoretically predict wetting pressure better than YL model, it still does not match the experimental LEP, as this model fails to address those irregularities occurring in both radial and axial direction.

1.6.2.3. Kim and Harriott Model

Purcell (1950), in the pursuit to understand the interaction between oil-reservoir rocks and water to determine the pressure difference across the oil–water interface, considered the pores as doughnut-shaped holes. In his model, an axial variation of the pores was included but did not consider the radial variation of the pores, thus assuming circular pore cross-section. In his model, when the pressure increased, the three-phase contact line radius between the water filling the pores and the oil pushing through them gradually decreases to the minimum radius r (see **Figure 1.15 A)** and then gradually increases.

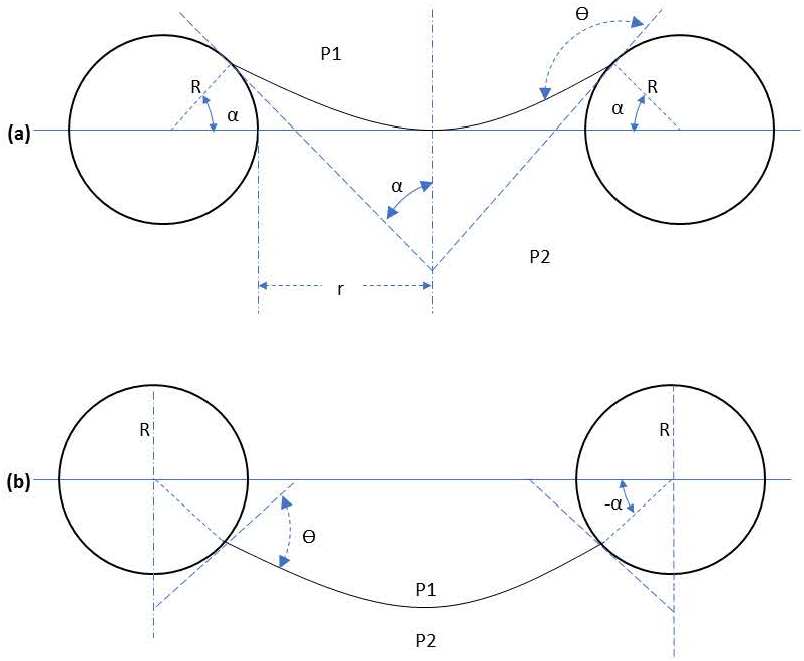

Figure 1.15 Purcell model of doughnut shaped pores of oil-reservoir rocks. Original from [136]

Building on this gained knowledge, Kim and Harriott [134] adapted Purcell's model and further expanded it to consider PTFE membranes as an array of uniform fibers intersecting at fixed angles and used it for deriving for the LEPw. The final derived equation is presented in Eq. 1.12.

$$\Delta P = \frac{2\gamma}{r}\frac{\cos(\theta-\alpha)}{1+\left(\frac{R}{r}\right)(1-\cos\alpha)} = \Delta P = \frac{2\gamma}{r}\cos\theta_{eff} = LEP \qquad \text{Eq. 1.12}$$

Where θ the CA, γ is is the surface tension of the wetting liquid, r is the pore radius, R is the fiber radius and α is the structural angle accounting for the axial deviation of the pores.

Kim and Harriott also introduced to the equation what they defined as the effective CA (Θ_{eff}) which can be calculated using Eq. 1.13.

$$\sin(\theta-\alpha) = \frac{\sin\theta}{1+(r/R)} \qquad \text{Eq. 1.13}$$

Eq. 1.12 shows that greater the r/R ratio the larger the effective contact angle. Kim and Harriott's model was both theoretically and experimentally validated using a PTFE membrane (0.2 µm) with various wetting liquids.

However, Zha et al. [137] pointed out that the deviation of any irregular pore structure from a cylindrical capillary needs to be further described by two parameters:

1. The hydraulic radius (r_h), reflecting the radial deviation from a circle,

2. The structural angle (α), reflecting the pores deviation from the vertical axis. It is an important factor that needs to be considered for liquid displacement in porous media and LEP does not occur at the narrowest part of the widest pore but at a certain value of α [137].

However, this model is not without its redundancies. As per this model, wetting could only occur when the contact angle is below 90° with very small r/R ratio. On the other hand, Franken's model even without the use of r/R ratio could predict that liquids having a CA greater than 0 would spontaneous wet the membrane, thereby partially disproving the application of this model. Furthermore, Kim and Harriott's model also requires the measurement of the effective CA inside the pores and the r/R ratio, which was not directly possible at the time.

However recently, researchers using transient laser interferometry technique investigated the evolution of the shape of the liquid-vapor interface in micropillar arrays during evaporation In the study, they could measure the absolute location and shape of the meniscus and calculated the contact angle and the capillary pressure [138]. This was done for a hydrophilic capillary, but this technique can be adapted for also hydrophobic capillary too, thus opening a new way for determining cos θ_{eff}.

In Kim and Harriott's model, the users have to assume that the roughness of the surface is an indicator of the roughness inside the pores [139]. This leads to the problem of how to calculate/predict the r/R ratio, as it is difficult to determine this ratio inside the membrane pore and the predicted α, leading to considerable variation in LEP determination.

Thus, further efforts were made to improve Kim and Harriott's model with the objective to predict wetting pressure or LEP better.

1.6.2.4. Adapted Kim and Harriott's Model

To improve on the R/r ratio, Guillen-Burrieza et al. [140] used two methods. Firstly, by using Cassie–Baxter relationship between the apparent advancing contact angle (ACA, θ^*_{adv}) and the intrinsic contact angle (θ_{adv}).

$$\cos\theta^{*}_{adv} = -1 + \frac{1}{D^{*}}[(\pi - \theta_{adv})\cos\theta_{adv} + \sin\theta_{adv}] \qquad \text{Eq. 1.14}$$

Where: D^{*} is a dimensionless spacing ratio. D* was defined by Rijke (1968) and was confirmed by Elowson (1984) while studying the hydrophobicity features of ducks feathers as $D^{*}=(R+r)/R$.

The second method was to use Atomic Force Microscopy (AFM) to obtain information on the membrane structure. Using AFM, a topographic profile was obtained where the valleys would be considered as pores (r) while the peaks were assumed to be the fibers/nodes (R). The authors theorized that the roughness of a surface could be interpreted as amplitude. However, the spatial distribution of the morphological elements on the surface (i.e., fibers, pores, etc.) is the ultimate factor that determines the contact angle and the LEP of the membrane. AFM profiles were used to identify the roughness amplitude, the defect spatial distribution and, density [140].

To validate their model and technique, five membranes were coated with the same hydrophobic monomer,1. The samples included two stretched PTFE membranes, one unsupported PVDF membrane, one track-etched PC membrane, and a nylon membrane. While keeping all parameters constant for the various membranes studied, it was found that the YL model and its modification proposed by Franken were unsuitable for predicting LEP for most membranes as presented in **Figure 1.16.** The model proposed by Kim and Harriott was closer to the reality with stretched PTFE membranes only. While the modified Kim-Harriot's model based on the Cassie–Baxter model and AFM predicted close for PTFE and PVDF membranes but over/underpredicted for PC and Nylon membranes.

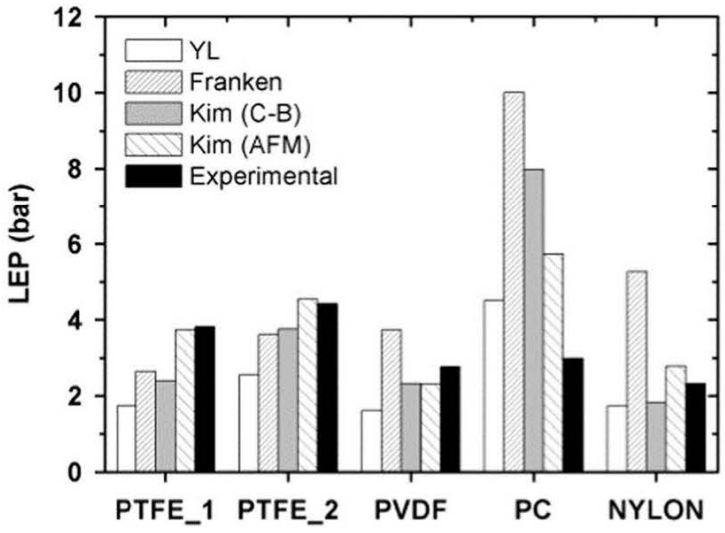

Figure 1.16 Theoretical LEP values as predicted by various models for the 5 membranes. Original from [140]

To continue the efforts in building more predictable LEP model, Servi et. al [143] provided a further improvement on LEP theory by modifying Purcell model and provided experimental proof using fibrous nylon membranes and presented the validity of this model for CA in the range of 63 - 129°. However, tests on other membrane materials were not reported.

In the end, it can be concluded that no single available model could exhibit good predictability for all membrane types used in membrane distillation. However, recent advancement in LEP prediction using multiphase computational fluid dynamics (CFD) has presented a very interesting approach to resolve LEP and pore wetting [144]. In this paper, the authors concluded that CFD simulation provided LEP results that were closer to the reality that an increase in pore length of the membrane could potentially improve wetting resistance. There is still much room for further development of theoretical models for predicting wetting pressure (LEP_w) in membrane distillation.

1.6.3. Conductivity measurement

The agreement between field and lab tests results strongly suggests that membrane wetting greatly contributes to the deterioration of the distillate quality [69]. Several authors have reported using conductivity measurements of the MD permeate [70,124] to identify wetting occurrence At present conductivity measurement is the standard *in-situ* technique to evaluate wetting in any MD configuration. This technique is being actively used by several authors to determine pore wetting in membrane distillation (especially in DCMD) [145]

By using conductivity probes, on the feed, permeate side of the membrane and measuring the progressive increase in conductivity, a slope can be developed, and wetting rate on the membrane can be estimated. The wetting rate can be defined as the slope of the registered rise in conductivity in µS/cm.h. Guillen-Burrieza et al. [103] first defined the wetting rate for the DCMD process. **Figure 1.17** presents a DCMD operation of a PVDF membrane with progressive salt rejection (SR), wetting rate, and wetting time. There is potential to expand this method to other MD configurations. However, this method would be only able to detect wetting if a sufficient number of pores or all pores are compromised, and partial or total wetting had occurred.

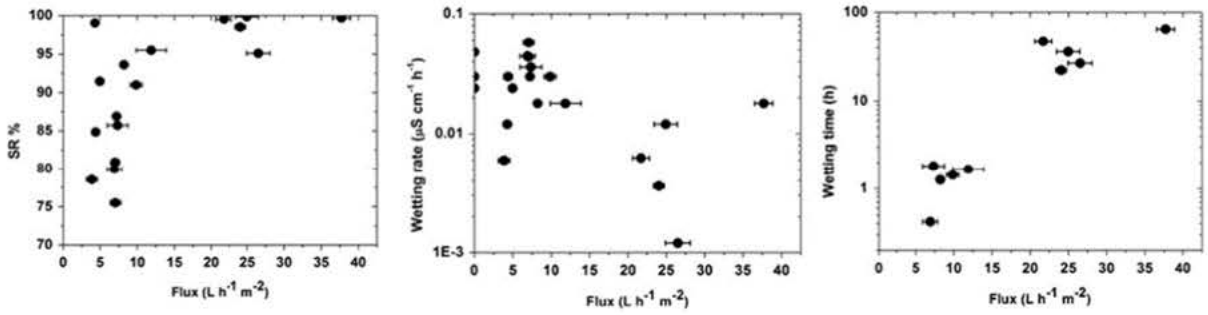

Figure 1.17: DCMD results from the experimental matrix. From left to right: DCMD flux versus salt rejection factor (SR %), wetting rate (µS h−1) and wetting time (h). [103]

1.7. Emerging methods for wetting detection

Recently efforts have been made for wetting detection in MD, and some promising innovative methods are emerging. One of them is an *ex-situ* method, based on scanning electron microscopy coupled with X-ray dispersion spectroscopy, and literature also presents interesting approaches to detect wetting *in-situ*, such as the volumetric method, the MD-electrochemical cell, and the impedance spectroscopy, that will be discussed in this chapter.

1.7.1. Electron microscopy and X-ray dispersion spectroscopic techniques

Scanning electron microscopy (SEM) is a high magnification microscope technique which uses a focused electron beam to produce images of a sample. SEM analysis requires necessary sample preparation for both top view and cross-section of the membrane using either Gold or Carbon. During SEM operation generated primary electrons result in low energy secondary electrons from a studied sample, which reveals its topographic nature. These primary electrons can also be backscattered, producing images with a high degree of atomic number (Z) contrast resulting in ionized atoms on the sample surface leading to X-ray emission or Auger electron ejection. These emitted X-rays are characteristics of the elements on the sample and are measured by an EDX (energy-dispersive X-ray spectroscopy) detector [146].

In membrane distillation, SEM/EDX (scanning electron microscopy and X-ray dispersion spectroscopy) analysis is often used in membrane autopsies to visualize the membrane surface or the cross-section [147–149]. SEM analysis is often conducted to understand membrane surface morphologies and defects. However considering wetting, SEM alone would not be enough for wetting detection. Here coupling EDX and SEM analysis can make wetting detection possible. As it can show the penetration of the salt (which in most cases stays in the liquid phase of the feed) into the membrane cross-section. Studies on membrane contactors [150] and another one on MD [68] presented autopsies with

detection of salt across the membrane cross-section (see **Figure 1.18**). The presence of these salt traces was attributed to membrane wetting, and potential evaluation of these salt traces could be considered used as a powerful tool to investigate pore wetting. This technique will be further explored and developed in Chapter 2 and 3.

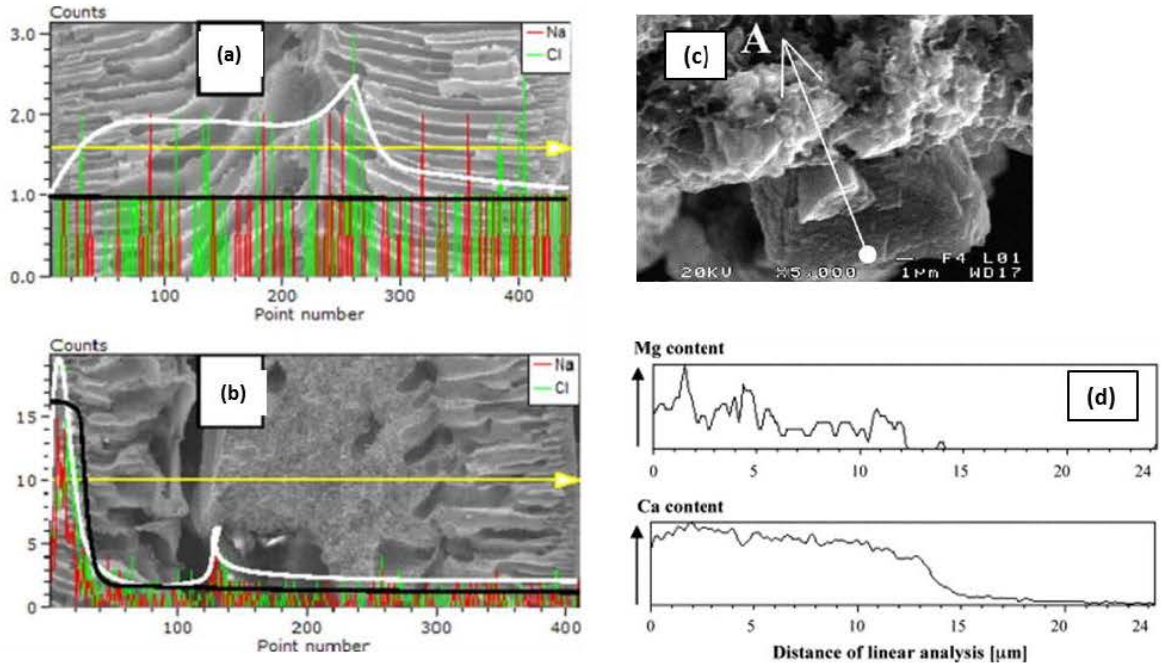

Figure 1.18: SEM-EDX spectra of 800X for membranes used for membrane contactors (a) PEI-12-IC (b) PES-15 (white lines: observed EDX trend, black lines: ideal EDX trend).[150] (c) Traces of salts inside the membrane wall (d)SEM–EDX line analysis of the Ca and Mg concentration [68]

1.7.2. Volumetric method

Most MD membranes are hydrophobic microfiltration membranes with a porosity of 60-80%. Implying that, if a known volume of liquid is fed to the membrane surface with pre-defined membrane properties, operating condition and permeate flux there is a possibility to estimate the total volume of liquid that entered in pores by a mass balance. Two research works developed variations of this method to detect and understand global wetting in membrane distillation. The first was by Peña et al.[79] using DCMD followed by Lawson and Lloyd [151] for VMD.

In the VMD experiment [151], the level in the feed tank was maintained by adding measured amounts of fresh water to the feed tank every 15 to 30 min. The flux was calculated by plotting the cumulative volume added to the feed versus time and taking the slope. If the volume versus time data did not fall on a straight line, then either wetting or fouling was assumed to occur. However, neither wetting nor

fouling was observed during the experiments. Thus, no conclusive data was obtained on wetting and the procedure is open to further research and development.

1.7.3. MD-electrochemical cell

Another approach for *in-situ* measurements would be by adding an electrically conductive layer on the membrane module. This approach makes the feed and permeate sides of the membrane compartment as an electrochemical cell where the membrane itself acts as a barrier while the conductive layer acts as an electrode. This method was proposed and evaluated by artificially inducing wetting (adding 10% wt. ethanol) by reducing the surface tension of feed [152]. The electrodes used on feed and permeate side were a stainless-steel mesh and carbon cloth respectively. **Figure 1.19** presents the change in both anodic and cathodic current after wetting was induced at 60 min. The advantage would be localized wetting detection to a single module in a multi-module system. However in a single module system, it would work the same way as measuring the conductivity of the permeate as proposed by others [103,124].

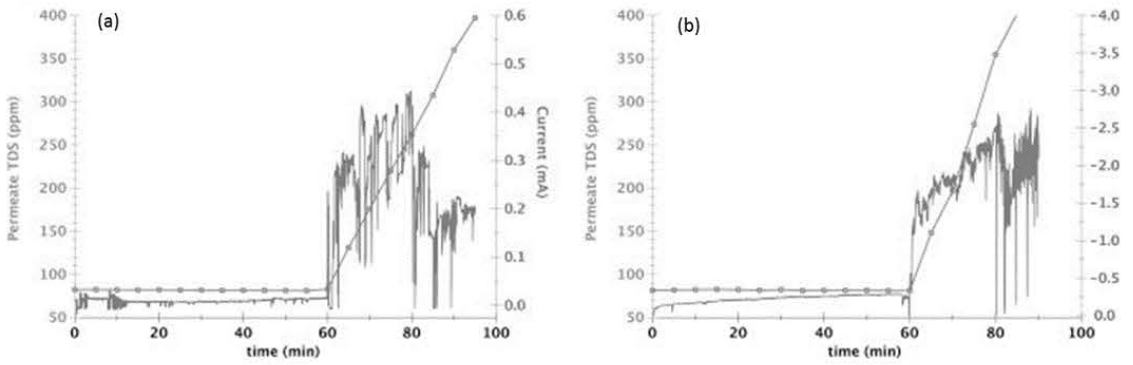

Figure 1.19: Permeate TDS and current for a) anodic and b) cathodic voltage applied in DCMD system treating salt water ([152]**)**

1.7.4. Impedance spectroscopy

By measuring the electrical response of a system upon application of alternating potentials (similar to [152]) but with a wide spectrum of frequencies, Chen et al. [153] using electrochemical impedance spectroscopy (EIS) were able to detect wetting before it was observed by conductivity probes in DCMD configuration. Ideally, in this configuration the membrane cell acts like a capacitor storing potential due to the air trapped inside the membrane pores. At the stage where surface wetting is transitioning towards partial wetting, a decrease of the average distance between the two interfaces (feed liquid interface: air trapped inside the membrane pores: permeate liquid interface) simultaneously decreases the resistance of the membrane. As the distance between the 2 interfaces decreases there

is an increase in the capacitance of the air trapped inside the pores leading to a reduction of the overall system impedance. **Figure 1.20** presents normalized impedance after inducing wetting reagent (Triton X-100) at 2 different concentrations. Measuring impedance could be a promising solution for *in-situ* measurement of mechanisms of wetting in direct contact membrane distillation and would be worth exploring in all the other membrane distillation configurations.

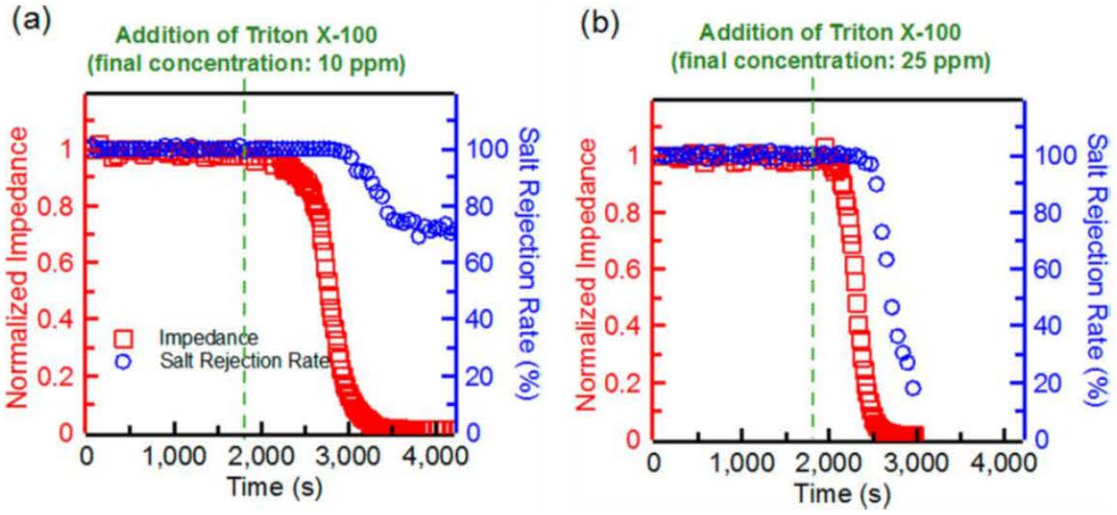

Figure 1.20: Impedance across the PVDF membrane and salt rejection rate in DCMD experiments in the presence of (a) 10 ppm Triton X-100 and (b) 25 ppm Triton X-100*[153]*

1.8. Comparison between wettability and wetting detection methods

Though most *ex-situ* methods can give information on changes the membrane surface (leading to wetting) on a local scale but not while the process in progress. On the other hand, conductivity based wetting rate, volumetric methods, MD-electrochemical cell and measuring impedance can give global information on wetting during the process in a single module MD unit. Additionally, it should be noted that in membrane contactors, thermal conductivity detectors are used for wetting detection [154–156] but they have limited utility in membrane distillation as only 2 of the membrane configurations, i.e. VMD and SGMD would be able to benefit from this technique as the detector is principally a gas sensor. An essential aspect of developing *in-situ* method would be wetting prevention but most of the methods using conductivity present the aftermath of total and strong partial wetting but not surface and slight partial wetting. In this regard, measuring impedance over the membrane surface seems to be a promising technique which needs to be further explored and developed. However, this technique does not provide information on local wetting like all other *in-situ* methods. A comparative assessment of the advantages and disadvantages of the presented methods/techniques for identifying wetting in membrane distillation are presented in **Table 1.8.**

Table 1.8: Comparison between *in-situ* and *ex-situ* methods for detecting wetting/wettability

Method	Principle	Advantage	Limitation	Information obtained
Contact angle	Surface energy	• Simplicity • Gives immediate information about hydrophobicity of the material and surface tension of sample liquid • Extensively studied by various authors	• Higher risk/impact of impurities • Results depend on the consistency of the operator • Not representative only relative to the measured location • Characterizes wettability but not wetting itself	Wettability
LEP	Provoked intrusion of liquid by filtration	• Simplicity • Standardized method • Extensively studied by various authors	• Only gives information on the largest pore • Varies with temperature and feed used	Wettability: Total liquid intrusion
SEM/EDX	Electron microscopy / Energy-dispersive X-ray spectroscopy	• Local information on wetting • User-friendly operation • Fast results • Applicability in several MD configurations	• Ex-situ • Destructive analysis • Sample preparation can result in artefacts	Salt penetration in the membrane pores
Conductivity measurement	Conductivity and mass balance	• In-situ • Simple to setup and retrofit into existing pilots • Cheap	• No information on the liquid vapor interface and surface wetting	Wetting: partial / complete wetting at global scale
Volumetric	Mass balance	• In situ • Needs no specialized equipment	• Sensitive • Needs pre-calibrated curve to interpret wetting	Wetting: surface / partial wetting at global scale

Method	Principle	Advantage	Limitation	Information obtained
		• Wetting can be studied at operating conditions	• Membrane movement inside the cell may affect the reading • Need skilled operator	
MD - electrochemical cell	Measuring electric current	• In situ • Potential expanded to large scale plants	• Fabricating and maintaining electrically conductive layer • Mass transfer resistance due to the conductive layer	Wetting: partial pore wetting
Electrochemical impedance spectroscopy	Impedance	• In situ • Potential expanded to large scale plants	• Maybe be only useful in DCMD where 2 interfaces are in contact to the membrane surface	Wetting: partial pore wetting and total wetting at global scale
Thermal conductivity detector	Thermal conductivity	• In situ • Used in membrane contactors	• Maybe be only useful in SGMD and VMD applications • Emerging method with proof of concept for MD still to be developed	Wetting: partial pore wetting

1.9. De-wetting and regeneration

The next step if the membrane is wet during MD operation is to remove the feed liquid with solutes trapped in the pores and potentially utilize the membrane again. At present, little attention has been given to de-wetting and regeneration strategies for membranes after they get wet. The documented literature presents studies done on DCMD and VMD configurations only [9,118,124,157–161]. Different de-wetting strategies like solvent evaporation, oven drying, vacuum drying, water rinsing and drying, 5 wt.% HCl solution followed by drying, microwave irradiation, inverting membranes, intermittent operation with drying out and pressurized air backwashing are being proposed in literature with varying degree of effectiveness.

Table 1.9: De-wetting strategies after membranes wetting occurred and wetting regeneration potential

Strategy	Config	Material / Membrane / Type	Wetting regeneration			Ref.
			No	Partial	Full	
Solvent evaporation	VMD	PVDF /Durapore GVPH / FS	x	x	●	[159]
	DCMD	MD 020 CP 2N / HF	x	x	●	
Oven drying	VMD	PVDF / Durapore GVPH / FS	x	x	●	
	TDCMD	MD 020 CP 2N / HF	●	●	x	
Vacuum drying	VMD	PVDF/ Durapore GVPH / FS	x	x	●	
	DCMD	MD 020 CP 2N / HF	●	x	x	
Water rinsing and drying	DCMD	PP / Accurel PP S6/2, Akzo Nobel /HF	●	●	x	[158]
	DCMD	PVDF / (Memtek), PVDF/PTFE (fabricated)/ HF	x	●	x	[124]
5 wt.% HCl solution followed by drying	DCMD	PP / Accurel PP S6/2, Membrana/HF	x	x	●	[118]
Microwave irradiation	VMD	PP /HF	x	●	●	[160]
Inverting membranes	DCMD	PP, PTFE / HF and FS (Several manufacturers)	x	●	x	[157]
Intermittent operation with drying out	AGMD	PTFE / FS	●	x	x	[9]
Pressurize air backwashing	-	PVDF / Millipore Immobilon-PSQ / FS	x	●	x	[161]

Note: FS (Flat sheet), HF (Hollow fiber), ● observed, x not observed

To assess the effect of the different regeneration techniques researchers [159] conducted tests on both hollow fibers and flat sheet membranes using drying with/without solvent and vacuum drying. A summary of the observations are tabulated in **Table 1.9,** and procedure is documented in their paper [159]. It was concluded that solvent evaporation in an oven is an effective method for hollow fiber membranes if soaked in ethanol before evaporation and this technique was not effective using vacuum

drying. While for the flat sheet membranes regeneration using elevated temperature, with and without soaking in solvent and vacuum drying was effective. Alternatively, rinsing membranes with fresh distilled water, later purging with air and subsequent drying was conducted[158] and [124]. In both cases, it was concluded that partial to no regeneration occurred since the salts present in the pores causes a rapid rewetting during the following hours of operation. Gryta [118], used five wt.% HCl solution followed by drying and it was found successful for membrane re-generation. While another study suggested using microwave irradiation as a quick way of recovering wetted membranes in VMD but did not provide any proof of concept [160].

In general, for lab scale modules it is recommended to open the membrane module and dry out the samples at elevated temperatures with or without rinsing with water and solvents like ethanol. However, there are exciting opportunities in de-wetting and regeneration strategies. As increasingly research proves the utility of membrane distillation for different applications. Active research needs to focus on effective de-wetting strategies for pilot and full-scale plants. Without the potential to re-generate membranes this technology will not be adopted at commercial scale. With a lack of focus on this aspect of research, some researchers have taken the other direction and have started to test discarded MD membranes as microfiltration membranes [162].

1.10. Conclusions and perspectives

In English

Today the risk of wetting occurrence is one of the significant limitations for the industrial development of membrane distillation in various areas, even if the potentiality of MD is very high for process intensification and better use of energy by coupling with renewable or lost energy sources. However, in literature, a mix-up occurs between wetting, wettability and the word "wetting" is often used more like an assumption than with real proofs of evidence and with a qualification of the wetting mechanism. This is making it difficult to draw reliable and valid conclusions on the impact of process operating conditions and or membrane characteristics on wetting and its mechanisms. On the other side the number of studies directed towards pore wetting, or even reporting it, is low but increasing rapidly.

It was essential to define correctly and distinguish the concepts of wettability (risk of wetting occurrence) and wetting (real occurrence during process operation) and to develop a common terminology for wetting mechanisms that could be used by the scientific community. It is also vital to evaluate wetting in MD with proper tools to detect it at both global and local scale. A unified approach

of wetting determination is required, for a better understanding of wetting and of the parameters that can influence it.

This chapter attempted to define pore wetting and distinguish it from wettability, with also an additional effort to categorize different wetting mechanisms at the pore scale. It also reports on the conventional or emerging methods for evaluating wetting and wettability, in the hope that this would help future studies to reconsider the influence of various parameters on the basis of both a unified definition of wetting and an appropriate method to detect and quantify wetting.

At present wettability in commonly evaluated by LEP and CA, while wetting is detected by conductivity measurement. It should also be noted here that at present CA and LEP_w are generally measured at standard temperature and with ultra-pure water. However, the wetting potential of a membrane depends on the fluid properties (e.g., surface tension) in contact with the surface. Thus, reporting CA and LEPw with ultra-pure water (@ 20°C) does not directly benefit the studied MD process. CA and LEPw need to be measured at the intended operating temperature with the initial and final feed solution. This may help in revealing the actual interaction of feed and the intrinsic membrane properties for better operation and wetting prevention. Though these techniques are simple and commonly used they reveal little information on the reality of wetting that can occur during process operation, and which will depend on feed properties, process operating conditions, and membrane properties.

Nevertheless, some emerging techniques appear that could help to develop new knowledge on wetting and on the parameters that influence it. The DDTI method is an *ex-situ* method and requires destruction of membrane samples, but it is very informative and, with the help of 2 indicators it allows both to qualify the wetting mechanisms at a local scale, and to quantify total and partial wetting (intrusion of liquid in pores). In-situ techniques like volumetric measurement, electrochemical cell and impedance can potentially reveal much more information than the commonly used methods.

Overall these emerging techniques (both *ex-situ* and *in-situ*) have their advantages but also show some limitations. The SEM/EDX technique can be informative but needs further development to interpret wetting. The development of a methodology based on SEM/EDX technique is explored in **Chapter 2** and the methodology's capacity to understand the influence on operational parameters in membrane distillation is explored in **Chapter 3**. As the state of the *in-situ* art techniques detects only evidence of total wetting at the global scale on the whole membrane, there is still an acute need to develop an *in-situ* technique that could be more informative on the wetting mechanisms, and that could allow to exploring wetting at local scale during operation. This application of such a tool could be a powerful

for better characterization and evaluation of wetting and the development of effective wetting mitigation strategies. Due to this need, the development of an *in-situ* technique for wetting visualization is explored in **Chapter 4.**

En Français

Aujourd'hui, le risque de mouillage est l'une des principales limites du développement industriel de la distillation membranaire dans différents domaines, même si son intérêt est avéré pour l'intensification des procédés et une meilleure utilisation de l'énergie en couplant des sources d'énergie renouvelables ou perdues. Cependant, dans la littérature, une confusion se produit entre mouillage et mouillabilité, et le mot « mouillage » est souvent utilisé davantage comme une hypothèse que comme une preuve concrète et une qualification du mécanisme de mouillage. Cela rend difficile de tirer des conclusions fiables et valables sur l'impact des conditions de fonctionnement du procédé et / ou des caractéristiques de la membrane sur le mouillage et ses mécanismes. Par ailleurs, le nombre d'études orientées vers le mouillage, ou juste sa mention, est faible mais augmente rapidement.

À notre avis, il est très important de définir correctement et de distinguer les concepts de mouillabilité (risque de mouillage) et de mouillage (occurrence réelle au cours du processus) et de développer une terminologie commune pour les mécanismes de mouillage pouvant être utilisée par la communauté scientifique. Il est également essentiel d'évaluer le mouillage en DM avec de bons outils pour le détecter à l'échelle globale et locale. Une approche unifiée de la caractérisation du mouillage est nécessaire pour une meilleure compréhension de ses mécanismes et des paramètres qui peuvent l'influencer.

Ainsi, cette revue a tenté de définir le mouillage des pores et de le distinguer de la mouillabilité, avec un effort pour classer les différents mécanismes de mouillage à l'échelle des pores. Elle présente également les méthodes courantes ou émergentes d'évaluation du mouillage et de la mouillabilité, dans l'espoir que cela pourrait aider les futures études à reconsidérer l'influence de divers paramètres sur la base d'une définition unifiée du mouillage et d'une méthode appropriée pour détecter et quantifier le mouillage.

Actuellement, la mouillabilité est couramment évaluée par le LEP et le CA, tandis que le mouillage est détecté par une mesure de conductivité. Il convient également de noter qu'à l'heure actuelle, CA et LEPw sont généralement mesurés à température standard et avec de l'eau ultra pure. Cependant, le potentiel de mouillage d'une membrane dépend des propriétés du fluide (par exemple la tension superficielle) en contact avec la surface. Ainsi, la mesure de CA et LEPw avec de l'eau ultra pure (à 20

° C) ne correspond pas directement au processus de DM étudié. CA et LEPw devraient être mesurés à la température de fonctionnement prévue, et avec la solution d'alimentation étudiée, en début et fin de process. Cela pourrait aider à révéler l'interaction réelle entre l'alimentation et les propriétés intrinsèques de la membrane pour un meilleur fonctionnement et une meilleure prévention du mouillage.

Bien que ces techniques soient simples et couramment utilisées, elles fournissent peu d'informations sur la réalité du mouillage qui se produira pendant le fonctionnement du procédé et qui dépendra des propriétés de l'alimentation, des conditions de fonctionnement du procédé et des propriétés de la membrane.

Cependant, certaines techniques émergentes pourraient aider à développer de nouvelles connaissances sur le mouillage et sur les paramètres qui l'influencent. La méthode DDTI est une méthode *ex-situ* et nécessite une destruction des échantillons de membrane, mais elle est très informative et, à l'aide de 2 indicateurs, elle permet à la fois de qualifier les mécanismes de mouillage à l'échelle locale et de quantifier le mouillage total et partiel (intrusion de liquide dans les pores). Les techniques in situ telles que la mesure volumétrique, la cellule électrochimique et l'impédance peuvent potentiellement révéler beaucoup plus d'informations que les méthodes couramment utilisées.

Dans l'ensemble, ces techniques émergentes (à la fois *ex-situ* et in situ) ont leurs propres avantages mais présentent également certaines limites. La technique SEM/EDX peut être informative mais nécessite un développement supplémentaire pour interpréter le mouillage. Le **Chapitre 2** explore le développement d'une méthodologie basée sur la technique SEM / EDX et le **Chapitre 3** sur la capacité de la méthodologie à comprendre l'influence sur les paramètres opérationnels de la distillation membranaire. L'état de la technique *in-situ* ne détecte que les signes de mouillage total à l'échelle globale sur toute la membrane. Il existe toujours un besoin urgent de développer une technique in situ qui pourrait être plus informative sur les mécanismes de mouillage, et qui pourrait permettre d'explorer le mouillage à l'échelle locale pendant le fonctionnement. Cela pourrait constituer un outil puissant pour mieux caractériser et évaluer le mouillage et pour élaborer des stratégies efficaces d'atténuation du mouillage. En raison de ce besoin, le développement d'une technique in situ de visualisation par mouillage est présenté au **Chapitre 4.**

Acknowledgments

I would like to thank ANR (The French National Research Agency) Programme: Innovation technologique pour analyser, remédier ou réduire les risques environnementaux (DS0102) 2014 for funding Project WETMEM. (ANR-14-CE04-0008

Preface to Chapter 2

As presented in the organizational flowchart below, the overall goal of the thesis was to deepen the knowledge on wetting in membrane distillation. **Chapter 1** revealed wetting is primarily defined and interpreted by liquid entry pressure and an effort was made to re-interpreted and re-defined wetting as a phenomenon that occurs at the pore scale. Evidently, there was a lack in suitable technique to visualize and characterize wetting mechanisms at the pore scale. Therefore **Chapter 2** is dedicated to developing new methodologies and indicators using an ex-situ tool for visualizing, characterize and interpret wetting at pore scale in membrane distillation. The developed ex-situ tool and methodology will further be used in **Chapter 3** to understand the effects of operating conditions on wetting.

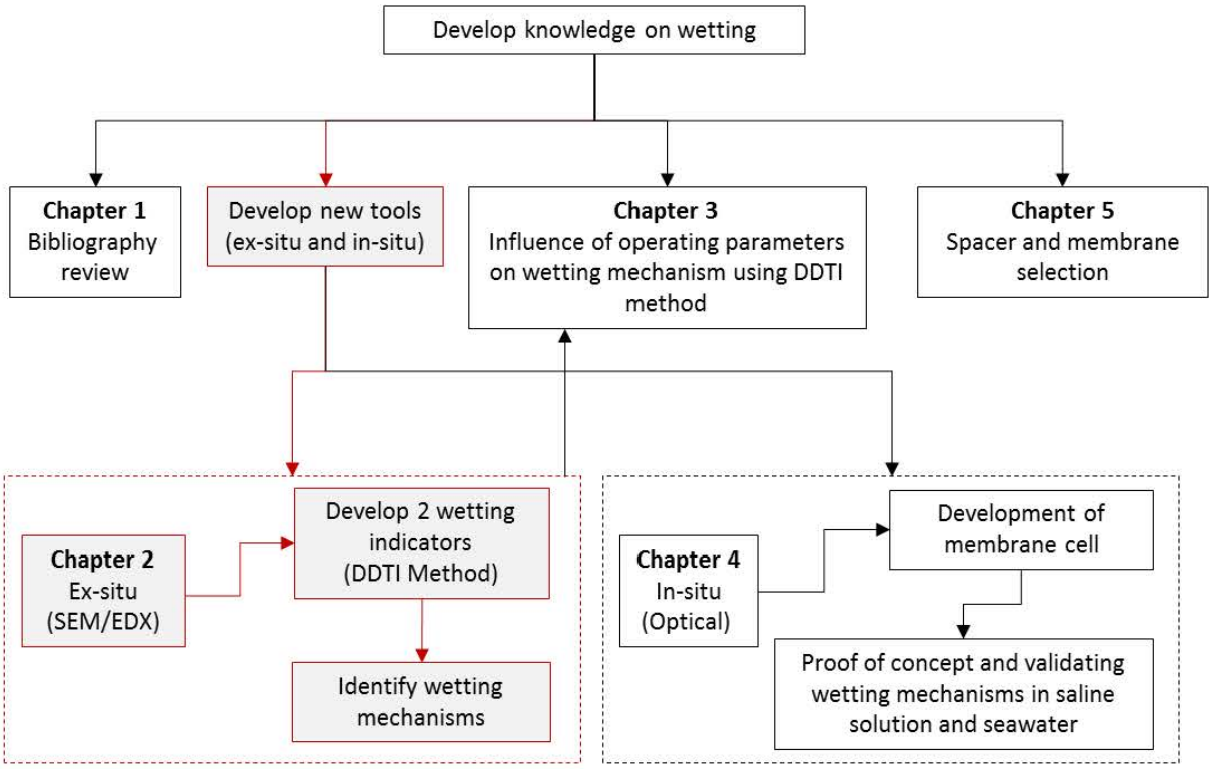

Chapter 2 : Visualizing and evaluating wetting in membrane distillation: New methodology and indicators based on Detection of Dissolved Tracer Intrusion (DDTI)

Summary of objective (in English)

The risk of membrane wetting is often considered as a setback to the development of membrane distillation (MD). Liquid entry pressure (LEP_w) is the main wettability indicator but it only gives information on the first event of total liquid intrusion in the biggest pore. To better understand wetting mechanisms at the pore scale, a dedicated experimental methodology is required. This chapter is aimed to develop and validate a methodology to locally characterize the occurrence of two possible forms of wetting in membrane distillation: partial pore wetting and total pore wetting. The principle of the developed method was based on the *ex-situ* detection of a tracer (salt) intrusion by SEM-EDX, after operation of the membranes in vacuum membrane distillation (VMD) using a saline solution.

Résumé de l'objectif (en français)

Le risque de mouillage de la membrane est souvent considéré comme un verrou pour le développement de la distillation membranaire (MD). La pression d'entrée de liquide (LEP) est le principal indicateur de mouillabilité, mais il ne donne que des informations sur le premier événement d'intrusion totale de liquide dans le plus grand pore. Pour mieux comprendre les mécanismes de mouillage à l'échelle des pores, une méthodologie expérimentale dédiée est nécessaire. Ce chapitre vise à développer et à valider une méthodologie permettant de caractériser localement l'apparition de deux formes possibles de mouillage en distillation membranaire : le mouillage partiel des pores et le mouillage total des pores. Le principe de la méthode développée repose sur la détection ex situ d'une intrusion de traceur (sel) par SEM-EDX, après utilisation des membranes en distillation membranaire sous vide (VMD) à l'aide d'une solution saline.

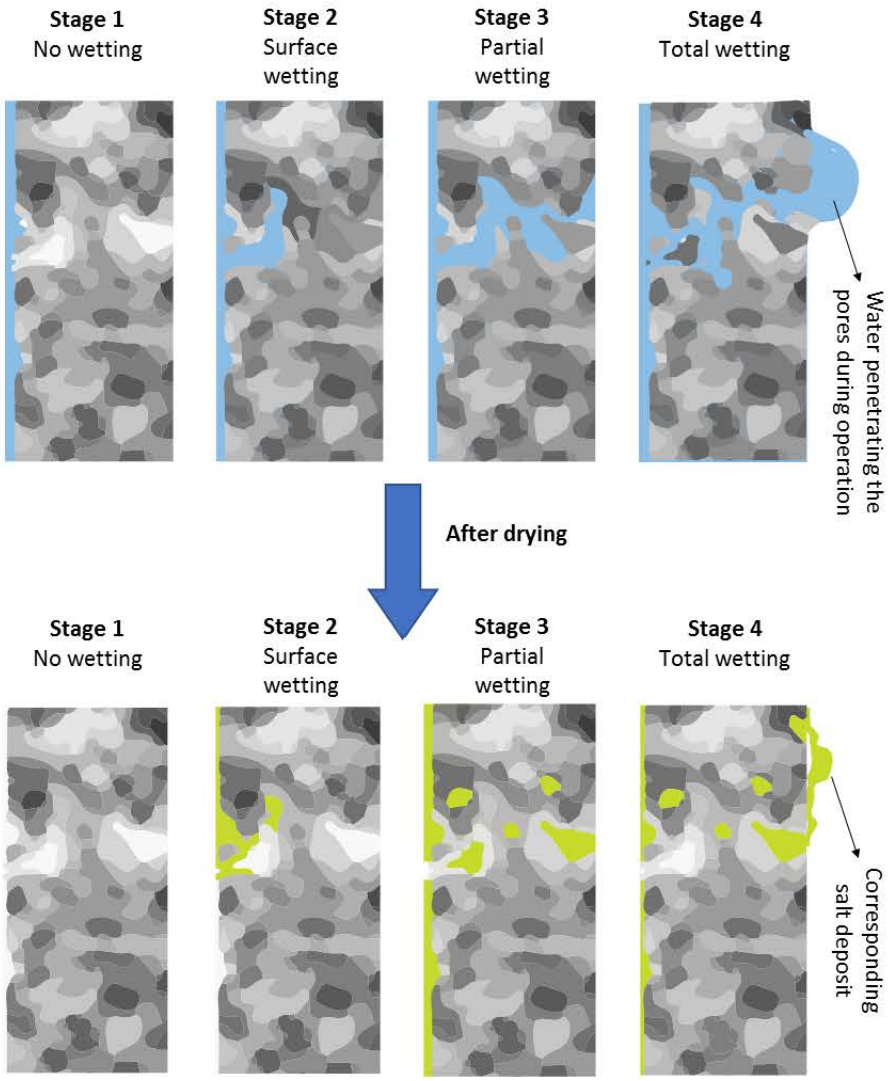

Graphical abstract

2.1. Introduction

2.1.1. Context and issues of MD in desalination

Confronted with growing world population, water shortage, diminishing freshwater resources, degradation of the quality of freshwaters and of climate change, the capacity to provide people with drinking water and good quality water is a key issue for the 21st century. Today, seawater desalination appears as a major alternative to produce drinking water in many countries, and in some areas, desalination is no longer a marginal or supplemental water resource but can be the major resource for both domestic and industrial supplies [163]. Based on lab-scale and more recently semi-industrial scale experiments, membrane distillation (MD) has been demonstrated as an interesting alternative for brackish or seawater desalination [7,164]. MD was developed by Findley in the 1960's [19]. It involves the evaporation of water through the pores of a hydrophobic macroporous membrane [21]. The

driving force is the vapor pressure difference between the two sides of the membrane. Operating on the principle of separation via phase equilibria, the hydrophobic membrane supports a liquid/vapor interface, which is supposed to be located at the membrane pore inlet. The membrane merely acts as a physical barrier between the two phases and has no influence on the process selectivity. However as it enhances the contact area for vaporization, this process is called a membrane contactor and is considered as a way for process intensification [6,22,32,33,165,166].

The interest of MD for seawater desalination was established in the last decade. It is largely linked to the facts that MD can theoretically retain all non-volatiles and that the quality of the treated water does not depend on the quality of the saline water resource, that can be seawater or a highly salted concentrate from RO or geothermal [11] desalination plants. With a possibility to increase water recovery and to reduce the volume of reverse osmosis brines [4] and the opportunity to couple the process with low grade heat from industrial waste heat [8,9], solar[10] or potentially even geothermal energy[11], MD is currently being viewed as a potential 3rd generation desalination technology for our future needs.

In this context, developing membranes, industrial-scale modules and adequate process for a sustainable long-term operation of MD for desalination are great issues and there is a large potential market for this technology.

2.1.2. Problematics of wetting in membrane distillation

With the sudden boom and relatively high potential application of this technology, many water companies and researchers are interested in using existing hydrophobic membranes for various MD applications. To further MD into full-scale commercial application, one of the major challenges it faces is for the membrane to remain dry during the process. A possible brake to the development of MD is thus related to the major potential risk of dysfunction of MD, which is currently expressed as "membrane pore wetting". Indeed, in the process, the required water quality will be only obtained if the mass transfer through the pores only occurs by diffusion of the vapor that is formed at the pore inlet. Alternatively, permeate quality is compromised if some liquid is transferred by convection through some pores, which could be the case if some pores are wetted by the feed or by the concentrate. Pore wetting during operation is still considered as a major risk of dysfunction by potential end-users. The process efficiency and its long-term feasibility might be clearly dependent on the properties of the membrane used as a support for the liquid/vapor interface. However, some of the factors that influence pore wetting are identified such as pore size distribution, membrane hydrophobicity, operating pressure, quality of the feed water [21], their quantitative effects are not

well known and cannot be predicted. Moreover, the reality of wetting occurrence during MD operation is rarely reported and documented.

Wetting and the parameters that might influence wetting are not completely understood, even if many attempts have been made both by manufacturing membranes designed for MD [167,168] and controlling/adding/changing operating parameters [102,103,160,169]. Different forms of wetting mechanisms have been proposed by Gryta [68] for direct contact membrane distillation. It was suggested that, under any given operating conditions, a membrane could be subjected to four forms of wetting: non-wetted pores, surface wetted, partially- wetted and wetted pores (See **Figure 2.1**).

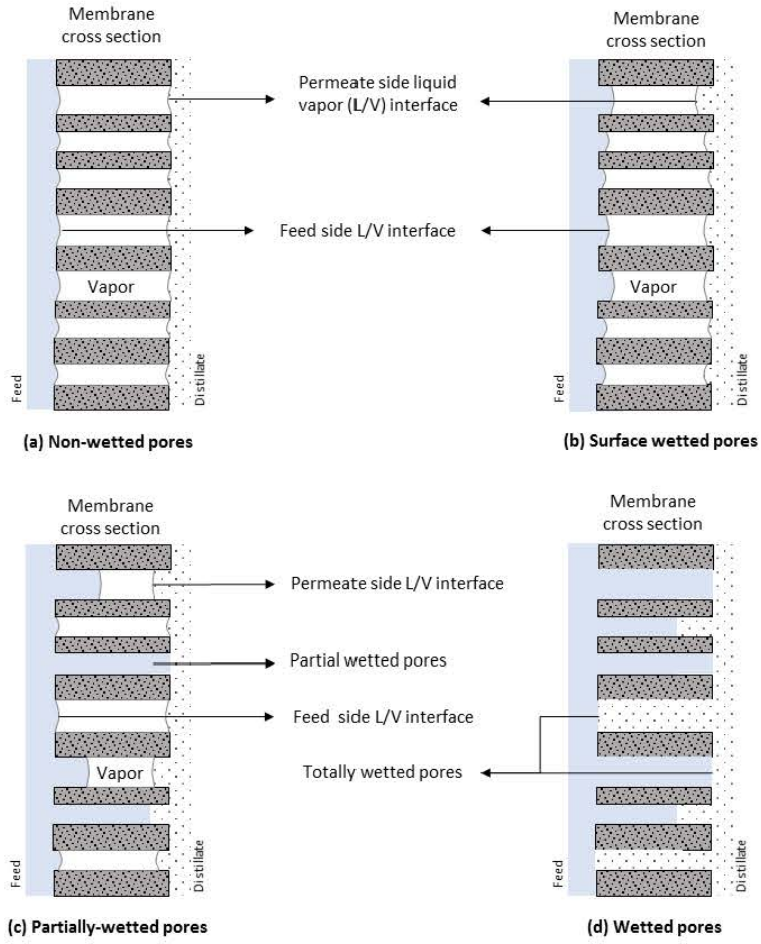

Figure 2.1: Schematic representation of various forms of membrane wettability in DCMD process: (a) non-wetted pores; (b) surface-wetted pores; (c) partial-wetted pores; and (d) wetted pores (adapted and redrawn from [68]) (to be viewed in color)

At the scale of pores, it can be considered that the mechanisms proposed correspond to:

a) Non-wetted pores

b) Sub-surface liquid intrusion in most pores
c) Total intrusion of liquid (passage of water through the total pore length) in some pores and partial intrusion in the others
d) Total liquid intrusion in all pores

Liquid entry pressure (LEP_w) is the method currently being used by both researchers and membrane manufacturers as a tool to identify the potential of membrane wetting. It is also one of the major criteria to select membranes to be used for membrane distillation. Liquid entry pressure (LEP_w) or "Wetting pressure" was defined in 1989 [24], as the pressure that must be applied onto pure water ($_w$) before a drop of water is observed in the permeate of a dry membrane, which means that the water has completely passed in the biggest pore (r_{max}). LEP_w is thus obtained after complete water intrusion (total wetting) in this pore. According to Franken model, LEP_w can be calculated using Eq. 2.1 :

$$LEP_w = \frac{-2B\gamma\cos\Theta}{r_{max}} \qquad \text{Eq. 2.1}$$

Where; Θ is the contact angle (CA) between the wetting liquid and the hydrophobic membrane, r_{max} (m) is the maximum pore radius, B is a pore geometry factor and Υ represents the surface tension of water.

Even though LEP is an indication of membrane wettability but, by definition, it does only provide information on the first event of total liquid intrusion in the biggest pore, and not on wetting relative to the other wetting mechanisms. Thus, there is an acute need to better understand wetting and to identify various forms of wetting such as surface wetting or partial wetting and more generally liquid intrusion in MD membrane pores. This requires an experimental methodology to obtain information on liquid intrusion during membrane distillation operation.

2.1.3. Concept of the new methodology and objectives of the study

The concept of the methodology is based on the following principle: if liquid passes the pores and if it contains tracers (salts) it would be possible by SEM-EDX to find traces of salts on membrane surface on the permeate side, if total liquid wetting, or inside pores for partial wetting.

Indeed, ideally in MD, water molecules in the feed side pass through the hydrophobic membrane towards the permeate side in vapor phase only whereas the non-volatile tracer (salt) would not be vaporized. This leads to a concentration of tracer at the L/V interface. In case complete penetration of the liquid occurs inside the pores, after drying, some traces of the salt may be found both inside the membrane pores and on the permeate side of the membrane surface. If the liquid/vapor interface is

located on the feed side (as proposed in the standard definition of membrane distillation [170]), the tracers (salts) should not penetrate inside the membrane under normal operating conditions and no trace of salt may be found. But on the other hand, if the interface moves from the feed side of the membrane surface and totally passes through some pores, there could be noticeable salt traces on the permeate side of the membrane. It would be then possible to detect these traces of salts on the membrane by SEM-EDX. Such observations of salt traces by SEM-EDX have been made after the autopsy of a wetted membrane in DCMD, and traces of salts were attributed to liquid intrusion [68]. Later, the principle of detecting traces of salts by SEM/EDX analysis was proposed for evaluating partial pore wetting in a gas/liquid membrane contactor used for the adsorption of CO_2 [150]. Membranes were operated in gas/liquid absorption using an aqueous NaCl solution as an adsorbent. The NaCl solution circulated in the lumen side and CO_2 flowed on the shell side at a constant flow rate. After a specific period of time membranes were then dried and analyzed by SEM-EDX. Traces of Na and Cl were observed throughout the membrane cross-section and mainly at the pore inlet, which was explained by partial pore wetting. On 4 membrane samples, 3 showed no significant traces of salts and then no wetting occurrence, and for the last membrane, only slight surface wetting was observed on the lumen side. The authors pointed out that the proposed method is still imperfect and could be improved. However, they suggested that it could be a good tool to investigate pore wetting for various membrane contactors.

The concept of our method, dedicated to membrane distillation and named Detection of Dissolved Tracer Intrusion (DDTI), consists in using a saline feed during MD operation and to use SEM-EDX afterward to detect traces of salts, which can constitute an evidence of wetting occurrence. If validated, this method could be used to compare and qualify some membranes or in studies for a better understanding of conditions that favor or prevent wetting. The present chapter aims then 1) to explain the DDTI methodology that was developed based on this principle, 2) to test it for standard conditions of VMD on MD membranes, 3) to define new wetting indicators that could be obtained from the developed experimental methodology. As a preliminary step of the study it was necessary to produce a proof of concept, that is to say, to validate the principle of the DDTI method, to show that pore wetting can be detected for a large range of operating conditions and to check which wetting mechanism can be identified.

2.2. Material and methods

2.2.1. General principal of the DDTI methodology and description of the key steps

The method that is proposed here to systematically assess wetting is based on the following principle: the membrane is first characterized for its properties and later used for MD with a solution containing

a tracer (saline solution). After sample preparation, the membrane is subjected to different wetting or wettability characterization methods (respectively SEM/EDX and LEP) for comparison. A generalized protocol is proposed and presented in **Figure 2.2.**

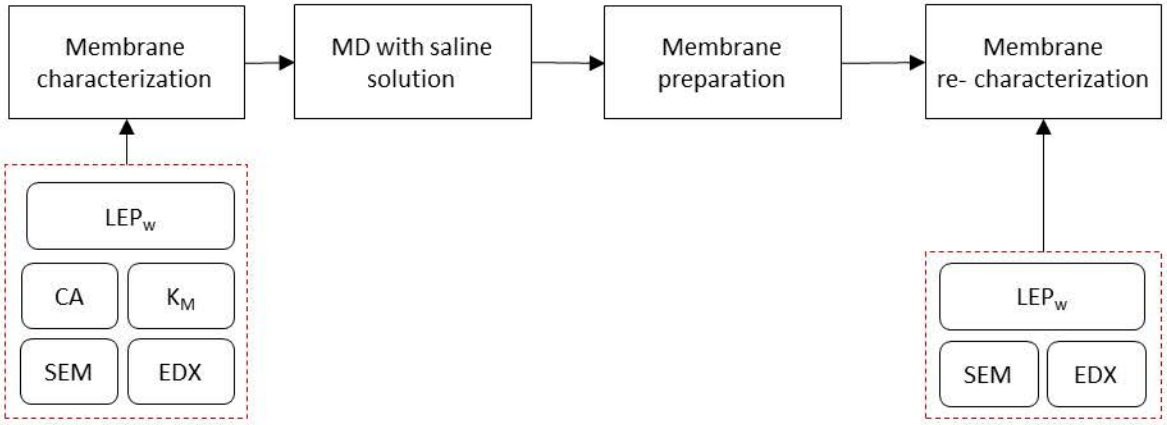

Figure 2.2: General protocol of the DDTI method

In this chapter, to develop the methodology, different choices have been made. Tracer solutions with NaCl salt as a tracer (choice explained in **Section 2.5**) at different concentrations (22 - 310 g/L) were used. The MD configuration used was Vacuum Membrane Distillation (VMD) in cross-flow mode (Reynolds = 2191) at 42.5°C. Vacuum pressure was maintained at 60 mbar until constant permeate mass was collected (225 g). Durapore (PVDF) membranes of 0.22 µm (nominal pore size) were used in this study. These membranes were first characterized for their properties **(Section 2.2.4**).

The developed method is not limited by the above mentioned operating conditions, membrane or configuration. DDTI using NaCl for VMD is presented here as a case study. In the future, tracer and parameters can be modified, depending on the intended application and MD process. The criteria for the choice of the tracer also include the feasibility of its detection by SEM/EDX.

2.2.2. Vacuum membrane distillation (VMD) pilot plant

The description of the VMD pilot plant used in this study is presented in **Figure 5.2**. A prepared saline feed of (4L) was fed into the jacketed feed tank (R1), which was heated by a hot water bath. R1 was stirred at 350 rpm with a magnetic stirrer so that the salts do not precipitate in the tank until the desired temperature was reached. The feed was pre-heated in a heat exchanger (E1) and fed in cross flow to the MD module using a magnetic pump at a flow rate that could be controlled to a cross flow velocity of 1.77 m/s on the membrane surface; in the range of Re 2191. The rectangular flat sheet membrane module is made of two polypropylene blocks of 20 mm thickness secured by two 10 mm thick stainless-steel plates. The internal feed side channel dimensions were 87.6 x 47.5 x 0.5 mm

(length x width x depth) with an edge radius of 8 mm. The membrane (M1) enclosure had an active surface area of 4.16 10^{-3} m^2 (See Supplementary Data Figure C2.1). On the permeate side, the required vacuum pressure was achieved using a vacuum pump (Vacuubrand (1000 - 3 mbar)) and set by an inline vacuum sensor. The vacuum pipe was heated to prevent the vapor from condensing inside the vacuum pipeline and the measurement of vapor flow rate could be as much representative. Finally, a cold trap was used after the vacuum pump to condense the permeate using a cold-water bath regulated at -4°C.

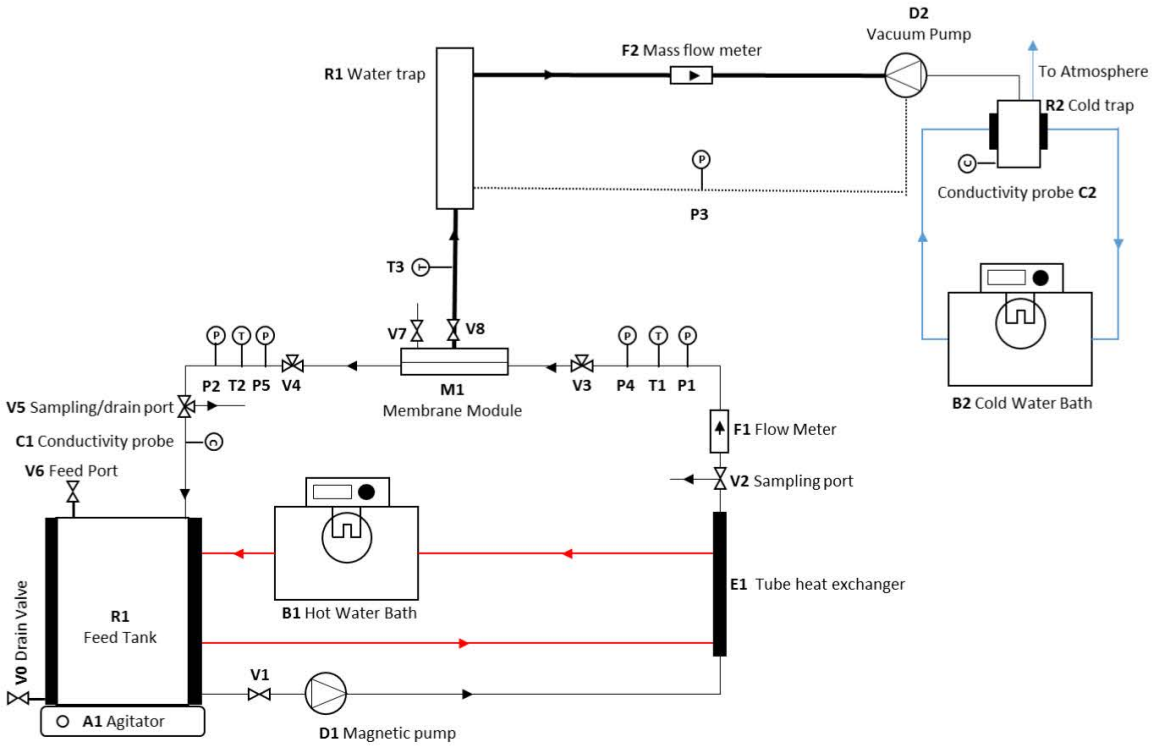

Figure 2.3: Schematic of vacuum membrane distillation setup (to be viewed in color)

A variable area flow meter (0-250 L/h) (F1) allowed to measure the inlet liquid feed flow rate. A mass flow meter, F2, (Bronkhorst, 0-60 g/h) was used to determine the permeate flow rate. Water trap (R1) were used to protect the mass flow meter and vacuum sensor in case the membrane breaks, and water directly leaks into the vacuum pipeline. Pt type temperature sensors and pressure sensors allowed to measure module inlet (T1, P1) and outlet (T2, P2) parameters and permeate (T3, P3) properties. All sensors were calibrated before using and connected to a computer for data logging. Feed and concentrate samples were taken from sampling ports (V2 and V5).

2.2.3. Liquid entry pressure measurement

LEP_w was measured both on virgin and used membranes to evaluate the effect of operating parameters on this indicator. LEP_w measurements were performed using ultra-pure water at 20°C. The

experimental protocol to obtain the LEP_w is based on the observation of the first drop of permeate during a pressure step filtration operation. A 50-mL Amicon filtration stirred cell with a membrane secured inside an O-ring was firstly filled with ultrapure water using a pressure vessel. Then a pressure of 0.1 bar was applied using filtrated pressurized air (5 µm) and maintained for 10 minutes. Later the pressure was increased every 10 minutes with a step of 0.1 bar and the permeate line was constantly observed (visually) for the first drop of liquid inside the tube. The corresponding pressure value was noted as LEP_w. This test was repeated 3 times and the averaged value reported for both virgin and used membranes. If a leak in the stirred cell was detected the experiments were repeated.

2.2.4. Characteristics of the MD membrane

Durapore (0.22 µm PVDF) membranes were used in this study. These membranes have been extensively studied and characterized by several researchers under various membrane distillation configurations [171,172]. They are manufactured using phase inversion technique [173]. Following are the membrane characteristics measured in this study: thickness (by SEM), contact angle, porosity, Surface free energy (SFE), LEP_w and Knudsen permeability coefficient (K_M).

Contact angle (CA) and surface free energy (SFE) measurements were performed both on virgin and used membranes using Drop Shape Analyzer – DSA25 (Kruss) and the results post-processed in accompanying software (ADVANCE). For the experiment protocol, guidelines from Drelich were considered for reproducible results [174]. CA was measured using a drop of 28-35 µl deionized water at 20°C while SFE was assessed using deionized water and di-iodomethane solutions. Ellipse (Tangent-1) fitting method and OWRK model was used for determining CA and SFE respectively. Each sample was analyzed 6-8 times over the feed side membrane surface. Membrane porosity was determined gravimetrically according to the protocol described by Nejati et al [175]. Membrane permeability was measured based on the protocols outlined by Dao et al [172]. The Knudsen permeability, K_M was calculated using Eq. 2.2 and Eq. 2.3.

$$J_{H_2O} = k_k * \Delta P_{H_2O} = k_k * (P_m^* - P_p) \qquad \text{Eq. 2.2}$$

Where, J_{H2O} is the permeate flux, k_k is mass transfer coefficient of the membrane, ΔP_{H2O} is difference in partial pressure of water on both sides of the membrane, P_m^* is vapour pressure of pure water at the membrane's conditions; P_p is partial pressure of water in the permeate side (equal to vacuum pressure as the permeate is only composed of water).

$$k_k = \frac{2}{3}\frac{\varepsilon \cdot r}{\chi \delta R T_m}\sqrt{\frac{8RT_m}{\pi M_{H_2O}}} = \frac{K_M}{\sqrt{M_{H_2O}}} \qquad \text{Eq. 2.3}$$

Where ε is porosity of the membrane; r is radius of the pores; χ is tortuosity factor; δ is thickness of the membrane; R is ideal gas constant; M_{H2O} is molar mass of water, K_M is Knudsen permeability and T_m is temperature at the membrane surface. To facilitate comparison, all reported Knudsen permeability are expressed at the same reference temperature T_{ref} = 20 °C [7].

Permeability measurements for the membrane were performed in MD mode using the VMD pilot plant. Deionized water (0.8 µs/cm) at 35°C was used in laminar flow regime with successively varying the vacuum pressure (ΔP_{H2O}) between 3.5 and 5 kPa. The value obtained for K_M at 20 °C is 3.07E-06 $mol^{1/2}.m^{-1}Kg^{-1/2}$.

Table 2.1: Properties of the virgin reference membrane (Durapore, GVHP29325 by Millipore)

Material	K_M ($mol^{1/2}.m^{-1}Kg^{-1/2}$)	R_{avg}, (µm)	Rmin (µm)	Rmax (µm)	Porosity ε (MG) (%)	Thickness δ (µm)	Contact angle Θ (°)	SFE (mN/m)	LEP_w (kPa)	Ref
PVDF	3.07 x 10^{-6}	-	-	-	75.1	114.4 ± 0.9	117±3	11.55 ± 3.80	205 ± 8.66	This study
	3.45 x 10^{-6}	0.22	0.2	0.35	71.3 / 32.74*	117.7	-	-	204	[6,53,172]

*Note: *Surface porosity*

Table 3.1 presents the virgin membrane characteristics for both observed in this study and in literature. Based on this **Table**, it is noticeable that the value of LEP_w obtained in this study is very close to the one reported in the literature. In the same way the K_m value in this study is in good accuracy globally to studies and reviews conducted by others [172].

2.2.5. Tracer solutions

To develop a wetting detection methodology using tracer intrusion, the choice was made to use NaCl (as a tracer), as it is a major constituent of seawater and of interest in desalination, small enough to enter the pores by convection and easily detectable by SEM/EDX. Different concentrations (22, 166 and 310 g/L) were used to develop the protocol, with the aim to check which are the more favorable for the wetting detection. The choice of the range of concentration was done to cover the range from brackish water to solutions used in MD crystallizer [158], where wetting has been reported. The saline

solution was prepared using crystalline powder NaCl (Purity grade ≥99 %) diluted in ultra-pure water at different concentrations. For each experiment, 4L of the solution was prepared and pre-heated to the desired temperature before the solution was fed to the vacuum membrane distillation setup. For each concentration (22, 166 and 310 g/L), two different solutions were prepared and tested. A feed solution without salt served as blank. The pH of all solutions was 7.

2.2.6. Sampling strategy

It was decided to collect samples on the studied membrane across the surface starting at the feed inlet 0 – 0.02 m, between 0.03 – 0.06m (just above the vacuum port) and finally on the feed outlet port (0.07– 0.08 m) as presented in Figure 2.4. Sample collection and preparation techniques are illustrated and explained in the following section.

Based on this sampling location, samples were cut using a CO_2 laser (Arketype Jade L6090, Precision: ± 10 µm) at speed: 14, power: 12, to avoid membrane burning during cutting. Depending on the cleaning procedure (see 4.2), membranes were sampled at different locations for SEM/EDX and LEP analysis (see **Figure** *2.4*).

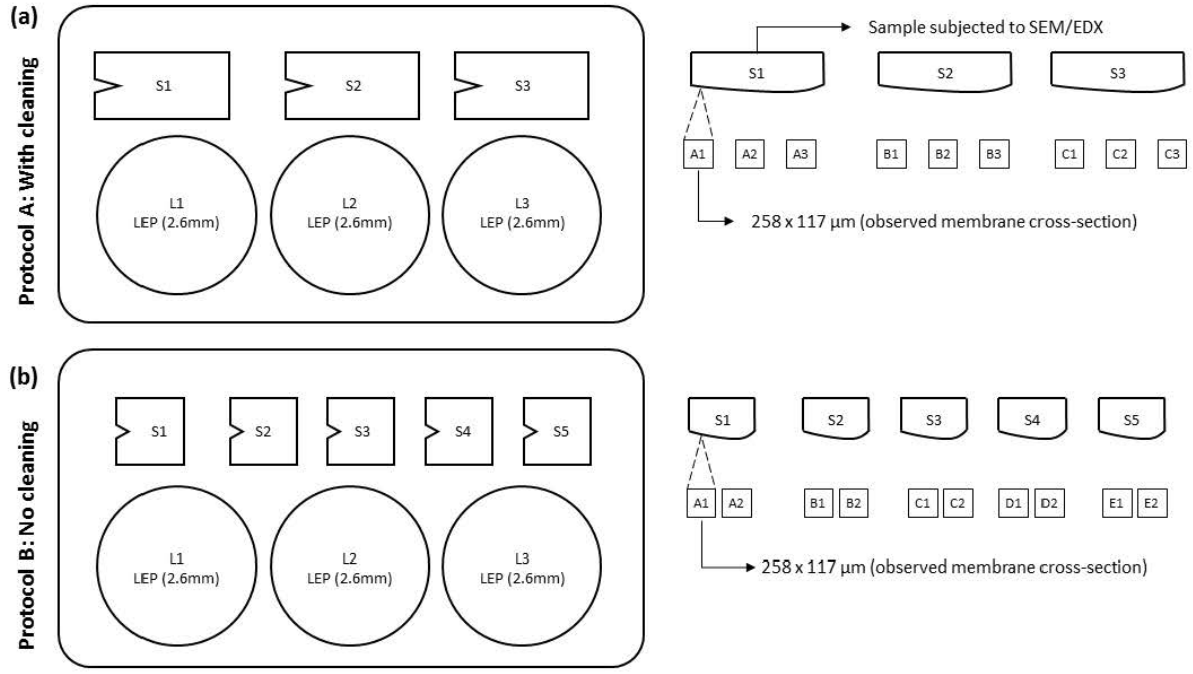

Figure 2.4: Sampling on the membrane surface for (a) after cleaning and (b) without cleaning

For MD experiments followed by cleaning (see **Figure** *2.4* (a)), after each experiment, the membrane was sampled at three locations (S1, S2, and S3) of 2 cm^2 for SEM/EDX analysis and three locations (L1, L2, and L3) for LEP analysis respectively. The prepared samples (S1-3) were further analyzed under

SEM/EDX at three locations on each sample. At each location, 258 x 117 μm (length x cross-section) was visualized. For example, sample S1 of 2 cm^2 was cut from the membrane and prepared for SEM/EDX experiments. On this sample, location A1, A2 and A3 was visualized for wetting detection.

For MD experiments without cleaning (see **Figure 2.4**(b)) greater number of samples was taken in anticipation that more heterogeneity could occur than when cleaning was not performed: five samples (S1, S2, S3, S4, and S5) of 1 cm^2/ membrane were taken for SEM/EDX analysis. Each sample (for e.g. S2) was analyzed at two locations (for e.g. B1 and B2).

In both cases LEP analyses were conducted at 3 locations on the membrane surface with ϕ 2.6 cm at L1, L2 and L3, where, L1 was located at the feed entrance, L2 on the center of the membrane and L3 on the feed outlet.

For SEM/EDX analysis, after the membrane was washed and dried, the samples were cut to its appropriate dimensions and dipped in liquid nitrogen for 5s and broke from the middle using 2 sets of plastic tweezers. The cross-section of one of the broken piece was observed by SEM-EDX after carbonization. Attention should be made to prepare the conductive layer for SEM/EDX using carbon instead of gold.

2.2.7. Detection of tracer by SEM-EDX

Scanning electronic microscope (JEOL, JSM-6400) coupled with X-ray energy-dispersive spectrometry (EDX) (Bruker, XFlash 6130) were used with accompanying software (ESPRIT 1.9) for sample analysis. The high tension of the SEM was 20 KeV and the resolution of the EDX detector was 125 eV with a detector surface area of 30 mm^2. In case of polymer membranes like PVDF and PTFE membranes, carbon and fluorine are ignored for analysis or used just to verify the samples. Typically, the resolution of EDX is 1 μm laterally and about 2 μm in depth. With respect to a 2-D image for each element, the spectral resolution is related to the time constant used when collecting the spectrum. The longer the process time, the better the resolution will be and the narrower the peaks. In this study, samples were exposed for 90 - 120 s.

A generalized protocol for wetting detection using SEM/EDX is described. After acquiring the SEM cross-section of the membrane sample, further EDX analysis was done for elements of interest (in this study; F, Na, Cl, and Fe). Fluorine was used for verifying the sample while sodium and iron micrographs were not used. After the SEM and Cl micrographs are calibrated and converted into 8-bit images in ImageJ. Later these images are merged into composite images. After signal treatment, finally, the gray values for Cl were plotted for permeate surface and the membrane cross-section to detect the trace

of Cl. The Cl traces were used for wetting detection. The gray values (indicated by the pixel brightness from 0 to 255) corresponds to the amount of Cl ion detected through the membrane cross-section. Higher the gray value, greater Cl detected on the cross-section. It should also be noted that before data interpretation proper signal treatment is necessary especially where samples have no salt traces as the signal to noise ratio in these samples can be significantly high. This is due to the small elemental size of Cl (17) and the threshold of the detector. For the flowchart protocol of wetting detection using DDTI method see supplementary data Figure C3.1.

2.3. Results and discussions

2.3.1. Proof of concept of DDTI method

The first step was to obtain a proof of concept for the DDTI methodology, that is to say, to verify that intrusion of salt can be detected in relation with proven wetting occurrence. For that 2 different situations with regards to wetting, were provoked for the same membrane:

- Case A: Total pore wetting was provoked by operating the membrane in a filtration mode at a pressure higher than the LEP. Indeed, in that case, it can be safely assumed that the saline solution should pass through the membrane and traces of salts should be detected by SEM-EDX. This test was performed with a tracer (NaCl solution at 35 g/L).
- Case B: VMD was operated below the LEP but at high tracer concentration (310 g/L) in order to check if any wetting mechanisms were occurring and detectable.

To check the sensitivity of the method a third experiment was performed (Case 0), that consists of a blank with no tracer.

The same membrane was used for all 3 experiments. For cases B, and 0 membranes were operated on the VMD pilot plant (see 2.2) with the following operating conditions: temperature = 42.5°C; Reynolds = 2191 and vacuum pressure = 60 mbar. While for case A, the same membrane was subjected to total pore wetting using LEP equipment (see 2.3). For the 3 cases, after operation (without cleaning the membrane surface), SEM/EDX micrographs were obtained and from these figures, the intensity profile of Cl along the membrane thickness was plotted after a proper signal treatment (**cf. 2.6**). For each case, the SEM micrograph and the intensity profile of Cl obtained is presented in **Figure 2.5.**

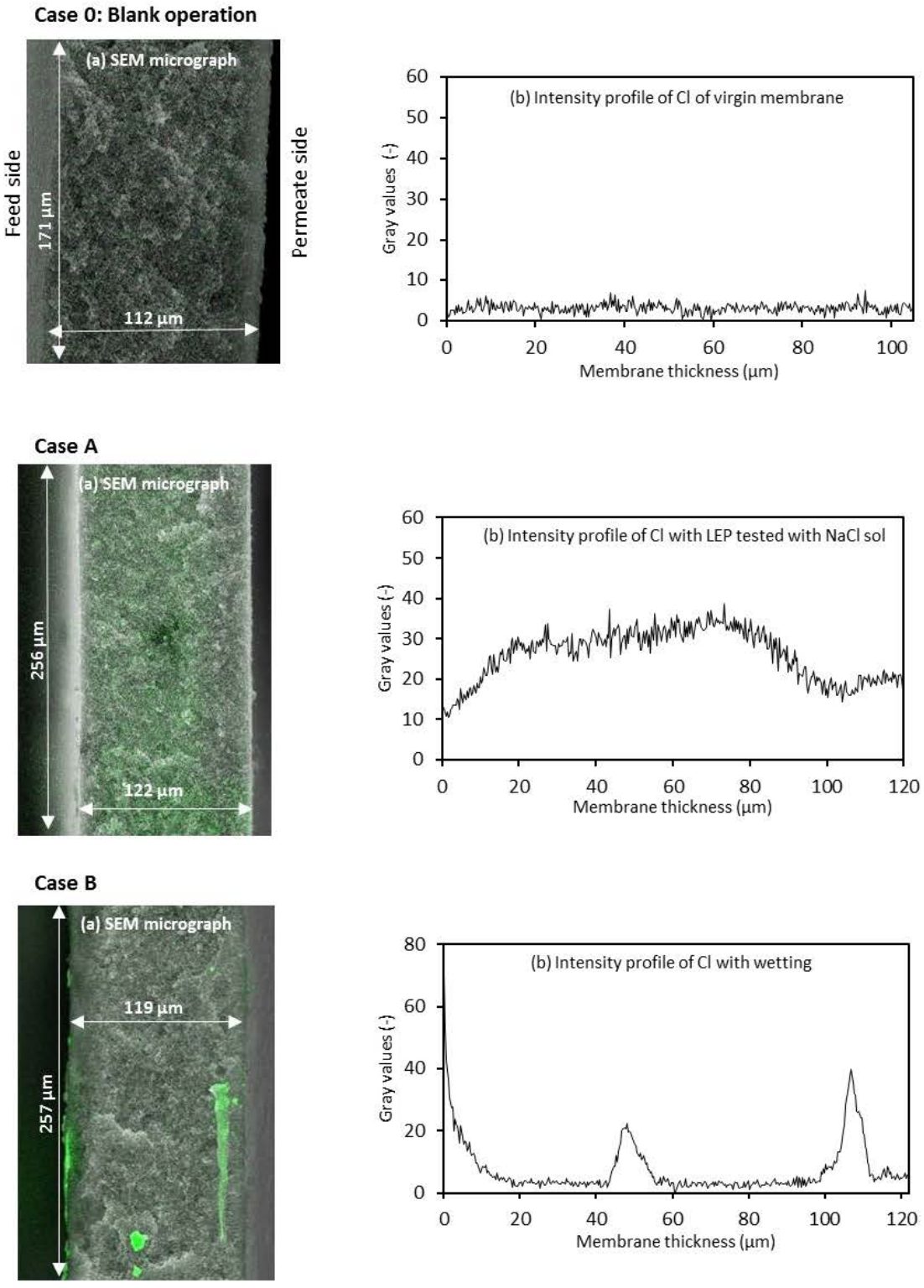

Figure 2.5: Stacked SEM/EDX micrographs with intensity profile of Chloride element of Case 0: Blank operation (with water) Case A: provoked total pore wetting by pressure higher than LEP using 35g/L NaCl solution and Case B normal VMD operation with 310 g/L NaCl solution (to be viewed in color)

It can be confirmed that for Case 0 (after the blank operation), no Cl was observed, neither on the surface nor on the membrane cross-section. The small intensity across the membrane sample is attributed to noise. Thus, for the membrane sample corresponding to a provoked total pore wetting, case A confirms that intrusion of salt occurred (with the intrusion of water) and that traces of Cl could be detected along the membrane thickness/cross-section. So, this experiment confirms that the DTTI concept could be applied at least when total pore wetting occurs.

For case B it can be noted that the gray value of Cl ions is more intense near the feed side than on the permeate side. This might indicate a slight intrusion of the liquid/vapor interface inside membrane pores that corresponds to surface wetted pores. The intensity profile also shows 2 peaks corresponding to Cl traces, one located just before the middle of the sample and one close to the permeate side. After comparison with the reference (Case 0), this can only be explained by partially wetted pores at a localized scale. Finally, for case B, even if the operation was performed at a difference of partial pressure lower than LEP, SEM-EDX allows detecting both surface wetted pores and partial pore wetting. At the same time in comparison with the properties of the virgin membrane, contact angle showed a significant reduction in hydrophobicity (CA= 63° for the used membrane), which can be consistent with wetting occurrence.

These results allow confirming the application of SEM/EDX micrographs to detect the presence of salt in correlation with an intrusion of liquid inside membrane pores (Case A). It can also confirm that SEM/EDX micrographs can reveal wetting by the partial intrusion of liquid into pores through the membrane cross-section by studying the salt left by liquid penetration during operation. This validates the proof of concept of the DDTI method that will be fully developed in the next paragraph.

2.3.2. Development of the general protocol of the DDTI method and of its different steps

Based on the wetting observations made using SEM/EDX, a generic protocol of the DDTI method to identify and evaluate two wetting mechanisms (total wetting and partial pore wetting) in membrane distillation was developed (**cf.** 2.1). Note that this protocol was developed for the VMD process but could also be used to characterize the wettability of any hydrophobic membrane used in a membrane contactor process. The major issue in this part of the study was to define precisely the impact of the membrane cleaning procedure (after MD operation) and definition of the cleaning method in order to obtain information on different wetting mechanisms.

Two different options were studied for the step in between MD operation with the tracer solution and SEM-EDX, before removing the membrane from the MD cell: cleaning or no cleaning. The two

corresponding protocols are introduced in **Figure 2.6**. For protocol A, that is to say the one with cleaning, the membrane module was first removed from the pilot and all the feed water was drained from the membrane module. Then, *in-situ* cleaning was conducted using deionized water until the conductivity of the feed drops to 5-50 µS/m at Re 100 to prevent additional wetting. During this period, no vacuum was applied, and the introduced deionized water was not heated to prevent any further membrane distillation. The objective of this *in-situ* cleaning was to ensure removal of most salts traces on the feed side of the membrane surface and to avoid pollution of the permeate side during manipulations of the membrane. Then the membrane was removed from the membrane cell, and its surface was dried with lens cleaning paper (Whatman N0 105 Lens Tissue) in order to reduce external contamination on the membrane surface. This kind of paper leaves no fibers on the membrane and is chemically pure and free from silicones and other additives. The membrane was then dried in a desiccator for 12 hours to ensure no water was left inside the membrane samples. For protocol B, that is to say the one without cleaning, just after the MD experiment with the saline solution has been completed, the membrane was removed from the membrane cell and covered in a protective box with lens cleaning paper and dried in a desiccator at room temperature.

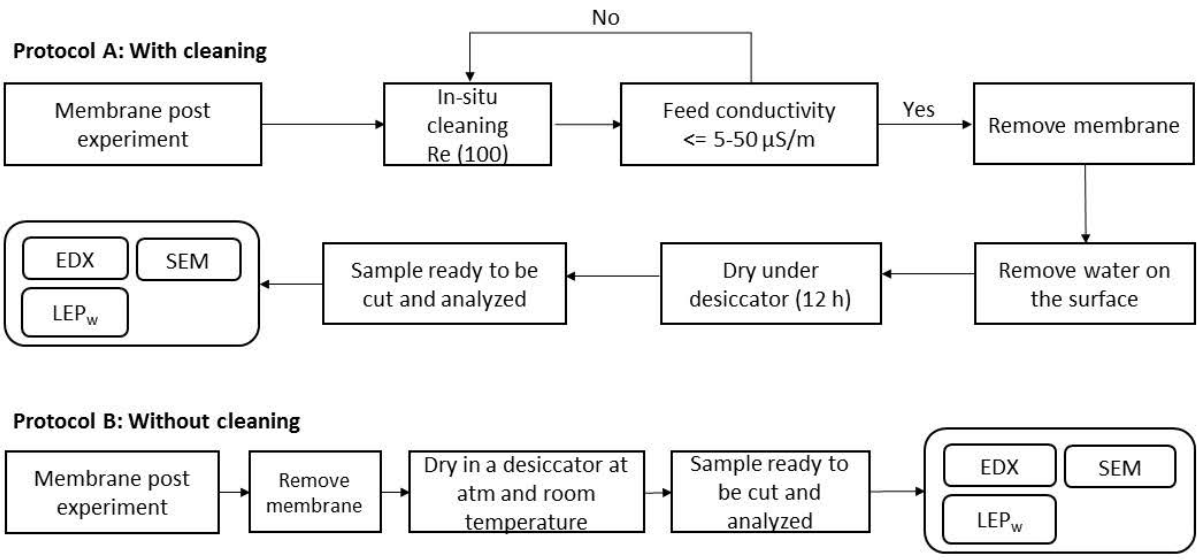

Figure 2.6: Cleaning protocol for membranes after each experimental run

The impacts of cleaning or not cleaning the membrane after the MD operation on the Cl intensity profiles obtained along the membrane thickness are presented in **Figure 2.7**. It can be clearly seen when cleaning (Protocol A) is being used, the Cl trace intensities on the permeate side surface could be visualized and graphed but the partial intrusion of salts on the feed side (which could be the trace of partial wetting) was not visible. With protocol A, if salt is detected on the permeate side, as the membrane has been carefully cleaned on the feed side before being removed from the cell, we could

be fairly confident that the salt was present on the permeate side and has not been introduced when the membrane was removed from the cell. Presence of salt is thus a trace of total wetting. However, in most cases, no more trace of salts was detectable on the feed side, due to cleaning protocol.

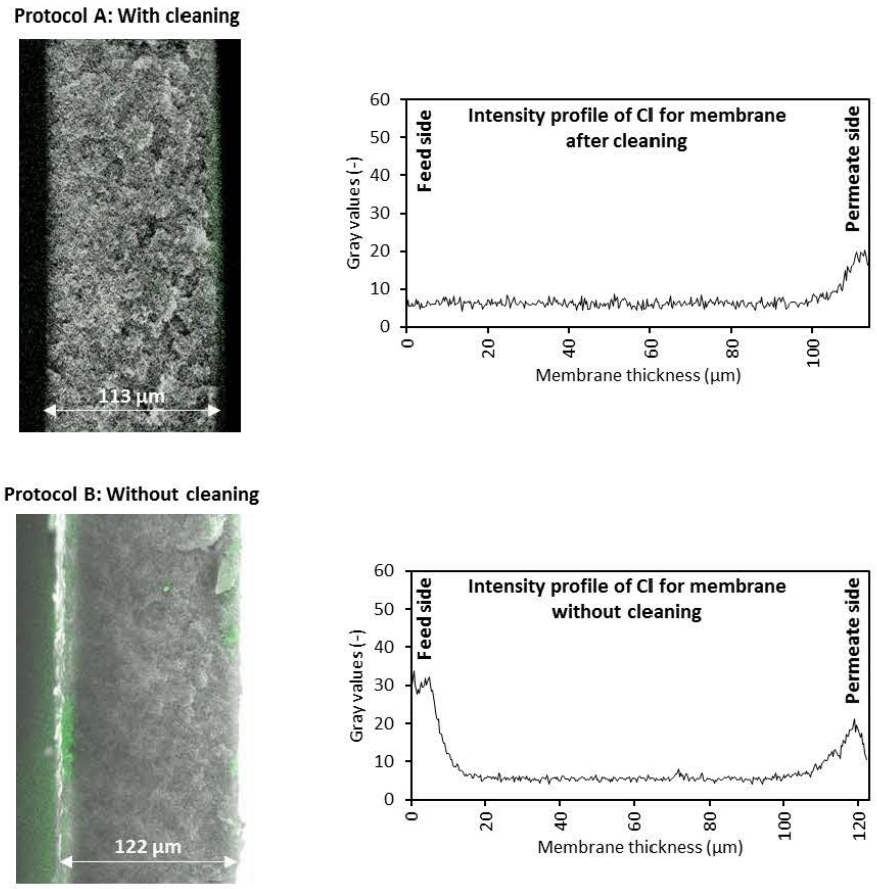

Figure 2.7: Example of intensity profile of Protocol (A) with cleaning and (B) without cleaning (to be viewed in color)

However, without cleaning (Protocol B) both surface wetting (partial intrusion in pores) and total wetting could be visualized. But, as the permeate side might have been polluted with salts when the membrane was removed from the cell, if information on total wetting is researched, then it is better to conduct cleaning. With cleaning, the liquid layer that was close to pore inlets and in the first part of pores on the feed side was removed and liquid intrusion could not be observed – so if this information is researched no cleaning (Protocol B) should be performed.

To better visualize and interpret liquid intrusion in pores, a graphical representation of the effect of cleaning/no cleaning is presented in **Figure 2.8**. When cleaning was conducted (Protocol A) two cases of wetting were observed. They are presented in **Figure 2.8** (a and b) where (a) represents membrane

surface were some surface and partial wetting have occurred and (b) where complete penetration of liquid had occurred.

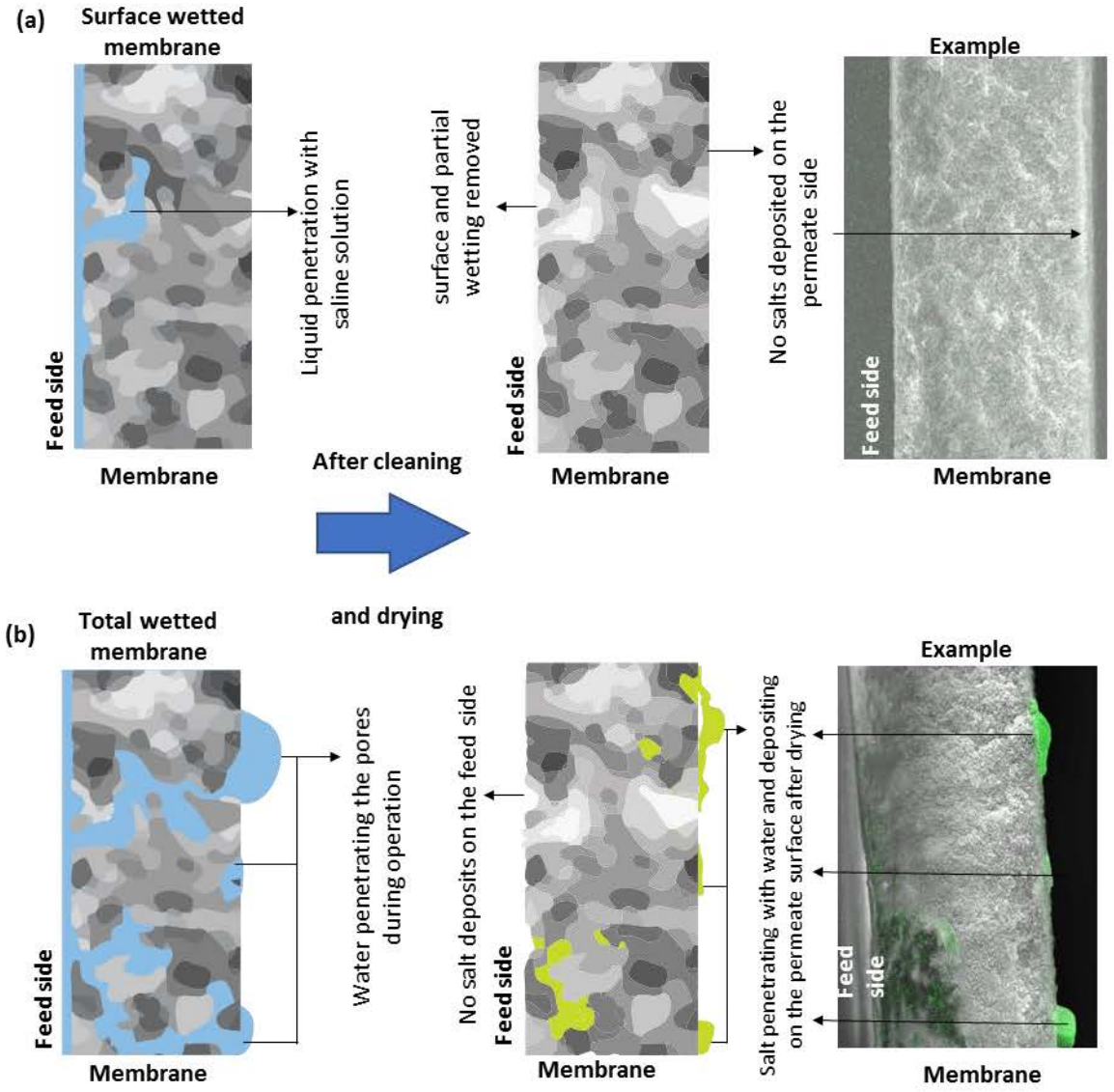

Figure 2.8: Representation of salt traces before and after cleaning (protocol A) and actual SEM/EDX micrographs: (a) in the case of surface and partial wetting and (b) in the case of total wetting (to be viewed in color)

For Protocol B, where no cleaning was conducted after the MD operation, **Figure 2.9** represents a case where complete wetting had occurred. The salt traces, left after the water had evaporated, can be observed. **Figure 2.9** also presents an actual SEM/EDX micrograph where complete wetting had occurred, and salt traces were observed on the feed side, within the membrane pores and also on the permeate side of the membrane. In cases where a lot of liquid was present salt traces where of random crystal shapes and sizes based on the liquid penetration.

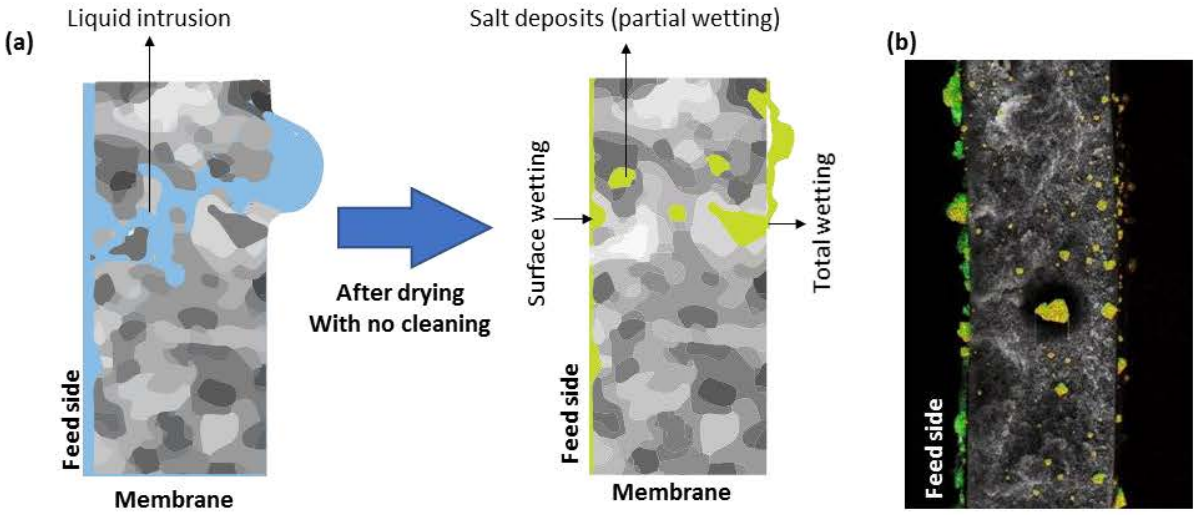

Figure 2.9: Representation of salt traces with no cleaning (protocol B) and SEM/EDX micrograph in the case of total wetting (to be viewed in color)

Furthermore, to confirm the effects of cleaning or not, SEM/EDX micrographs of 2 membranes subjected to the same operating conditions (42.5°C, Re = 2191 and 310 g/L NaCl solution) are presented in ***Figure 2.10*** in the case (a) of cleaning and (b) without cleaning. Here it can be seen that under the same operating conditions wetting visualization was possible, with the main difference being that the membrane subjected to cleaning had no salts on the feed side and the one without cleaning had salt traces on the feed side.

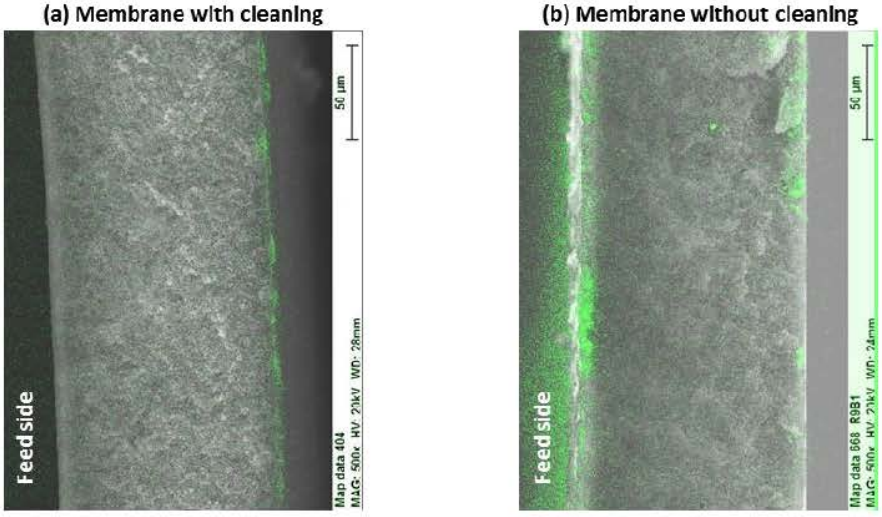

Figure 2.10: Effect of (a) cleaning and (b) not cleaning at the same operating conditions (to be viewed in color)

2.3.3. Definition and results of wetting indicators

Based on the cleaning strategies, wetting observations could be categorized into distinct forms using the following two indicators:

- A proportion of totally wetted surface area (ω_s), that can be obtained from the information on salt traces on the permeate side membrane surface only, which represents a rate of total liquid intrusion.

- An average rate of liquid intrusion in the pore (called pore wetting ratio) (ω_p): that can be obtained by visualizing the salt traces through the membrane thickness only.

The definitions and interpretations of these two indicators are summarized in the following sub-sections.

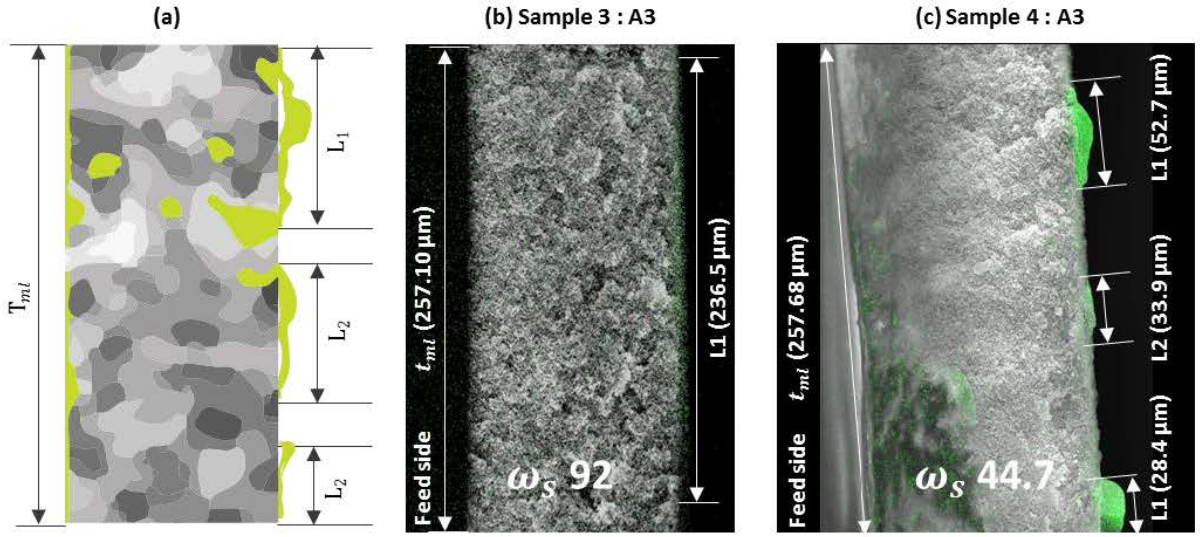

Figure 2.11: Totally wetted surface (a) graphical representation of the ω_s analysis conducted on the membrane surface (b) example on location A3 with 166 g/L and (c) location A3 with 310 g/L (to be viewed in color)

2.3.3.1. Totally-wetted surface ratio (ω_s)

In case where cleaning was conducted, salt traces on the permeate side could be visualized without risk of contamination by the feed side. Presence of salts in this place indicates a complete passage of water in some pores, which represent a fraction area of the membrane that is totally wetted.

The proportion of totally wetted surface, namely totally-wetted surface ratio (ω_s) is defined as the proportion of the length in the permeate side covered by salt to the total observed length of the membrane as expressed in Eq. 2.4.

$$\omega_s = \frac{\bar{pl}}{T_{ml}} \times 100 \qquad \text{Eq. 2.4}$$

Here $\bar{pl}$ (µm) is the sum of the observed wetted length on the permeate side only and T_{ml} is the total length of the observed membrane in µm. **Figure 2.11 (a)** is a graphical representation of the ω_s analysis conducted on the membrane surface, while **Figure 2.11 (b and c)** are examples of proportion of totally-wetted surface (ω_s) observed respectively in Location A3 for 166g/L and 310 g/L.

Table 2.2: Summary of totally-wetted surface analysis conducted samples 1 to 4 using SEM/EDX

Feed	NaCl	Totally-wetted surface (ω_s)									Average (ω_s)	
	(g/L)	A1	A2	A3	B1	B2	B3	C1	C2	C3	Mean	S. D
1(Blank)	0	0	0	0	0	0	0	0	0	0	0	0.00
2	22	0	0	0	0	0	0	0	0	0	0	0.00
3	166	0	0	92	0	0	0	0	0	0	10.2	28.91
4	310	100	0	44.7	100	0	10.5	96.4	96	68.5	68.5	38.21

ω_s was measured at pre-defined locations on the membrane surface after being used in the VMD pilot with tracer solutions. The data and values of ω_s obtained from Eq. 4 are reported in **Table 2.2**. It can be noted that the blank essay and feed, in any location, lead to ω_s values of 0 (no wetting). ω_s values for feed 3 -A3 and feed-A3 were 92 and 44.7 respectively, which means that 92 and 44.7 % of the observed permeate side of the membrane surface was covered by salts in each sample respectively. It would be also interesting to note that the only wetted surface observation in feed 3 was acquired from A3, which was located very close to the feed side inlet port, which could be explained by local absolute pressure in this place, which might favor liquid intrusion in pores. Most wetting occurred on the feed 4 at the highest tracer concentration. In 9 sampling locations for feed 4, seven locations showed wetted surface while two did not lead to wetted surface observation. Additionally, by using the mean value it can be noted that wetting occurrences were becoming more frequent at the highest tracer concentrations with an average ω_s reported at 68.5 ± 38.2 %.

The objective of studying the influence of tracer concentrations was to determine the best conditions to characterize wetting. Here it appears that tracer concentrations clearly influence the answer that will be given in terms of wetting indicators for a membrane or MD set of operating conditions.

Operation of the procedure at concentrations close to the one that will be used during real operation might be more representative of what will happen, but operations at higher concentrations might be a way to amplify wetting processes, which could be interesting if the objective is to use the methodology to compare different innovative membranes in order to select the one to be developed and manufactured at industrial scale. Based on the results, wetted surface (ω_s) indicator can be considered as a good tool for evaluating total wetting with regard to the limits of operating conditions and membrane used. The SEM/EDX micrographs of the membrane cross-section described in this section can be found in supplementary data Figure C3.4.

2.3.3.2. Pore wetting ratio (ω_p)

In a case where no cleaning was conducted, surface wetting (from feed side) and partial wetting can be visualized through the membrane surface and cross-section. Thus, in this case wetting was only interpreted using salt traces inside the membrane cross-section. These salt traces are left after liquid intrusion in pores. The average rate of liquid intrusion in pores was termed as pore wetting ratio (ω_p).

Pore wetting ratio (ω_p) can be defined as the proportion of liquid intrusion under a given operating condition detected by the intensity profile of an element of interest through the cross-section of the membrane. It is a rate of liquid intrusion in the membrane thickness expressed as the ratio of the wetted distance (δ_l) divided by the total distance, i.e. membrane cross-section/thickness(δ_m).

In this study, liquid intrusion in pores was detected by Cl intensity through the membrane cross-section and can be expressed as Eq. 2.5.

$$\omega_p = \frac{\delta_l}{\delta_m} \times 100 \qquad \text{Eq. 2.5}$$

δ_m is the membrane thickness in µm.

δ_l is the deepest position (µm), through the cross-section of the membrane, where a peak of significant intensity compared to the signal baseline can be observed (see Figure 2.5– Case B where peaks have been observed). The most remarkable result is that all wetting mechanisms proposed by Gryta leading to different mechanisms of wetted pores could be visualized thanks to the new DDTI methodology, by interpreting the salt traces left by the liquid intrusion. **Figure 2.13 (a)** presents for each different assumed mechanism of liquid intrusion in the pores its evidence based on the corresponding salt traces.

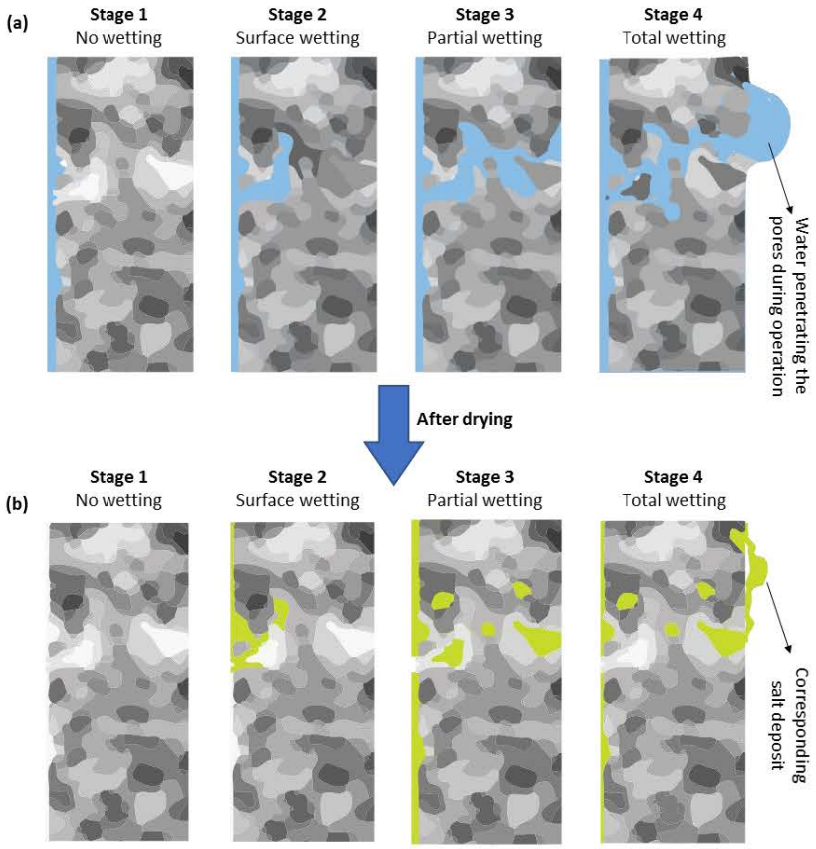

Figure 2.12: Representations of various mechanisms of wetting presented with (a) liquid intrusion into the pores with the corresponding (b) salt traces visualized/analyzed by DDTI method (to be viewed in color)

Ideally in MD, molecules with low vapor pressure in the feed side pass through the hydrophobic membrane towards the permeate side in their vapor phase only and no liquid penetration occurs through the cross-section of the membrane and no wetting is observed **Figure 2.12 ((a) Stage 1).** The process dysfunction occurs when liquid penetrates the pores and starts to induce wetting. If the saline liquid penetrates just below the feed side membrane surface and traces of salts can be found inside membrane it can be deemed as surface wetting and water intrusion can be visualized in **Figure 2.12 ((a) Stage 2)**. While the corresponding salt traces can be seen in on **Figure 2.12 ((b) Stage 2).** Deeper intrusion of the liquid towards the permeate side can be termed as partial wetting **Figure 2.12 (Stage 3).** Finally, when most pores are compromised, and liquid starts to penetrate the membrane, this can be considered as complete wetting **Figure 2.12 (Stage 4).** The resulting salt traces occur not only on the membrane pores but also on both the membrane surfaces too (**Figure 2.12 ((b) Stage 4)**.

For each experiment, a plot can be obtained where the x-axis represents the non-dimensional horizontal distance through the cross-section of the membrane surface (x/δ_m), which allows

comparison of membranes having different thicknesses, and the y-axis the vertically averaged pixel intensity (gray values). Figure 2.14 shows examples of different shapes of curves that can be obtained. On a given curve, if different peaks of significant intensity are observed, the position of the deeper peak (higher value of x) corresponds to δl which is used to calculate ω_p. In case that no real peaks are observed but a continuous and significant gray value level, it means that traces of salts were observed all along the membrane length which corresponds to total wetting. In that case, ω_p value is taken equal to 100 %.

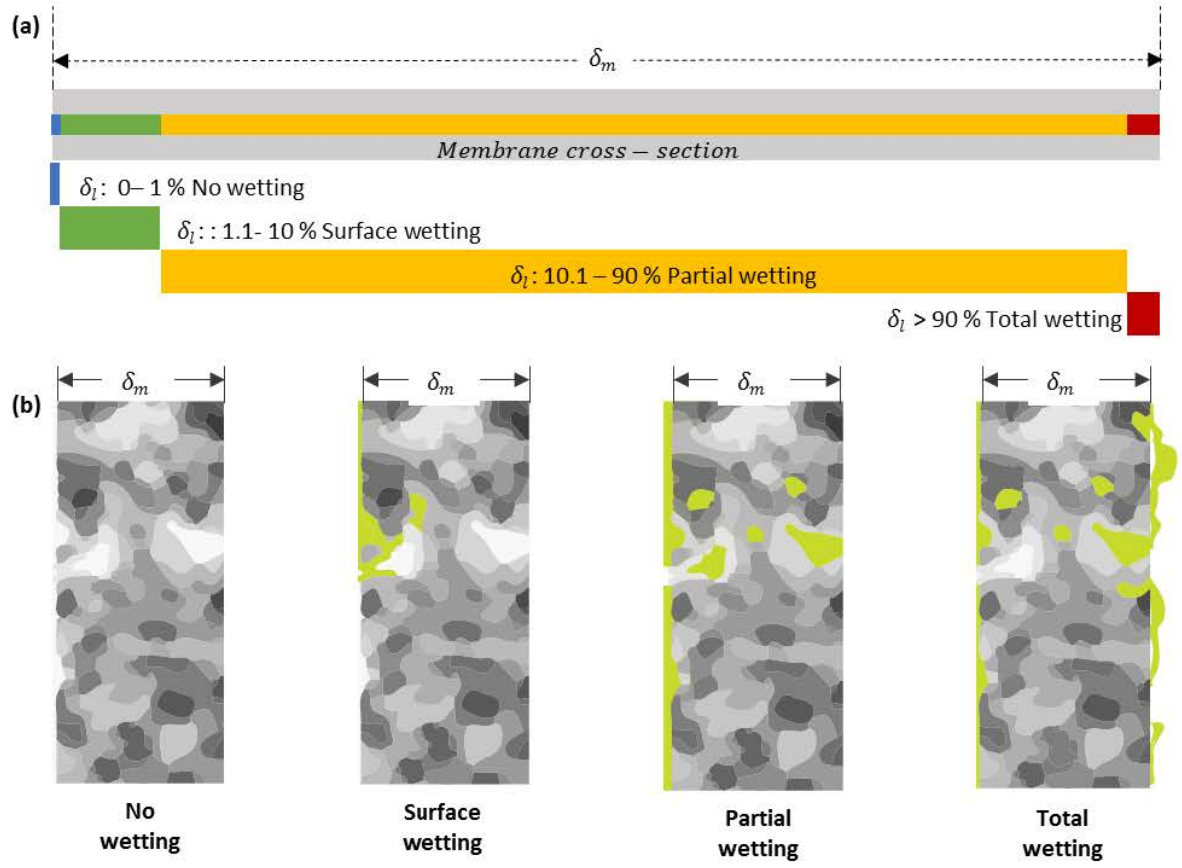

Figure 2.13: (a) Further classification of wetting under pore wetting ratio (ω_p) (b) Representation of various mechanisms of pore wetting in membrane distillation detected DDTI method (to be viewed in color)

Based on our observations the following classification of pore wetting mechanisms were further established as presented in **Figure 2.13** as a function of ω_p value.

- No wetting: if ω_p(0 - 1 %)
- Surface wetting: if ω_p (1.1-10 %)
- Partial wetting: if ω_p (10.1-90 %)

- Total wetting: if ω_p (> 90 %)

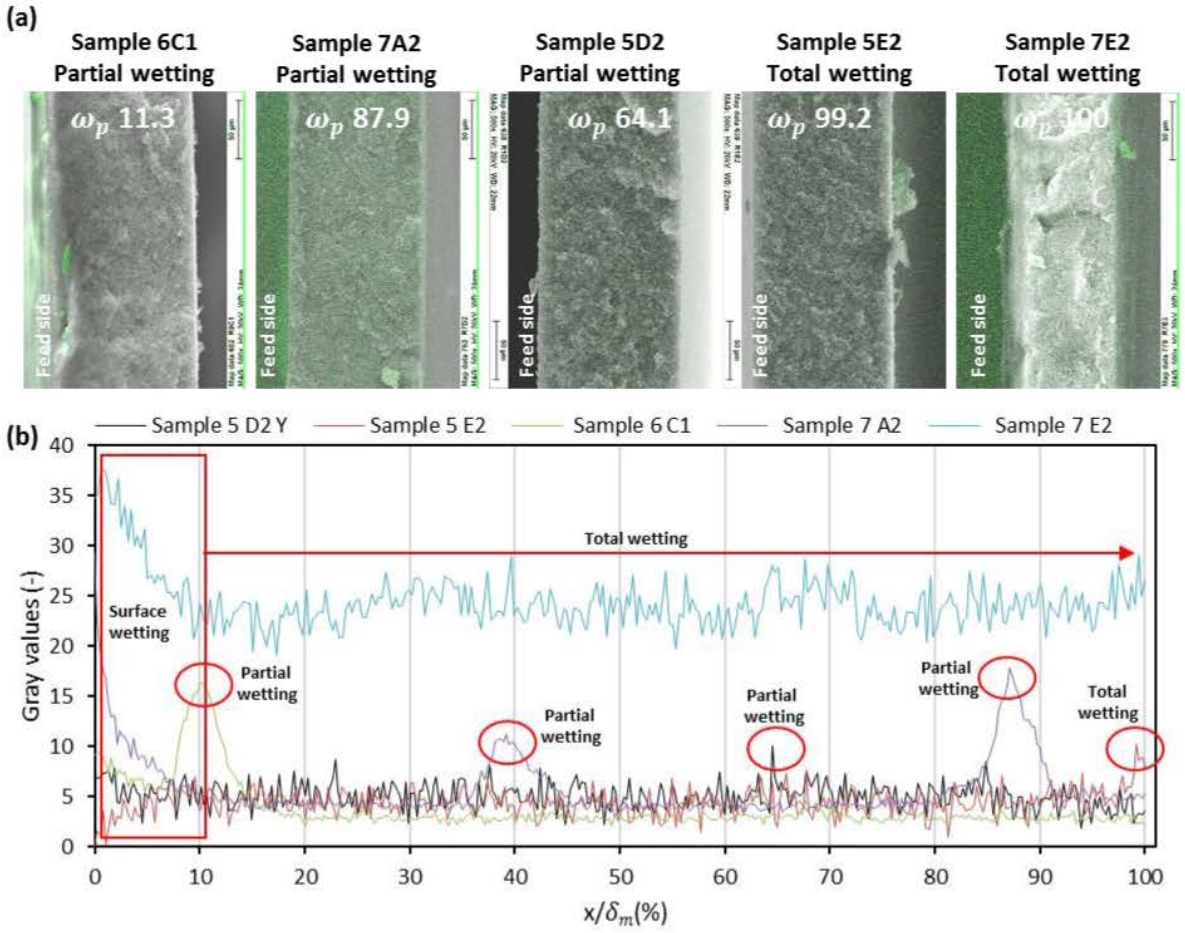

Figure 2.14: Examples of wetting occurrences observed in the studied samples (to be viewed in color)

Based on the above interpretation **Figure 2.14 (a)** presents SEM/EDX micrographs with various wetting mechanisms observed with tracer solutions 5, 6 and 7 (at different sampling locations). **Figure 2.14 (b),** presents the intensity profile in the cross-section in samples. Firstly, it can be noted that as no cleaning was performed, surface wetting can be now observed in several samples (e.g. in samples 6C1 and 7A2). For these samples, though surface wetting was observed but partial wetting and total wetting were also observed as indicated by ω_p of 11.3 and 87.9 % respectively. Additionally, in sample 5D2, though no surface wetting was observed but partial wetting was observed as indicated by ω_p of 64.1. This reveals the complexity of wetting in membrane distillation and all forms of wetting may or may not be visualized depending on the location.

Let us now consider total wetting, in samples 5E2, 7E2. In both cases, salt had penetrated through the cross-section of the membrane to the permeate side, but the shapes of the curve are different (respectively peaks and continuous high intensity). In sample 5E2, total wetting was interpreted by

observing the ω_p as the deepest peak intensity observed through the cross-section of the membrane was at 99.2, while in sample 7E2 total wetting was considered as 100% **Figure 2.14 (b).** The SEM/EDX micrographs used for pore wetting ratio can be found in supplementary data Figure C3.5.

Based on the above description and example interpretation, ω_p measurements were conducted on the membranes (feed 5, 6 and 7) and the data (ω_p and Median) are reported for the sampling location (A1, A2, B1, B2, C1, C2, D1, D2, E1, and E2) at the highest tracer concentration in **Figure 2.15.** It is interesting to note that all forms of wetting are observed, depending on the location. In all sampling locations, surface wetting was existing, while at location A2 and C2 partial pore wetting was observed frequently through the membrane cross-section. Finally, in two cases D2 and E2 complete wetting had occurred where the median pixel intensity was observed to be 20.6 and 24 respectively. It can be noted that in these 2 cases, the high Cl intensity throughout the membrane sample was seen as in the case where wetting was induced by operating in filtration mode (**Figure 2.5 Case B**).

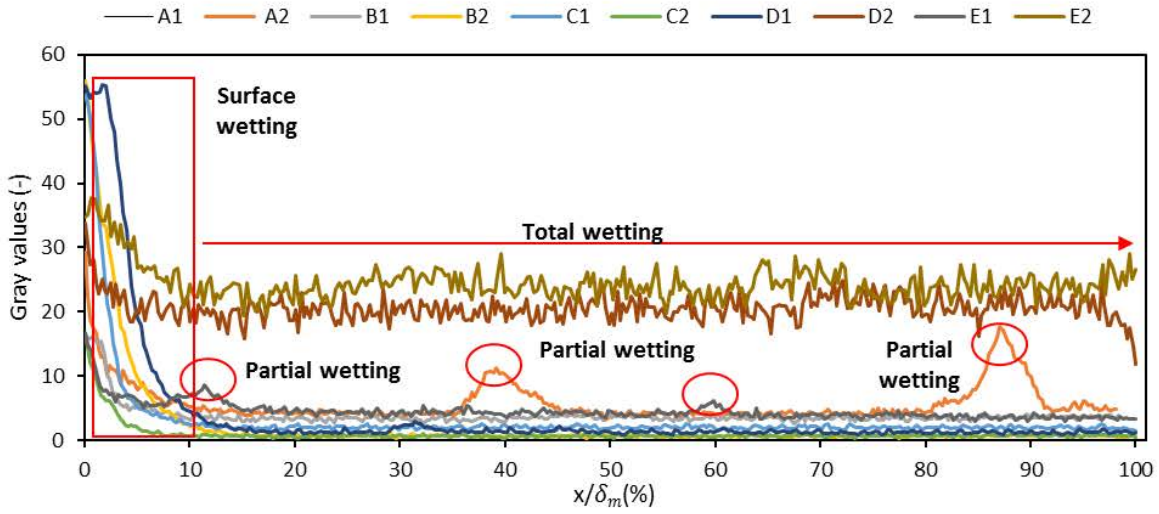

Figure 2.15: Pore wetting observations in function of the sampling location for 310 g/L (to be viewed in color)

2.3.4. Comparing the wetting observations with LEP

There has been a lot of effort by various researchers over the decade to improve the theoretical accuracy of LEP measurements and verifying it by experimental methods and recently CFD to better understand and predict wetting in membrane distillation [120,134,140,144]. Regardless, LEP is good wettability indicator but it does not give deeper information on wetting itself and on its possible mechanisms during operation or post operation.

In this study, LEP measurements were conducted at 3 locations (L1 at the feed inlet, L2 in the middle of the membrane and L3 at the feed outlet port) at the highest tracer concentration and the average and standard deviation values are summarized in **Table 2.3**. LEP values varied between 150 and 190 kPa respectively, and according to these global values and to the current use of LEP, no wetting would be predictable for the operating conditions. However, as presented before all forms of wetting were observed with the DDTI method. Though, the DDTI method is a more pertinent tool to detect wetting or to predict wettability, when used for membrane screening.

Table 2.3: LEP measurement at different locations

Feed	NaCl(g/L)	Liquid entry pressure (kPa)				
		L1	L2	L3	Average	S.D.
1(Blank)	0	210	210	195	205	9
4	310	190	180	150	173	21
7	310	180	190	190	187	6

2.4. Conclusions and perspectives

In English

Up to now the most common criteria for the evaluation of wetting/wettability were conductivity increase in the permeate, contact angle, and LEP. In fact, among these different criteria, the increase of conductivity is an *in-situ* way to evaluate wetting and traduces wetting in its operational reality, but it only informs on total wetting. Contact angle and LEP measurements are only wettability indicators. Even if they can be used at the end of the process to evaluate the evolution of wettability during operation they only inform respectively on changes in membrane hydrophobicity or on the ability for total wetting. They do not provide information on other wetting mechanisms, such as surface or partial wetting.

Here we have both illustrated and given proof of concept that, in MD, wetting can be both visualized and studied thanks to a new methodology, named Detection of Dissolved Tracer Intrusion (DDTI). This method is quite simple and is based on the use of equipment that are available in most laboratories. After a liquid penetrates through the membrane, traces of salts can be found on the surface and pores as it progressively passes through and that these traces can be detected by SEM/EDX and considered as an evidence of wetting. Thus, by studying the location of the liquid penetration using SEM analysis of salts, it was demonstrated that the DDTI method allows the visualization and identification of the

four wetting mechanisms and that at the local scale all forms of mechanisms can co-exist in different locations of a membrane.

Based on these principles, two complementary indicators were elaborated and established as relevant indicators to evaluate wetting in membrane distillation: totally- wetted surface ratio (ω_s) and pore wetting ratio (ω_p). These indicators reveal much more information, notably on wetting mechanisms, than "wetting pressure" observed by measuring LEP. They can be used together or separately for comparing wettability of membranes under given operating conditions. A summary on these indicators is presented in **Table 2.4**

Table 2.4: Interests and complementary information from the 2 indicators

Wetting indicator	Totally-wetted surface ratio (ω_s)	Pore wetting ratio (ω_p)
Definition	The proportion of the length in the permeate side covered by salt to the total observed length of the membrane	The proportion of liquid intrusion in the membrane thickness expressed as the ratio of the wetted length divided by the total length
Cleaning	Yes	No
Advantages	• Local information on wetting • Potentially applicable in many membrane distillation configurations and membrane contactors (except DCMD) • Evaluates total wetting at the global scale of membrane surface • Do not inform on partial or surface wetting • Is more sensitive than LEPw	• Evaluates liquid intrusion in pores and allows quantification of surface and partial wetting • Can also be used to evaluate total wetting at the scale of one pore • Much more refined technique
Drawbacks	• Not an *in-situ* method • Requires sampling and destruction of membrane sampling • Does not inform on surface or partial pore wetting	• Does not inform on total pore wetting at the scale of the membrane

With regard to these tools/ methods to be transferred to other membrane distillation configuration, total wetted surface (ω_s) and pore wetting (ω_p) may also be valid at least for all configurations where a liquid is not being circulated on the permeate side to recover vapor like VMD, SGMD, and AGMD. Further development of the methodology will be necessary to adapt it to other configurations. For these processes, the DDTI principle could be used effectively for benchmarking newly developed or commercially available membranes and operating conditions and the module designs for their potential use for various applications and intensification levels.

A systematic use of comprehensive wetting indicators in the early stages of membrane development will be a powerful tool to orientate the elaboration strategy and to select the membranes of the future, with the highest chances to develop membranes with low (or measured) risk of wetting. Membrane aging could also be deeply studied and understood with these tools at a local scale. The wetting indicators developed here can be used as a tool to better understand the impact of the operating conditions and feed solution on the membrane morphology leading to wetting. As it reveals information on local wetting at different locations and thus on the impact of membrane cell geometry and design, which would not have been previously possible. This tool could also be interesting to understand the process dynamics of wetting to have some objective elements of decision for the process optimization, such as for example with regards to cleaning and de-wetting strategies in membrane distillation.

En Français

Jusqu'à présent, les critères les plus couramment utilisés pour évaluer le mouillage / mouillabilité d'une membrane en distillation membranaire étaient l'augmentation de la conductivité dans le perméat, l'angle de contact et le LEP. En fait, parmi ces différents critères, l'augmentation de la conductivité est un moyen in situ d'évaluer le mouillage et traduit le mouillage dans sa réalité opérationnelle, mais elle n'informe que sur le mouillage total. L'angle de contact et les mesures du LEP ne sont que des indicateurs de mouillabilité. Même s'ils peuvent être utilisés à la fin du processus pour évaluer l'évolution de la mouillabilité en cours de fonctionnement, ils ne renseignent respectivement que sur les changements d'hydrophobicité de la membrane ou sur la capacité de mouillage total. Ils ne fournissent pas d'informations sur d'autres mécanismes de mouillage, tels que le mouillage superficiel ou partiel.

Ici, nous avons à la fois illustré et prouvé que, en MD, le mouillage peut être à la fois visualisé et étudié grâce à une nouvelle méthodologie, appelée Détection de l'intrusion de traceurs dissous (DDTI). Cette méthode est assez simple et repose sur l'utilisation d'équipements disponibles dans la plupart des laboratoires. Après la pénétration d'un liquide dans la membrane, on peut trouver des traces de sels à la surface ainsi que dans les pores au fur et à mesure de son passage. Ces traces peuvent être détectées par SEM / EDX et considérées comme une preuve de mouillage. Ainsi, en étudiant l'emplacement de la pénétration de liquide à l'aide d'une analyse SEM de sels, il a été démontré que la méthode DDTI permet de visualiser et d'identifier les quatre mécanismes de mouillage et qu'à l'échelle locale, toutes les formes de mécanismes peuvent coexister à différents endroits d'une membrane.

Sur la base de ces principes, deux indicateurs complémentaires ont été élaborés et définis comme indicateurs pertinents pour évaluer le mouillage en distillation à membrane : le rapport de surface totalement mouillée (ω_s) et le rapport de mouillage des pores (ω_p). Ces indicateurs révèlent beaucoup plus d'informations, notamment sur les mécanismes de mouillage, que la « pression de mouillage » observée en mesurant la LEP. Ils peuvent être utilisés ensemble ou séparément pour comparer la mouillabilité des membranes dans des conditions de fonctionnement données.

En ce qui concerne ces outils / méthodes à transférer dans une autre configuration de distillation à membrane, les indicateurs développés (ω_s et ω_p) peuvent également être valables au moins pour toutes les configurations dans lesquelles un liquide ne circule pas du côté du perméat comme la VMD, la SGMD et la AGMD. Le développement de la méthodologie sera nécessaire pour l'adapter à d'autres configurations. Pour ces procédés, le principe de la DDTI pourrait être utilisé efficacement pour évaluer des membranes nouvellement développées ou disponibles dans le commerce, pour tester des conditions de fonctionnement, ainsi que pour concevoir des modules en vue de leur utilisation potentielle dans diverses applications et niveaux d'intensification.

L'utilisation systématique d'indicateurs de mouillage dès les premiers stades du développement de la membrane sera un outil puissant pour orienter la stratégie d'élaboration et pour sélectionner les membranes du futur, avec les meilleures chances de développer des membranes avec un risque de mouillage faible (ou mesuré). Le vieillissement des membranes pourrait également être étudié en profondeur et compris avec ces outils à l'échelle locale. Les indicateurs de mouillage développés ici peuvent être utilisés comme un outil pour mieux comprendre l'impact des conditions de fonctionnement et de la solution d'alimentation sur la morphologie de la membrane conduisant au mouillage. En effet, cet outil révèle des informations sur le mouillage local à différents endroits et donc sur l'impact de la géométrie et de la conception des cellules à membrane, ce qui n'aurait pas été possible auparavant. Cet outil pourrait également être intéressant pour comprendre la dynamique du processus de mouillage afin de disposer d'éléments de décision objectifs pour l'optimisation du processus, comme par exemple en ce qui concerne les stratégies de nettoyage et de démouillage en distillation à membrane.

Acknowledgments

I would also like to thank Fabric'INSA and Dr. Benoit Viallet, Stephanie Reyjal, and Simon Cayez from the physics department of INSA Toulouse for providing equipment's and sharing their expertise. ANR (Agence Nationale de la Recherche) Programme : Innovation technologique pour analyser, remédier ou réduire les risques environnementaux (DS0102) 2014 also needs to be thanked for for funding project WETMEM (ANR-14-CE04-0008).

Preface to Chapter 3

The development of the DDTI methodology with its two wetting indicators in **Chapter 2** gives an opportunity to understand wetting as a local phenomenon and visualize and evaluate its occurrences at the pore scale. The bibliography review (**Chapter 1**) presents an ambiguity on the effects of operating parameters and feed characteristics and their interactions on wetting. Therefore, **Chapter 3** (see flowchart below) is dedicated to understanding the effects of three operating parameters with the totally wetted surface ratio (wetting indicator 1) and the effect of salt concentration on the proportion of liquid intrusion using pore wetting ratio (wetting indicator 2) on a membrane surface using the DDTI methodology. This chapter also distinguishes between wettability and wetting by evaluating the information obtained by classical wettability tools (liquid entry pressure, contact angle, and surface free energy) and newly developed wetting indicators. Finally, the chapter concludes by giving some recommendations for the studied membranes and operating parameters to prevent wetting occurrences during operation.

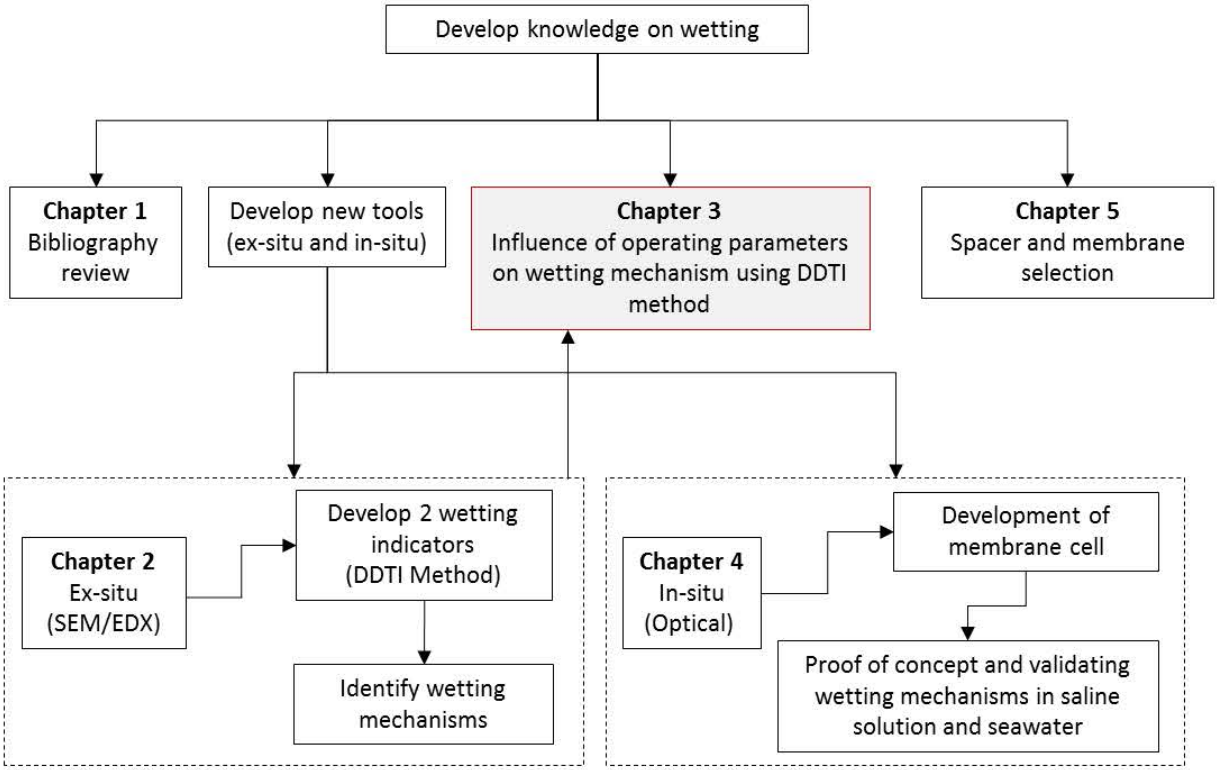

Chapter 3 : Study on the influence of some operating conditions on wetting and wettability in vacuum membrane distillation

Summary of objectives (in English)

This chapter is aimed to evaluate the effects of operating parameters (temperature (T_f), Reynolds number (Re), and salinity (C_f)) on wettability (contact angle (CA), liquid entry pressure (LEP_w) and surface free energy (SFE)) and wetting indicators evaluated with Detection of dissolved tracer intrusion (DDTI) method. Vacuum membrane distillation was considered with a 0.22 µm PVDF membrane and in a very large range of NaCl salinity (22 to 310 g/L). In a first step, the effects and interactions of the operating parameters on the totally wetted surface ratio (ω_s) was studied using Box Behnken design of experiments (DOE). In a second step, the effect of salt concentration on the proportion of liquid intrusion was studied using pore wetting ratio (ω_p) together with wettability tools.

Résumé des objectifs (en français)

Ce chapitre est destiné à évaluer les effets des paramètres de fonctionnement (température (T_f), nombre de Reynolds (Re), et salinité (C_f)) sur la mouillabilité (angle de contact (CA), pression d'entrée de liquide (LEP) et surface d'énergie libre (SFE)) et sur les indicateurs de mouillage évalués avec la méthode Detection of dissolved tracer intrusion (DDTI). La distillation membranaire sous vide a été effectuée avec une membrane en PVDF de 0,22 µm et dans une très large plage de salinité de NaCl (22 à 310 g/L). Dans un premier temps, les effets et les interactions des paramètres de fonctionnement sur le « totally wetted surface ratio » (ω_s) ont été étudiés à l'aide du plan d'expériences (DOE) de Box Behnken. Dans un deuxième temps, l'effet de la concentration en sel sur la proportion d'intrusion de liquide a été étudié à l'aide du « pore wetting ratio » (ω_p) associé à des outils de mouillabilité.

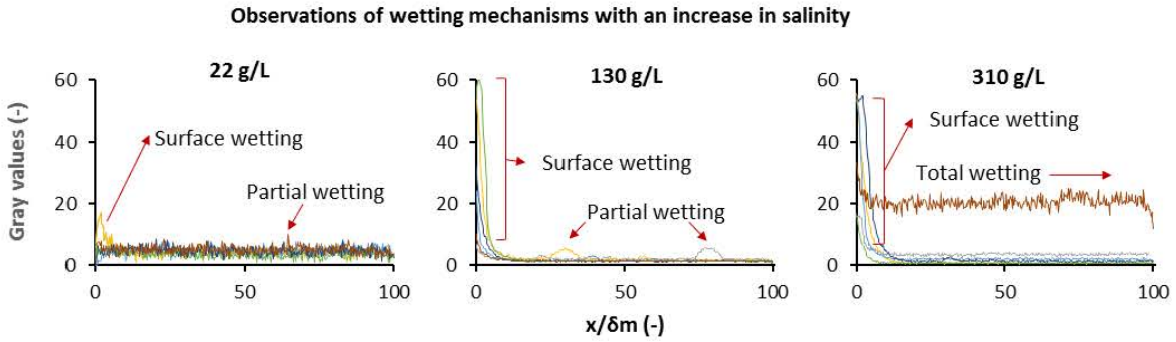

Graphical abstract

3.1. Introduction

With the rising challenges of water security due to population growth and climate change, the 2030 Agenda for Sustainable Development Goals (SDG) by United Nations recognizes the importance of Goal 6 to ensure the availability and sustainable management of water. Over 2 billion people lack safe drinking water with water demands being expected to increase by nearly one-third by 2050. Better technological and managerial solutions are needed to offset these problems and tackle them at its core. Thereby the current focus is towards desalination of the oceans. Analysts forecast the global market on desalination to have an annual growth rate of 8.6 % during the period 2018-2022 [2]. Membrane distillation (MD) can treat hypersaline solutions with substantially greater salinities than reverse osmosis with similar footprint [22] and thus RO and MD can be coupled [7]. MD can also be associated with renewable energies, like solar energy [8].These major differential advantages arouse a growing interest for the industrial development of this technology.

However, membrane wetting has been regarded as one of the primary barriers for the industrial implementation of MD process [16,17] even if the risks of wetting occurrence and of the related process dysfunction are not well understood and qualified. To further this technology into a commercial application, one of the major challenges it faces is for the membrane pores to remain non-wet during the process to preserve a good permeate quality [15].

Wetting can be defined as the effective intrusion of water inside pores, at different stages [176] :

- Sub-surface liquid intrusion in most pores, (surface wetting)
- Partial intrusion in some pores and total intrusion of liquid (passage of water through the total pore length) in the others (partial wetting)
- Total liquid intrusion in all pores (total wetting)

Total wetting can be detected by the degradation of permeate quality.

With the accelerated interest to apprehend wetting, both *ex-situ*[176] and *in-situ*[153] detection tools have been developed to evaluate and understand this phenomenon. Moreover, wetting in membrane distillation is commonly evaluated by interpreting wettability potential of the membrane using contact angle (CA), surface free energy (SFE) and liquid entry pressure (LEP) measurements. However, many studies utilize these wettability indicators to give some conclusions about wetting, even if these indicators have not proven to be precisely predictive. So, confusion exists in the literature between wetting and wettability.

At present, most studies are ambiguous on the effects of operating conditions and feed characteristics and their interactions on wetting. However, some information can be distinguished that really relies on wetting [102,107,117]. For example, the effects of varying flowrates and temperatures at constant salinity in the DCMD process were illustrated by using the rise in conductivity (wetting rate, $\mu S\ min^{-1}$) employing mass balance[103]. It was concluded that at the higher feed temperatures (50 and 60°C) the time to wet the membrane could be possibly delayed, whereas, the effect of flow rates on wetting was considered marginal. Other observations made using SEM, pore size distribution (PSD) to study the microstructure evolution of membrane pores at different temperatures concluded that exposure to high temperature (40 – 70 °C) could induce wetting [102]. Thus, the effects of process parameters on wetting are unsettled, and a more systematic approach still needs to be developed. Only a few available studies are directly addressing assessing the effects of operating parameters [103,107,117] on wetting. Some papers consider the composition of feed solution[74,121], but for oil emulsions.

Therefore, the overall objective of this study, focusing on the possible application of MD for desalination, is to analyze the influence of operating parameters and feed salinity on wetting mechanisms in vacuum membrane distillation. This analysis will be supported by

- An *ex-situ* characterization of wetting using the Detection of Dissolved Tracer Intrusion (DDTI) method that has been previously developed in our group [176], allowing to obtain two indicators: the totally wetted surface ratio (ω_s) , and the pore wetting ratio (ω_p)
- Determination of wettability by classical indicators (contact angle, surface free energy, and liquid entry pressure).

The first part of this study aimed to qualify the effects and interactions of temperature, Reynolds number, and salinity on total wetting (evaluated thanks to ω_s) and on wettability. The experimental strategy was based on Design of experiments (DoE). Whereas the second part of this study aimed to

study the influence of salt concentration on the intrusion of the liquid/vapor interface inside pores, that is to say, to characterize partial pore wetting using ω_p as the wetting indicator. A wide range of salt concentrations (NaCl) were considered (22 to 310 g/L).

3.2. Material and methods

This section presents, the detailed description, and motivation of the two strategies used for understanding wetting influences of operating parameters, the membrane and its characterization, experimental setup, and finally wetting detection tools. Overall the effects of three process parameters on wetting were studied: feed temperature (T_f), Reynolds number (Re), and salinity (C_f) in vacuum membrane distillation (VMD). **Figure 3.1** illustrates the overall methodology. After the initial membrane characterization, the overall study was architectured in two independent parts where wetting was evaluated based on the two developed tools and compared with wettability indicators.

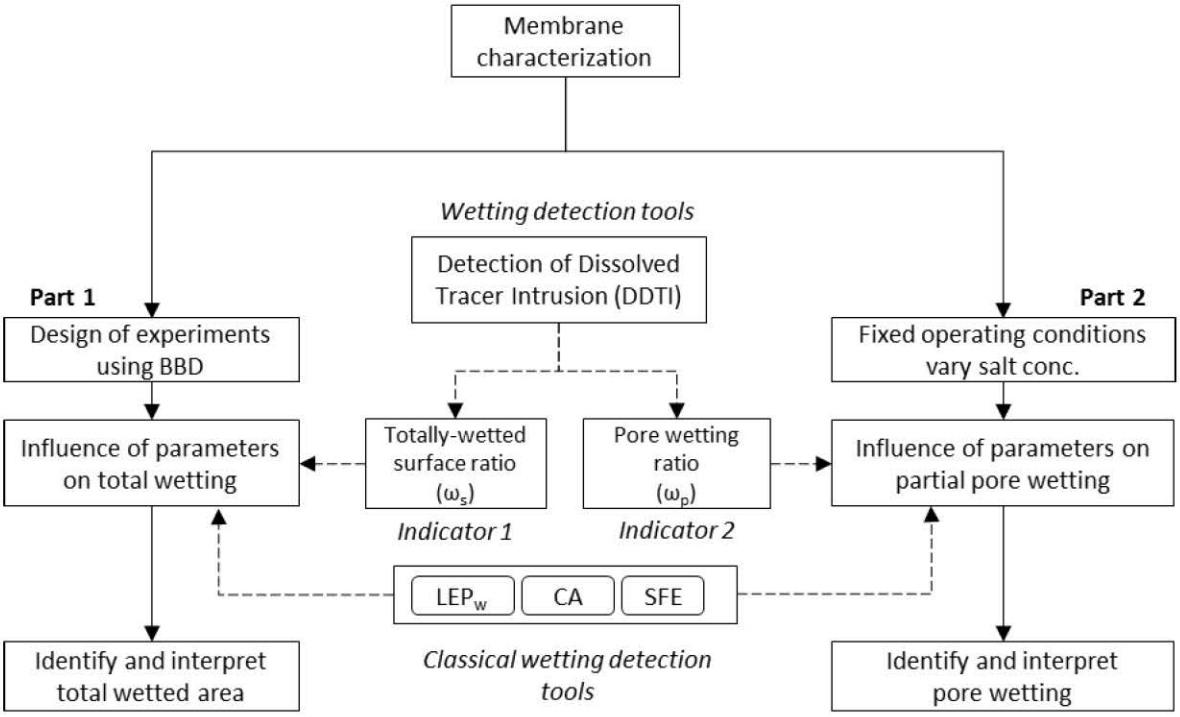

Figure 3.1: Overall methodology to evaluate the effects of MD parameters on wetting

3.2.1. Part 1: Influence of parameters on total wetting using design of experiment (DoE)

A Response surface methodology (RSM) called Box-Behnken design (BBD) *[177]* was used, which is quite similar to central composite design (CCD). BBD is a class of rotatable or nearly rotatable second-order designs based on three-level incomplete factorial designs. BBD can be used to screen factors

with big ranges based on the generated responses. The number of experiments (N) required for the development of BBD is defined in Eq. 3.1.

$$N = 2k(k - 1) + C_0 \quad \text{Eq. 3.1}$$

Where, k is number of factors and C_0 is the number of central points.

Application of Response Surface Methodology (RSM) for characterizing membranes and optimization process is not new in membrane distillation. This methodology has been applied to configurations like DCMD [103,178,179], SGMD [180], AGMD [181] for both membrane and process optimization. The DoE was prepared using Design Expert (V10) considering the three selected operating factors. **Table 3.1** presents the low and high values of each factor. Feed temperatures (T_f) varied between 35 – 50 °C, whereas the Reynolds number (Re) between 382 – 4000 and the salinity (C_f) from 22 to 310 g/L of NaCl respectively. 17 experimental runs were generated using BBD, where the design points were randomized. The assigned values for the temperature (T_f) were discretized, whereas continuous values assigned for flow rate (Re) and salt concentration (C_f). Some repeat experimental runs (Run 2, 3, 6, 10 and 15) were inbuilt to ensure statistical validity.

The vacuum pressure and the total permeate volume produced for each experiment were kept constant at 6 kPa and 225 g of permeate respectively, regardless of the operating conditions. Only after the operating factors reached their desired values, experiments commenced. Experimental runs took between 4 h to 3 days depending on the operating conditions. Each experimental run had five responses (R1-5): R1: Flux ($Kg.m^{-2}.h^{-1}$), R2: CA (°), R3: SFE (mN/m), R4: LEP at 3 locations (bar), and R5: ω_s at 9 locations.

Table 3.1: Factors with their minimal and maximal level used for Box-Behnken design

Factor	Name	Units	Min.	Max	Mean	S.D.
A	Temperature (T_f)	°C	35	50	42.5	5.303
B	Reynolds number (Re)	-	382	4000	2191	1279.16
C	Salinity (C_f)	g/L	22	310	166	101.82

Analysis of variance (ANOVA) tests were performed for response surface with the reduced quadratic model using the partial sum of squares - Type III. For each response (R1-R5) data was analyzed and transformed to generate statistically valid models. The assessed model factors were A, B, C, AB, AC, BC, A^2, B^2, and C^2 for each response. For the fitting model, F-value tests were conducted to compare the source's mean square to the residual mean square to determine the model's significance. Finally,

the model equations were established and reported to understand the interactions within the designed space. Additionally, a comparison between experimental and model predicted data were performed to ensure the model validity.

3.2.2. Part 2: Influence of operating parameters on partial pore wetting

The effect of only varying salinity (C_f) while fixing temperature and vacuum pressure commonly used in VMD was studied. Here the feed salinity was varied from 22 - 310 g/L NaCl (cf. **3.2.4**) while the other operating conditions were fixed (T_f: 42.5 ± 0.19°C, Re 2191 and vacuum pressure 6 ± 0.011 kPa). For each experimental condition 225 g of water (a constant volume) was collected as permeate. Depending on the salt concentration the experiment lasted between 9.6 h to 24 h.

3.2.3. Properties of the membrane used in this study

A PVDF microporous membrane (Durapore, GVHP29325) was used in this study. This membrane has been extensively studied by several authors for various MD configurations [7,37,182]. The virgin membrane was 117.2 ± 0.9 µm thick with an average porosity 0.75 (ε). The contact angle and surface free energy were experimentally determined to be 124 ± 2.8° and 11.5 ± 3.8 mN/m, respectively. The average pore size and the max pore size (R_{max}) were determined to be 0.28 µm (R_{avg}) and 0.89 µm (R_{max}) using ASTM E1294 (89), respectively. The Knudsen permeability coefficient (K_M) and liquid entry pressure (LEP_w) of the membrane were experimentally determined to be 3.59 E-06± 2.38 E-07 $mol^{1/2}.m^{-1}Kg^{-1/2}$ and 2.04 ± 0.86 bar respectively using techniques previously described [176].

3.2.4. Saline solutions preparation

Saline solutions were prepared using NaCl (> 99% pure, Fisher Scientific, France) diluted in ultra-pure water. The range of salt concentrations (22- 310 g/L) was chosen to cover concentrations observed from brackish waters [183] to reverse osmosis brines/concentrates, and to membrane distillation crystallizers [117]. For each experimental run, a 4L solution was prepared and the saline solution was pre-heated before each experimental run.

3.2.5. Vacuum membrane distillation setup and operating conditions

The prepared saline solution was fed into the feed tank heated by a hot water bath in the vacuum membrane distillation (VMD) setup (Figure 3.2). K-type sensors (accuracy ±1.6 %) were used for measuring temperature before the module feed inlet (T1) and at the module retentate outlet (T2). The feed velocity on the membrane surface (Area = 4.16 x 10^{-3} m^2) was controlled using a flow meter

(Krohne, 0-250 L/h) by adjusting a magnetic pump in a closed loop. The Reynolds number (Re) was calculated using Eq. 5.12.

$$Re = \frac{\rho . D_h . v}{\mu} \qquad \text{Eq. 3.2}$$

Where, ρ is the fluid density (kg/m^3), D_h is the effective diameter (m), v is the average fluid velocity inside the feed compartment (m/s) and μ is the dynamic fluid viscosity (kg/m.s). The values for the constants (ρ, v, and μ) at different operating temperatures(T_f) were taken from standard reference [184].

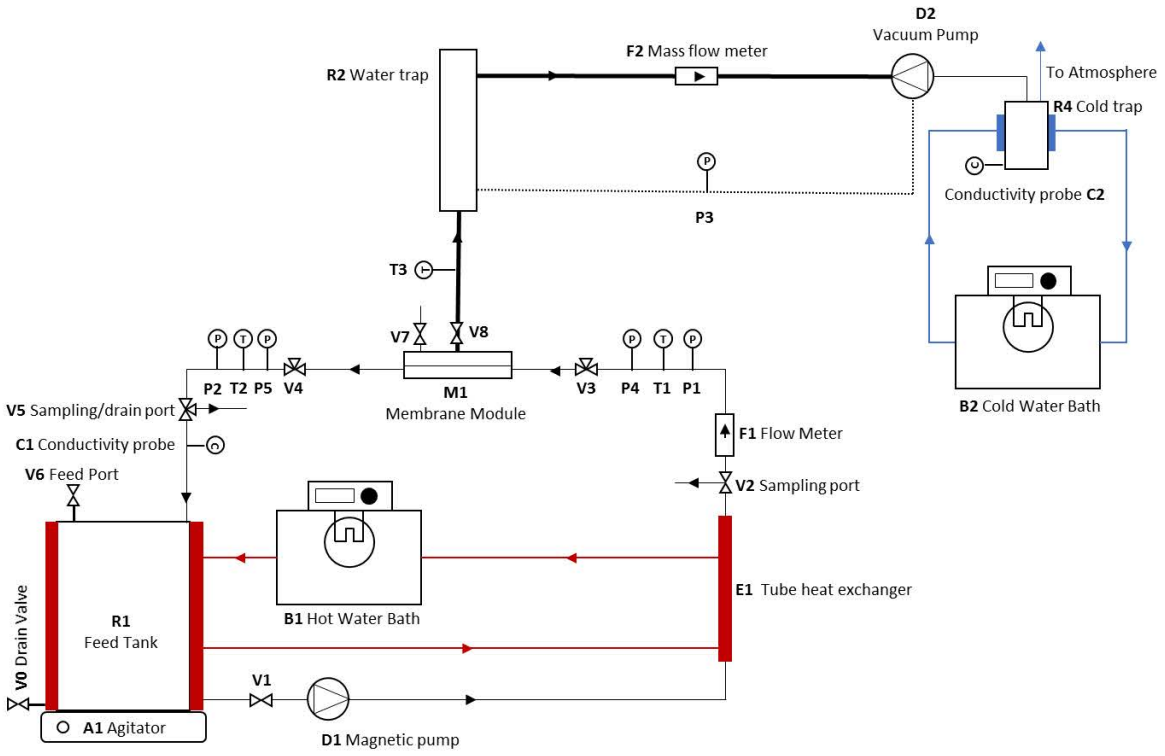

Figure 3.2: Schematic of vacuum membrane distillation setup (to be viewed in color)

The membrane was supported by a spacer on the vacuum side only. Temperatures, pressures, conductivities were measured at the feed inlet and outlet sides and at the permeate side. All sensors logged data onto a computer for the total duration of each experiment. The VMD setup was insulated to prevent heat loss. A detailed description of the experimental setup can be found elsewhere [176]. The permeate flux was calculated using a mass flow meter using Eq. 5.11.

$$J = \frac{\text{vapor massic flux}}{1000 \times A} \qquad \text{Eq. 3.3}$$

Where J is flux ($Kg.m^{-2}.h^{-1}$), vapor flux (g/h) and A (active membrane area, m^2)

3.2.6. Wetting detection tools

The two indicators obtained with the Detection of Dissolved Tracer Intrusion (DDTI) method were used together with wettability indicators like contact angle (CA), surface free energy (SFE), and liquid entry pressure (LEP_w). Following sub-section introduces a brief description of wetting and wettability detection tools. These tools were used together for understanding the influence of the operating parameters towards wetting in membrane distillation.

3.2.6.1. The Detection of Dissolved Tracer Intrusion (DDTI) method

This method was developed and validated in a previous study [176]. It exploits the fact that during MD operation if wetting occurs, solutes (tracers) in the feed can progressively penetrate through the membrane cross-section. The traces of salt left by the liquid intrusion inside pores (attesting partial wetting) or on the permeate side (attesting total wetting) can be detected coupling scanning electron microscopy (SEM) and X-ray dispersion spectroscopy (EDX) micrographs. Liquid intrusion in pores was detected by Cl^- intensities on the membrane permeate surface for the ω_s ratio and through the membrane cross-section for the ω_p ratio.

It allowed defining two indicators namely;

- Totally-wetted surface ratio (ω_s), which quantifies total wetting
- Pore wetting ratio (ω_p), which quantifies the intrusion of liquid inside the membrane

A brief description of the definitions, criteria's and governing equations of each indicator are presented in the following sub-section. Detailed protocols, cleaning strategies, and sampling techniques were described in a previous paper [176].

3.2.6.1.1. Totally-wetted surface ratio (ω_s)

Totally-wetted surface ratio (ω_s) is defined as the proportion of the membrane length in the permeate side covered by salt to the total observed length of the membrane as expressed in ***Eq. 3.4***

$$\omega_s = \frac{\overline{pl}}{T_{ml}} \times 100 \qquad \text{Eq. 3.4}$$

Here $\overline{pl}$ (µm) is the sum of the observed wetted length on the permeate side only and T_{ml} is the total length of the observed membrane in µm.

This indicator was used (cf. **3.3.1**) after cleaning the membrane surface, each membrane was assessed at 9 locations; 3 samples near the feed inlet (A1-A3), 3 on the membrane surface (B1-B3) and 3 at the feed outlet (C1-C3) with an observed cross-section of about 258 µm. After totally-wetted surface ratio analysis, the averaged value for the nine samples were used for further analysis.

3.2.6.1.2. Pore wetting ratio (ωp)

Pore wetting ratio (ω_p) is defined as the proportion of liquid intrusion under a given operating condition detected by the intensity profile of an element of interest through the membrane cross-section. It is a rate of liquid intrusion in the membrane thickness expressed as the ratio of the wetted distance (δ_l) divided by the total distance, i.e., membrane thickness(δ_m)as expressed in Eq. 3.5

$$\omega_p = \frac{\delta_l}{\delta_m} \times 100 \qquad \text{Eq. 3.5}$$

Using the following classification, wetting mechanisms were established as a function of ω_p value.

a) No wetting: if ω_p(0 - 1 %)
b) Surface wetting: if ω_p (1.1-10 %)
c) Partial wetting: if ω_p (10.1-90%)
d) Total wetting: if ω_p (> 90 %)

This indicator was used (cf. **3.3.2**) for each membrane at 10 places (2 samples near the feed inlet A1 – 2), 6 on the membrane surface (B1 – D2) and 3 at the feed outlet (E1 – E2) with an observed cross-section of about 258 x 117 µm. No cleaning of the membrane surface was done before using this indicator. After sample analysis, data treatment was performed for further analysis and interpretation.

3.2.6.1.3. Liquid entry pressure

LEP_w measurements were conducted on both virgin and post experimentation membrane surfaces to evaluate the effects on "wetting pressure." LEP_w of each membrane was assessed at 3 locations (feed inlet, membrane surface, feed outlet) and an averaged value and standard deviation were reported. Standard protocols of LEP_w measurements were used [176].

3.2.6.1.4. Contact angle and surface free energy

Contact angle (CA) and surface free energy (SFE) analyses were conducted on both virgin and used membranes using Drop Shape Analyzer (DSA25, Kruss). For analysis, deionized water (for CA and SFE) and di-iodomethane (for SFE) solutions were used. The results were post-processed using the accompanying software (ADVANCE). For the experimental protocol, standard guidelines and definitions were considered for reproducible measurements of CA and SFE [123,174]. Ellipse (Tangent-1) fitting method was used for estimating the CA. While OWRK Model was used for estimating SFE. Analyses were conducted on each sample using a 28 – 35µl drop using a calibrated syringe with respective solutions at 20°C for CA and SFE respectively. 6-8 samples were used over the active membrane surface (feed side) with averaged results and standard deviation reported.

3.2.6.1.5. Conductivity

Additionally, conductivities were measured both in the feed and in a condensate flask on the permeate side (see **Figure 5.2** C1 & C2) using calibrated conductivity probes (CONDUCELL 4UHF ARC PG-120, Hamilton).

3.3. Results and discussions

3.3.1. Part 1: Potential influence of operating parameters on total wetting

Table 4.2 presents the results obtained in part 1 of this study. Overall it can be noted from **Table 4.2**, that under respective operation conditions the flux varied between about 0 to 11.5 $Kg.m^{-2}.h^{-1}$, the contact angle varied between 67.6 – 118.9°, the SFE ranged between 13.9-50.1, LEP varied between 120-205 kPa and finally the totally wetted surface (ω_s) was between 0 (No wetting) to 78.3 % (total wetting observed in every sample but to a varying degree).

While comparing wettability indicators with the one of the virgin membrane (CA_{ref} 124°, SFE_{ref} 11.5 mN/m and LEP_{ref} 2.05 bar) it can be noted that the operating conditions influenced these membrane properties to a varying degree. At 50°C regardless of the C_f and Re, the CA was 113.9±1.9° which was close to CA_{ref}. It is clear that for all other runs CA was lower than to CA_{ref}, and that SFE was always higher than SFE_{ref} which means that operation makes the membrane more hydrophilic. LEP was very close to LEP_{ref} for 4 runs but lower for all the others. This suggests that wettability was affected during these runs. As for wetted surface analysis, in most studied cases wetting was not found for other runs than for the ones at C_f 166-310 g/L, were wetting observations were persistent but to varying degrees (9 – 78%).

In **Table 4.2** it can be seen that at the lowest saline concentrations (C_f 22g/L), ω_s was in its limit of detection, which means that total wetting was not observed, even by varying Re and T_f. In the replication runs (runs 2, 3, 6 , 10 and 16, all at T_f 42.5, Re 2191, C_f=166 g/L), the dispersion for flux was 4.3 ± 0.5 $Kg.m^{-2}.h^{-1}$, showing quite a good repeatability whereas there were significant variations in CA, SFE were respectively 95.6 ± 18.1 °, 30.7 ± 14.3 mN/m and a slight variation in LEP 1.8 ± 0.2 bar. During these replicates ω_s was 0% for 3 runs and reached 10 % for one run.

It appears that the more repeatable responses are the ones that are measured at a global scale (LEP is measured at the scale of the whole membrane area) and a higher dispersion is observed for the more local indicators, which are based on membrane sampling. Thus, the dispersion can be attributed to membrane heterogeneity. This is indicative that membrane wetting is a localized phenomenon and can vary over the membrane surface depending on membrane morphology. In the following of this chpater, this question will be studied in detail (cf. **3.3.2)**. Similar variations in flux and wetting occurrences can also be seen under the same operating conditions on the repeated runs in **Table 3.2**. These variations can be attributed to the localized morphological changes and interactions on the membrane surface.

In the following section of this work, based on the factors and responses shown in **Table 4.2**, empirical equations were generated to describe ω_s **(**Eq. 3.6**)** and wettability indicators (CA(Eq. 3.7), SFE (*Eq. 3.8*) and LEP) as functions of input process parameters (T_f, Re, C_f). These equations can be valid only for the operating conditions presented here, while the VMD system was operated under constant volume mode (225 g) using the presented membrane cell geometry and membrane.

Table 3.2: Influences of T_f, Re and C_f on flux, wettability indicators (CA, SFE, and LEP_w) and totally wetted surface indicator (ω_s)

Run	Factor A	Factor B	Factor C	Response 1	Response 2	Response 3	Response 4	Response 5
	T_f (°C)	Re (-)	C_f (g/L)	Flux ($Kg.m^{-2}.h^{-1}$)	CA (°)	SFE (mN/m)	LEP_w (bar)	ω_s (%)
1	42.5	4000	22	6.3	116.4	13.9	2.00	0.0
2	42.5	2191	166	3.5	104.2	22.8	1.95	0.0
3	42.5	2191	166	4.3	67.6	41.7	1.40	10.0
4	35	2191	310	0.02	82.5	38.1	1.73	78.0
5	35	2191	22	1.2	107.9	14.6	1.70	0.0
6	42.5	2191	166	4.6	112.0	19.9	1.97	0.0
7	50	382	166	6.9	116.3	19.7	1.57	11.0
8	42.5	4000	310	1.4	103.5	34.6	1.77	9.0
9	42.5	382	310	1.4	92.7	29.7	1.73	68.0
10	42.5	2191	166	4.6	87.6	50.1	1.63	0.0
11	50	2191	310	2.8	114.3	18.8	1.50	32.0
12	50	2191	22	11.5	113.3	23.3	2.05	0.0
13	42.5	382	22	3.8	118.9	16.1	1.43	0.0
14	35	382	166	0.4	90.6	22.2	1.20	5.0
15	50	4000	166	10.1	111.7	25.3	1.53	0.0
16	42.5	2191	166	4.5	106.4	18.9	1.80	1.0
17	35	4000	166	1.1	74.8	40.1	1.60	24.0
Min				0.02	67.6	13.85	1.2	0
Max				11.47	118.9	50.1	2.05	78
Mean ± S.D.				4.03±3.2	101.2±15.7	26.45±10.7	1.6±0.23	14.1±24.2

3.3.1.1. Relationship between the totally-wetted surface ratio (ω_s) and operating parameters

Considering ω_s, a natural log transformation ($y' = \ln(y + k)$) was required to fit the model with a constant (k) of 0.078. It shows that ω_s principally depends on salinity (C_f) and to a lesser extent to temperature (T_f) and Reynolds number (Re). The resulting model equation is presented in Eq. 3.6.

$$\ln(\omega_s + 0.08) = -9.33 + (0.16T_f) + (4.67 \times 10^{-3}Re) + (0.021C_f) - (1.18 \times 10^{-4}T_fRe) \quad \text{Eq. 3.6}$$

To understand the generated model's accuracy, the values computed with Eq. 3.6 were plotted against the experimental values in **Figure 3.3**. For ω_s, the computed and the experimental data are in good agreement for lower values, but computed values are higher than the experimental one at higher values corresponding to totally wetted surface. So, the Eq. 3.6 is over-estimating ω_s when wetting becomes severe (cases of run 4 and 9, both corresponding to a salt concentration of 310 g/L).

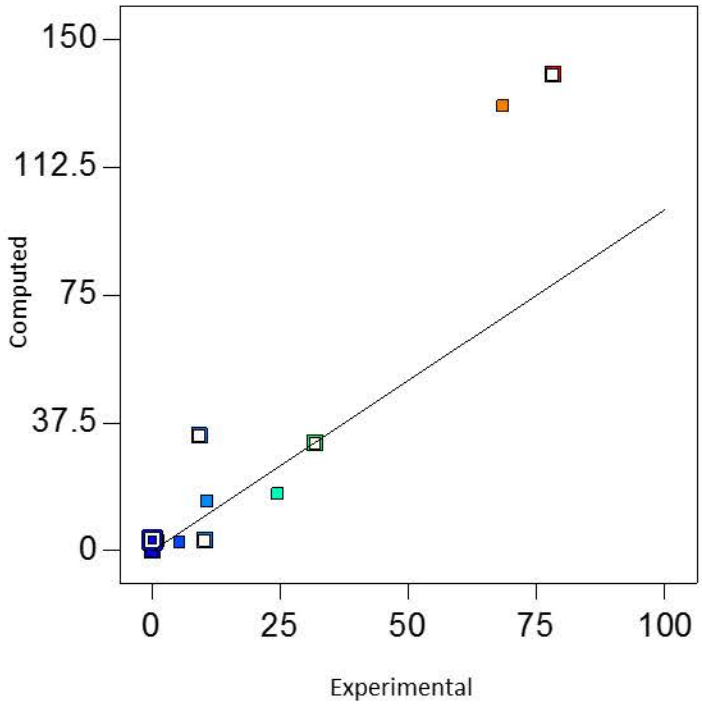

Figure 3.3: Computed value vs experimental data for the totally wetted surface ratio ω_s

These observed variations in computed data might be due to the limitation of BBD itself or to the fact same some parameters that may be influent have not been considered initially in our experimental

strategy. Zolgharnein et al. [185], have emphasized that although BBD is derived from a cube based design, however, it is a spherical design, so the edges of this design (extreme combinations of factors) are not concealed in this approach. Consequently, the model avoids the extreme combination of operating conditions thus it has greater variability at the extremities of the design space. Thus, it is safe to point out that Eq. 3.6 is only valid under the range of studied operating conditions, and as said before for moderate values of ω_s. Interpretation based on extreme operating conditions and saline concentrations should be dealt with considerable reservations. However, the model can be used to visualize the possible tendencies in the parameters interactions.

Using Eq. 3.6, ω_s was computed for saline concentrations of 22 (a), 166 (b) and 310 g/L (c) and **Figure 4.4** introduces the interactive effects of temperature and Reynolds number on ω_s. The x-axis presents the temperature (T_f) in the range of 35 - 50°C and the y-axis presents the Reynolds number (Re) from 382 to 4000 respectively. The lines introduced on each graph are the iso-ω_s lines and the colors are blue when ω_s is close to 0 (no wettability) and red when ω_s approaches 100%.

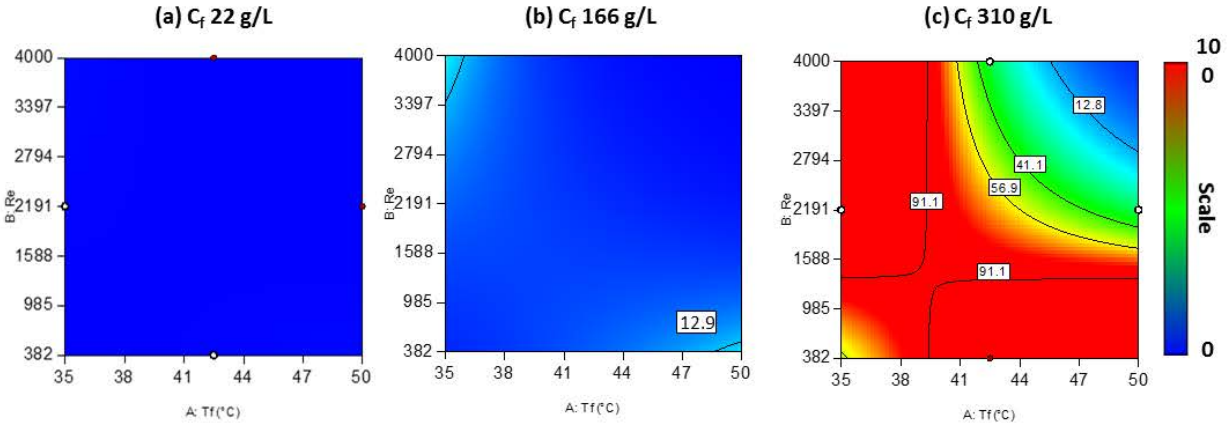

Figure 3.4: Computed values of totally-wetted surface ratio (ω_s) at (a) 22 g/L (b) 166 g/L and (c) 310 g/L NaCl concentrations (to be viewed in color)

As represented in **Figure 4.4** (a) low values of ω_s, attesting non-occurrence of total wetting (low values of ω_s), are observed for the lowest saline concentrations (C_f 22g/L), in all the range of T_f and Re values. As the salinity (C_f) increases to 166 g/L NaCl, (Figure 4.4 (b)), ω_s is quite low in all the experimental area and a slight increase is observed at the two extremities i.e. with the combination of highest Re (4000) and lowest temperature (35°C) and lowest Re (382) at high T_f (50°C), where computed value of ω_s was 13 % (to be compared to 24 and 11% for the corresponding experimental runs, runs 17 and 7). At the highest saline

concentration, the model predicts that total wetting could become significant in a large area of the experimental domain and mainly for the lower temperatures (T_f 35 – 42.5°C). Both Re and T are influencing wetting. Depending on these parameters, wetting could be low (about 13 %) or high (91 %) if temperature or Re are low. This might be explained by the fact that for at this high concentration and for low Re and low temperature, the local salt concentration at the membrane surface might be close to saturation and crystallization at the membrane surface could be a kind of inducer of pore wetting.

In conclusion, for concentrations of 22 to 166 g/L total membrane wetting is low and is poorly affected by T_f and Re. Whereas for very high concentrations of 310 g/L, the influence of T_f and Re becomes sensitive and the choice of these values is determinant to avoid wetting. Both high temperature and high Re values are required in the process otherwise totally-wetted surface ratio can become significant.

As previously stated, factors like temperature and Reynolds number had a lower influence than salinity on wetting in this study. Normal operating conditions (T_f $(35-50°C), Re(382-4000)$) within this range do not affect wetting greatly for the current operation mode and membrane. However, if data obtained from flux, CA and SFE responses are considered, it can be concluded that T_f at $35°C$ would not be a suitable operating condition (under any Re and C_f) for membrane distillation with a vacuum pressure of 6 kPa in this PVDF membrane. As the driving force in VMD is the difference between the partial pressure of the feed solution and the applied vacuum, therefore at lower temperatures, the driving force is reduced resulting in low fluxes. Additionally, as the process progresses, the feed salinity further increases due to the mass transfer across the membrane, resulting in further reduction of the driving force. This eventually results in heightened changes of nucleation sites on the membrane surface thereby increasing wetting occurrences.

In the narrow feed channel, increasing the Re not only reduces the concentration polarization effect but also increases the hydrostatic pressure experienced by the membrane surface. As a result, some of the biggest pores on the membrane surface get compromised therefore resulting in pore wetting. This is due to the local hydrostatic pressure generated by the fluid flow on the membrane surface exceeding the membranes intrinsic liquid entry pressure (LEP_w). Gryta [107] reported that the hydrodynamic conditions influenced total wetting in some membrane pores (observed using a rise in conductivity in the permeate) and suggested the hydraulic pressure to be maintained as low as possible to restrict wettability.

3.3.1.2. Relationship between the wettability indicators and operating parameters

Regarding contact angle (CA), based on the experimental run and after ANOVA tests, no transformation was required to fit the experimental data for establishing a relationship between CA and the operating parameters. Only two operating parameters, T_f and C_f are required to obtain CA, as presented in Eq. 3.7.

$$\mathrm{CA} = 39.75 + 1.66\mathrm{T_f} - 0.055\mathrm{C_f} \qquad \text{Eq. 3.7}$$

For SFE, an inverse transformation ($y' = \left({}^{1}/_{y+1}\right)$ was required to fit the model with constant (k) of -0.81. After ANOVA tests, it was found that the interactions between operating parameters and SFE energy can be described by Eq. 3.8.

$$\frac{1}{(\mathrm{SFE} - 0.81)} = 0.14 - (1.81 \times 10^{-3}\mathrm{T_f}) - (6.5810^{-4} \times \mathrm{C_f}) + (1.31 \times 10^{-5}\mathrm{T_f C_f}) \qquad \text{Eq. 3.8}$$

These equations integer the fact that SFE does not depend on Re but shows a dependency on temperature($\mathrm{T_f}$) and salt concentration ($\mathrm{C_f}$).

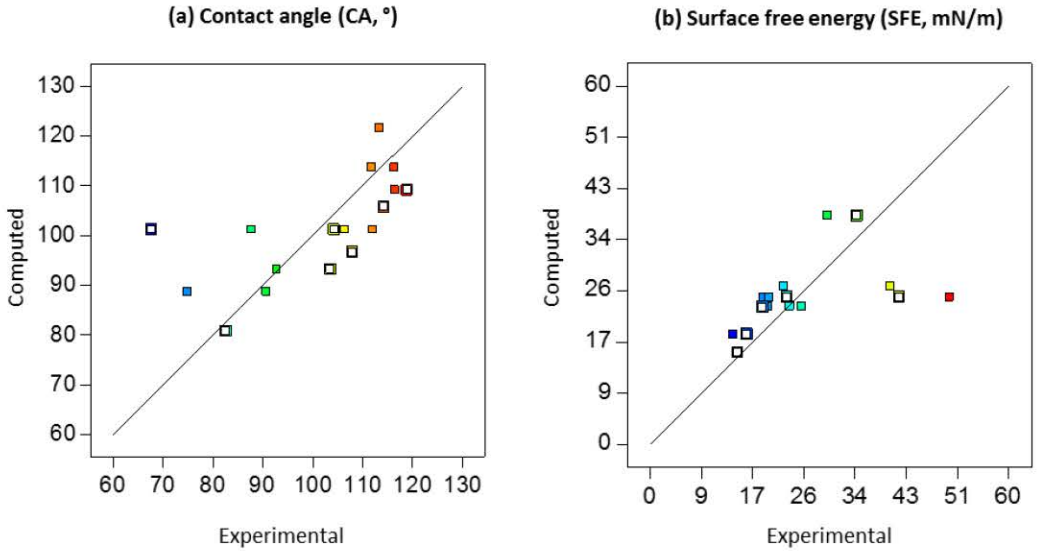

Figure 3.5: Computed value vs experimental data for (a) contact angle and (b) surface free energy

Concerning LEP, it varied between 1.5 – 2.05 bar during Runs 1- 17 even though the operating conditions varied significantly (**Figure 3.6(e)).** It can be observed w.r.t the standard deviation that the LEP_w fluctuated between 0.06- 0.5 bars within all the samples but did not deviate as compared to LEP_{ref} 2.05 bar. Based on

ANOVA tests under the studied conditions, no correlation could be established between LEP and the operating conditions. In the present study, the only information that could be deduced was that a decrease in LEP was observed after each experimental run compared with the LEP_{ref}.

As for CA, the computed values are higher than the experimental ones for the lowest values (below 80°), but the accuracy is good above this limit value. Similarly, accuracy is good for SFE for most data with three exceptions at the higher end as seen in ***Figure* 3.5(b)**. The calculated values obtained for Contact angle (CA) and Surface free energy (SFE) and the experimental values of LEP_w are presented in Figure 3.6.

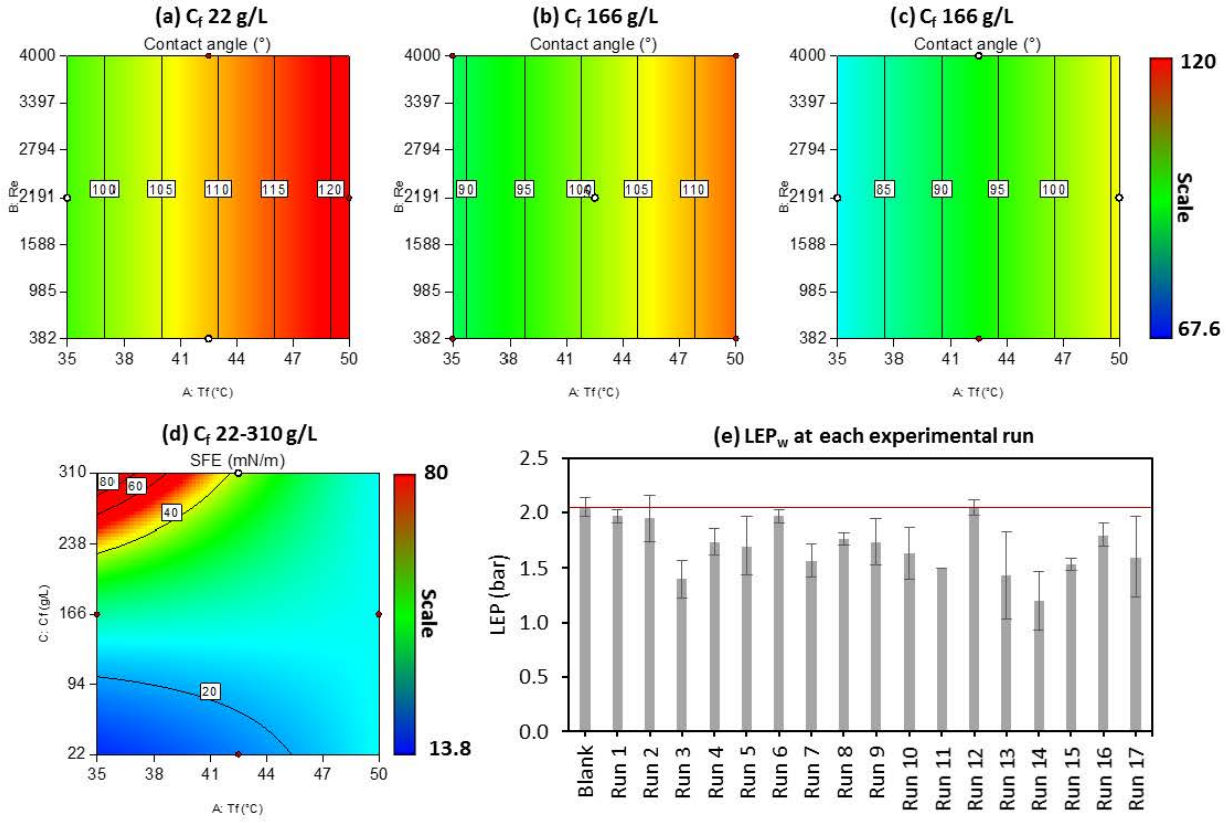

Figure 3.6: Calculated values at (a) 22 g/L (b) 166 g/L and (c) 310 g/L NaCl concentrations for Contact angle (d) SFE at 22-310 g/L NaCl and (e) experimental values of LEP for the 17 runs (to be viewed in color)

Figure 3.6 shows clearly that whatever the concentration, CA is not influenced by Re (which is not a parameter in Eq. 3.7) but is influenced by T_f. For each concentration (see Figure 3.6 **a, b and c**), CA increases with an increase in temperature, and it is close to the CA of the virgin membrane at the higher temperature (50°C). These results on the influence of temperature are in contradiction with the observations [102] reporting a reduction in contact angle with an increase in temperature for samples tested with 35 g/L NaCl

solutions. For the lower C_f value(22 g/L), the contact angle computed by Eq. 3.7 (Figure 3.6 (a, b, c)) is always lower than the one of the virgin membrane, and thus a loss of hydrophobicity occurs, and the lowest obtained value was 67.6°. This is consistent with literature reporting significant variation in CA even at low saline concentrations. For example, loss in membrane hydrophobicity was observed after 1 [127] to 30 h [126] of operation with seawater in DCMD configuration. When salinity increases from 22 g/L Figure 3.6 (a) to 166 g/L Figure 3.6 (b) and 310 g/L Figure 3.6 (c), the value of CA obtained at the lower temperature (35°C) decreases, meaning that the membrane becomes less hydrophobic. At this temperature, for 166 g/L the CA was about90°, and corresponds to the limit of hydrophobicity. For 310 g/L the CA was 81°, which corresponds to hydrophilicity.

The lower the surface free energy higher the membrane hydrophobicity with lesser tendency to interact with the feed solution. **Figure 3.8 (d)** shows that SFE is close to the one of the virgin membrane (11.55+ 3.8 mN/m) for low temperatures and low concentrations. Its value increases when concentration increases and its maximal value (50.1 mN/m) is observed at the highest concentration and lower temperature. It is noticeable that this set of operating conditions also corresponds to the highest value of ω_s, and thus high SFE are correlated with a high proportion of total wetting.

3.3.2. Part 2: Influence of operating parameters on partial pore wetting

In the second part of the study, in order to better understand the influence of salt concentration at the early stage of wetting, that is to say during liquid intrusion in pores, independent experiments were performed at varying saline concentrations C_f with identical other operating conditions (cf.**3.2.2**). Both pore wetting, and wettability were assessed using the pore wetting ratio ω_p and the 3 wettability indicators: CA, SFE and, LEP_w.

3.3.2.1. Influence of salinity on pore wetting ratio (ω_p)

All the studied membranes were sampled at the same locations to reduce bias based on sampling locations. Pore wetting ratio for each location on the studied membrane are summarized in **Table 3.3** and the Cl^- intensity profiles (for B1-D2) are presented in **Figure 3.7.**

Based on the ω_p evaluation, for a salinity of 22 g/L, no wetting was observed for 5 samples, whereas surface, partial and total wetting were observed at 3, 1 and 1 locations respectively. As the salinity increases, the number of no wetting observations ($\omega_p = 0$) could be seen to be diminishing. As seen in **Table**

3, for all salinities at least 1 sample was observed to have total wetting, and the worst situation is observed for salinity of 250 g/L where total wetting (ω_p = 100) had occurred at 6 sampling locations.

Table 3.3: Pore wetting ratio at each sampling location on the membrane surface

Salinity	Pore wetting ratio (ω_p)									
(g/L)	A1	A2	B1	B2	C1	C2	D1	D2	E1	E2
22	2.2	0	3.5	3.5	0	0	0	64.5	0	99.2
35	3.4	2.2	100	1.6	0	0	2.5	2.4	0	0
60	100	0	99.7	1.6	100	1.8	2.3	10.9	1.5	2.3
100	0	1.2	30.8	100	2.3	84.8	1.7	0.6	0	98.1
130	0	0	78.6	56.8	60.3	4.4	2.8	0	100	2
166	2.4	2.3	97.1	2.1	11.3	1.3	2.7	0	2.4	0.3
200	100	2.8	0.8	1.9	0.6	0	0.6	1.3	2.4	1.7
250	0.6	1.7	100	100	100	100	100	100	2	0
310	2.2	87.9	2.1	2.6	2.5	10.1	2.5	100	0.9	100

The variation in ω_p is an indication of motion of the L/V interface at the local scale. To reveal more information about the influence of salinity on wetting mechanisms, analysis of different wetting mechanisms can be made by comparing the different gray value profiles obtained for the membranes subjected to different salinities. As nine saline solutions were studied they were categorized into 3 broad groups considering the salinity of the solution as follows:

1. Low to medium salinity (22, 35, 60 g/L NaCl solutions): **Figure 3.7** (a,b,c)
2. Medium to high salinity (100, 130, 166 g/L NaCl solutions): **Figure 3.7** (d,e,f)
3. High to hyper-salinity (200, 250, 310 g/L NaCl solutions): **Figure 3.7** (g,h,i)

In each **Figure**, the x-axis is the membrane cross-section while the y-axis is the Cl^- intensity profile through the membrane cross-section at sampling locations (B1-D2) which are in the more central part of the filtration cell, where the flow is well established. At low to medium salinity, a progressive increase in surface wetting can be observed. As the salinity increases from 22 to 60 g/L NaCl, more and more sampling locations present surface wetting. Whereas, partial wetting was only detected at C_f 22 g/L and total wetting was observed at both 35 and 60 g/L NaCl concentrations.

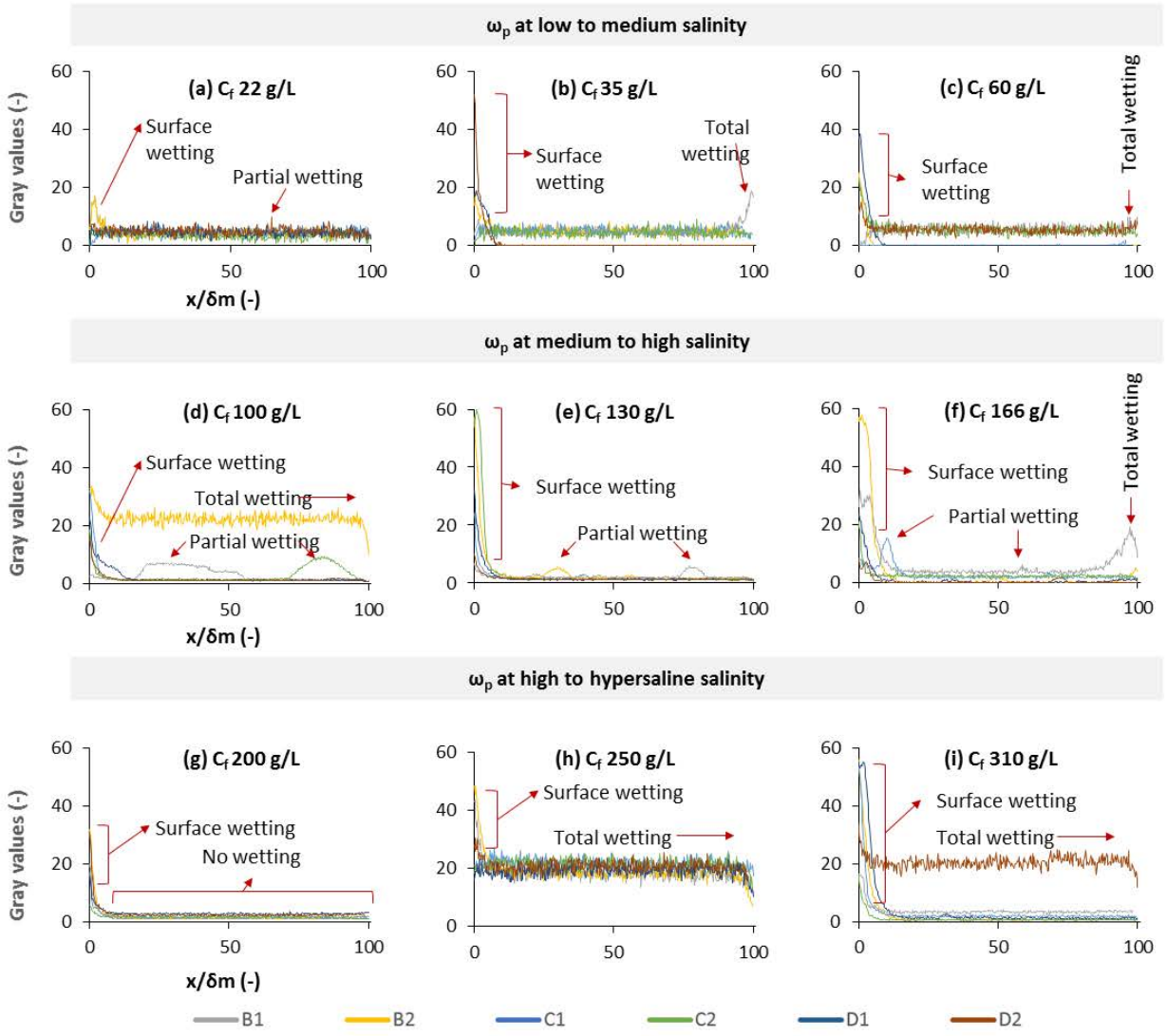

Figure 3.7: Sampling membrane cross-section for Cl^- intensity at (a,b,c) low to medium salt concentrations (d,e,f) medium to high salt concentrations (g,h,i) high to hypersaline salt concentrations (to be viewed in color)

Observations at medium to high feed salt concentration (100-166g/L), show that surface wetting started to become dominant with an increase in observations as compared to no wetting for this range of salinity. In **Figure 3.7** (d,e & f), various Cl^- peak intensities at different sampling locations can be observed indicative of partial wetting. Some of these observations are labeled on the **Figure** for easier visualization. These observations are attributed to a slight motion of L/V interface inside pores. Also, it must be noted that some cases (or locations) of partial wetting and total wetting are also observed in this group (for example in locations E1 and B1).

At high to hypersaline concentration (200- 310g/L NaCl), the behavior is very different at 200 g/L and at higher concentrations. Only surface wetting or no wetting was observed at 200 g/L NaCl solution in the central parts of the cell (locations B1-D2). At C_f 250 and 310 g/L surface wetting was also observed.

Moreover, for most locations at 250 g/L and one location at 310 g/L the profile corresponds to a uniform high intensity of Cl^- across all the membrane cross-section. This is the proof of intrusion of liquid along all the membrane thickness that is to say of total pore wetting, occurring at the local scale. It means that the L/V interface has been disrupted, leading to the convective transportation of the feed through the membrane pores. It can be deduced that greater interactions between the feed solution due to salinity, and maybe to crystallization due to saturation at the membrane surface could lead to frequent wetting occurrences. However, at this stage the link between crystallization and wetting (according to our definition) is not established. Literature complements the evidence of an increase in wettability at higher salt concentrations [158,186]. A general trend emerges that the frequency of surface, partial and total wetting increases from low salinity to hypersaline concentrations and that, for the studied membrane, the occurrence of total wetting becomes significant for the more hypersaline solutions.

3.3.2.2. Influence of partial pressure and saline solution on sampling location for wetting

Due to the observations of various wetting mechanisms at all studied salinities, an effort was made to visualize the effects of the partial pressure of the saline solution (**Figure 3.8**(a)) at one location and salinity (**Figure 3.8**(b)) concerning all sampling locations. **Figure 3.8**(a)) presents the averaged value of pore wetting ratio at locations C1 and C2 as a function of the difference in partial pressure on both sides of the membrane (using Eq. 3.9)

$$\Delta P_{H20} = P_m - P_p = \alpha_{H20}.P_m^* - P_p \qquad \text{Eq. 3.9}$$

Where, ΔP_{H20} is the difference in partial pressure on both sides of the membrane (kPa), α_{H20} is the activity coefficient of water calculated at 42.5°C using PHREEQC-2, χ_{NaCl} molar fraction of water with NaCl in the feed solution and P_m^* is the partial pressure (kPa) of pure water at 42.5°C and P_p is the partial pressure of water on the permeate side.(kPa)

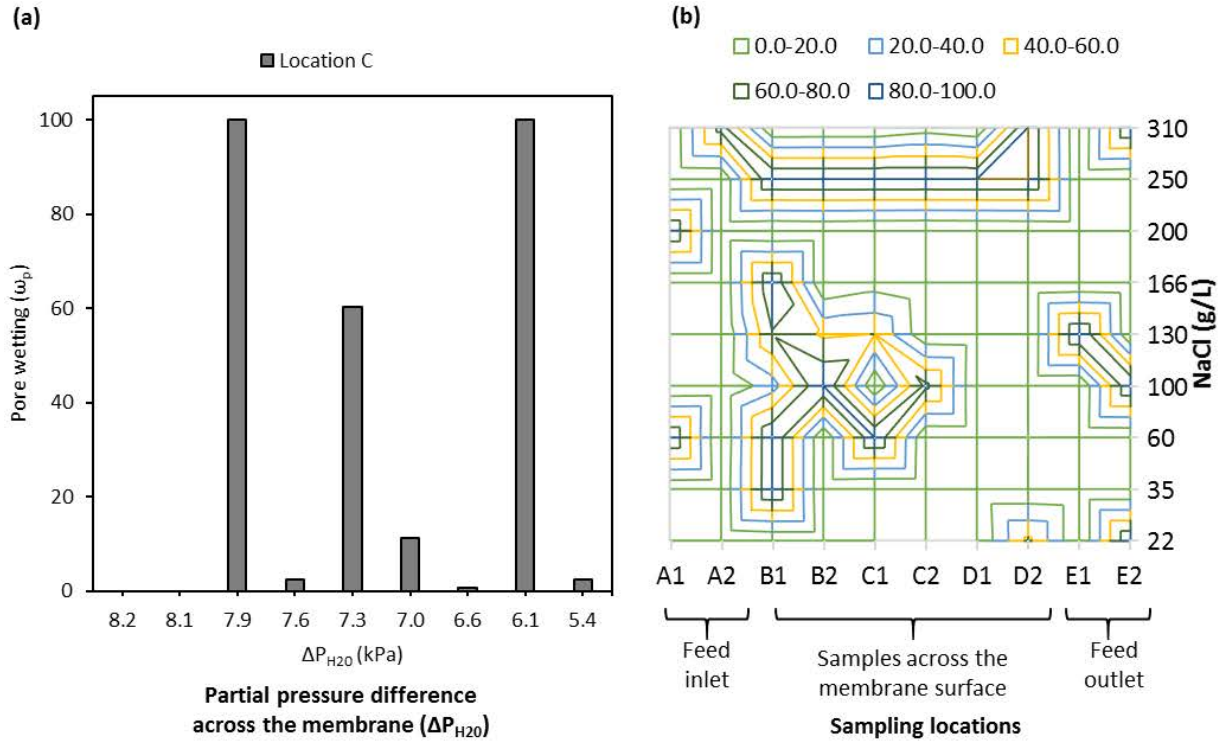

Figure 3.8: Location based pore wetting (ω_p) (a) at location C on the membrane surface for different ΔP_{H20} and (b) at all sampling locations at different NaCl concentrations (to be viewed in color)

In **Figure 3.8**(a)) it can be observed that at a given location (C) under the same operating conditions (T_f 42.5°C and Re 2191) there is no relationship between ω_p and partial pressure. However, it can be noted that at the higher partial pressure of 8.2 and 8.1 kPa (that is to say C_f 22 and 35 g/L) no pore wetting was observed. By taking into account the partial pressure difference (ΔP_{H20}) experienced by the membrane, pore wetting ratio (ω_p) at this location (C) fluctuates to varying intensities. One possible explanation for this random comportment is that ω_p is measured at the local scale and that the heterogeneity of membrane morphology at the local scale (surface charge, roughness and pore size distribution) might be responsible for these large variations.

On the other hand, **Figure 3.8** (b) presents ω_p as a 2D plot, where the sampling location from A1 to E2 are represented on the x-axis, while the y-axis presents all the studied salinities. A color code was defined, where ω_p is categorized by groups of 20 depending on the intensity, where 0-20 being no to little pore wetting and 80-100 being total pore wetting. Based on this **Figure**, it can be inferred that most wetting occurrences on the membrane surface were observed near to the feed inlet (Sampling locations A1-C1)

and some across the membrane surface with few observations on the feed outlet. This is indicative of the influence of pressure drop on wetting from the feed inlet to the feed outlet on the membrane surface. However, several occurrences of various wetting mechanisms can be observed at high to hypersaline solution at C_f 200 to 310 /L.

The membrane cell used in this study is designed like conventional flat sheet cell, and similar to commercially available MD filtration cells for laboratories where the feed inlet and outlet ports of the membrane module are located directly under the membrane surface at each end. This creates a high-pressure zone at the inlet, some low-pressure zones at the outlet and some dead zones on the edge of the membrane. This high pressure drop on the membrane surface may be more favorable to induce wetting as demonstrated by more wetting observations close to the feed inlet port. So, in order to avoid wetting a specific attention should be paid to module design to limit the risk of wetting in these specific areas. The DDTI method could be an interesting tool to help orientate the design, by testing different configurations. See supplementary data for Chapter 4 for more information.

3.3.2.3. Influence of salinity on wettability indicators

Wettability indicators present similar trends as the first part of this study. **Figure 3.9** shows clearly that CA and SFE have a linearity with salinity. Where CA is a linear decreasing function of the salt concentration and surface free energy is also linearly increasing as a function of the concentration which could be attributed to a negative interaction of increasing salinity on this membrane surface after operation. The increase in salinity globally implies loss of membrane's hydrophobicity as compared to CA_{ref} and SFE_{ref}. The fluctuation in standard deviation within each sample varied greatly for both CA and SFE, indicating the heterogeneity of interactions on the membrane surface.

With respect to liquid entry pressure here again, as in the first part of this study, this parameter appears as very constant and without sensitivity to salinity. The only definitive interpretation could be that LEP fluctuated with a slight decrease from the membranes virgin properties.

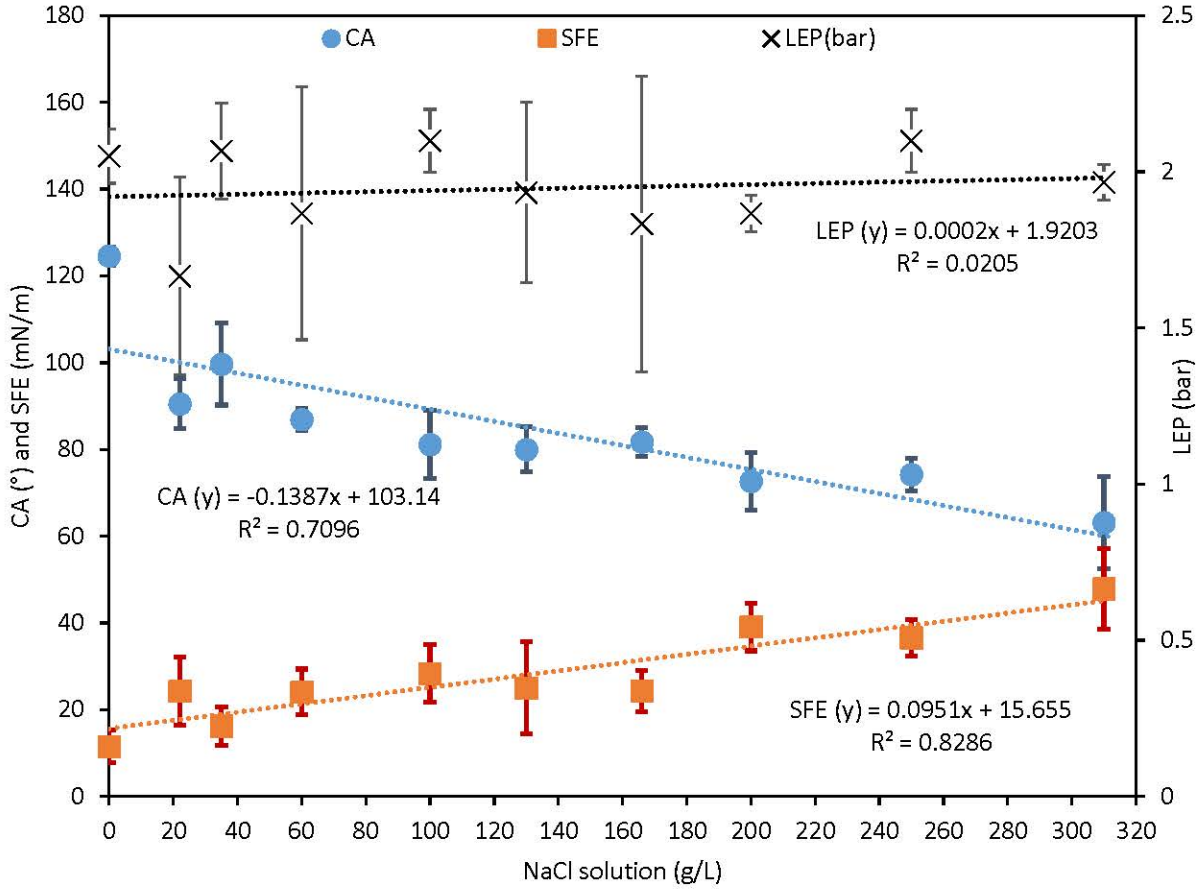

Figure 3.9: Relationship between saline concentration and wettability parameters (a) contact angle (CA), surface free energy (SFE) and Liquid entry pressure (LEP)

However, it is interesting to note that after washing the membrane surface with D.I. water there was a significant restoration of the membrane wettability indicators (CA and SFE) as compared to CA_{ref} and SFE_{ref}. As seen in **Figure 4.10 (a and b)** after washing, contact angle was restored to 90° but to varying degrees and linearity could not be established. Comparatively, the SFE after washing did reduce but fluctuated greatly both within the same sample and across salinities. No linear trends could be observed for the cleaned membranes for both wettability indicators. This rather reveals the discrepancy in interactions on the membrane surface even after cleaning.

Further research and interpretation are needed on SFE as contributions towards polar and disperse interaction on the membrane surface were not the same as in virgin membrane. As PVDF material has only disperse component and after being subjected to the operating conditions with increasing solute concentrations there was a significant increase in polar interactions. Even though it may seem like the

overall SFE had reduced but the surface properties were modified. However, the evaluation of the capability to restore the non-wetting properties of a wetted membrane is still to be performed.

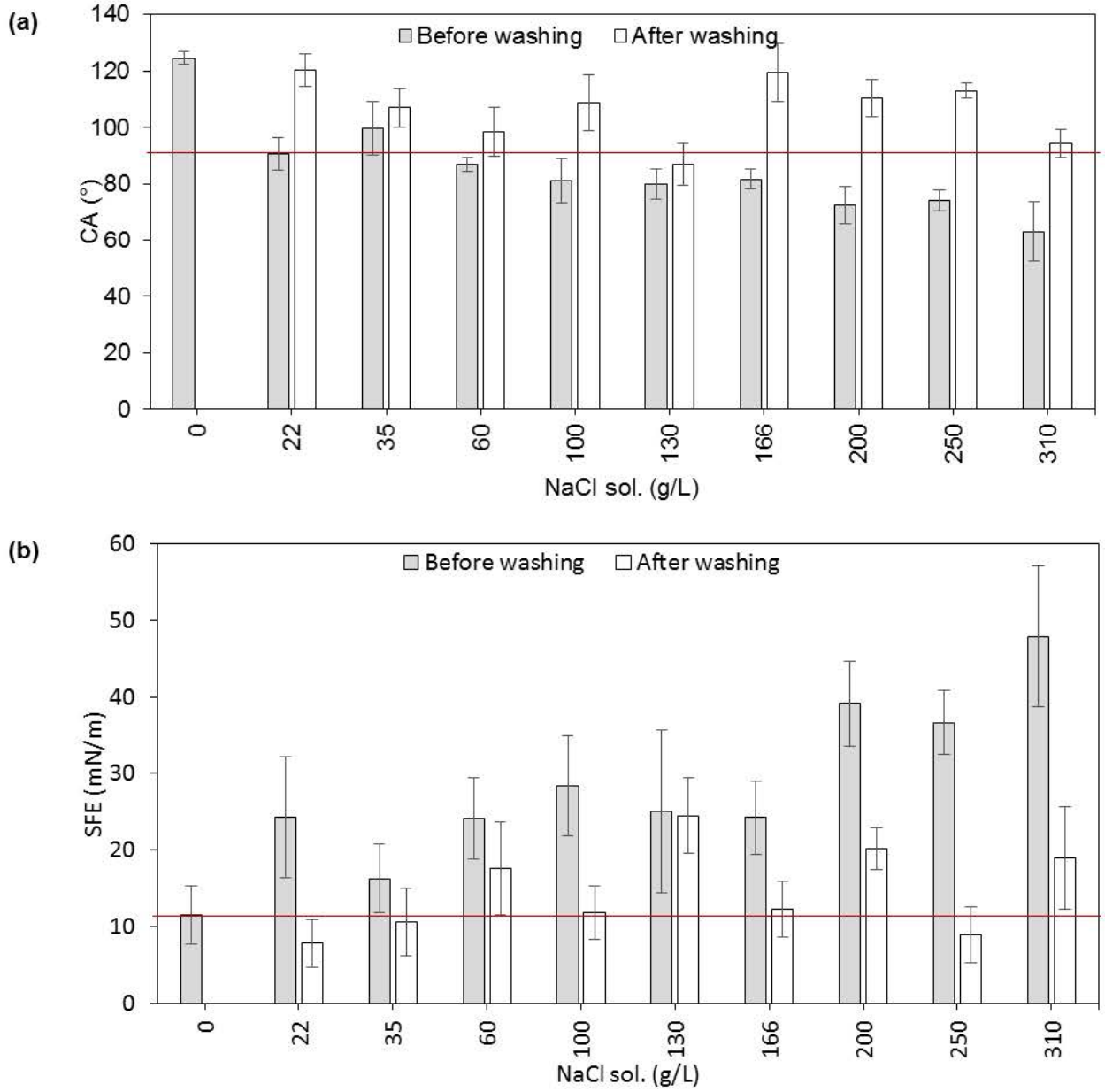

Figure *3.10*: *Wettability indicators (a) contact angle (b) surface free energy before and after cleaning the membrane surface*

3.4. Conclusions and perspectives

In English

The growing interest in commercializing membrane distillation necessitates a deeper understanding to choose better membranes and operating parameters to prevent the risk of wetting. This study aimed at understanding the potential interactions of temperature (35 – 50°C), Reynolds number (400 – 4000) and salinity (22 – 310 g/L NaCl solution) on wetting during VMD operation with a PVDF membrane (0.22 µm). Wetting was evaluated using the recently developed DDTI method together with wettability indicators (LEP, CA and SFE).

In the first part of the study the interactions between the operating parameters on total wetting were studied using a Box Behnken design of experiments. The generated model did reveal some complex interactions between the three operating parameters on totally wetted surface ratio (wetting indicator) and wettability indicators (CA and SFE) with salinity (C_f) being a more sensitive parameter. At feed salinities lower than 166 g/L NaCl, totally wetted surface ratio (ω_s) was marginally affected by a change in temperature and Reynolds number. However, at hypersaline concentrations (C_f 310 g/L), an increase in temperature and Reynolds number facilitated avoiding total wetting. Contact angle and surface free energy are the intrinsic membrane properties which were only affected by the temperature and salinity, but no interactions were identifiable considering Reynolds number. Though care should be taken as the models do diverge at the extremities of the design space resulting in discrepancies in computes and experimental values.

In the second step of the study, the feed temperature (42.5°C) and Reynolds numbers (2199) were fixed while the feed salinity was varied to quantify liquid intrusion in the PDVF membrane pores using the pore wetting ratio (ω_p). It appears that an increase in salinity primarily induces surface wetting which later results in either partial or total wetting with an evidence of total wetting only for hypersaline concentrations (higher than 200 g/L). However, it is clear that CA and SFE vary linearly with salinity as membrane hydrophobicity decreases and surface interactions increase with an increase in salinity. However, LEP is not significantly affected by salinity and remains almost constant

As a conclusion, this study showed that the operating parameters must be chosen carefully to prevent wetting and that for hypersaline solutions the choice of the membrane itself is a key issue. Future studies could continue using the DDTI method to further determine the conditions for making membrane

distillation even more reliable. Focus could be given on the influence of vacuum pressures and on membrane screening in order to select some membranes that are less sensitive to hypersaline solutions. Additionally, special attention should be paid in designing membrane distillation modules to reduce the impact of wetting occurrences due to local hydrostatic pressure.

En français

L'intérêt croissant pour la commercialisation de la distillation membranaire nécessite une meilleure compréhension afin de choisir de meilleures membranes et paramètres de fonctionnement permettant de limiter le risque de mouillage. Cette étude vise à comprendre les effets potentiels de la température (35 - 50 ° C), du nombre de Reynolds (400-4000) et de la salinité (22-310 g / L de solution de NaCl) sur le mouillage au cours d'une distillation membranaire sous vide menée avec une membrane en PVDF (0,22 pm). Le mouillage a été évalué à l'aide de la méthode DDTI récemment mise au point et avec des indicateurs de mouillabilité (LEP, CA et SFE).

Dans la première partie de l'étude, les effets des paramètres de fonctionnement sur le mouillage total ont été étudiés à l'aide d'un plan d'expériences Box Behnken. Le modèle généré a révélé des interactions complexes entre les trois paramètres de fonctionnement sur le rapport de surface totalement mouillée (indicateur de mouillage) et les indicateurs de mouillabilité (CA et SFE), la salinité (Cf) étant un paramètre plus sensible. Aux salinités d'alimentation inférieures à 166 g / L de NaCl, le rapport de surface totalement mouillé (ws) était peu affecté par un changement de température et du nombre de Reynolds. Cependant, à des concentrations hypersalines (Cf 310 g / L), une augmentation de la température et du nombre de Reynolds a permis d'éviter le mouillage total. L'angle de contact et l'énergie libre de surface sont des propriétés intrinsèques de la membrane qui ne sont affectées que par la température et la salinité, et pas par le nombre de Reynolds. Il faut toutefois faire attention car les modèles divergent aux extrémités de l'espace de conception, ce qui se traduit par des écarts importants entre valeurs calculées et valeurs expérimentales.

Dans la deuxième étape de l'étude, la température de l'alimentation (42,5 ° C) et le nombre de Reynolds (2199) ont été fixés, et seule la salinité de l'alimentation a varié. L'étude a consisté à quantifier l'intrusion de liquide dans les pores de la membrane de PDVF en utilisant le rapport de mouillage des pores (wp). Il semble qu'une augmentation de la salinité induise principalement un mouillage de surface qui se traduit par la suite par un mouillage partiel ou total avec une preuve de mouillage total uniquement pour les

concentrations hypersalines (supérieures à 200 g / L). Il est également apparu que le CA et le SFE varient linéairement avec la salinité à mesure que l'hydrophobicité de la membrane diminue et que les interactions de surface augmentent avec une augmentation de la salinité. Cependant, la salinité n'affecte pas le LEP de manière significative et reste presque constant.

En conclusion, cette étude a montré que les paramètres de fonctionnement doivent être choisis avec soin pour éviter le mouillage et que, pour les solutions hypersalines, le choix de la membrane elle-même est un problème clé. Les études futures pourraient continuer à utiliser la méthode DDTI afin de déterminer plus en détail les conditions pour rendre la distillation membranaire encore plus fiable. L'accent pourrait être mis sur l'influence des pressions de vide et sur le criblage des membranes afin de sélectionner des membranes moins sensibles aux solutions hypersalines. De plus, une attention particulière doit être accordée à la conception des modules de distillation à membrane afin de réduire l'impact des phénomènes de mouillage dus à la pression hydrostatique locale.

Acknowledgements

I would like to thank Mr. Tianyi Zhang for his support for wettability analysis of Part 2 this chapter. Fabric'INSA and the physics department of INSA Toulouse are acknowledged for providing access to laser cutter and to SEM/EDX respectively. Additionally, I would like to thank ANR (Agence nationale de la recherche) Programme : Innovation technologique pour analyser, remédier ou réduire les risques environnementaux (DS0102) 2014 for funding projet WETMEM (ANR-14-CE04-0008).

Preface to Chapter 4

By using the wetting indicators developed in **Chapter 2** and utilizing them in **Chapter 3** leads towards the conclusions that wetting is strictly localized and its occurrence on the membrane surface under the same operating parameters may vary greatly depending on the local hydrodynamics and membrane morphologies. The techniques developed in **Chapter 2** are only capable of identifying wetting occurrences after the MD process has ended. Therefore, there was a need to identify wetting mechanisms *in-situ* to better understand the nature of wetting propagation during the MD process. In **Chapter 1**, the most common in-situ technique for wetting is conductivity measurements and this tool only indicates the occurrence of total wetting in some pores and does not give any information on the location of the wetting occurrence on the membrane surface. Therefore, **Chapter 4** is dedicated to the development of an optical tools that allows to identify and visualize *in-situ* occurrences of wetting mechanisms. **Chapter 4** details on the development of a new membrane module, optical device and the image treatment algorithm that can visualize wetting propagation at a macro and meso scales. Finally, the observations from the optical tool (at meso scale) are compared and validated using the wetting indicators developed previously in **Chapter 2.**

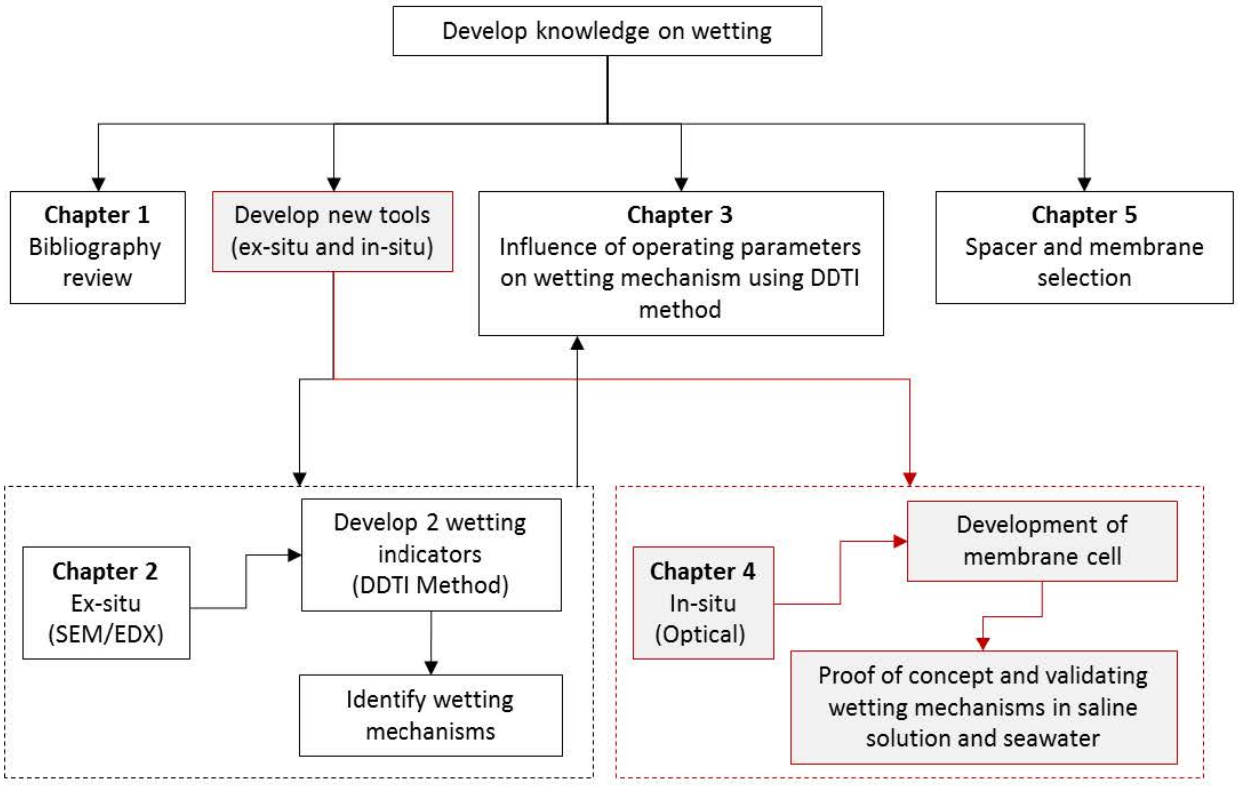

Chapter 4 : An *in-situ* optical tool for visualizing and understanding wetting propagation in membrane distillation: The proof of concept

Summary of objective (in English)

This chapter describes the development of a new optical tool to detect *in-situ* wetting in vacuum membrane distillation. With this objective, the theory of wetting detection exploiting the phenomenon of light transmission is developed, and the proof of concept of this optical tool is validated using scanning electron microscopy and x-ray dispersion spectroscopy. The tool was additionally tested in standard operating conditions (feed temperature 40°C, laminar flow and vacuum pressure 6kPa) for vacuum membrane distillation with water, saline solution, and seawaters. Controlled wetting was inducted using surfactant after 30 min of operation and wetting progression could be effectively visualized. Additionally, the scalability (macro and mesoscales) of this tool was verified and wetting was visualized at different locations on the membrane surface and compared with the global wetting observation

Résumé de l'objectif (en français)

Ce chapitre décrit le développement d'un nouvel outil optique de détection in situ du mouillage en distillation membranaire sous vide. Dans cet objectif, la théorie de détection de mouillage basée sur le phénomène de transmission de la lumière est développée, et la preuve de concept de cet outil optique est validée grâce à la microscopie électronique à balayage. L'outil est ensuite testé dans des conditions opératoires standards (température d'alimentation de 40°C, régime laminaire et pression de vide de 6 kPa), pour la distillation membranaire sous vide de différentes solutions d'alimentation, notamment une solution saline synthétique et des eaux de mer réelles. Le mouillage de la membrane est provoqué au bout de 30 min d'opération, grâce à l'ajout de surfactant, et la progression de ce mouillage peut être effectivement visualisée. Enfin, l'évolutivité de l'outil (échelle globale et locale) a été validée. La progression du mouillage a en effet pu être visualisée à l'échelle locale (entrée, milieu et sortie de la membrane) et comparée à l'observation du mouillage à l'échelle globale.

An optical tool for localized wetting visualization in membrane distillation

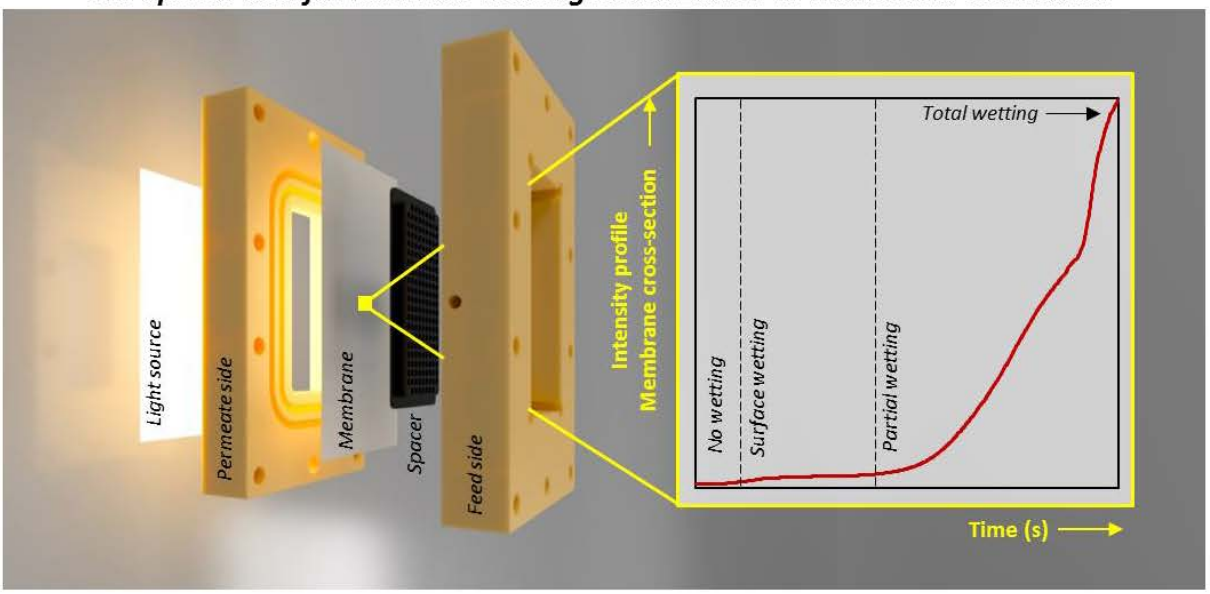

Graphical abstract

4.1. Introduction

Several authors use LEP and CA as tools to determine the wettability potential of a membrane together with tools like AFM [115], FTIR [36,118], SEM/EDX [68] etc. However, primarily all these tools/methods are *ex-situ*. Though most *ex-situ* methods can give information on wettability potential on a local scale, however, these tools are unable to give any information on the movement of the liquid-vapor interface leading to wetting. In the previous chapters wetting mechanisms were determined by the DDTI method (traces left by the saline intrusion with the movement of the L/V interface in the membrane pores after the operation). [176] yet still, SEM/EDX is a destructive technique.

On the other hand, significant efforts have been made to develop and adapt non-invasive techniques for membrane processes [187]. Though most of these techniques are not translatable to membrane distillation. Presently, measuring conductivity [70,124] in the permeate is the most used *in-situ* wetting detection technique. Some other technics are being currently considered are volumetric methods [151], measurement of electric current using a conductive layer on the membrane compartment [152] or impedance across the membrane [153]. All these methods provide only global information. There is an acute need to develop a simple technique that can combine the advantages of both *in-situ* and *ex-situ* techniques and detect localized wetting on the membrane surface during operation.

The objective of this study is to develop an optical tool based on the light transmission to visualize wetting *in-situ*. The principle of this method is based on the modification of the refractive index when the L/V interface penetrates inside the membrane. The issue is to develop equipment able to detect

this modification and to demonstrate that the obtained signal can be related to wetting occurrence. The primary objective of this study is to provide the proof of concept by validating the concept of light transmission to detect localized *in-situ* wetting in vacuum membrane distillation. The second part will aim to use this validated tool to study wetting in different feed solutions for a given membrane and finally an attempt was made to compare and distinguish wetting progression at the global scale and compare it with wetting progression at local scales at different locations on the membrane surface under the same operating conditions.

4.2. Theory of light transmission in hydrophobic membrane

For any material, when light falls on it, part of this light is absorbed, transmitted, reflected and scattered. These interactions determine the material transparency at a given wavelength of light. The amount of light scattered versus the amount transmitted determines the transparency of the material. A membrane is a porous matrix of fibers with air inside and surrounding it, implying a membrane with 75% porosity is in fact 25% material (membrane fibers) and the rest is air. Under ambient conditions (standard temperature and pressure STP) when light falls on such a membrane (Refractive index (N_D)1.48 [188]) together with air (N_D 1), the majority of the light gets scattered or reflected and only a part of the light gets transmitted. This results in a membrane which is opaque white due to light scattering. This scattering depends on a variety of variables (E.g. intrinsic properties, pore size, uniformity etc.) including the difference in refractive index between the membrane material and the medium (air) inside/surrounding it. Therefore, if the medium (air) inside the membrane can be replaced by a medium (e.g. water N_D 1.33) with a similar refractive index (N_D) as the one of the membrane material, the overall membrane can seem to be translucent and ideally approaching transparent due to this refractive index matching. A described example of this refractive index matching is presented on the **Figure 5.1** below.

Figure 5.1 (a) visualizes a PVDF membrane, where all the light falling on it is scattered resulting in the membrane to look like an opaque white sheet of plastic similar to a sheet of paper. However, when water was forced into the same PVDF membrane, refractive index matching occurred as the membrane pores were filled with water with a closer refractive index to the membrane one. This results in a membrane translucent with greater light transmission (**Figure** 5.1 (b)). Exploitation of this phenomenon can be utilized in membrane distillation to determine the degree of wetting at a localized scale during operation.

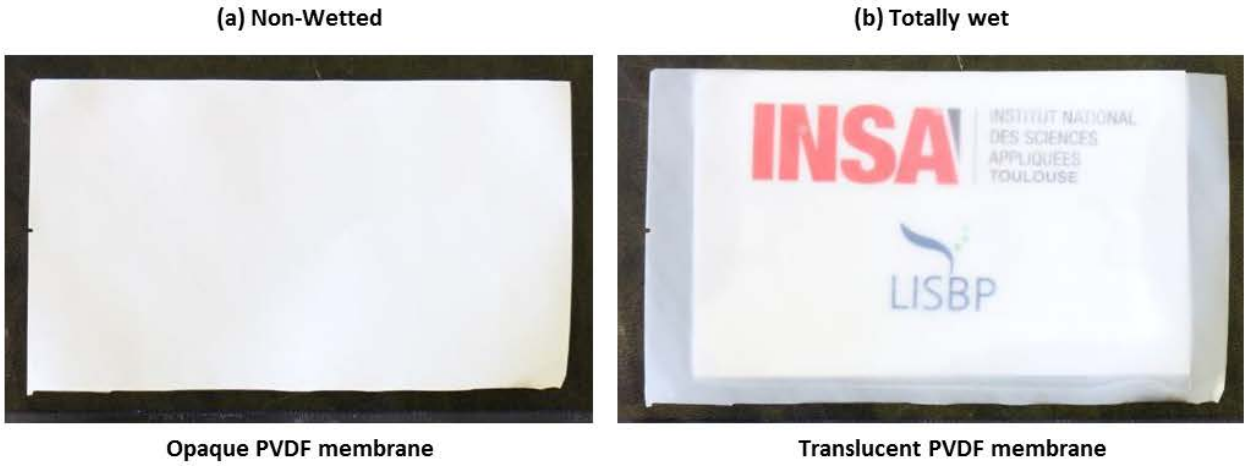

Figure 4.1: Light transmission through the same PVDF membrane (a) under non-wetted conditions (b) under totally wetted conditions using water (to be viewed in color)

To better understand the theory of light transmission in the membrane pores, a graphical representation of a membrane cross-section subjected to vacuum membrane distillation and observed at microscale is presented in **Figure 4.2.** The membrane cross-section was illuminated with a light source from the feed side. Here 2 cases are presented. In the case of Figure 2 (a), the liquid-vapor interface is located on the feed side of the membrane. Here the light transmission from the feed side to the permeate side is low due to the miss matching refractive indexes between liquid, membrane and partial air/vacuum inside the membrane cross-section. However, when the interface moves inside the membrane and total wetting occurs on the membrane cross-section (see **Figure 4.2 (b)),** light transmission increases due to the matching refractive indexes of liquid and membrane material. Thus, light transmission increases, and light scattering reduces significantly. Indeed, the light that was being initially reflected under no wetting condition is now being transmitted by refraction causing the membrane to be ideally transparent while being totally wet. Therefore, by using a camera/or a light sensor, a change in pixel intensity or light intensity can be identified while keeping all the other parameters constant. An exploitation of this phenomenon will result in identifying the movement of the liquid-vapor interface under a steady-state operation of membrane distillation.

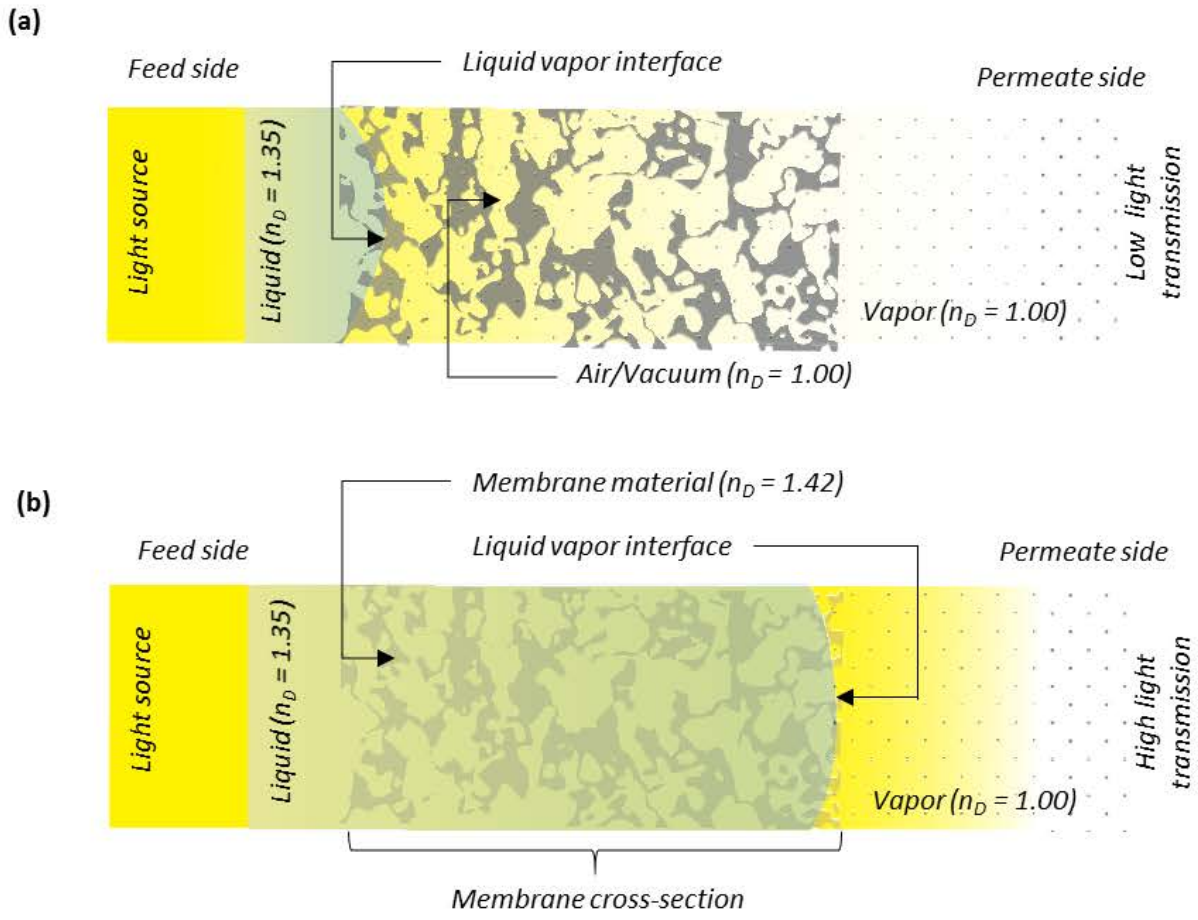

Figure 4.2: Graphical representation of light tramission through the membrane cross-section at microscale (a) where no wetting had occurred (b) where total wetting has occurred (to be viewed in color)

4.3. Material and methods

4.3.1. Vacuum membrane distillation setup

The overall setup was similar to previously studied vacuum membrane distillation setup **(Chapter 2 & 3)**. The membrane cell was designed differently than the conventional membrane cell and is described below.

4.3.2. Membrane module

The cell was designed and fabricated to have viewing windows on both sides of the membrane module to observe the active membrane surface during operation. The rectangular flat sheet membrane module was made of two 20 mm C-PVC blocks secured by two 10 mm thick stainless-steel plates. As presented in **Figure 4.3 (a),** the module was designed with viewing windows both on the feed and the

permeate side with glass (borosilicate) windows that could withstand high temperatures with 90 % light transmission for 350 – 2000 nm wavelength.

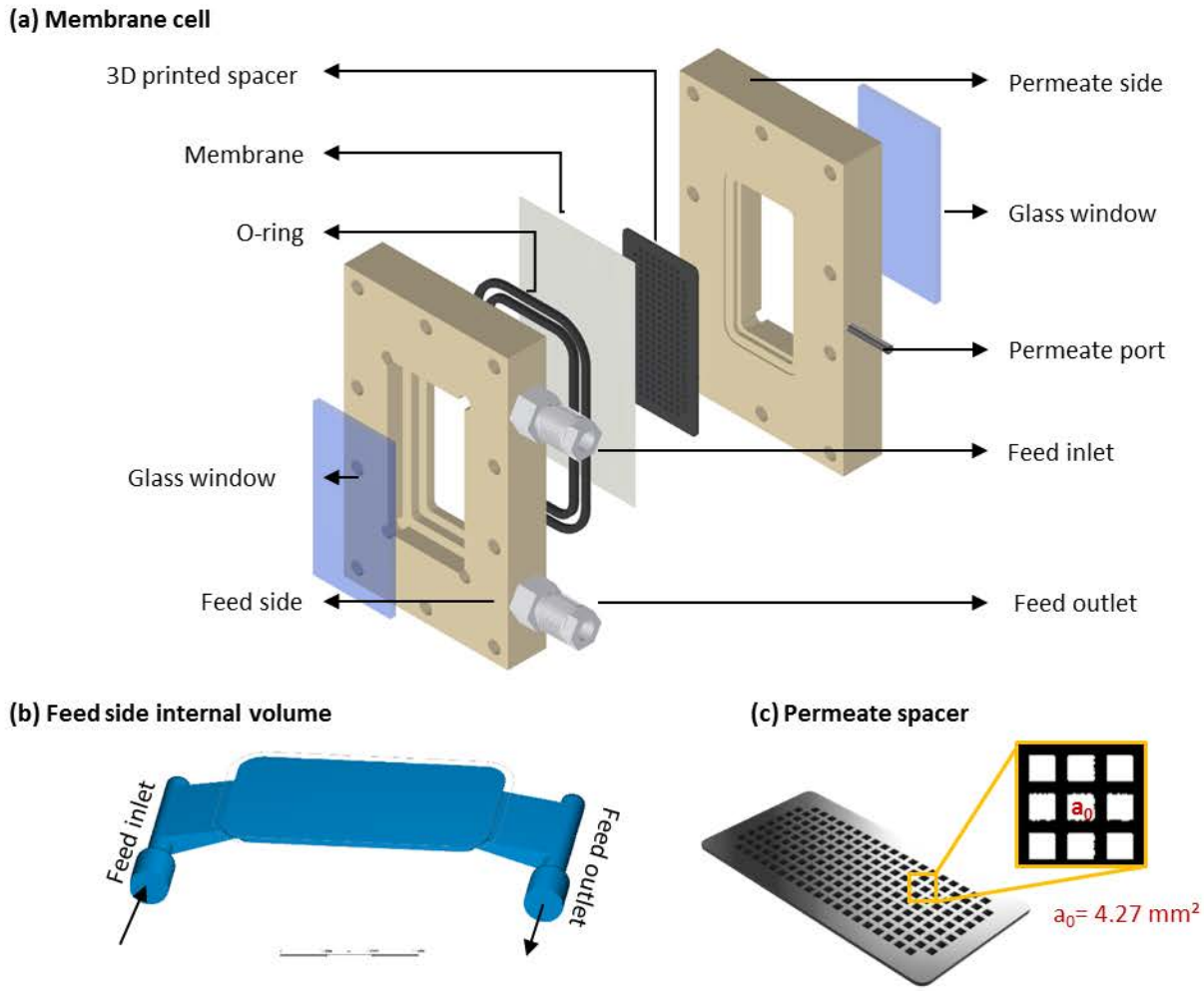

Figure 4.3: (a) Membrane module design (b) feed side internal geometry (c) 3-D printed spacer (to be viewed in color)

The internal feed side channel dimensions were 79 x 41 x 12 mm (length x width x depth) with an edge radius of 7.5 mm. The internal feed side membrane cell volume is presented in **Figure 4.3 (b)**. It can be seen that the feed inlet and outlet ports moved to the sides to have the active membrane surface in view and to reduce the impact of hydrostatic pressure at the feed inlet. The enclosure membrane had an active surface area of 3.24 x10^{-3} m^2 and was secured by two O-rings on the feed side.

4.3.3. Spacer design

The advent and accessibility to manufacture custom parts using 3D printing has led to several researchers developing and using custom spacers designs for membranes processes like RO[189,190]

and MD[191]. A 3D printed spacer was introduced on the permeate side to support the membrane during operation. The spacer had 185 openings with an open area (a_{oi}) of 4.27 mm²/opening (see **Figure 4.3 (c)**) determined by image processing. This results in the visualization of only 7.94 x10^{-4} m² or ~27.4 % of the active membrane surface. All wetting visualization in this study are limited to these 185 openings or 7.94 x10^{-4} m² or ~27.4 % of the active membrane surface.

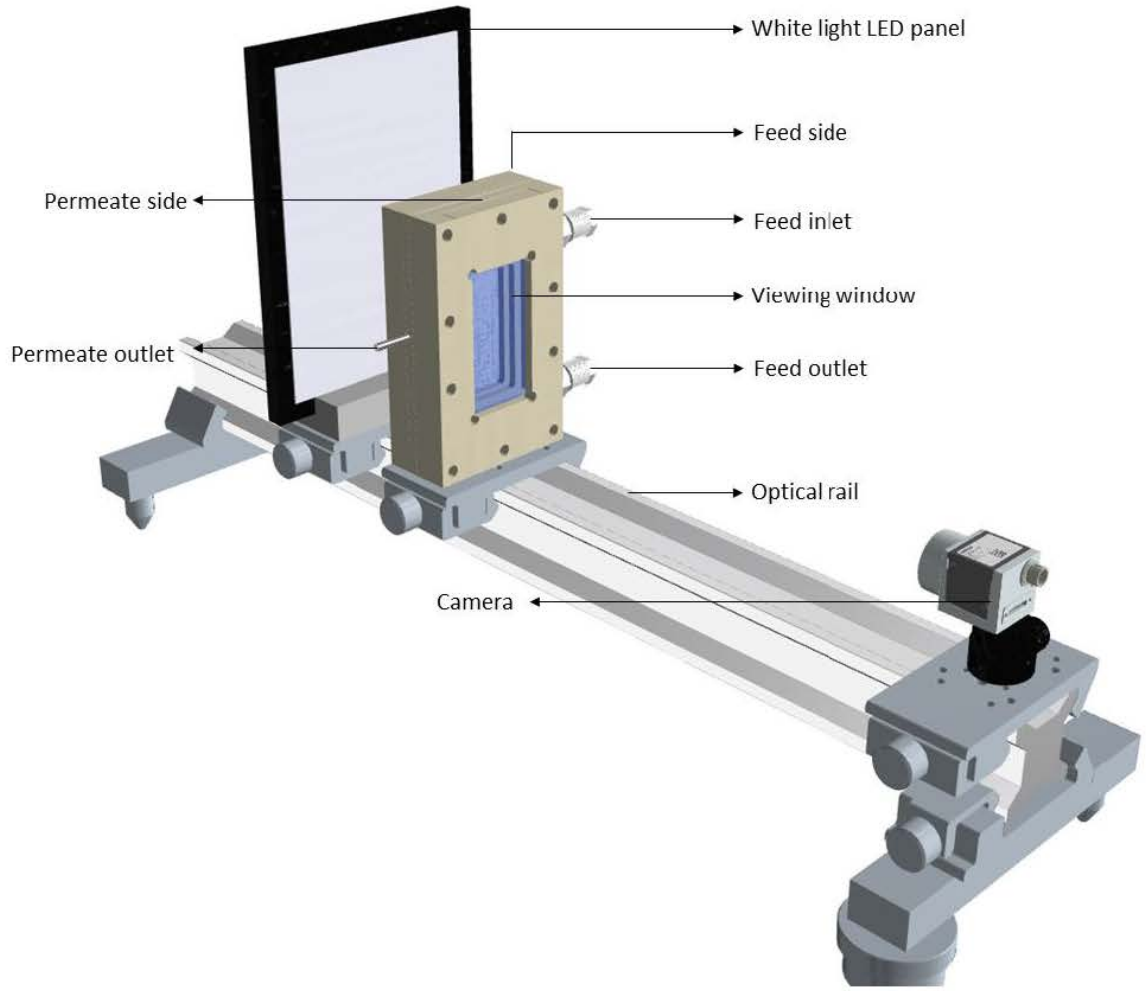

Figure 4.4: Optical system for localized wetting visualization (to be viewed in color)

4.3.4. Optical wetting detection device

The optical system consists of a LED panel, membrane cell, and camera (Basler ace acA1300-200uc with a 16mm lens) (see **Figure 4.4**). The whole setup was fixed and aligned on an optical rail for stability using optomechanical clamps. The white light LED panel (Metaphase Technologies) was used as the light source which emitted a uniform intensity. The feed side of the membrane surface faced the light source while the permeate side faced the camera. The camera was focused and calibrated to view the membrane surface through the spacer. Each image was 1200 x 600 pixels in RGB. The overall system

has a resolution of 13 pixels/mm or ~77 µm/pixel. The optical setup was designed and manufactured in-house.

During operation, the whole system was placed inside the VMD pilot plant with the feed and permeate ports of the membrane module connected to their respective pumps and setups. The camera recorded images each second for the entire duration of the experiment. The viewing window on the permeate side was heated to avoid vapor condensation. The whole system was covered with a matte black paper and cloth to avoid external light interference and noise.

4.3.5. Membrane and its characterization

Durapore membrane (0.22µm, PVDF) were used in this study. This membrane has been previously characterized (Chapters 2, 3 and 4). The virgin membrane was 117.2 ± 0.9 µm thick with an average porosity 0.75 (ε). The contact angle and LEPw of the virgin membrane were 124 ± 2.8° and 2.04 ± 0.86 bar respectively. The Knudsen permeability coefficient (K_M) was experimentally determined in this membrane cell using temperature variation method [172] for laminar flow (2.75E-06 ± 1.1E-07 $s.mol^{1/2}.m^{-1}.kg^{-1/2}$) at the reference temperature of 20°C.

4.3.6. Operating conditions

The temperature on the feed side was fixed at 40±1°C with a feed flow rate ~ Re ≤ 400, while the vacuum pressure was held at 6kPa. The feed solution (**cf. 4.3.7**) was pre-heated to the desired temperature before circulating on the membrane surface. The vacuum membrane distillation set-up was operated for 1 hour per experiment. For each experiment, the feed solution was circulated in the membrane cell for 30 min. After that, the surfactant was injected into the feed tank to reach a final concentration of 12.5 mg/L. The objective of this injection is to provoke membrane wetting and to check if the optical system can detect it. Data for temperature (feed inlet and outlet, permeate), vacuum pressure and conductivities (feed side and permeate flask) were collected and logged during the experimental run. Whereas, images of the membrane surface illuminated from the feed side were taken using a camera on the permeate side at 1 Hz for 1 hour.

The following assumptions were made for *in-situ* wetting detection with light transmission:

- No wetting on the membrane is assumed until steady state of temperature, vacuum pressure and permeate flux is achieved
- Unidirectional wetting from the feed side to the permeate side is assumed

4.3.7. Characterization of feed solution without and with surfactant

A total of 4 feed solutions were studied: water (as a control/blank), saline solution and two seawaters. The blank was de-ionized water, the saline solution was prepared to achieve NaCl concentration of 35 g/L using crystalline NaCl salt (VWR, France) and deionized water. Seawater were collected at 2 locations in the Mediterranean Sea (Location 42°50'48.0"N 2°56'33.4"E and 43°40'42.1"N 7°13'51.4"E). The samples were analyzed for conductivity, turbidity, pH, UV absorbance at 254nm.All analytical measurements were conducted at least 3 times.

Table 4.1: Feed solution properties

Parameters	Unit	Blank / D.I. Water	Saline solution	Seawater 1	Seawater 2
Conductivity	**mS/cm**	0	51	43.8	51.1
pH	-	6.8	7.0	7.8	7.9
Turbidity	**NTU**	0.06	0.01	0.34	0.09
Absorbance UV_{254nm}	-	0	0	0.06	0.012
Refractive index	-	1.33241	1.33849	1.33754	1.339
Surface tension	**mN/m**	72	73.5	73.9	72.8

Note: All measurements are reported for 25°C

Additionally, surface tension and refractive indexes of the feed solution, and the contact angle of the feed solution on the membrane surface were also analyzed and the protocols are described subsequently (**cf. 4.3.7.1 and 4.3.7.2**). **Table 4.1** presents the properties of pure water, saline solution and the seawaters termed as SW1 and SW2 respectively. Both seawaters were pre-filtered using a 0.45 µm filter to remove sand and other large particles that may interfere with the measurements. Considering salinity (using conductivity measurements), SW1 was less saline than the prepared saline solution and SW2.

Here it should also be noted that SW1 was collected from the inlet of a fish farm in a lake adjoining the Mediterranean Sea. This resulted in freshwater or surface water intrusion in SW1 that reduced salinity. It should be noted that SW1 contained higher organics matter as reported by Monnot et. al [192] studying seawater samples from the same location. This is not the case with SW2 where the salinity (measured by conductivity) is similar to the saline solution prepared at 35 g/L NaCl in the lab. Whereas considering pH, water and saline solutions had a pH close to neutral whereas both seawater samples were slightly basic. The surface tension and refractive indexes of all the three solutions were close to the blank solution.

A surfactant was added to all the feed solutions during experimentation to induce wetting, as surfactants (SDS and Triton X) have been previously reported to induce wetting in membrane distillation [121,153,193]. In this study, laboratory grade Triton X-100 (Sigma Aldrich, France) was used as a wetting inducing agent at 12.5 mg/L for all feed solution samples. The optimal concentration for wetting detection was determined after several tests conducted earlier. The change in feed solution properties and wettability indicators (LEP and CA) due to surfactant addition during operation are elaborated later (**cf. 4.4.2**)

4.3.7.1. Surface tension and contact angle

The surface tension of the feed solution was measured using the pendant drop method and later the contact angle of these feed solutions with and without surfactants on the membrane surface were also measured using Drop Shape Analyzer – DSA25 (Kruss) at 25°C. The results were post-processed in accompany software (ADVANCE). Tests were repeated over 10 times with average, and standard deviation reported.

4.3.7.2. Refractive index

The refractive index (N_D) of these solutions were measured at 25°C using a refractometer (RM50 LiquiPhysics, Mettler Toledo). The samples were analyzed over three times with average, and standard deviation reported.

4.3.7.3. Wettability and wetting indicators

Two classical wettability indicators (Liquid entry pressure and contact angle) and one wetting indicator from DDTI method previously developed were used in this study. LEP and CA characterization were conducted on virgin membranes using feed solutions before and after adding surfactants. Whereas, pore wetting ratio was used in validating the proof of concept and for interpreting localized wetting visualization. The acquired images were post-processed in ImageJ. The following algorithm was developed and implemented (see **Figure 4.5**).

4.3.8. Image treatment

From each experiment 3600 images of 1200 x 600 pixel were collected which visualized 27.4 % of the active membrane surface (7.94 x10^{-4} m^2) through the spacer and the glass window. The images were taken from the permeate side of the membrane surface with the light source located on the feed side.

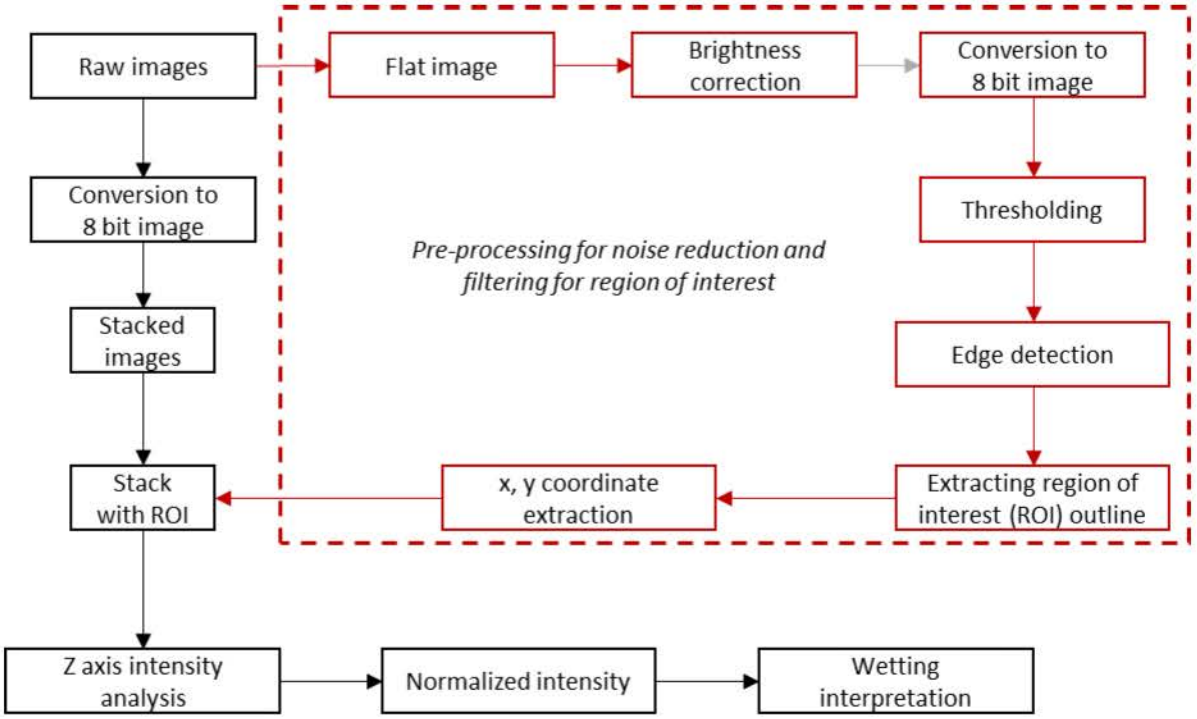

Figure 4.5: Flowchart for image processing algorithm for *in-situ* wetting detection

Firstly, the raw images were calibrated, converted to 8-bit images and stacked. Later, using a flat image (where no wetting was observed, and the membrane was operating at steady state) the dark regions of the image were suppressed by extracting the region of interest (ROI's) by using brightness correction and threshold. Later edge detection of the bright regions of this image was conducted and polygon mask were fitted on these regions of interests (ROI's). These ROI's were labeled and the x, y positions of these extracted and superimposed to the stacked images. Each ROI was labeled from 1-185 as presented in **Figure 4.6**. No further data treatments were conducted as the noise in the acquired data

were very low (0.8 – 1.7 gray values). Finally, the average intensity all to ROI's on the Z axis were determined, and the intensity was normalized for interpreting wetting mechanisms.

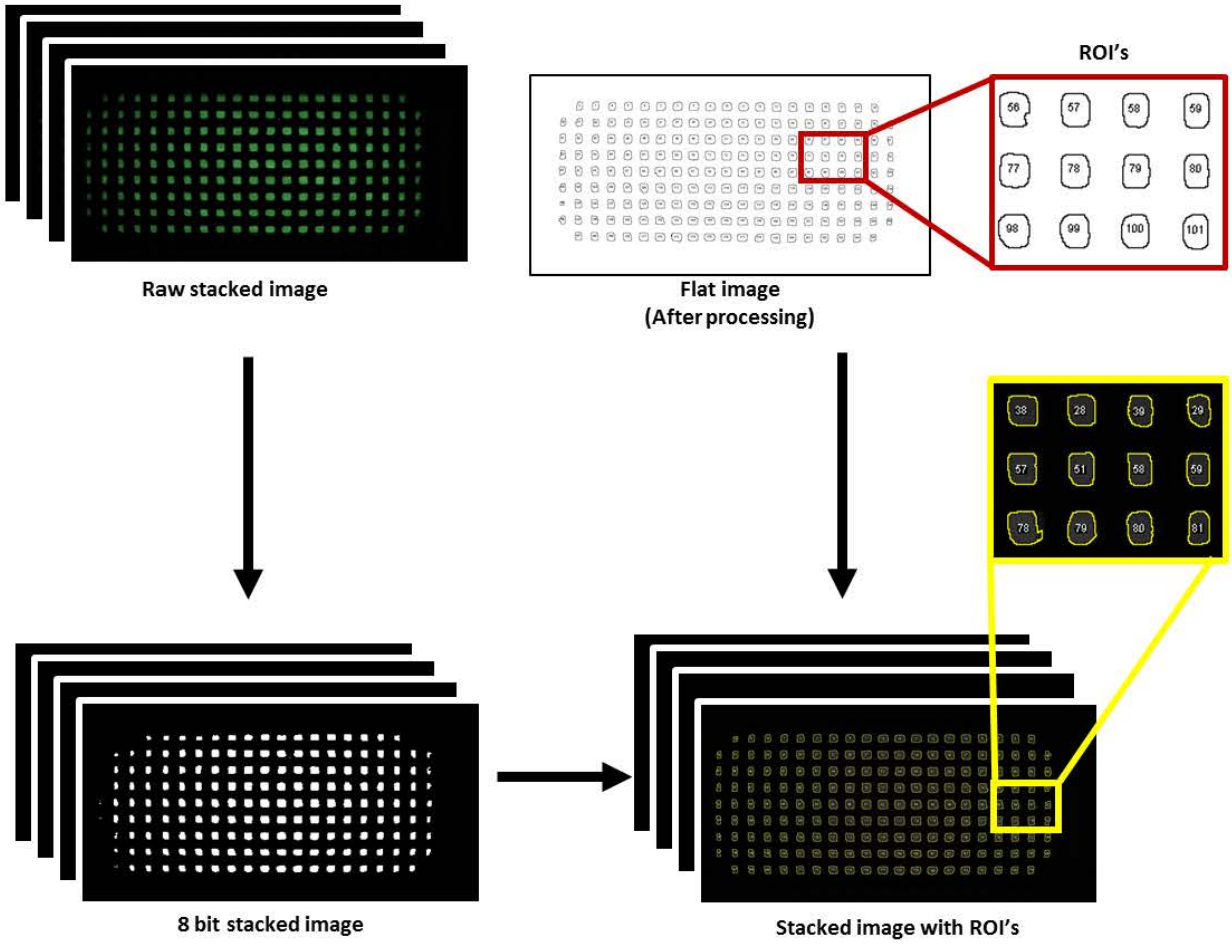

Figure 4.6: Representation of the image processing algorithm with actual images acquired from an experiment (to be viewed in color)

The averaged intensity values for the ROI's were calculated using Eq. 4.1 and presented over time.

$$I_{avg}(t) = \sum_{i=1}^{N}\sum_{j=1}^{M}\frac{I_{ROI}(x_i, y_i)}{LM}(t) \qquad \text{Eq. 4.1}$$

Where I_{avg} is the overall average intensity of all region of interests (I_{ROI}) observed over time (t). Whereas, $\frac{I_{ROI}(x_i,y_i)}{LM}$ is the average intensity at one ROI at location x_i and y_i with a location coordinates enclosed by NM observed over time (t).

Additionally, the average intensities were normalized to facilitate the wetting propagation through the membrane cross-section using Eq. 4.2

$$N = \frac{(I_{observed} - I_{initial})}{(I_{max} - I_{intial})} \quad \text{Eq. 4.2}$$

Where N is the normalized light intensity, $I_{observed}$ is the intensity of one image at time (t) and I_{max} is the intensity of an image captured when total wetting had occurred and finally, $I_{initial}$ was the flat images where no wetting had occurred after steady-state operation was achieved.

4.3.9. Wetting visualization at different scales

Using the above image treatment, we have the ability to choose and analyze wetting propagation at a global or a local scale as presented in **Figure 4.7**. The evaluations of these scales are detailed in the following paragraphs.

4.3.9.1. Macro scale

If the choice is made to evaluate wetting progression considering all the 185 ROI's as seen in **Figure 4.7** (a), wetting analysis using *Eq. 4.1* and Eq. 4.2 would be considered at the macro scale or the global scale of the membrane surface. Wetting analysis at this scale would result in an average increase in light intensity of all ROI's in time during the entire duration of the experiment.

It should be noted here that the results sections from **4.4.1 and 4.4.2** utilizes wetting propagation considering all the ROIs.

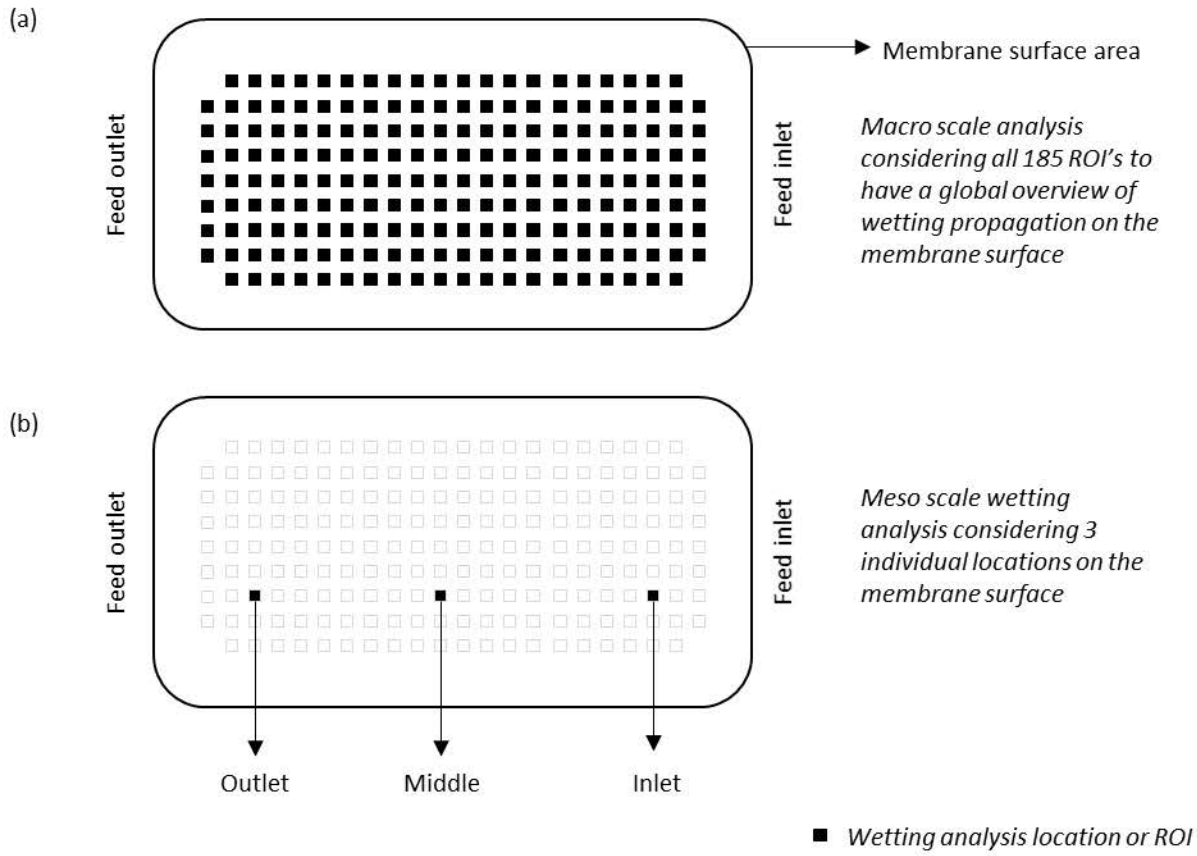

Figure 4.7: Wetting analysis with highlighted regions of interest (ROI) (a) at macro scale or global scale (b) at meso scale or local scale

4.3.9.2. Meso scale

At present, the finest tools that have been developed or used for determining *in-situ* wetting are at the scale of the membrane. For example, conductivity measurement and recently developed impedance-based technique. The information that can be derived from conductivity measurements is that some pores have been compromised and total wetting has occurred. Wetting is considered at the global scale of the active membrane surface area and not at a local scale. However, as presented in Chapter 3, wetting may not occur at all locations simultaneously as it is a localized phenomenon. If such a local analysis is deemed necessary, we can choose to apply the same image treatment algorithm and equations on an individual ROI (4.2 mm^2 or at the mesoscale) and have greater detail on wetting at this scale. Therefore, to illustrate the difference in wetting propagation at different scales, 3 ROI's were selected on the membrane surface where; one is close to the membrane surface close to the inlet, one at the middle of the membrane and one close to the outlet of the membrane surface as illustrated in **Figure 4.7 (b)**. The difference in wetting propagation at these 3 locations will be compared to the wetting propagation at the macro scale to illustrate the effectiveness of this optical tool better.

4.4. Results and discussions

4.4.1. Proof of concept and validation using DDTI method

The proof of concept of wetting detection using light transmission consisted of provoking wetting on a membrane and observed the drying/de-wetting of the membrane pores using the optical device. These observations can later be validated using pore wetting ratio from the DDTI method previously developed. These observations could then be associated with the wetting mechanisms with the idea to observe the wetting kinetics.

Experiments were conducted by operating the VMD pilot with:

- **Case 1:** A membrane submerged in saline solution (35g/L NaCl) with 500 ppm of surfactant for a week to ensure total wetting. Then the membrane was installed inside the membrane module. The change in light intensity was observed through the membrane cross-section during the drying of the membrane for 1 hour. During this time no feed was injected into the membrane cell (as membrane was already wet and would have let water pass through membrane feed side to the permeate side), but a vacuum of 6kPa was still applied, and all other operating conditions were maintained the same.

- **Case 2:** A reference membrane operated with saline solution (35g/L NaCl) only, for which no wetting is expected (according to previous results) and observing the change in light intensity for 1 hour through the membrane cross-section during VMD operation.

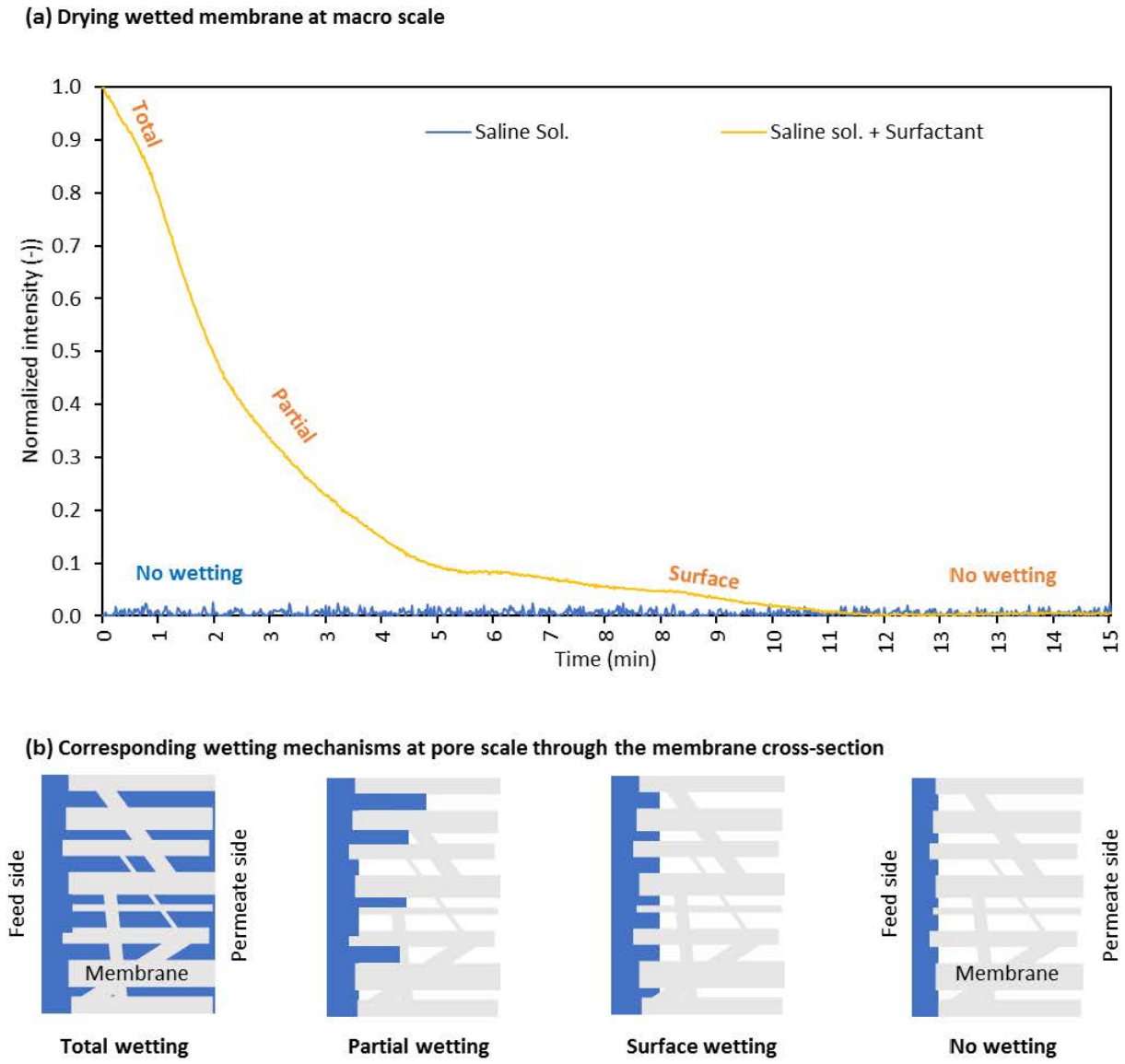

Figure 4.8: In-situ visualization and graphical representation of wetting mechanism (to be viewed in color)

The resulting normalized intensity profile of these 2 cases are presented in **Figure 4.8(a)** for 15 min only. Indeed, the membrane subjected to surfactant (case 1) had a higher intensity at the beginning, indicative of total wetting, and as the membrane progressively dried with the water evaporation inside the membrane pores, total wetting transitioned to partial wetting. Finally, when all the water had evaporated, and the membrane dried entirely, the intensity reduced to its lowest value indicative of no wetting. At the same time for case 2 where no surfactant was introduced, no wetting was observed during the total experimental duration. These observations are at macroscale but are representative of the transiting wetting mechanisms observed at the pore scale as illustrated in **Figure 4.8 (b)** (for case 1).

To validate the above hypothesis, scanning electron microscopy with x-ray dispersion spectroscopy were conducted on samples acquired from Case 1 and Case 2. Detailed protocols of sample preparation and SEM/EDX analyses can be found elsewhere (**Chapter 2**, [176]). An average intensity profile of Chlorine across the membranes subjected to both cases are presented in **Figure 4.9(a)** whereas **Figure 4.9(b)** presents the SEM/EDX micrographs of these membranes. Indeed, high Chlorine traces across the membrane sample subjected to surfactant (Case 1) allow validating that total wetting was prevalent in this sample. Whereas for the membrane subjected to the saline solution only (Case 2) no traces of Chlorine on the membrane cross section was found, indicating no wetting had occurred.

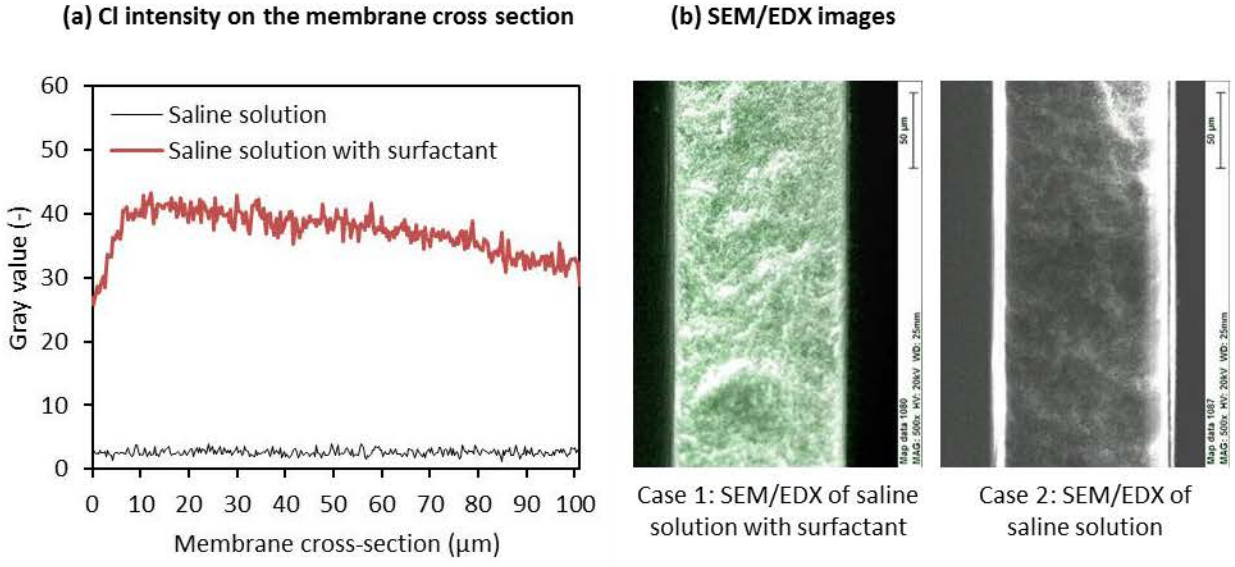

Figure 4.9: (a) Chlorine intensity on the membrane cross-section (b) SEM/EDX micrographs for case 1 and case 2 (to be viewed in color)

These preliminary results allow validating the proof of concept that an increase in light intensity at steady state operation can be linked to a wetting propagation inside the membranes. In the following section, the membrane was subjected to various feed solutions under steady-state operation, in order to better illustrate and understand wetting mechanisms.

Table 4.2: Feed properties and wettability parameters before and after surfactant injection

Parameters	Unit	Blank / D.I. Water	Without surfactant			With surfactant		
			Saline solution	Seawater 1	Seawater 2	Saline solution	Seawater 1	Seawater 2
Conductivity	**mS/cm**	0.0	51	43.8	51.1	51.5	41.1	49.5
pH	**-**	6.8	7	7.8	7.9	7.2	7.9	8.0
Turbidity	**NTU**	0.06	0.01	0.34	0.09	0.30	0.42	1.16
Absorbance UV_{254nm}	**-**	0.000	0.000	0.060	0.012	0.049	0.093	0.048
Refractive index	**-**	1.33241	1.33849	1.33754	1.33900	1.33851	1.33719	1.33830
Surface tension	**mN/m**	72.0	73.5	73.9	72.8	62.3	64.1	57.1
Contact angle	**°**	123.7	125.9	125.3	123.7	122.1	123.6	119.3
LEP	**bar**	2.03	1.97	1.43	1.50	1.73	1.33	0.87

Note: All measurements are reported for 25°C

4.4.2. Influence of surfactant on feed properties, wettability parameters and flux

Table 5.2 presents the properties of the different solutions used in this study before and after addition of the surfactant in the feed solution where deionized water was used as a control/blank. All measurements were conducted at 25°C and the seawaters were pre-filtered with a 0.45 µm membrane before characterization. Considering the different feed properties, an addition of the surfactant generally increased the pH to slightly basic for all samples even though the turbidities of the samples were still clear. Similarly, it could be seen that all samples with an addition of surfactant had an overall increase in refractive index compared to the blank solution. However, after addition of the surfactant, there was a slight reduction in the refractive indexes in the samples. The principal changes in the feed that can be highlighted is a 15 – 22 % reduction in the surface tension of the feed solution after surfactant addition, implying the wetting potential of the feed solutions had increased.

Concerning the wettability parameters of the feed solutions with the studied membranes, both contact angle and liquid entry pressure were measured. Only a 2-4 % reduction in contact angle was observed, however, LEP presented a 7 to 42 % reduction. It can be seen for LEP that wetting potential of the feed solution after surfactant addition had significantly increased. It worthy to mention that these measurements were taken at standard temperature and pressures. Elevated temperature feed solution with surfactant would have a significant reduction in surface tension thereby increasing the risk of wetting under the operating conditions [193].

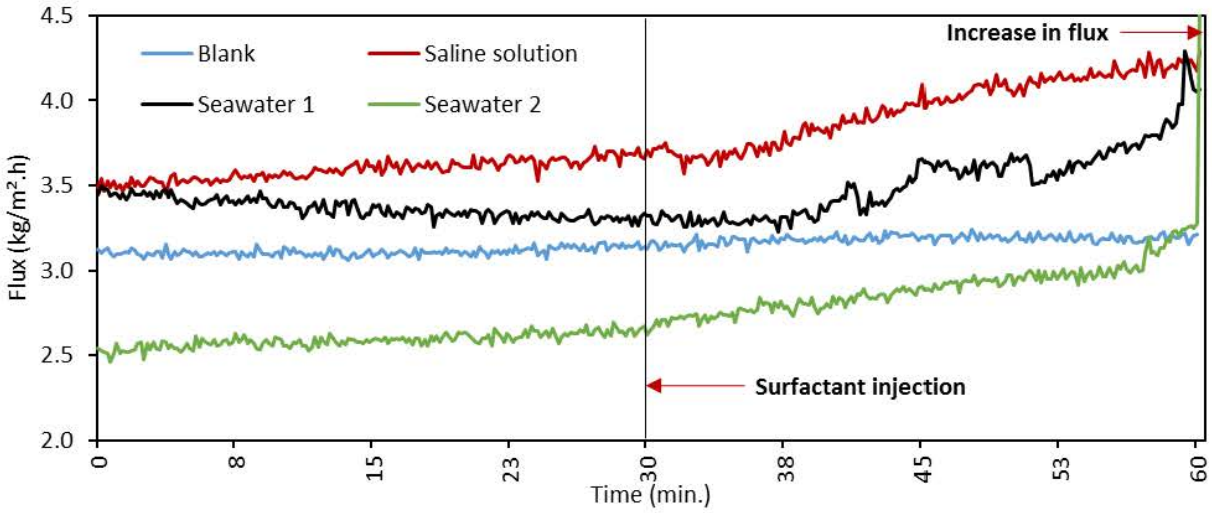

Figure 4.10: Flux response for the feed solutions (to be seen in color)

Figure 4.10 summarizes the flux response in the studied samples under fixed operating conditions. Depending on the samples the flux varied between 2.5 and 3.5 Kg/m².h and generally could be considered stable during the first 30 minutes of operation. However, after addition of the surfactant, a linear trend in flux could be observed. This may be attributed to the inward movement of the liquid-vapor interface thereby decreasing the vapor diffusion path and temporarily increasing the flux. Similar observation of an increase in flux leading to wetting, later on, was also observed by Gryta[70]. After 55 min of operation, the vapor flux started to be unstable, and feed solution could be seen to pass through the membrane in its liquid state confirming total wetting had occurred at some location or locations on the membrane surface during operation.

4.4.3. Visualizing induced wetting with different feed solutions

In this section, the different previously described solutions (**cf. 4.3.7**) were used as feed to visualize wetting progression under same steady-state operating conditions for 1 hour while using deionized water as blank. Wetting was provoked after 30 min by injecting a surfactant (Triton x) into the feed solution to reach a final concentration of 12.5 ppm (**cf. 4.3.6**).

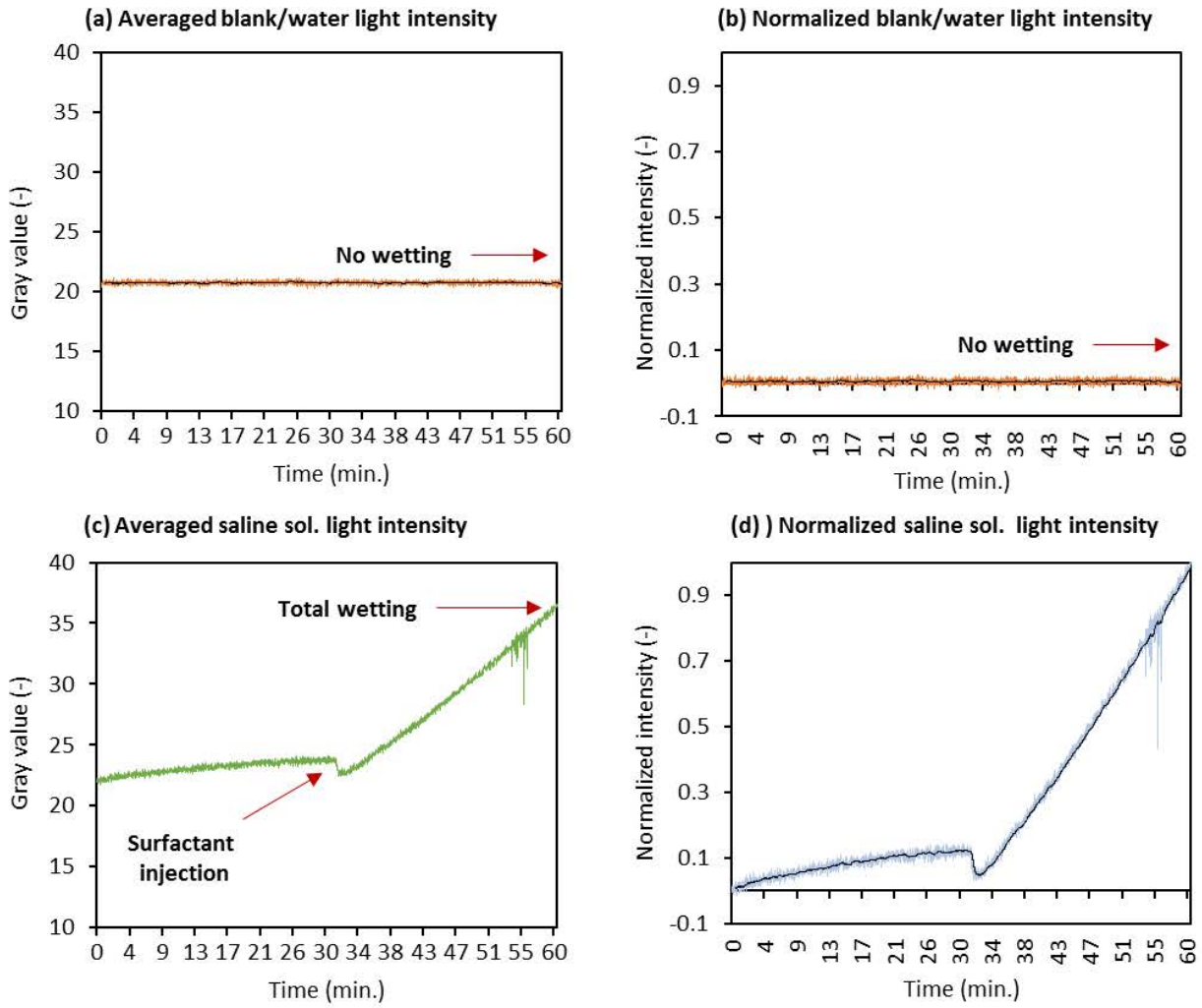

Figure 4.11: Averaged and normalized light intensities during experimental run (a, b) blank/water and (c, d) saline solution with surfactant injection after 30 min

4.4.3.1. Blank and saline solution

Figure 4.11 presents the light transmission with (a) water (blank) and (c) saline solutions for the entire duration of the experiment. In the case of blank, the intensity did not change during the entire operation, and this state could attribute towards the steady operating conditions where no wetting occurs. As the feed contained neither salts nor the surfactant; the feed conductivity stayed stable 3.37±0.07 µs/cm. The normalized graph on the right side (**Figure 4.11 (b)**) also presents the same information. During the total duration of the experiment, no feed liquid had appeared on the permeate side of the membrane surface.

However, considering the saline solution (see **Figure 4.11 (c)**), it can be seen that the light transmission slightly increased as the experiment continued. This increase in light intensity can be postulated as the inward movement of the L/V interface. However, just after the addition of the surfactant at the ½ hour

mark, a sudden drop in light intensity can be observed with a significant increase in light transmission soon after. By the end of the experiment, liquid water started to appear on the permeate side of the membrane module validating total wetting had occurred on the membrane surface. Considering the normalized data (**Figure 4.11 (d)**), it can be seen that surfactant addition introduced these molecules at the membrane interface which lead to a rapid reduction in light intensity. The surfactant interacts with the membrane surface inducing a less hydrophobic property, as well as a reduced membrane contact angle, leading to wetting.

4.4.3.2. Seawaters

As the principle application of membrane distillation is for desalination, the application of wetting detection using the optical technique was also tested for real seawaters. Considering light intensities (see **Figure 4.12**), it can be noted that both samples had lower light transmission than observed for either blank or saline solution. This may be due to additional solutes dissolved in seawater. For the first ½ hour SW1 performed more like the blank with no increase in wetting intensities. However, after the surfactant injection, the intensity dropped like for saline solution but to a lesser extent and then it started to increase. Here the signal was noisy so a running average filter (n=30) was introduced to better visualize the trend in data. The significant noise in the signal was introduced by the surfactant interacting with this seawater sample and generating small bubbles in the circulating feed samples. As these bubbles passed in front of the visualized membrane surface, they created momentary dark regions resulting in the noisy signal. However, a general trend in the increase in light signal could be still observed.

Considering SW2, this sample had a similar intensity profile as the saline solution. Here it can be noted that there was a slight increase in intensity before the surfactant injection, implying an inward movement in the L/V interface. However, after the surfactant injection, wetting progressed in the same manner as the saline solution. As the surfactant accumulated on the membrane surface there again was a reduction in the intensity and later wetting propagation occurred until a state of total wetting was observed. Total wetting was confirmed by the accumulation of the liquid feed in the permeate side of the membrane. For additional information please check supplementary data for **Chapter 4**.

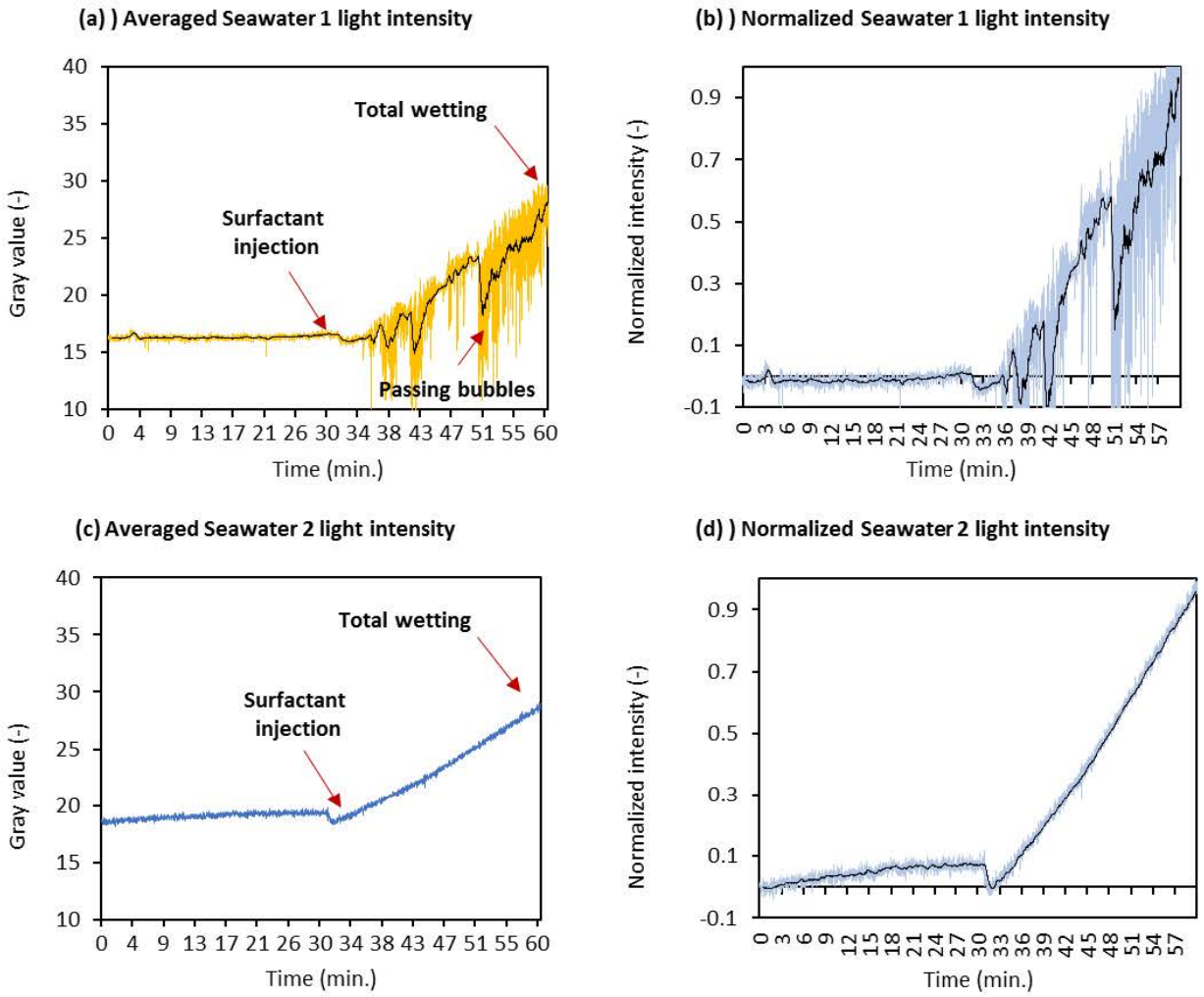

Figure 4.12: Averaged and normalized light intensities during experimental run (a and b) seawater 1 (c and d) seawater 2 with surfactant injection after 30 min

4.4.4. Difference in wetting propagation at macro and meso scale at different locations

Using this optical tool, we can further differentiate wetting occurrences at a more local scale for example at meso scale (0.01 to 30 mm) and compare it with the scale of the membrane. **Figure 4.13** presents the 4 curves of normalized intensity for the membrane surface at the inlet, middle, outlet and the global intensity for the membrane subjected to the saline solution with the surfactant added at 30 min. The data's presented in **Figure 4.13** are a moving average filter (n=15) to reduce signal noise. Here it can be observed that the global curve match closely to the data sampled at the middle until the surfactant is added. However, wetting propagation at the feed outlet surpasses wetting propagation observed at the inlet and middle of the membrane after surfactant addition. Wetting induction at the feed outlet was faster than that for the inlet and middle even though the overall curves mimic the same linear trend as the global scale. This difference in normalized light intensity is indicative of the

change in wetting rate experienced by the same membrane at different locations under the same operating conditions. This level of detail *in-situ* localized wetting progression was not possible with the current state of the art.

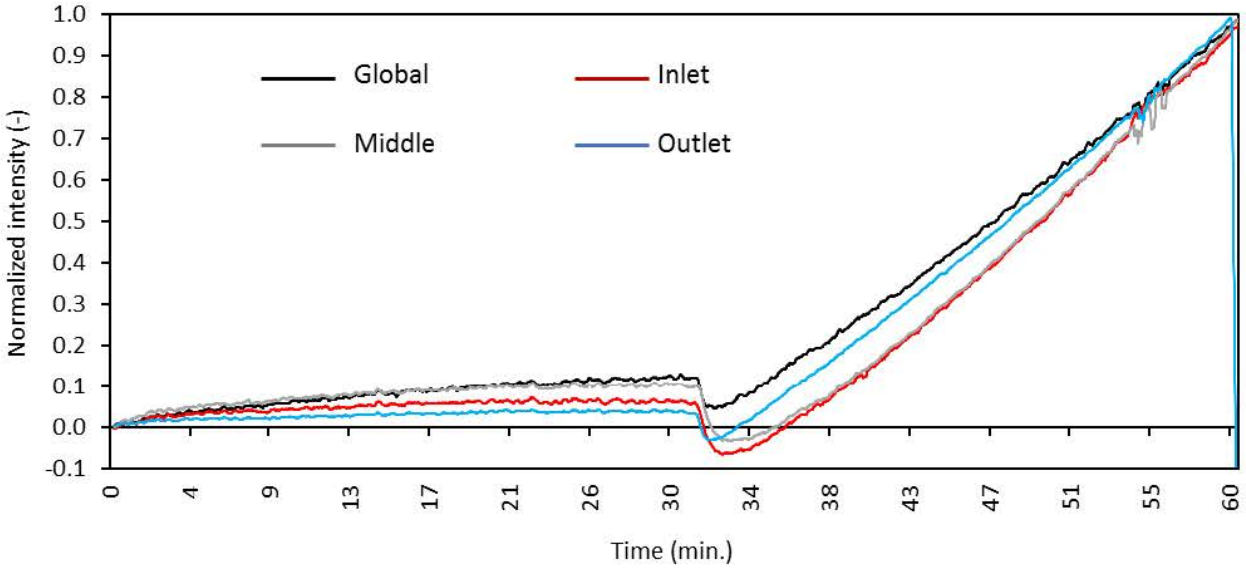

Figure 4.13: Comparing wetting progression on the membrane surface at global and local scales: inlet, center and outlet – (To be seen in color)

Additionally, after the experiment, the membrane was sampled at the inlet location, and Cl^- was profiled by SEM-EDX across the membrane cross-section using pore wetting ratio (ω_p) as presented in **Figure 4.14 (a and b)**. Here the progressive change in light intensity can be interpreted by the Cl traces left by the feed solution. The chloride deposits on the feed side membrane cross-section are indicative of an inward movement of the L/V interface leading to surface wetting. The same surface wetting mechanism can also be seen with a slight increase in light intensity from 0- 29 min (see **Figure 4.14**(c)). However, after surfactant injection, an increase in light intensity could be observed as the liquid vapor interface moved inside the membrane cross-section. At the end of the experiment, the highest intensity (indicated by Normalized data = 1) was observed, indicative of a total wetting and this can be confirmed by the Cl deposits on the permeate side of the membrane cross-section ((see **Figure 4.14**(b)) Pore wetting ratio also confirms that the total wetted state of the membrane as Cl- peaks can be seen at ω_p of 97.2 % of the membrane cross-section.

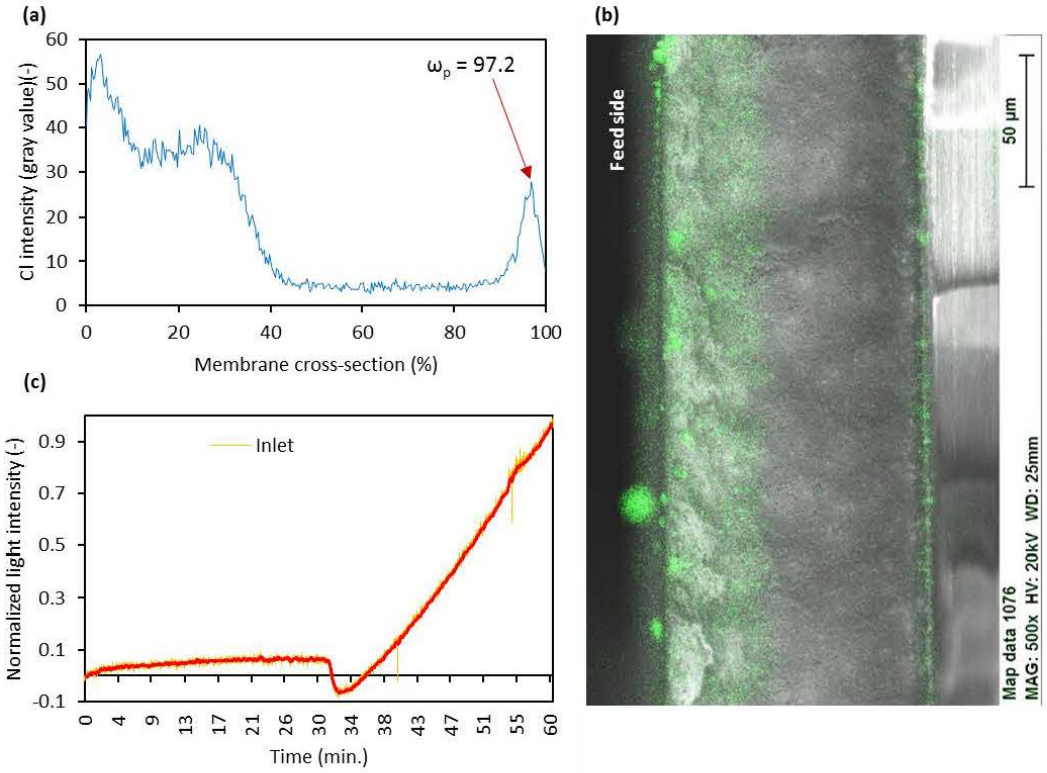

Figure 4.14: (a) Chlorine Intensity profile of membrane cross-section (b) SEM/EDX micrograph of the membrane cross-section (c) Normalized *in-situ* light transmission of at the the same location with saline solution (to be seen in color)

Wetting progression at the inlet (mesoscale) can be validated by the SEM/EDX micrographs at the pore scale. Similar observations can be made all over the membrane surface and used to identify the propagation of wetting mechanisms at different locations. This would enable us to better understand the influence of feed solutions, operating conditions and process hydrodynamics at a local scale during operation.

The scale and resolution of the wetting observation will depend on the resolution of the camera/sensor setup and area of the membrane visualized. Wetting may not be visualized where the membrane surface is covered for example with the spacer. Wetting propagation may be evaluated on the membrane by precisely determining and correlating SEM/EDX and light at different stages of wetting.

4.5. Conclusions and perspectives

In English

In this study, a non-invasive *in-situ* optical tool was developed and tested for visualizing wetting propagation in membrane distillation. The proof of concept that *in-situ* wetting can be detected using light transmission was provided and validated using DDTI method. The tool was tested with saline solutions and seawaters with controlled wetting induced by the surfactant. The optical tool was able to provide information on wetting mechanisms in the studied solutions. The developed tool is adaptable and can visualize wetting at both global and local scales. Earlier this level of scalability could be only possible using *ex-situ* techniques like SEM/EDX.

Table 4.3: Advantages and challenges of the developed optical tool

Advantages of the optical tool	Challenges to be addressed in future studies
• In-situ tool which can evaluate and visualize wetting propagation and mechanisms at the global and local scales	• Wetting visualization is limited by the optics of the camera used therefore wetting can be visualized but not at the scale of the pores (i.e., microscale)
• Can be adapted to the main membrane distillation configurations	• Opaque particles / or translucent feed solutions and scaling/fouling may block visualization of the wetting mechanism
• Non-invasive and Non-destructive	• Utilization limited to steady state as water properties, and operating parameters may influence light transmission
• Easy to setup and could be coupled with existing membrane cells with adaptations to visualize the membrane surface	• Thin, durable spacers designed to make more of the membrane surface available for visualization, ideally approaching 100 % surface visualization.

The developed tool is simple and can be easily adapted to all membrane distillation configurations for example; DCMD, SGMD, AGMD, and VMD with suitable adaptation the membrane module. With this optical tool, the effects of operating parameters (temperatures, flow rates, local hydrodynamic conditions, feed salinities, time and membrane, etc.) on *in-situ* wetting can be evaluated. Additional to wetting detection techniques, there is a growing interest in membrane regeneration after wetting. In this study, the proof of concept was based on the observation of de-wetting with the optical method, which also appears as a promising tool to elaborate de-wetting strategies. **Table 4.3** summarizes the current advantages of this optical wetting detection tool and further challenges that need to be addressed to make this tool even better.

En Français

Dans cette étude, un outil optique *in-situ* et non invasif a été développé et testé pour visualiser la propagation du mouillage en distillation membranaire sous vide. La preuve de concept selon laquelle le mouillage in situ peut être détecté par transmission de la lumière a été fournie et validée par la méthode DDTI. L'outil a été testé avec des solutions salines et des eaux de mer réelles, en induisant le mouillage grâce à l'ajout d'un surfactant. L'outil optique a pu fournir des informations sur les mécanismes de mouillage avec les solutions étudiées. L'outil développé est adaptable et permet de visualiser le mouillage à des échelles globale et locale. Auparavant, ce niveau d'évolutivité n'était possible qu'avec des techniques *ex-situ* telles que SEM / EDX.

L'outil développé est simple et peut être facilement adapté à toutes les configurations de distillation membranaire par exemple ; DCMD, SGMD, AGMD et VMD avec une adaptation appropriée du module membranaire. L'utilisation de cet outil optique permet d'évaluer *in-situ* les effets des paramètres de fonctionnement (températures, débits, conditions hydrodynamiques locales, salinités des solutions, durée et membrane, etc.) sur le mouillage. Outre les techniques de détection de mouillage, la régénération de la membrane après mouillage suscite actuellement un intérêt croissant. Dans cette étude, la preuve de concept reposait sur l'observation du « démouillage » par la méthode optique, qui apparaît alors également comme un outil prometteur pour élaborer des stratégies de démouillage.

Acknowledgements

I would like to thank Ms. Manon Montaner for working together to construct the membrane cell and the optical device. Mr. Claude Leman and Dr. David Laupsien are acknowledged for sharing their experience on optics, opto mechanical systems and data treatment respectively. Acknowledgement are also extended to Mr. Evrard Mengelle, Dr. Mathias Monnot, Fabric'INSA and the physics department of INSA Toulouse for providing access to 3D printer, collection of Seawater 1, laser cutter and SEM/EDX respectively. As always I would like to thank ANR (Agence nationale de la recherche) Programme: Innovation technologique pour analyser, remédier ou réduire les risques environnementaux (DS0102) 2014 for funding projet WETMEM (ANR-14-CE04-0008).

Preface to Chapter 5

As seen through **Chapter 1,2, 3 and 4** the selection of an appropriate membrane becomes vital as it pose a risk of wetting under different operating conditions. Today commercial membranes used or studied for MD process are generally microfiltration membranes, but they were not specifically designed for MD operation. Thus, introducing an important challenge of fabricating good membranes that can lower the risk of wetting. Therefore, under the framework of the ANR project WETMEM, the two partners (Institut Européen des Membranes (IEM) and Laboratoire Réactions et Génie des Procédés (LRGP), Nancy) took the task of exploring different membrane fabrication techniques. **Chapter 5** is dedicated to analyzing these fabricated membranes for their effectiveness for wetting resistance by evaluating for their intrinsic properties and permeabilities as compared to commercial membrane available in the market. Additionally, it was revealed during the bibliography review (**Chapter 1**) that selection of a suitable spacer also becomes important as they can introduce additional mass transfer resistance (lowering permeability) and cause mechanical failure on membranes utilized for MD. These 2 topics are explored and studied in this chapter under vacuum membrane distillation for selection of a good spacer and membrane that may be suitable to be utilized in vacuum membrane distillation.

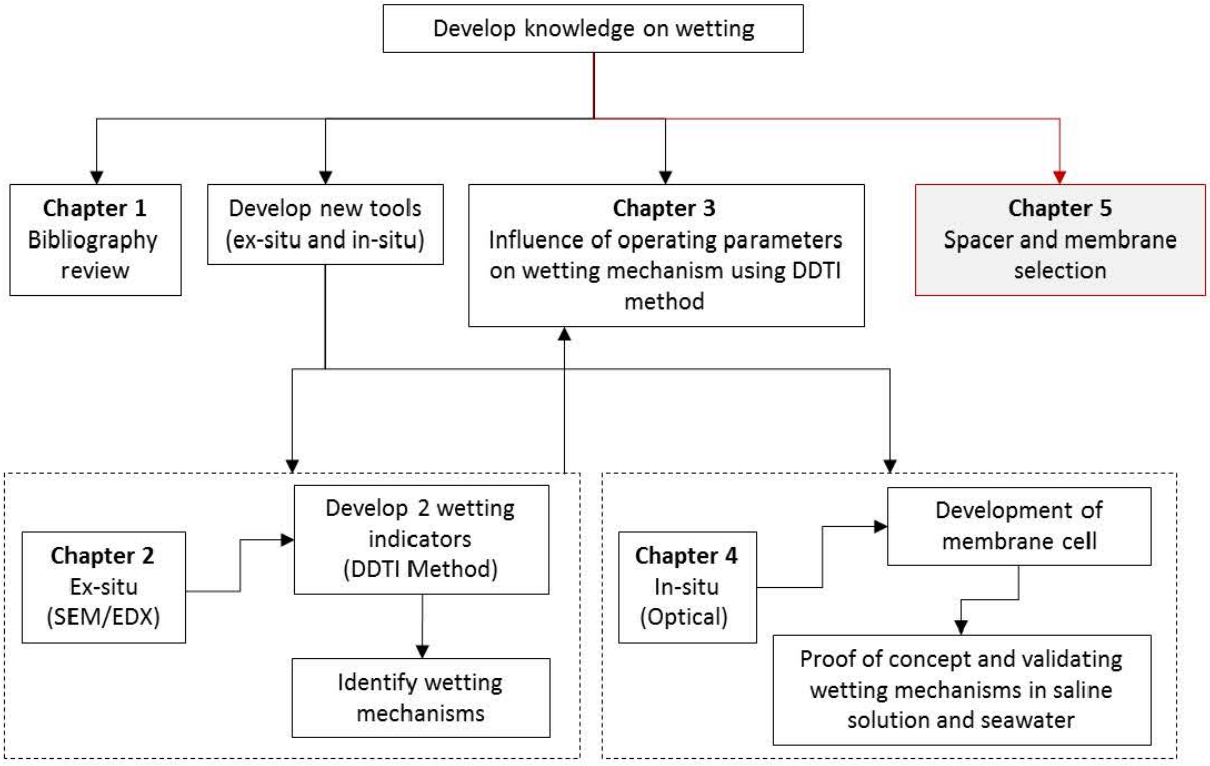

Chapter 5 : Choice of spacers and characterizing membranes in vacuum membrane distillation

Summary of objective (in English)

Geometrical characterization of 9 spacers and their effectiveness for utilization as a single spacer to support the membrane for vacuum membrane distillation were evaluated. All spacers were assessed based on permeability and pure water flux under constant operating conditions using the same PVDF membrane (0.22 µm Durapore membrane). It was found that a polypropylene-based coarse spacer with a 53.54 % open area was better than the other studied spaces. This spacer was implemented as the default spacer for studying membranes under vacuum membrane distillation pilot. The second objective of this chapter was to characterize 23 membranes (commercial and fabricated by partners) under the framework of the ANR project (WETMEM). These membranes were characterized and evaluated for their intrinsic properties (thickness, contact angle, liquid entry pressure) and permeabilities.

Résumé de l'objectif (en français)

Le premier objectif de ce chapitre est d'étudier l'effet de différents espaceurs sur la mesure de perméabilité d'une membrane. Il s'agit d'évaluer si la géométrie, ou le matériau de l'espaceur peuvent significativement modifier la mesure de perméabilité de la membrane. Dans cette optique, la caractérisation géométrique de 9 espaceurs est effectuée. Tous les espaceurs sont comparés en mesurant, avec chacun, la perméabilité de la membrane et le flux d'eau pure (membrane Durapore en PVDF de 0,22 µm). Le premier résultat est qu'il est possible d'utiliser un seul espaceur, pour supporter côté perméat la membrane de distillation membranaire sous vide. Les résultats ont également montré que l'espaceur en polypropylène, ayant une surface ouverte de 53,54%, est celui qui présente la plus faible résistance au transfert. C'est cet espaceur qui est alors sélectionné pour la suite des expériences de distillation membranaire. Le deuxième objectif de ce chapitre est de caractériser 23 membranes (commerciales et fabriquées par des partenaires) dans le cadre du projet ANR (WETMEM). Les propriétés de ces membranes sont caractérisées (épaisseur, angle de contact, pression d'intrusion liquide) et leurs perméabilités sont mesurées et comparées.

5.1. Introduction

The first objective of this chapter was to study different spacers to be used in the vacuum membrane distillation cell and to compare their effectiveness in terms of membrane permeability and pure water flux measurements. The second aim was to characterize and compare commercial and fabricated membranes under the project framework of WETMEM. Intrinsic membrane properties and permeabilities were compared to evaluate the performance of membranes used in the vacuum membrane distillation pilot.

5.2. Materials and methods

The overall protocol followed in this chapter is presented in **Figure 5.1.** Firstly, for the spacer study, 9 spacers were geometrically characterized, and their properties evaluated. Following this evaluation, permeability and pure water flux of Durapore membrane (0.2 µm PVDF) with each spacer was assessed. Based on these results, the best spacer was selected for further testing both commercial and partner university membranes.

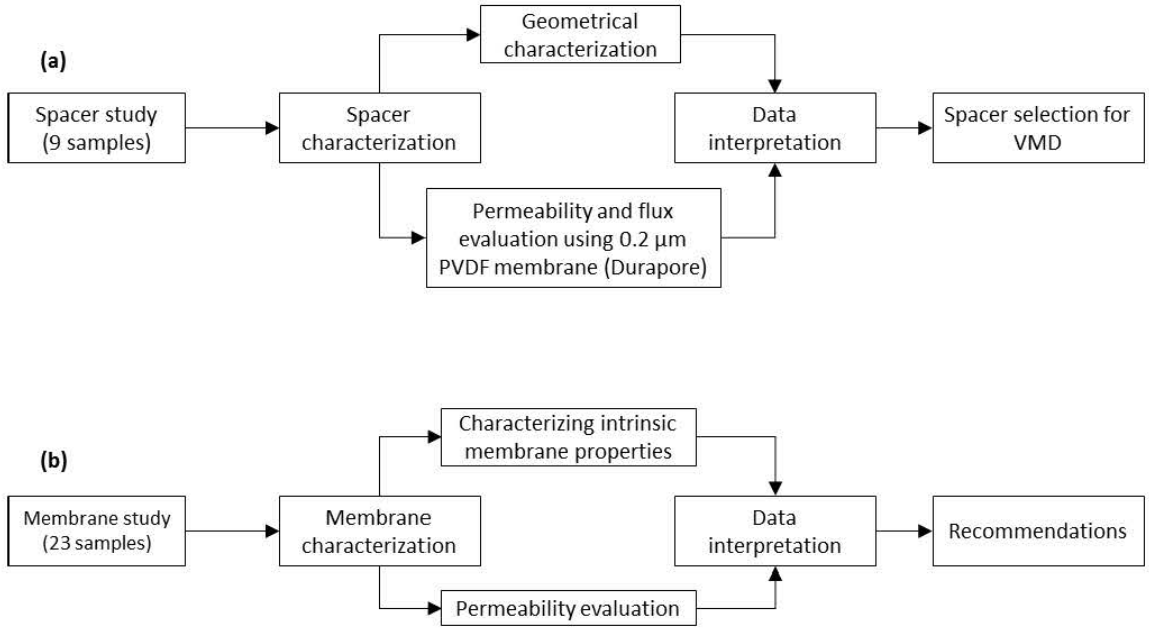

Figure 5.1: General protocol for (a) spacer study (b) membrane characterization and evaluation

In the second part of this chapter, 23 samples of different membranes were characterized: intrinsic membrane properties were evaluated and their performance in the VMD pilot were assessed thanks to permeability measurements. Description of the vacuum membrane distillation pilot, the membrane module and detailed characterization techniques and operating strategies used for each part of this study are elaborated in the following paragraphs.

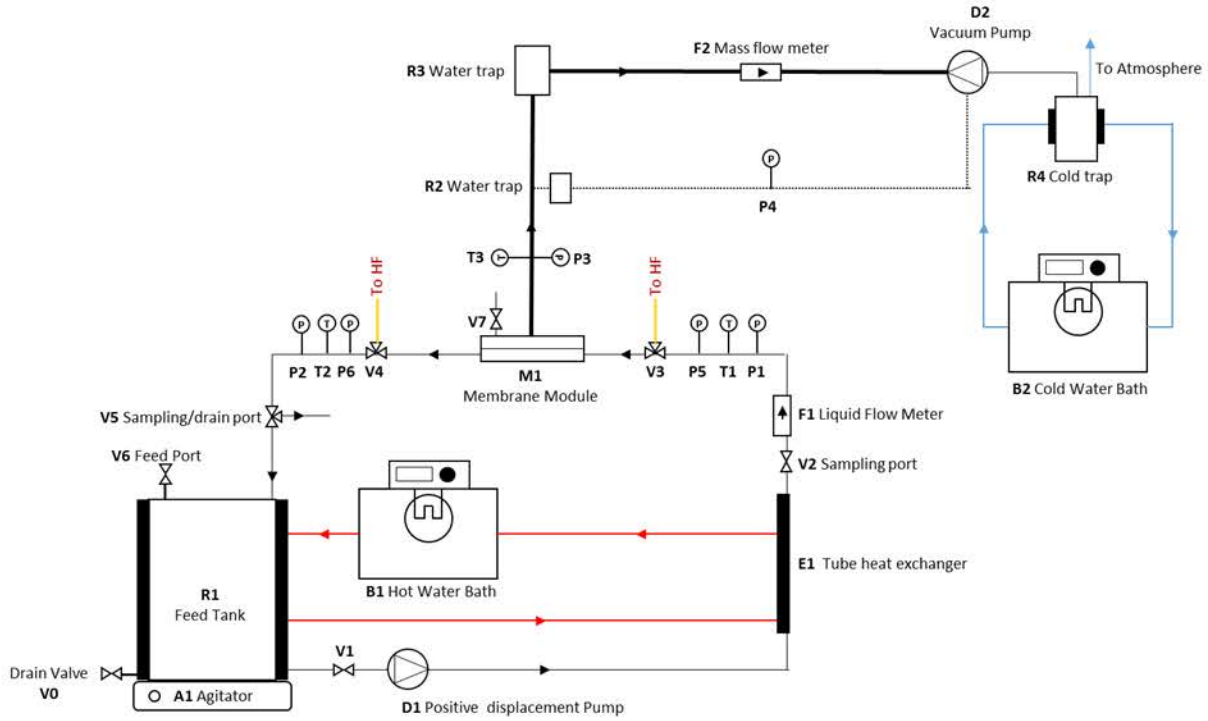

Figure 5.2: Schematic of vacuum membrane distillation setup (to be viewed in color)

5.2.1. VMD Setup and membrane module

Deionized water was used as a feed solution with 4L fed into the jacketed feed tank (R1), which was heated by a hot water bath (Model: 18202, Bioblock Scientific) as presented in **Figure 5.2**. A magnetic stirrer (Variomag, Thermo Scientific) set at 350 RPM was used inside R1 to have uniform temperature distribution. The feed side was operated in cross-flow mode. The feed solution, thanks to a magnetic pump (AB pump), passed through a tube heat exchanger (E1) and a flow meter (Krohne, 0-250 L/h) and entered the membrane module. The flow rate could be varied between 22 - 250 L/h corresponding to a Reynolds number Re 382 – 4000 (depending on the temperature of the feed). Feed temperature (using Pt type sensor) and operating pressure (E7, Bourdon Sedeme) were logged both before (T1, P1) and after (T2, P2) passing through the membrane module. Sampling ports (V2 and V5) were available before and after the membrane module. On the permeate side, the vacuum pressure was maintained using a vacuum pump (NT VARIO, Vacuubrand (1000 - 3 mbar)) and set by a vacuum regulator. A vapor flow meter (Bronkhorst, 0-60g/h) was used to determine the flux of the membrane. Two water traps (R2 and R3) were used to protect the mass flow meter and vacuum sensor in case of the membrane breaks. The vacuum pipe (TYGON® E-3603) was heated so that vapor did not condense on the pipeline and the mass flow meter could get the accurate readings. Finally, a cold trap was used after the vacuum pump to condense the permeate using a cold-water bath (18205, Bioblock Scientific (-4°C)). All sensors were calibrated before using and connected to a computer for data logging. Conductivity was

measured both in feed and condensed permeate using conductivity probes during the experimental run and values reported at 25°C.

As presented in **Figure 5.3**, the membrane module (M1) had an active surface area of 4.16 x 10^{-3} m² (See Supplementary Data Figure C2.1). The membrane was sealed using an O-rings with a spacer on the permeate side only. The whole membrane module was encased with 2 stainless steel blocks.

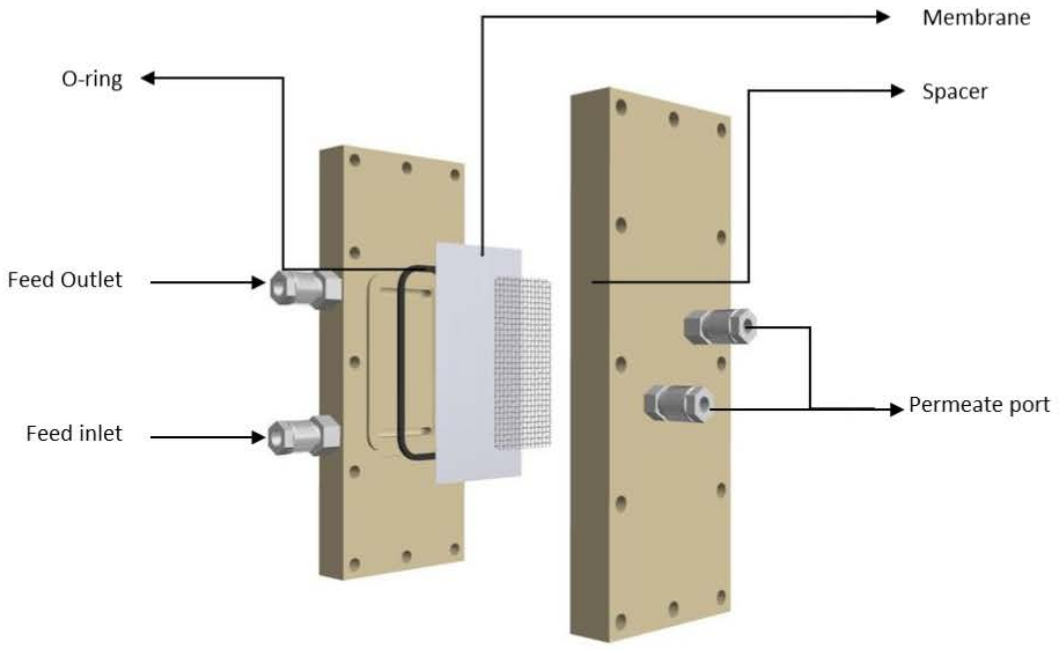

Figure 5.3: Membrane cell (to be viewed in color)

5.2.2. Membranes

5.2.2.1. Membrane studies

A total of 23 membranes were studied where most being either PVDF or PTFE membranes as listed in **Table 5.1.** The 2 commercial membranes from Millipore (M1a = Durapore, PVDF and M2a = Fluoropore, PTFE) have been extensively utilized in all membrane distillation configurations [4,37]. The average pore size of these membranes was 0.2 µm. Sumitomo membranes (M3 – M7) of different pore sizes (0.1, 0.2, 0.45, 1 and 5 µm) are PTFE membranes and have been used to a lesser extent [39]. The project partners provided 16 membranes (M8a – M23a) with the top side as the active layer, however, no information on the pore size was made available. The product numbers of each membrane, the material, with or without the support layer and fabrication techniques with their respective manufacturers are presented in **Table 5.1.** The membranes manufactured at Institut Européen des

Membranes (IEM) were PVDF membranes and were manufactured using different techniques as listed below:

- Liquid Induced Phase Separation (LIPS)
- Vapor Induced Phase Separation(VIPS)
- Mixing both methods

Detailed protocol for membrane fabrication can be found elsewhere [12,14] Additionally, fabrication techniques used for IEM membranes are briefly described below:

- Protocol A (LIPS2): Immersion in osmosis water
- Protocol B (VIPS + LIPS2): Exposition to water vapor and then immersion in osmosis water
- Protocol C (VIPS + LIPS1 + LIPS2): Exposition to water vapor, immersion in alcohol (duration time t1 or t2) and then immersion in osmosis water
- Protocol D (LIPS1 + LIPS2): Immersion in alcohol (duration time t1 or t2) and then immersion in osmosis water. Some membranes were prepared by a variant of this protocol called Modified Protocol D.
- Protocol E: (LIPS1+ VIPS + LIPS2): Immersion in alcohol (duration time t1), exposition to water vapor and then immersion in osmosis water.

Whereas the membrane manufactured by Laboratoire Réactions et Génie des Procédés (LRGP), Nancy were microporous membranes (0.22µm GVHP0010) coated with a dense layer. The M21a membrane was coated with TPX Polymethylpentene whereas M22a was coated with Poly[4,5-difluoro-2,2-bis(trifluoromethyl)-1,3-dioxole and M23a with poly(1-trimethylsilyl-1-propyne) respectively. Detailed fabrication techniques can be found elsewhere [13].

Table 5.1: Membranes used in this study

Sr.no	Ref.	Material	Support layer	Manufacturer	Product no.	Fabrication	R_{avg}, (m)
1	M1a	PVDF	No	Millipore	Durapore	Phase inversion	2.20E-07
2	M2	PTFE	Yes	Millipore	Fluoropore	-	2.00E-07
3	M3	PTFE	No	Sumitomo	HP-01-30	Stretching	1.00E-07
4	M4	PTFE	No	Sumitomo	HP-020-30	Stretching	2.00E-07
5	M5	PTFE	No	Sumitomo	HP-045-30	Stretching	4.50E-07
6	M6	PTFE	No	Sumitomo	WP-100-100	Stretching	1.00E-06
7	M7	PTFE	No	Sumitomo	WP-500-100	Stretching	5.00E-06
8	M8a	PVDF	No	IEM	16SGO 84	Protocol D t1	-
9	M9a	PVDF	No	IEM	16SGO 86	Protocol A	-
10	M10a	PVDF	No	IEM	16SGO 88	Protocol D t2	-
11	M11a	PVDF	No	IEM	16SGO 90	Protocol B	-
12	M12a	PVDF	No	IEM	16SGO 92	Protocol E t1	-
13	M13a	PVDF	No	IEM	16SGO 94	Protocol E t2	-
14	M14a	PVDF	No	IEM	16SGO 96	Protocol C t1	-
15	M15a	PVDF	No	IEM	16SGO 98	Protocol C t2	-
16	M16a	PVDF	No	IEM	M195a	Modified Protocol D t2	-
17	M17a	PVDF	No	IEM	M196a	Modified Protocol D t2	-
18	M18a	PVDF	No	IEM	M197a	Modified Protocol D t2	-
19	M19a	PVDF	No	IEM	M198a	Modified Protocol D t2	-
20	M20a	PVDF	No	LRGP	Durapore	Phase inversion	2.20E-07
21	M21a	PVDF	No	LRGP	N°F	Coating 2% PMP	-
22	M22a	PVDF+AF2400	No	LRGP	Teflon AF2	Coating	-
23	M23a	PVDF+PTMSP	No	LRGP	PTMSP (1)	Coating	-

Note: "a" implies active surface of the membranes

5.2.2.2. Characterization of intrinsic membrane properties

5.2.2.2.1. Thickness

The thicknesses of the membranes were also assessed using electronic micrometer, Schuts Model-134001. Each membrane was sampled at 5 locations, and the mean with standard deviation reported.

5.2.2.2.2. Contact angle

Contact angle (CA) analyses using deionized water were conducted using Drop Shape Analyzer (DSA25, Kruss) and the results post-processed in accompany software (ADVANCE). For the experiment protocol, guidelines and definitions from [123,174] were considered for reproducible measurements for CA. Ellipse (Tangent-1) fitting method was used for estimating the CA. Analyses were conducted on the sample using a drop of 28-35µl using a calibrated syringe with water at 20°C for CA. 6-8 samples were taken over the active membrane surface (feed side) with averaged results and standard deviation reported.

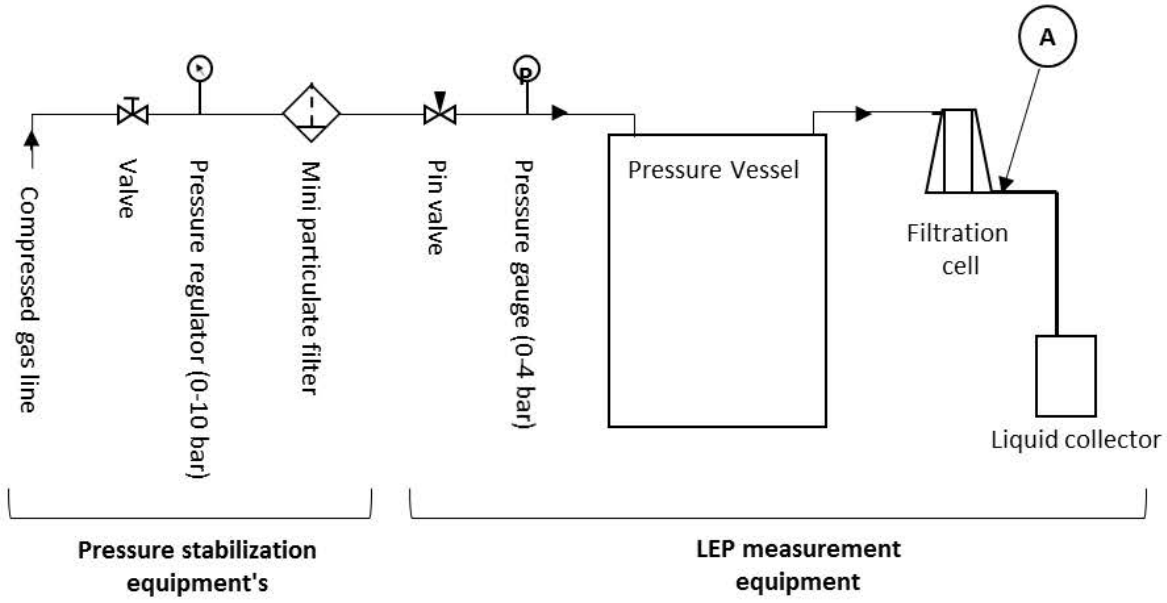

Figure 5.4: Schematics of liquid entry pressure measurement

5.2.2.2.3. Liquid entry pressure

Standard protocols of LEP_w measurements were used. The schematic of the complete setup used for the LEP measurements are presented in **Figure 5.4**. The experimental protocol to obtain the LEP_w is based on the observation of the first drop of permeate (at location A, **Figure 5.4**) during a pressure step filtration operation. A 50 mL filtration cell (Amicon stirred cell, Sartorius model no. 17530) was

used to secure a ϕ 25 mm hydrophobic membrane using an O-ring and filled with ultra-pure water using a pressure vessel. A pin valve (Norgaen, model no. D-70731) was used to control the applied pressure, and this pressure was measured by a gauge (IMT, 0-4 bar). To stabilizing the gas flow rate, the following series of pressure stabilizing equipment's were used: a gross valve (for air inlet), pressure regulator (SMC, 0-10 bar) and particle filter (5 µm).

5.2.2.2.4. Scanning electron microscopy

Scanning electronic microscope (JEOL, JSM-6400) was used with accompanying software (ESPRIT 1.9) for sample analysis. The samples were prepared and later coated with gold for visualizing the membrane surfaces. The high tension of the SEM was 20 KeV. EDX was not conducted in this part of the study.

Table 5.2: Spacer studied to be utilized in vacuum membrane distillation pilot

Reference	Mesh category	Brand / Model no.
Spacer 1	Coarse	Gantois / -
Spacer 2	Coarse	Millipore / Polypropylene backing for Fluoropore membrane
Spacer 3	Fine	Gantois / Woven mesh 304L n°110.22 fr0.112
Spacer 4	Coarse	Nitto Denko / Feed side spacer for RO membranes (USPA 2-4444)
Spacer 5	Coarse	Gantois / -
Spacer 6	Coarse	Sefar-Fyltis / 05-1020-W BC
Spacer 7	Coarse	-
Spacer 8	Coarse	Gantois / -
Spacer 9	Coarse	Gantois

Note: Fine mesh: 0.5 - 0.025 mm | Coarse mesh: 2 - 0.5mm

5.2.3. Spacers

5.2.3.1. Spacer study

A total of 9 spacers were studied as presented in **Table 5.2**. The spacers varied in thickness, open area, attack angle, and material. The spacers used in this study were categories into fine (*0.5 - 0.025 mm)* and coarse (*2 - 0.5 mm)* meshes using the standard convention. Before installing the spacers on the membrane cell, geometrical characterizations were conducted. Then spacer effects were evaluated by permeability and pure water flux measurements.

5.2.3.2. Geometrical characterization of spacers

As presented in **Figure 5.5**, yarn diameter (d), mesh opening (w) and filament angle (Θ) of the studied spacers were assessed using image processing with ImageJ [194]. All spacers used in this study were < 1.1 mm in thickness due to the practical constraints of the permeate channel. The following standard geometric characterizations were assessed: open area, mesh count, grammage, and thickness for characterizing the spacers.

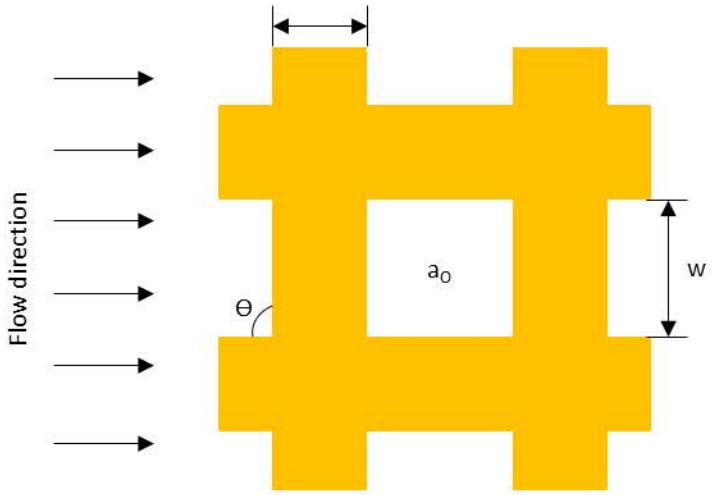

Figure 5.5: Schematic for a section of an ideal spacer

5.2.3.2.1. Open area

The open area was calculated using Eq. 5.1

$$a_{ot} = \frac{w^2 \times 100}{(w+d)^2} \qquad \textit{Eq. 5.1}$$

Where a_{ot} (%), is the calculated open area, w is the mesh opening (mm) determined by image processing and d is the yarn diameter (mm) determined by a screw gauge. To validate, the calculated open area was also compared to the image processed open area a_{oi} (%).

5.2.3.2.2. Mesh/strand count

The number of mesh/ cm of the spacer was also calculated based on Eq. 5.2.

$$n/cm = \frac{1000}{(w+d)} \qquad \textit{Eq. 5.2}$$

5.2.3.2.3. Grammage

Grammage is defined as the mass per unit area and calculated using Eq. 5.3

$$Grammage = \frac{Weight}{l \times b} \qquad Eq.\ 5.3$$

Where Grammage is expressed in g/m². The weight of each spacer was measured using Sartorius weighing balance (CP224s ± 0.1 mg), and area (l x b) was measured using an mm ruler.

5.2.3.2.4. Thickness

The thicknesses of the spacers were assessed by using an electronic micrometer, Schuts Model-134001. Each spacer was sampled at 5 locations and the mean with standard deviation reported. Geometrical characterization of each spacer was performed by image processing. The spacer images were calibrated/scaled using a ruler/ line gauge. The different spacers utilized in this study are presented in **Figure 5.6** and their characterization summarized in **Table 5.3.**

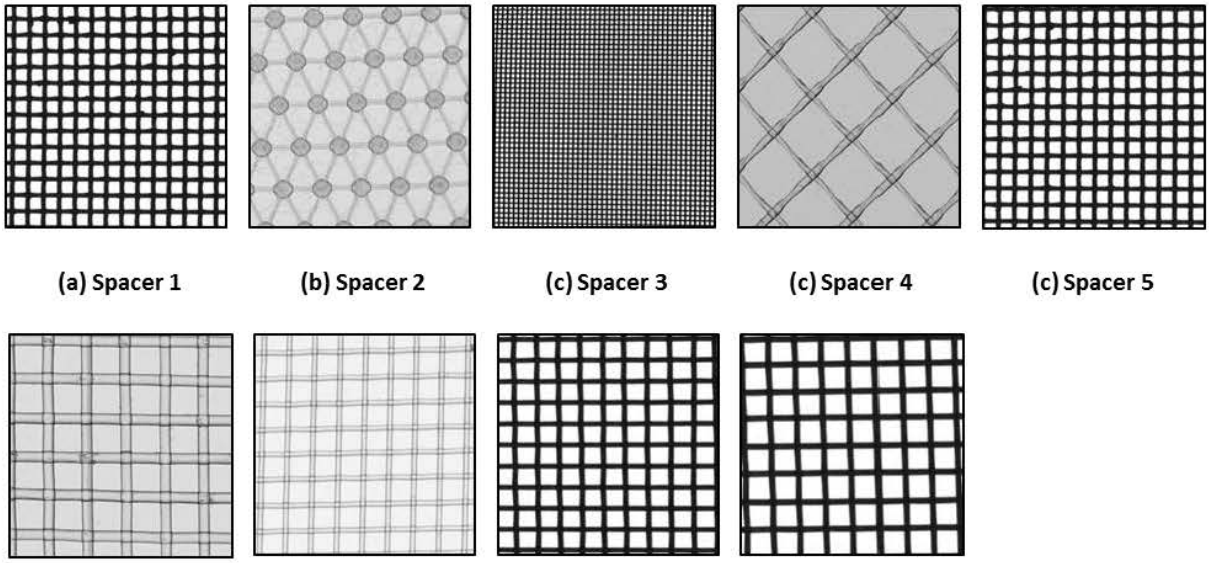

Figure 5.6: Images of the spacers utilized in this study

All spacers were <1 mm thick. Mesh opening (W) for most spacers utilized in this study were in the range of coarse meshes (0.7 – 3.36 mm) whereas only 1 fine spacer was utilized (Spacer 3). Spacer 1, 3, 5, 8 and 9 were stainless steel while Spacer 2, 4 and 6 were polypropylene with a thermal conductivity of 16 and 0.1-0.2 W/m. K respectively. The material property of spacer 7 was unknown however it is of polymer origin. The yarn diameters for the spacers were 0.14 – 0.55 mm. Based on

these physical characterizations open area (A_{ot}) was calculated both theoretically (Eq. 5.1) and using image analysis. **Table 5.3** presents both ways of analysis are in good agreement. The open area for the studied spacers varied between 44 to 76 % with most spacers being 50 - 60 % open area. In general, spacers with a high open area are more suitable for membrane distillation[195]. Indeed, high open areas would expose more membrane surface for permeation as spacers introduce additional mass transfer resistance. With the geometrical characterization, it would seem that spacer 4 with the 74 % open area should be a good spacer for utilization in the Vacuum membrane distillation pilot.

Table 5.3 Geometrical characterization of spacers used for vacuum membrane distillation

Ref.	Material	W, Mesh opening (mm)	d, Yarn diameter (mm)	Thickness (mm)	Attack Angle (°)	Calculated Open area, A_{ot} (%)	Image analysis Open area, A_{oi} (%)	Grammage (g/m^2)	Mesh count (n/cm)
Spacer 1	SS	0.70	0.30	0.64	90	49.0	49.7	1355.85	100
Spacer 2	PP	0.70	0.14	0.19	60	69.4	67.8	26.89	-
Spacer 3	SS	0.16	0.08	0.24	90	44.4	43.4	563.05	416
Spacer 4	PP	3.36	0.49	0.49	90	76.1	75.5	30.11	26
Spacer 5	SS	0.60	0.20	0.98	90	56.2	50.8	1460.80	125
Spacer 6	PP	1.50	0.55	0.84	90	53.5	51.2	151.98	48.8
Spacer 7	Polymer	1.04	0.39	0.58	90	52.8	53.9	140.04	69.9
Spacer 8	SS	1.1	0.30	0.66	90	61.7	60	1004.52	71.4
Spacer 9	SS	0.87	0.30	0.75	90	55.1	57.7	1086.45	85.7

Note: SS: 304 stainless steel | PP: Polypropylene

5.2.4. Permeability measurements used for both studies

Macro-porous hydrophobic membranes are characterized by four main parameters, i.e., thickness, δ (m), mean pore size (radius r), porosity, ε (defined as porous volume fraction relative to the total membrane volume) and tortuosity, χ (defined as the ratio of pore length to membrane thickness). Influences of each parameter to the permeability of the membrane are summarized by Lei et al. [196].

$$K_M \propto \frac{r\alpha\varepsilon}{\chi\delta} \qquad \textit{Eq. 5.4}$$

Here, K_M is the permeability, α may be equal to 1 or 2, depending on the predominant mass transfer mechanism within the membrane pores with Knudsen number, Kn > 1 or Kn < 0.01. It can be noted that membrane permeability is directly proportional to r, α, ε and inversely proportional to χ and δ.

Knudsen number is defined as the ratio of the mean free path to the pore size. As VMD works under vacuum (on the permeate side) the mean free path of water molecules is considerably larger than the pore size of the hydrophobic membranes (0.1–1 μm) used in the MD process. Consequently, mass transfer through the membrane is generally dominated by Knudsen mechanism. In the case of pure water, the molar flux J_{H2O} through the membrane is written as:

$$J_{H_2O} = k_k . \Delta P_{H_2O} = k_k . (P_m^* - P_p) \qquad \textit{Eq. 5.5}$$

Where, J_{H2O} is the molar flux of water; ΔP_{H2O} is difference in partial pressure of water on both sides of the membrane; P_m^* is vapor pressure of pure water at the membrane's operating conditions; P_p is partial pressure of water in the permeate side (equal to vacuum pressure as the permeate is only composed of water) and k_k is mass transfer coefficient of the membrane.

P*m can be calculated by Antoine Equation

$$P_m^* = \exp(A - \frac{B}{C + T_m}) \qquad \textit{Eq. 5.6}$$

Where T_m is the temperature at the membrane surface and the constant A is 23.1964, B is 3816.44, and C is -46.13.

While mass transfer coefficient k_k is expressed as

$$k_k = \frac{2}{3}\frac{\varepsilon \cdot r}{\chi \delta R T_m}\sqrt{\frac{8RT_m}{\pi M_{H_2O}}} = \frac{K_M}{\sqrt{M_{H_2O}}} \qquad \text{Eq. 5.7}$$

In Eq. 5.7, ε is porosity of the membrane; r is the radius of the pores; χ is tortuosity factor; δ is the thickness of the membrane; R is the ideal gas constant; M_{H2O} is molar mass of water, K_M is Knudsen permeability and T_m is the temperature at the membrane surface.

To facilitate comparison, all reported permeabilities are expressed at the same reference temperature T_{ref} = 20 °C by using the following equation developed by Dao et. al [7].

$$K_M(T_{ref}) = K_M(T)\sqrt{\frac{T}{T_{ref}}} \qquad \text{Eq. 5.8}$$

Where K_M (T) and K_M (T_{ref}) are Knudsen permeability values at temperature T and at reference temperature T_{ref}, respectively;

By combining (Eq. 5.5, Eq. 5.7, Eq. 5.8), a general equation for permeate flux calculation can be formulated as Eq. 5.9.

$$J_{H_2O} = \frac{K_M(T)}{\sqrt{M_{H_2O}}}\Delta P_{H_2O} = \frac{K_M(T_{ref})}{\sqrt{M_{H_2O}}}\sqrt{\frac{T_{ref}}{T}}\Delta P_{H_2O} \qquad \text{Eq. 5.9}$$

According to this equation, determination of permeability of hydrophobic membrane K_M can be performed by varying of trans-membrane partial pressure ΔP_{H2O} while recording the variation of corresponding permeate flux, J_{H2O}. Thus, the slope of the line presents the correlation between J_{H2O} and ΔP_{H2O} i.e., K_K which is further used to calculate the permeability K_M of the membrane. Variation of partial trans-membrane pressure ΔP_{H2O} can be conducted by either varying vacuum pressure at a constant bulk temperature (**pressure variation method**) or by varying bulk temperature at a fixed vacuum pressure (**temperature variation method**).

5.2.4.1. Pressure variation method

In the PV method, the variation of trans-membrane partial pressure difference ΔP_{H2O} was done by varying permeate pressure at a constant bulk temperature. Different values of the permeate flux, J_{H2O} could be achieved corresponding to each different value of the permeate pressure Pp. In this case, the two

parameters J_{H2O} and ΔP_{H2O} (Eq. 5.9.) are variables while the others are constant. A plot between two factors J_{H2O} and ΔP_{H2O} provides a slope, giving the value of mass transfer coefficient k_k (Equation Eq. 5.5). This value is then used for further calculating the Knudsen permeability, K_M at reference temperature, T_{ref} = 20 °C by the Eq. 5.8. Pressure variation method was adopted to test the permeability of the membranes based on the protocols outlined by the following thesis's and paper [172,197,198], [7].

5.2.4.2. Temperature variation method

In the TV method, the applied pressure is kept constant, and the bulk temperature is varied to achieve the trans-membrane partial pressure difference. A different value of the permeate flux (J_{H2O}) can be achieved corresponding to each different value of the bulk temperature. In this case, the two parameters, J_{H2O} and $\sqrt{\frac{T_{ref}}{T}}\Delta P_{H_2O}$ (Eq. 5.9) are variables while, $\frac{K_M(T_{ref})}{\sqrt{M_{H_2O}}}$ is a constant. The linear slope between the plot of J_{H2O} and $\sqrt{\frac{T_{ref}}{T}}\Delta P_{H_2O}$ is used to calculate K_K. Which in turn is used with α, to obtain the Knudsen permeability K_M at reference temperature, T_{ref} = 20 °C by the Eq. 5.10.

$$K_M(T_{ref}) = \alpha\sqrt{M_{H_2O}} \qquad \textit{Eq. 5.10}$$

Permeability determination using temperature variation method was used for characterizing and evaluating spacers utilized in vacuum membrane distillation pilot.

5.2.4.3. Flux measurements

The permeate flux was calculated using the vapor mass flowrate measured by the flow meter (g/h) using Eq. 5.11.

$$J = \frac{\text{vapor flux}}{1000 \times A} \qquad \text{Eq. 5.11}$$

Where, J is flux (Kg/m².h), and A (active membrane area, m²)

5.2.5. Operation strategies for permeability measurements

Ultrapure water was used as feed for all permeability measurements with each test conducted on a new membrane.

5.2.5.1. Spacer study

Normally, two spacers are used in most membrane distillation configurations [195,199]: one of the spacers is located on the feed side and the other one on the permeate side. However, in VMD there is an opportunity to use a single spacer on the permeate side which could serve the purpose of both stabilizing the membrane and creating turbulence for the feed to flow on the surface. Therefore, spacers were installed in the permeate channel and no spacers were installed in the feed channel of the module as presented in **Figure 5.2**. Due to the limitation of the permeate channel depth, all tested spacers were below 1.1 mm in thickness. The vacuum pressure was controlled at 7.4kPa. The feed temperature was varied between 35 – 60°C for both permeability measurements and pure water flux measurements. Temperature variation technique for permeability measurement was used. The feed flow was maintained at 150 L/h, corresponding to a Reynolds number of 2639 (at 40°C) and 3663 (at 60°C) (Eq. 5.12).

$$Re = \frac{\rho . D_h . v}{\mu} \qquad \text{Eq. 5.12}$$

Where, ρ is the fluid density (kg/m^3), D_h is the effective diameter (m), v is the fluid velocity inside the membrane chamber (m/s) and μ is the dynamic fluid viscosity (kg/m.s). The values for the constants (ρ, v, and μ) at different operating temperatures(T_f) were taken from standard reference [184]. The membrane used for the spacer study was the Durapore (0.22 μm, PVDF) membrane.

5.2.5.2. Membrane study

For each membrane, permeability measurements were conducted on their top side only using pressure variation method. Ultrapure water was used as feed for permeability measurements. The flow rate for membranes M1a –M7, M20a-M23a was set at 150 L/h (corresponding to a Reynolds number of ~ 2000), while for M8a - M19a, the flow rate was kept at a minimum (25 L/h) which corresponds to a Reynolds number 324 – 440 depending on the water temperature. The feed temperature was kept at 35 – 37°C (measured using Pt type sensor T1 and T2).

5.3. Results and discussions

5.3.1. Influence of the spacer on permeability and pure water flux measurements

The Durapore membrane permeability was measured with each spacer using temperature variation method. Each experiment was carried out using a new membrane, and every spacer was tested > 4 times.

The average permeability and standard deviation for each spacer are presented in **Figure 5.7.** It can be clearly seen that different spacers have varying degree influence on the permeability of the same membrane.

For comparable geometries (Spacers 1, 5, 6, 7 and 9), the effect of the spacer material (SS or PP) on membrane permeability was negligible For example, spacers with ~ 50 % open areas (see **Table 5.3**) performed similarly (permeability's 3.47 x 10^{-6} to 3.7 x 10^{-6} $mol^{1/2}.m^{-1}Kg^{-1/2}$) even though spacers 1, 5 and 9 were stainless steel while 6 and 7 were polymer-based spacers.

Spacer 2 performed the least under the same operating conditions, even though most geometrical properties of this spacer were similar to the other studied ones expect thickness. Spacer 2 was the thinnest with introducing only a 0.19 mm gap between the membrane surface and the permeate wall. It could be postulated that due to the low thickness of the spacer, the transmembrane vapor pressure experienced at different locations on the membrane surface was dissimilar and resulted in low vapor flow rate from these regions, thereby leading to low permeability.

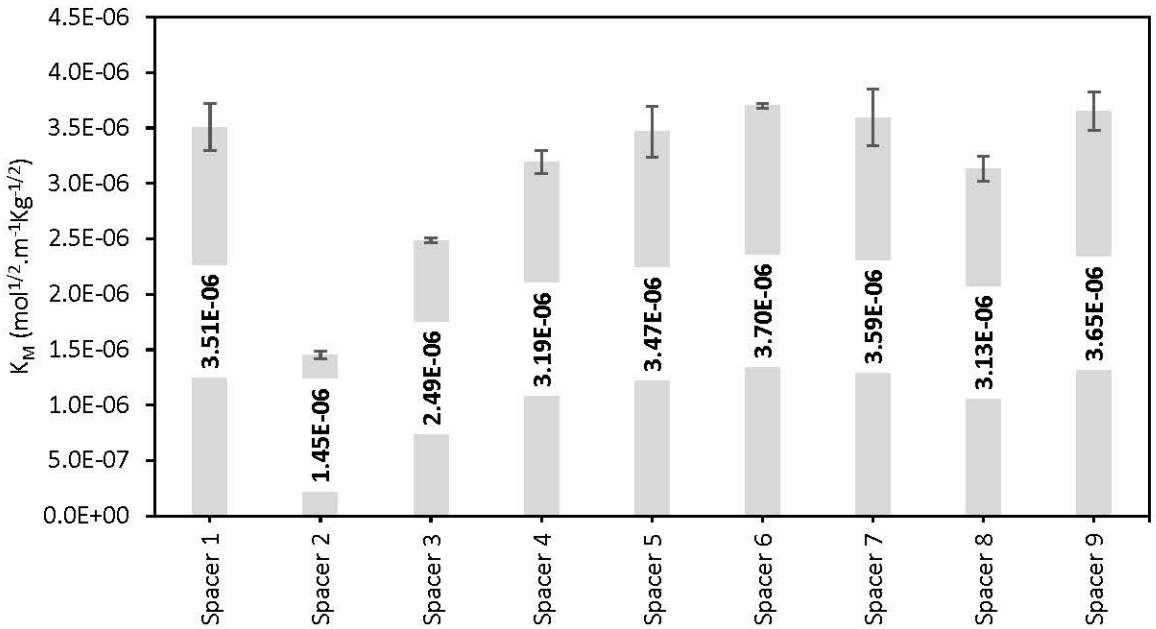

Figure 5.7: Average permeability of the membrane measured with different spacers

It was interesting to note that an increase in open area could not be coupled with an increase in permeability. Let us consider five spacers with a descending order of open area (Spacer 4 = 75.5 %, Spacer

2 = 67.8 %, Spacer 8 = 60 %, Spacer 6 = 53.4 %, and Spacer 3 = 44 %). Spacer 3 (fine mesh) with the least open area of 44 % was also found to be 2nd lowest in performance with an average permeability of 2.5 x 10^{-6} $mol^{1/2}.m^{-1}Kg^{-1/2}$. However, with this spacer, the membrane performed consistently with a low standard deviation of ±2.2E-08. Considering the membrane permeability with these spacers, it could be noted that the permeability did not linearly reduce based on the descending order of the open area. On the contrary membrane permeability was observed to be higher using Spacer 6 (3.70E-06 ± 1.94E-08 $mol^{1/2}.m^{-1}Kg^{-1/2}$) as compared to Spacer 4 (3.19E-06 ± 1.04E-07 $mol^{1/2}.m^{-1}Kg^{-1/2}$). Now considering the total range of open area, it would seem there is an optimum between low open area and high open area. Overall it could be seen that Spacer 6 with the highest permeability of 3.7 x 10^{-6} $mol^{1/2}.m^{-1}Kg^{-1/2}$ performed better than other spacers with least deviation ±1.8E-08.

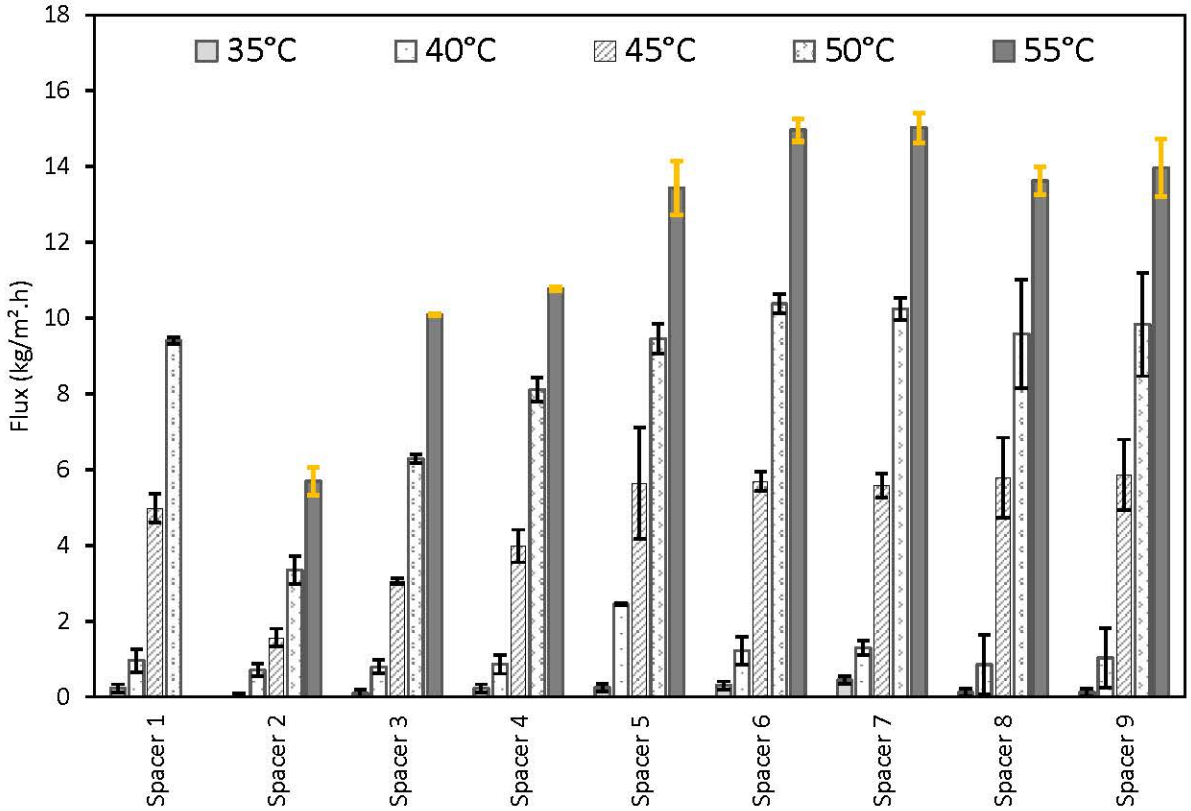

Figure 5.8: Pure water flux of membrane with the studied spacers at temperatures between 35 – 55°C

All spacers were also evaluated for their influence on the membrane concerning pure water flux under the same operating conditions (**cf. 5.2.5.1**) at different temperatures (35 -55°C). The average flux and standard deviation of 6 membrane samples with each spacer are plotted in **Figure 5.8**. Here it can be seen that at lower temperatures of 35 and 40 °C the difference in flux between the studied spacers were negligible, with a flux between 0 – 2.5 kg/m².h. However, at high temperatures, 45- 55°C the flux responses became

significant and distinguished non-performing spacers could be more vivid. With most spacers (1, 5, 6, 7, 8, and 9) the produced fluxes were in the range of ~ 5 – 5.9 Kg/m².h at 45°C with spacers 2 performing the least with 1.6 kg/m².h. Overall, it could be seen that spacers 4-9 performed better at 45 and 50°C. At 55°C, spacer 6 had a flux 2.6 times the flux of spacer 2. Finally, it should be noted that spacer 6 and 7 performed similarly at this temperature.

5.3.1.1. Spacer selection

Considering all the studied spacers it can be noted that spacers with an open area of 50 – 60 % performed better than others. Additionally, spacers with the least thickness performed the least for both permeability and pure water flux evaluation followed by the fine mesh spacer 3. In literature, spacer studies on direct contact membrane distillation also observed that coarse spacers induced turbulence and enhanced membrane flux than fine spacers [195]. A similar difference in flux and membrane permeability could be observed in this study. Spacer 6 performed consistently both for permeability and flux measurement with the least standard deviation; and this spacer would be used for all the studied membranes in the next section and chapters.

5.3.2. Membrane characterization

A total of 23 membranes were studied where 8 were commercial membranes, and 15 were membranes fabricated using different techniques. M1a to M7 were commercial membranes acquired by INSA Toulouse. M8a to M19a were membranes prepared by IEM, where M16a -M19a were made with the same fabrication techniques in different batches. Whereas M20a (Durapore 0.22 µm PVDF membrane) was as given as blank reference and M21-23a were different dense layer coating on a Durapore membranes provided by LRGP. The membranes in this study were characterized for their thickness, contact angle, and liquid entry pressure (LEP_w). Pore morphologies on the active surfaces were visualized using SEM, and membrane permeabilities were also determined.

2.3.2.1 Thickness

The thickness of the membranes used in this study varies from 30 to 220 µm (see **Figure 5.9**). Most PVDF membranes including commercial and fabricated by partner universities had a minimum thickness of 100 µm to a maximum of 171.4 µm, whereas the PTFE membranes were generally thinner with a minimum width of 30 µm (M3) and a maximum of 220 µm (M2 Fluoropore membranes). However, Fluoropore membranes had a support layer of 190 µm attached to it, and the membrane itself was 30 µm. It can also

be noted that for Sumitomo PTFE membranes (M3-M7), as the pore size increased from 0.1 – 5 µm, the thickness of the membranes also increased from 28.4 to 50.8 µm. It was communicated that this is due to limitation to produce stable membranes properties with a larger pore size of 1 and 5 µm. Indeed, it was also observed that commercial and dense membranes used in this study (M1-M7, M20a-M23a) had a low standard deviation concerning their thickness, whereas, manufactured PVDF membranes (M8a-M19a) had a more significant deviation from their average thickness. In literature, membranes of 10 - 220 µm have been reported to be used in membrane distillation for different applications [17,23,95–97]. A recent review recommended membrane thickness of 30 - 60 µm for low salinities and 200 - 700 µm for high salinity solutions in order to prevent wetting [58]. This implies that a flat sheet membrane may be more applicable at lower salinities whereas thick flat sheet membranes or hollow fiber membranes would be more applicable to hypersaline solutions.

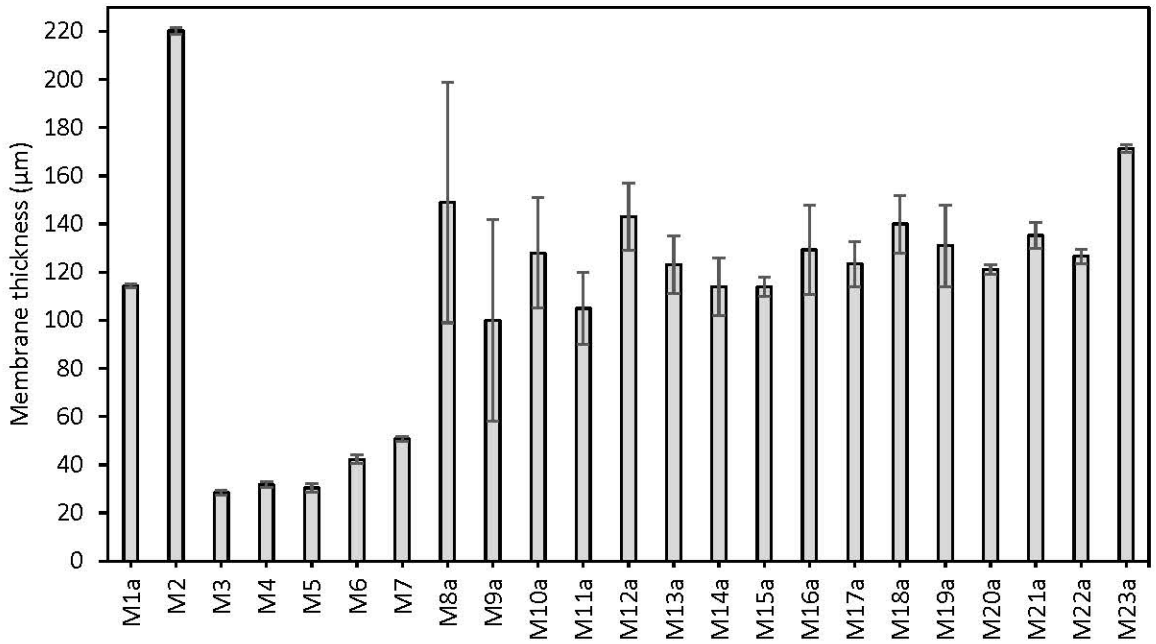

Figure 5.9: Thickness of the studied membranes

2.3.2.2 Contact angle

One of the primary criteria for membranes used for membrane distillation is hydrophobicity [24]. As per definition [123], hydrophobicity is defined by a stable contact angle of ≥ 90° between the membrane surface and a calibrated drop of water. As presented in **Figure 5.10**, all studied membranes had a contact angle higher than 90° except M8a with a contact angle of 70±5°. The highest observed contact angles were

between 130 to 135° for commercial PTFE membranes (M2,4-6) and PVDF membranes fabricated by IEM (M12, 18 & 19). Concerning contact angle, the average standard deviations for all membranes were ~ ± 2.35 °. In general PTFE membranes exhibited a higher contact angle of 131 ± 2.1 as compared to PVDF membrane with an average contact angle of 116 ± 2.5°. In literature, membranes with a contact angle of 80-160° have been utilized for membrane distillation [17,23,95–97] however for wetting prevention a CA >105° is recommended [58], and most membranes assessed in this study were above this CA.

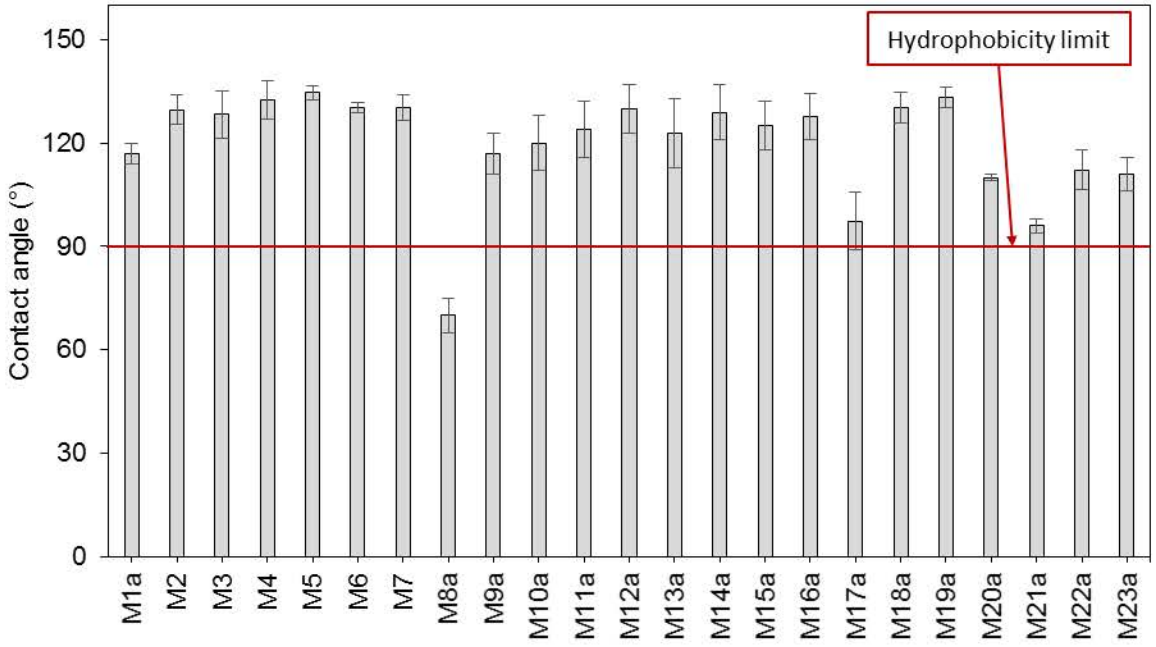

Figure 5.10: Contact angle of the active side of the membrane surface

2.3.2.3 Liquid entry pressure

A high LEP_w is a vital parameter for evaluating membranes utilized for membrane distillation [24]. Indeed, this tool is used as a primary technique to determine the minimum pressure a membrane can withstand before the liquid penetrates its pores. All membranes in this study were analyzed for their LEP_w under standard conditions (**Cf. 5.2.2.2.3**). As seen in **Figure 5.11**, most commercial membranes had a LEP > 2 bar apart from PTFE membranes with the average pore radius of 1 and 5 µm (M5 and M6). Fluoropore (M3) and the dense membrane by LRGP (M22a and M23a) had a LEP_w of above 4 bars (above the limit of the pressure sensor used). IEM membranes (M8a-M19a) performed to a varying degree depending on the fabrication technique. The best performing membranes from IEM (M16a-M19a) were observed to have

the highest LEP_w of 2.1 – 3.1 bar. In literature, a membrane with LEP_w of 0.5 - 4.6 bar had been reported [17,23,95–97], and LEPw > 2.5 bar is recommended to limit wetting risk [58].

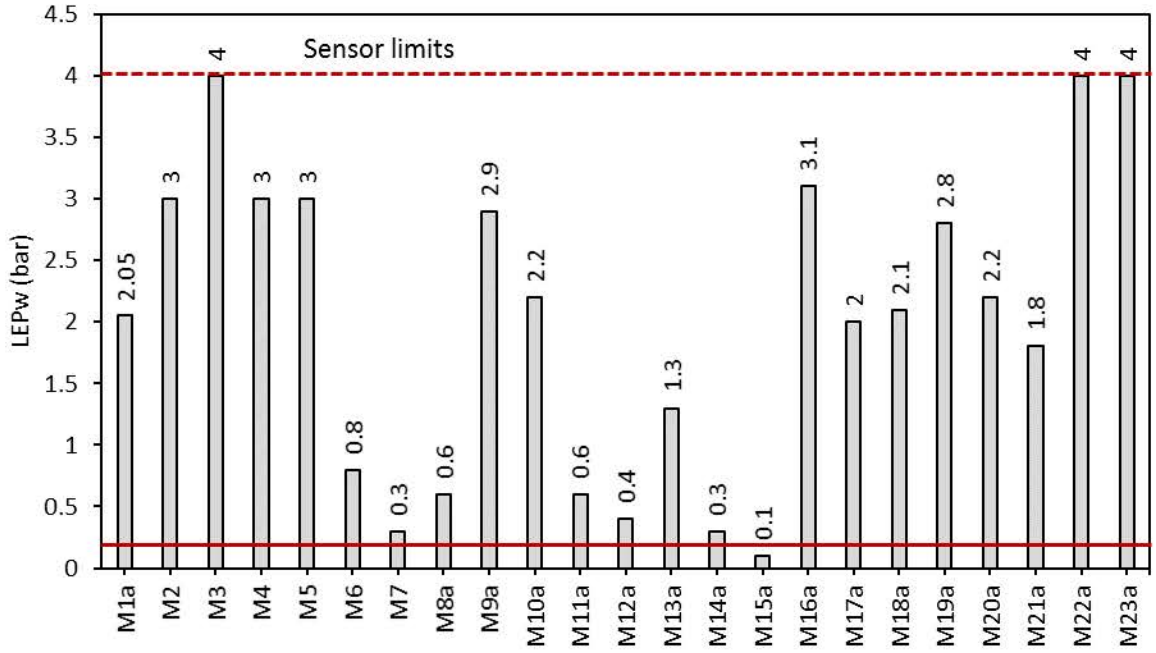

Figure 5.11: Liquid entry pressure of the active side of the membrane surface

2.3.2.4 Permeability evaluation

Permeability tests were conducted for each membrane using the pressure variation method. The permeabilities with the standard deviations of 9 membranes out of 23 are presented in **Figure 5.12**. The maximum permeability was observed for M2 (Fluoropore membrane) at 3.8E-06 ± 4.9E-07 $mol^{1/2}.m^{-1}Kg^{1/2}$. Concerning commercial membranes of similar pore size (~ 0.22 µm), Fluoropore membrane (M2) had a higher permeability than Durapore membrane (M1a) or Sumitomo membrane (M4) at the same operating conditions. Permeability's of M16-M19a were averaged as they were made using the same fabrication technique. With permeability of Side "a" of the membrane 3.18E-06 ± 4.4E-07 $mol^{1/2}.m^{-1}Kg^{1/2}$ performing lesser than side "b" with 3.48E-06 ± 3.4E-07 $mol^{1/2}.m^{-1}Kg^{1/2}$. However, membranes with a dense layer had the least permeability, with measured permeability for M22a (8.25E-08 $mol^{1/2}.m^{-1}Kg^{1/2}$) and M23a (8.26E-08 $mol^{1/2}.m^{-1}Kg^{1/2}$) being 2 orders of magnitude lesser than other fabricated and commercial membranes. Surprisingly, the permeability did not seem to increase with an increase in pore size but, on the contrary, decreased with an increase in pore size w.r.t Sumitomo membranes. *Eq. 5.4* presents that permeability is directly proportional to pore radius and inversely proportional to the

membrane thickness. This may be indicative of some permeability limits influenced by the membrane module that is yet to be explored.

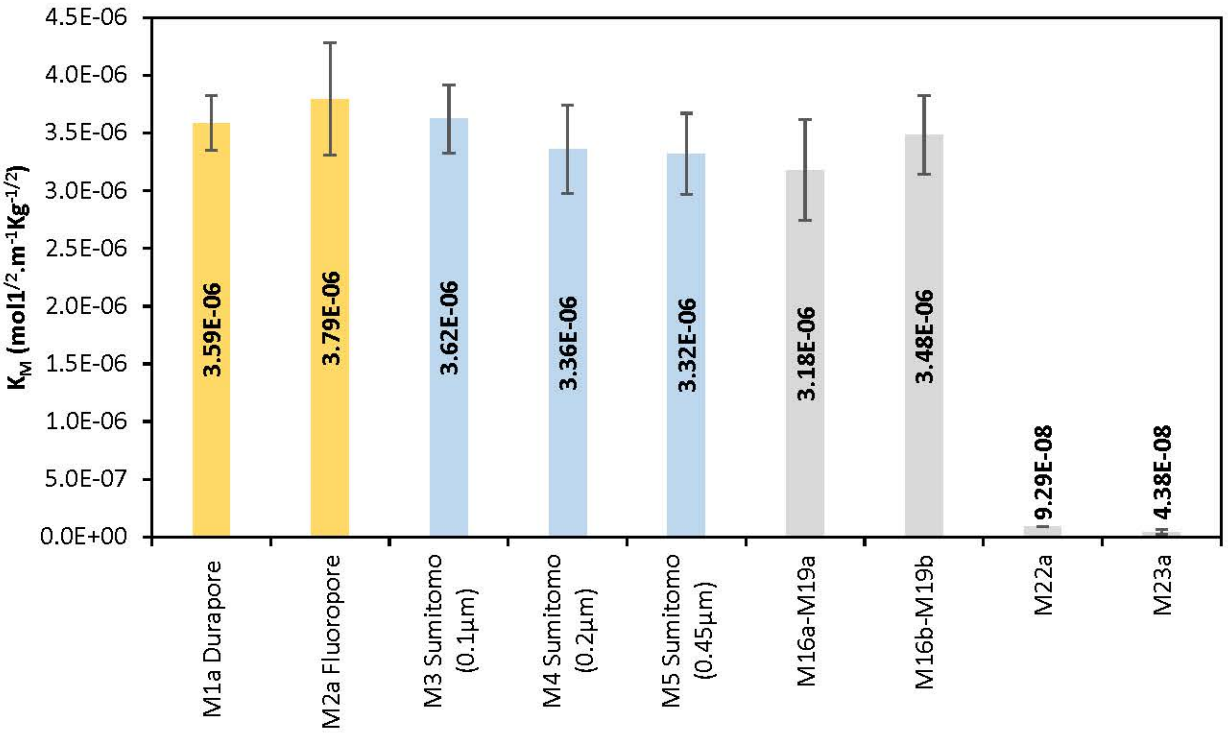

Figure 5.12: Permeability's of some studied membranes

The permeability for some commercial (M6 and M7) and fabricated membranes (M8a - M15a) could not be determined. Indeed, these membranes had low LEP_w (See **Figure 5.11**), and some were too fragile (low tensile strength) and had a significant variation in thickness (See **Figure 5.9**) and consequently let the water pass through the membranes during operation. Whereas, M21 did not generate any permeate due to dense layer even at the extreme limit of the pilot (with a feed flow rate of 250 L/h, feed temperature 60°C and the vacuum pressure of 0.3 kPa). Overall it can be noted that PVDF membranes (M16a-M19a) manufactured by IEM had a permeability similar to commercial available Durapore membranes (M1a). Their wetting resistance to saline solutions needs to be evaluated in the future. For example, data on flux and permeability for some membranes see supplementary data Figure C5.2.

2.3.2.5 Membrane surface observations

The active membrane surfaces were coated with gold and were observed under scanning electron microscopy under three magnifications of x30, x1000 and x6500 to understand the membrane

morphology. All commercial and LRGP membranes (except M20a Ref Blank) were observed under SEM while only a representative sample from IEM (M16-19) was observed under SEM. **Figure 5.13** presents the Millipore membranes while the **Figure 5.14** presents the Sumitomo membranes, and **Figure 5.15** presents the fabricated membranes from the project partners.

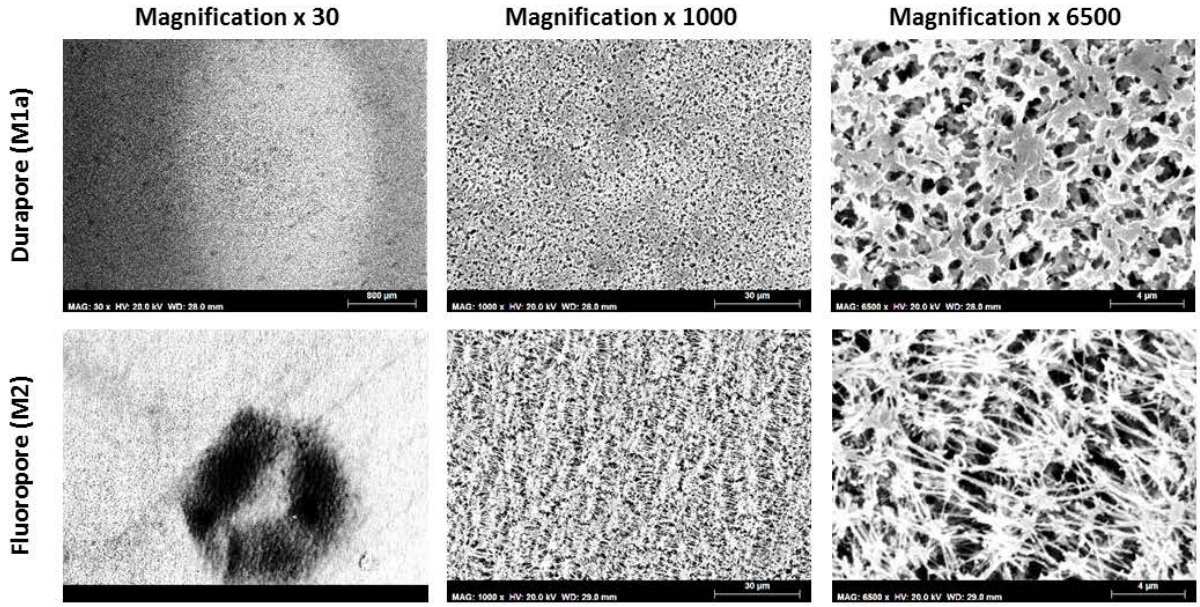

Figure 5.13: Millipore membrane surfaces at three magnifications of x30, x1000 and x6500 with Scanning Electron Microscopy

Figure 5.13 presents the two Millipore membranes of the same pore size of 0.22 µm. The difference in fabrication techniques can be clearly seen at x6500 magnification. The PVDF (Durapore) membranes are produced by phase inversion technique resulting in a globular morphology whereas PTFE (Fluoropore) membranes are produced using stretching and have elongated pore structures. As Fluoropore membranes are fused with a backing material, the compression marks left by the backing material can be seen on x30 magnification on the active surface (M2). Burrieza et al. [69], postulated that compaction by the backing material might facilitate wetting processes by allowing bridging of liquid water within the pores.

In **Figure 5.14**, it is interesting to visualize the gradual increase in the membrane pore size from 0.1 µm to 5 µm at x6500 magnification with the same PTFE stretched to achieve different pore sizes. At the lower magnification of x30, not much difference can be seen on the membrane surface however at x1000 and x6500 the evolution of the pore size become much more pronounced.

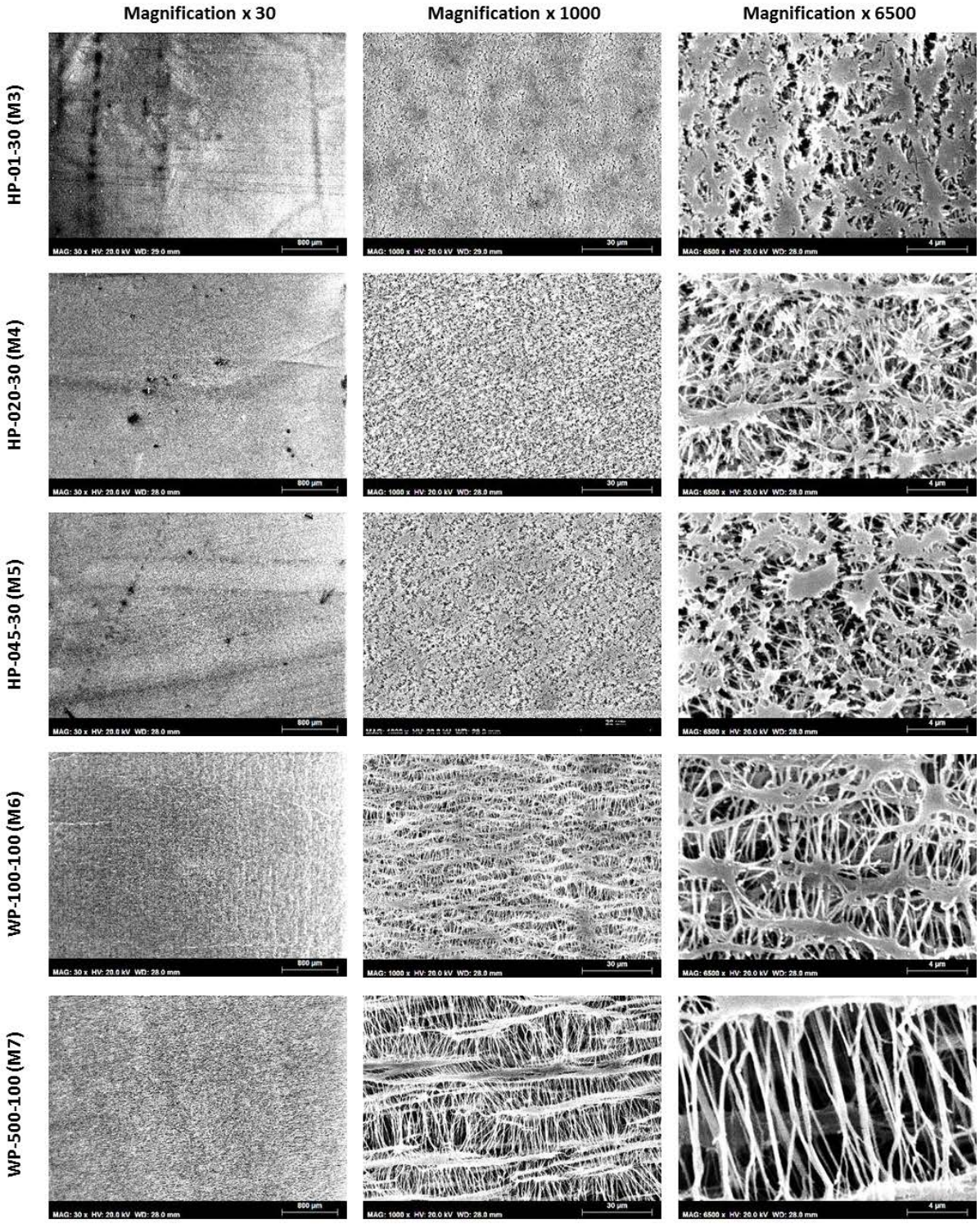

Figure 5.14: Sumitomo membrane surfaces at three magnifications at x30, x1000 and x6500 with Scanning Electron Microscopy

Similar to commercial PVDF membranes the membrane morphology of the representative sample IEM membrane for M16a-M19a was M195 (M18a) (see **Figure 5.15**) shows globular morphology at x1000 and x6500 magnification. For the three LRGP membranes, an active porous layer could not be visualized except for some evidence of porous layer for M18a at x6500. The active dense layers of the other 2 LRGP membranes could not be visualized at high magnifications.

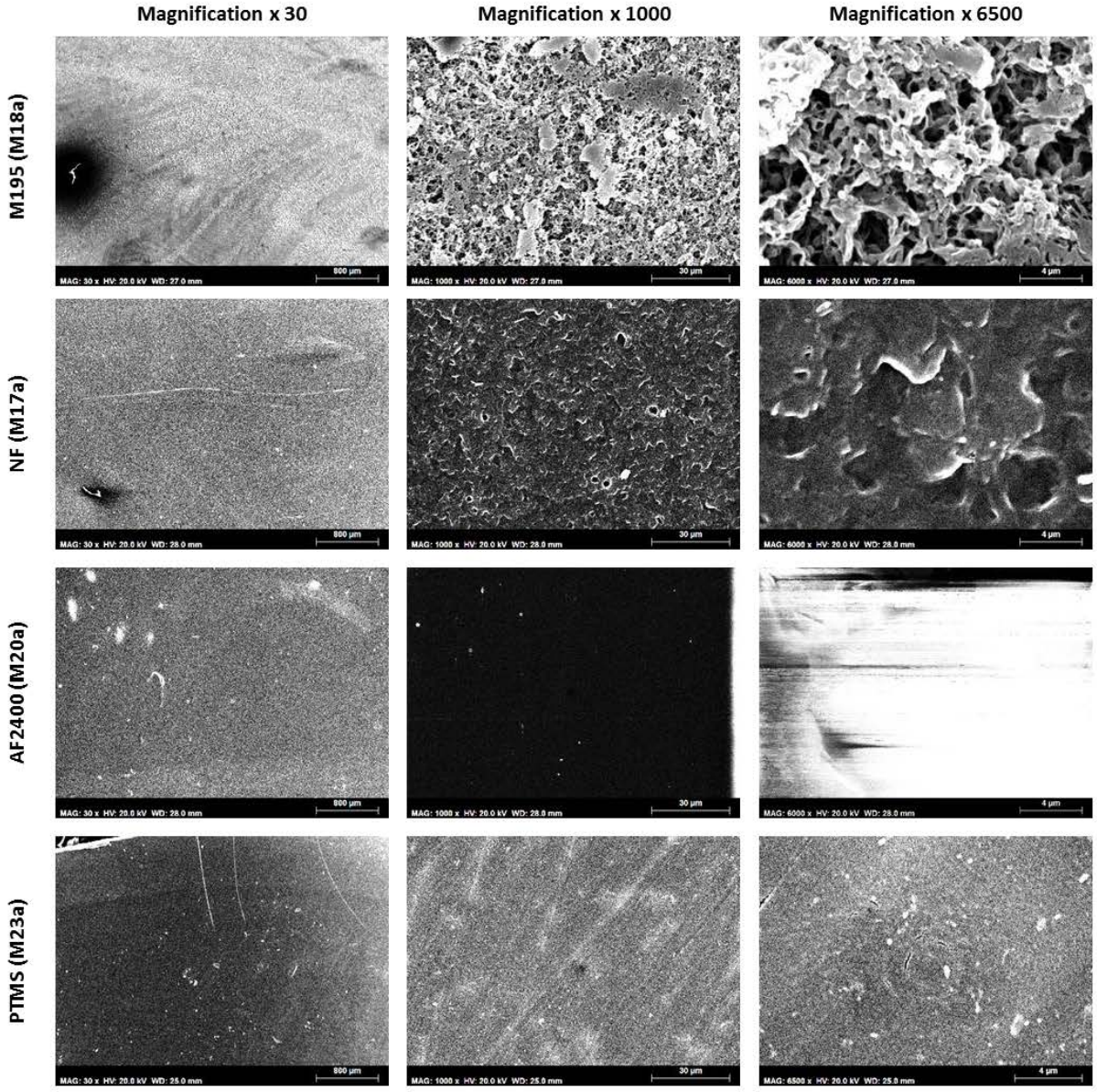

Figure 5.15: Membrane surfaces from partner universities at three magnifications at x30, x1000 and x6500 with Scanning Electron Microscopy

5.4. Conclusions and recommendations

In English

In this chapter, geometrical properties of 9 spacers were estimated and their effect on membrane permeability measurements was evaluated. It was found that a polypropylene-based coarse spacer with a 53.54 % open area was better than the other studied spaces for vacuum membrane distillation. Whereas no difference in membrane permeabilities was observed for polymer and metal spacer of comparable geometries. Successful utilization of a single spacer in vacuum membrane distillation could be an interesting approach to reduce the mass transfer resistance caused by 2 spacers in other configurations like DCMD.

Moreover, 23 samples of different membranes were characterized. The thickness, contact angle and LEP_w for most commercial and some fabricated membranes lie within the acceptable range that could be recommended to be utilized for various membrane distillation application. Membrane permeability of the fabricated PVDF membranes (M16a-M19a) provided by IEM had comparable properties to commercially available PVDF membranes. Utilization of dense membranes for membrane distillation needs further development to have comparable performances with respect to permeability. Their application in membrane distillation needs to be further explored.

En Français

Dans ce chapitre, les propriétés géométriques de 9 espaceurs, et leur effet sur la mesure de perméabilité d'une membrane commerciale (membrane Durapore en PVDF de 0,22 µm) ont été évalués. La faisabilité d'utiliser un seul espaceur, côté perméat, a été démontrée, ce qui constitue une approche intéressante pour réduire la résistance au transfert générée par deux espaceurs (comme en DCMD par exemple). Les résultats ont également montré que l'espaceur en polypropylène, ayant une surface ouverte de 53,54%, est celui qui présente la plus faible résistance au transfert.

D'autre part, 23 membranes différentes, provenant du commerce ou des partenaires du projet ANR (WETMEM), ont été caractérisées. Les valeurs d'épaisseur, d'angle de contact et de LEPw de l'ensemble des membranes testées correspondent à des gammes qui conviennent bien à la distillation membranaire. De plus, les membranes en PVDF fabriquées par l'IEM (M16a-M19a) ont des perméabilités comparables à celles des membranes commerciales. En revanche, l'utilisation de membranes denses pour la distillation

membranaire nécessite encore des développements afin d'obtenir des performances comparables aux membranes poreuses du commerce.

Acknowledgements

I would like to thank the project partners from European Institute des Membranes, Montpellier (Ing. Sandy Gosset, Dr. Jean-Pierre Mericq and Prof. Denis Bouyer) and Laboratoire Réactions et Génie des Procédés, Nancy (Dr. Tarik Eljaddi, Prof. Eric Favre and Dr. Denis Roizard) for fabricating membranes using novel techniques for the ANR projet WETMEM (ANR-14-CE04-0008). Special thanks extended to Prof. Roger Ben Aïm of Institut de la Filtration et des Techniques Séparatives (IFTS), Foulayronnes and Mr. Tetsuro Tamura from Sumitomo Electric for providing five commercial spacers and sending PTFE membranes of different pore sizes from Japan respectively.

Thesis conclusions and perspectives

Conclusions (In English)

Wetting characterization in membrane distillation has received restrained attention through the past four decades limiting the technological applications to labs and some demonstration projects. Since the early 2000's, there is a growing interest in manufacturing hydrophobic membranes and controlling operating conditions to prevent wetting occurrences. In the hope that newer membrane manufacturing techniques would be able to resist wetting under adverse operating conditions and salinities.

State of the art revealed our current stance on evaluating wetting phenomenon in membrane distillation is limited to global scale, and more often literature mixes up pore wetting, wettability and the word "wetting" without evidence and qualification of the wetting mechanism. This had made it difficult to draw reliable conclusions on the impact of operating parameters and/or membrane characteristics on pore wetting and its mechanisms. The current state of the art in evaluating wetting is based on experimentally determining liquid entry pressure, measuring the contact angle of the membrane and at best measuring conductivity of the permeate. All these techniques do not give information of pore wetting but instead on membrane's wettability (the potential of wetting) or failure of some membrane pores during operation. There has been a significant advancement in theoretical approaches for determining liquid entry pressure for wettability evaluation, but very little attention has been given to understand wetting at the pore scale and its dynamics (motion of the liquid vapor interface inside pores). Our collective knowledge on wetting is limited by the tools that are at our disposal in understanding it.

Thus, the general objectives of this thesis were directed towards shedding some light on the subject of wetting and develop some dedicated tools that could help in understanding it better at a local scale.

During the course of the thesis, the distinction between wettability and wetting was made more apparent. Though the state of the art of wettability indicators (LEP and Contact angle) indicates the change on the membrane at both global scale and local scales, however, we now know that wetting needs to be tackled at pore scales. In consideration of this effort, the DDTI (detection of dissolved tracer intrusion) method and wetting indicators were developed to define wetting and its mechanisms at pore scale. DDTI exploits the fact that tracer intrusion (salts) is limited at the liquid-vapor interface, and these traces can be visualized by coupling scanning electron microscopy and x-ray dispersion spectroscopy. DDTI is a robust

methodology that can be used to identify the occurring wetting mechanisms and to evaluate wetting at the scale of pores with its two indicators, i.e. totally wetted surface ratio (ω_s) and pore wetting ratio (ω_p). These wetting indicators were used together with the classical wettability indicators (LEP_w, CA and SFE) to understand the interactive effects of operating parameters on wetting on a PVDF membrane operated in vacuum membrane distillation. A wide range of salinities (22- 310 g/L NaCl) was considered together with temperatures and flow rates ranging from 35 – 50°C and laminar to turbulent respectively, using the Box-Behnken design of experiments. The interactions of the operating parameters were modeled. At salinities lower than 166 g/L NaCl solution, temperature and flow rates poorly affected the totally wetted surface (ω_s). However, for the hypersaline solution (<166 g/L), an increase in flow rates and temperature seem to prevent wetting occurrences

Additionally to ω_s, the pore wetting ratio (ω_p) revealed that surface wetting could be a precursor to partial and total wetting with an increase in wetting occurrences at hyper salinities. However, it is clear that CA and SFE vary linearly with salinity as membrane hydrophobicity decreases and surface interactions increase with an increase in salinity. However, LEP is not significantly affected by salinity and remains almost constant. Considering the interactive effects of the operating parameters on wetting it could be said that careful selection of operational parameters is vital for wetting prevention and that for hypersaline solutions the choice of the membrane itself becomes a key issue.

The growing interest to understand the influence of operating parameters and the need to regenerate membranes after being wet has necessitated the need of an *in-situ* tool for evaluating wetting propagation. Therefore, a non-invasive optical tool was conceptualized and developed for visualizing *in-situ* wetting propagation in membrane distillation. Based on the principles of light transmission, the theory of an increase in light transmission with an increased wetting was also described and illustrated. The proof of concept of this optical tool was validated using the pore wetting ratio obtained from the DDTI methodology. The tool was tested for its effectiveness using saline solutions and seawaters with controlled wetting induced by a surfactant. Using the optical tool and developed data treatment algorithms, the analysis was able to provide information on wetting progression with time for the studied solutions. The developed tool is adaptable to all major membrane distillation configurations and can visualize wetting at both global and local scales. Using this tool, the potential for operation control strategies for wetting prevention and regeneration of wetted membrane using different techniques could be better evaluated for membrane distillation.

Finally, under the project framework of **WETMEM**, several commercial available and fabricated membranes were assessed for their usability in vacuum membrane distillation to understand the influences of membrane properties on wettability. Membrane characterization together with permeability measurements and wettability assessment (LEP and Contact angle) of these 23 membranes revealed their applicability in vacuum membrane distillation. In general, PTFE membrane performed better than PVDF membranes considering their permeability. However, regardless of the polymer material, membranes with a pore size greater than equal to 1 µm and variable thicknesses (< 100 µm) had difficulty in holding that liquid-vapor interface and resulted in water passage under normal operating conditions. Membranes manufactured using stretching (PTFE) and phase inversion by a liquid (PVDF) showed much better Knudsen Permeability Coefficient than dense membranes. The applicability of dense membranes for membrane distillation is still at its infancy and suitability of an ultrathin dense layer membranes needs further exploration.

Perspectives (in English)

During the development of DDTI methodology, lighter elements (like Cl and Na) were used as tracers to detect liquid penetration. However low atomic numbers (less than 11 (Na)) are difficult to detect by EDX as the beryllium (Be) window used for protecting the SiLi detector in the EDX system limits the detection of elements with low atomic numbers due to the absorption of the soft X-rays. An improvement on the DDTI methodology would be to use tracers with higher atomic number to reduce the signal to noise ratio. Nevertheless, systematic use of the developed wetting indicators at the early stages of membrane fabrication and process optimization will be powerful tools to orientate operational strategies and to select the membranes of the future, with low (or measured) risk of wetting. More intrinsic parameters that were not considered earlier like membranes pore size distribution and thickness needs to be additionally considered with suitable quantification of the operational variables like vacuum pressures and time.

Also, the application optical *in-situ* wetting detection tools is limited to operational steady state conditions. Correlations can be established to compensate for the change in refractive index due to temperature so that wetting can also be visualized in unsteady state conditions. The use of higher resolution (for instance microscopy techniques) can be utilized to further improve the resolution of localized wetting visualization. Finally, to make the results obtained from optical tool quantitative towards wetting mechanisms,

correlations need to be established between pore wetting ratio from the DDTI methodology and wetting visualized on a local scale on the membrane surface.

Whereas, wettability indicators like CA, SFE, and LEP_w are measured at standard temperature with ultra-pure water. However, the wettability of a membrane depends on the fluid properties that it is in contact with during operation. It may be more advantageous to assess CA and LEP_w at the intended operating temperature with feed fluid. This may help in revealing the actual interaction of the feed solution and the intrinsic membrane properties for better operational control and wetting prevention.

The unified definition and the newly developed tools marks the beginning of better understanding on wetting in membrane distillation. There is still a lot of explorative research to be done to understand and thereby truly predict wetting. The methodologies and tools developed here are first steps in furthering our understanding of the wetting phenomenon in membrane distillation. Predictive pore wetting models can be now tested and improved based on the knowledge gained from these tools.

Membranes with good pore morphologies and exhibiting an excellent response to the wettability parameters (high LEP_w and CA) failed to operate in vacuum membrane distillation. Polymer based membranes used in MD are subjected to compression and deformation during operation leading to mechanical failure leading to wetting. Therefore, membrane tensile strength and thickness become important intrinsic properties that are under evaluated considering its contribution towards the overall membrane wetting resistance.

With the selection of appropriate membranes, polymer aging will eventually become an issue that will contribute to the wetting phenomenon. This aspect of research is at its infancy and could also be intensely studied and understood with these wetting tools. The *ex-situ* and the *in-situ* tools developed herewith in can be powerful to understand the impact of the operating parameters and feed solution on the membrane morphology leading to wetting. Researchers have time and again called for better membrane cell design and to study the impact of membrane cell geometry on pore wetting. This kind of study was not possible previously however with the developed tools the impact on cell geometry can now be studied with greater clarity. These tools could also be interesting to understand the process dynamics of wetting to have some objective elements of decision for the process optimization, such as with regards to cleaning and de-wetting strategies in membrane distillation.

By utilizing the optical *in-situ* tool, localized effects of operating parameters (temperatures, flow rates, local hydrodynamic conditions, feed salinities, time and membrane, etc.) on wetting can now be evaluated during the entire duration of an experiment. Considering the results obtained from the effects of operating parameters, further tests need to be conducted considering vacuum pressure and time as a variable for better operational strategies to prevent wetting in vacuum membrane distillation. The optical tool could help in understanding *in-situ* wetting propagation. The effects of different de-wetting strategies can now be evaluated which would be a vital concern for membrane ageing. With further experimental development using known fluid properties, the results from this tool can be compared with various wetting models.

Conclusions (en français)

La caractérisation du mouillage en distillation membranaire a reçu peu d'attention au cours des quatre dernières décennies, limitant les applications technologiques de ce procédé à l'échelle du laboratoire et à quelques projets de démonstration. Depuis le début des années 2000, on s'intéresse de plus en plus à la fabrication de membranes hydrophobes et au contrôle des conditions de fonctionnement pour éviter les phénomènes de mouillage. Dans l'espoir que les nouvelles techniques de fabrication de membranes leur permettront de résister au mouillage dans des conditions de fonctionnement et de salinité défavorables.

L'état de l'art a révélé que la position actuelle sur l'évaluation du phénomène de mouillage en distillation membranaire est limitée à l'échelle globale et que la littérature confond le plus souvent la perméabilité des pores, la mouillabilité et le mot « mouillage » sans preuves ni qualification du mécanisme de mouillage. Il était donc à ce jour difficile de tirer des conclusions fiables sur l'impact des paramètres de fonctionnement et / ou des caractéristiques de la membrane sur le mouillage des pores et ses mécanismes. L'état actuel de la technique en matière d'évaluation du mouillage est basé sur la détermination expérimentale de la pression d'entrée du liquide, la mesure de l'angle de contact de la membrane et au mieux la mesure de la conductivité du perméat. Toutes ces techniques ne donnent pas d'informations sur le mouillage des pores, mais plutôt sur la mouillabilité de la membrane (le potentiel de mouillage) ou la défaillance de certains pores de la membrane au cours du fonctionnement. Les approches théoriques pour déterminer la pression d'entrée des liquides et l'évaluation de la mouillabilité ont considérablement progressé, mais très peu d'attention a été portée sur la compréhension du mouillage à l'échelle des pores et de sa dynamique (mouvement de l'interface liquide/vapeur dans les pores). Notre connaissance collective sur le mouillage est limitée par les outils dont nous disposons pour le comprendre.

Ainsi, les objectifs généraux de cette thèse visaient à éclaircir le sujet du mouillage et à développer des outils dédiés qui pourraient aider à mieux le comprendre à l'échelle locale.

Au cours de la thèse, la distinction entre mouillabilité et mouillage est apparue plus clairement. Bien que l'état de la technique des indicateurs de mouillabilité (LEP_w et angle de contact) indique l'évolution de la membrane à la fois à une échelle globale et locale, nous savons toutefois qu'il est nécessaire de comprendre le mouillage à l'échelle des pores. Dans cet objectif, la méthode DDTI (détection d'intrusion de traceurs dissous), et des indicateurs de mouillage ont été développés pour définir le mouillage et ses mécanismes à l'échelle des pores. La méthode DDTI exploite le fait que l'intrusion de traceur (sels) est limitée à l'interface

liquide-vapeur et que ces traces peuvent être visualisées en couplant microscopie électronique à balayage et spectroscopie de dispersion de rayons X. La méthode DDTI est une méthodologie robuste qui peut être utilisée pour identifier les mécanismes de mouillage existants et pour évaluer le mouillage à l'échelle des pores avec ses deux indicateurs, à savoir le rapport de surface totalement mouillée (ω_s) et le rapport de mouillage des pores (ω_p). Ces indicateurs de mouillage ont été utilisés avec les indicateurs de mouillabilité classiques (LEP, CA et SFE) pour comprendre les effets des paramètres de fonctionnement sur le mouillage d'une membrane de PVDF fonctionnant en distillation membranaire sous vide. Une large gamme de salinités (22 à 310 g/L de NaCl), des températures allant de 35 à 50°C, ainsi que des écoulements laminaire et turbulent ont été testés, en utilisant le modèle d'expériences Box-Behnken. Les interactions des paramètres de fonctionnement ont été modélisées. À des salinités inférieures à 166 g/L de solution de NaCl, la température et les débits ont peu affecté l'indicateur « surface totalement mouillée (ω_s) ». Toutefois, pour la solution hypersaline (>166 g/L), une augmentation des débits de circulation et de température semble limiter les phénomènes de mouillage.

De plus, le rapport de mouillage des pores (ω_p) a révélé que le mouillage de surface pouvait être un précurseur du mouillage partiel ou total avec une augmentation des taux de mouillage en hyper salinité. Il est également apparu que le CA et le SFE varient linéairement avec la salinité, à mesure que l'hydrophobicité de la membrane diminue et que les interactions de surface augmentent avec une augmentation de la salinité. En revanche, la salinité n'affecte pas la LEP de manière significative. Compte tenu des effets couplés des paramètres de fonctionnement sur le mouillage, on pourrait dire qu'il est essentiel de choisir soigneusement les paramètres de fonctionnement pour prévenir le mouillage et que, pour les solutions hypersalines, le choix de la membrane elle-même devient une question essentielle.

La nécessité croissante de comprendre l'influence des paramètres de fonctionnement mais aussi de pouvoir régénérer les membranes après leur éventuel mouillage a rendu nécessaire la mise au point d'un outil in situ permettant d'évaluer la propagation par mouillage. Par conséquent, un outil optique non invasif a été conçu et développé pour visualiser la propagation du mouillage in situ au cours de la distillation membranaire. Basée sur les principes de la transmission de la lumière, le lien a pu être fait entre l'augmentation de la transmission de la lumière et l'augmentation du mouillage. La preuve de concept de cet outil optique a été validée à l'aide du taux de mouillage des pores obtenu selon la méthodologie DDTI. L'efficacité de l'outil a été testée à l'aide de solutions salines et d'eaux de mer en provoquant le mouillage par l'ajout d'un surfactant. À l'aide de l'outil optique et des algorithmes de traitement de données développés, l'analyse a permis de fournir des informations sur la progression du mouillage au cours du

temps pour les solutions étudiées. L'outil développé est adaptable à toutes les principales configurations de distillation membranaire et permet de visualiser le mouillage à l'échelle globale et locale. Grâce à cet outil, il serait possible de mieux évaluer le potentiel de stratégies de contrôle des opérations pour la prévention du mouillage et la régénération de membranes mouillées à l'aide de différentes techniques.

Dans le cadre du projet ANR WETMEM, plusieurs membranes commerciales et expérimentales ont été testées afin de déterminer si elles étaient utilisables en distillation membranaire, et de comprendre les effets des propriétés de la membrane sur la mouillabilité. La caractérisation des membranes ainsi que les mesures de perméabilité et l'évaluation de la mouillabilité (LEP et angle de contact) de ces 23 membranes ont révélé leur applicabilité à la distillation membranaire sous vide. En général, les membranes en PTFE ont obtenu de meilleurs résultats que les membranes en PVDF compte tenu de leur perméabilité. Cependant, quel que soit le matériau polymère utilisé, les membranes de pores supérieurs à 1 µm et d'épaisseurs variables (<100 µm) ont de la difficulté à maintenir cette interface liquide-vapeur et entraînent le passage de l'eau dans des conditions de fonctionnement normales. Les membranes fabriquées en utilisant l'étirement (PTFE) et l'inversion de phase par un liquide (PVDF) présentaient un coefficient de perméabilité de Knudsen bien supérieur aux membranes denses. L'applicabilité des membranes denses pour la distillation membranaire en est encore à ses balbutiements et la pertinence des membranes à couche dense ultra-fine nécessite une exploration plus approfondie.

Perspective (en français)

Au cours du développement de la méthodologie DDTI, des éléments plus légers (chlore et sodium) ont été utilisés comme traceurs pour détecter la pénétration de liquide, or un nombre atomique bas (moins de 11 (Na)) est difficile à détecter par EDX. La fenêtre au béryllium (Be) utilisée pour protéger le détecteur SiLi dans le système EDX limite la détection des éléments de faible nombre atomique en raison de l'absorption des rayons X mous. Une amélioration de la méthodologie DDTI consisterait à utiliser des traceurs avec un numéro atomique plus élevé afin de réduire le rapport signal sur bruit. Néanmoins, l'utilisation systématique des indicateurs de mouillage développés dès les premières étapes de la fabrication de la membrane et de l'optimisation des procédés constituera un outil puissant pour orienter les stratégies opérationnelles et sélectionner les membranes du futur, avec un risque de mouillage faible (ou mesuré). D'autres paramètres intrinsèques qui n'ont pas été pris en compte auparavant, tels que la distribution de la taille des pores et de l'épaisseur des membranes, doivent également être pris en compte avec une quantification appropriée des variables opérationnelles telles que la pression de vide et la durée.

De plus, les outils optiques de détection de mouillage in situ sont limités aux conditions de fonctionnement en régime permanent. Des corrélations pourraient être établies pour compenser le changement d'indice de réfraction dû à la température par exemple, de sorte que le mouillage puisse également être visualisé dans des conditions instables. L'utilisation de techniques de microscopie à résolution plus élevée, par exemple, peut être considérée pour améliorer encore la résolution de la visualisation du mouillage localisé. Enfin, pour rendre les résultats obtenus à partir d'outils optiques quantitatifs vis-à-vis des mécanismes de mouillage, des corrélations doivent être établies entre le taux de mouillage des pores (méthodologie DDTI) et le mouillage visualisé à l'échelle locale à la surface de la membrane.

D'autre part, les indicateurs de mouillabilité tels que CA, SFE et LEP_w sont mesurés à la température standard avec de l'eau ultra-pure, alors que la mouillabilité d'une membrane dépend des propriétés du fluide avec lesquelles elle est en contact pendant le fonctionnement. Il peut être plus avantageux d'évaluer CA et LEPw à la température de fonctionnement prévue et avec le fluide d'alimentation. Cela peut aider à révéler l'interaction réelle de la solution d'alimentation et les propriétés intrinsèques de la membrane pour un meilleur contrôle opérationnel et une meilleure prévention du mouillage.

La définition du mouillage proposée et les nouveaux outils développés marquent le début d'une meilleure compréhension du mouillage en distillation membranaire. Il reste cependant encore beaucoup de recherche à faire pour comprendre et donc véritablement prédire le mouillage. Les méthodologies et les outils développés ici sont les premières étapes pour approfondir notre compréhension du phénomène de mouillage en distillation membranaire. Les modèles prédictifs de mouillage des pores peuvent maintenant être testés et améliorés en fonction des connaissances acquises grâce à ces outils.

Les membranes présentant une bonne morphologie des pores et présentant une excellente réponse aux paramètres de mouillabilité (LEP_w et CA élevés) n'ont pas toujours bien fonctionné en distillation membranaire sous vide. Les membranes à base de polymère utilisées sont soumises à une compression et à une déformation pendant le fonctionnement, ce qui entraîne une défaillance mécanique conduisant à un mouillage. Par conséquent, la résistance à la traction et l'épaisseur de la membrane deviennent des propriétés intrinsèques importantes qui sont sous-évaluées compte tenu de leur contribution à la résistance au mouillage de la membrane.

Avec le choix de membranes appropriées, le vieillissement des polymères deviendra un problème qui contribuera au phénomène de mouillage. Cet aspect de la recherche est à ses débuts et pourrait également

être étudié et mieux compris avec ces outils de détection du mouillage. Les outils ex-situ et in-situ développés ici peuvent être performants pour comprendre l'impact des paramètres de fonctionnement et de la solution d'alimentation sur la morphologie de la membrane conduisant au mouillage. Les chercheurs ont à maintes reprises réclamé une meilleure conception des modules membranaires et l'impact de la géométrie des modules sur le mouillage des pores, qui n'aurait pas été possible auparavant, peut maintenant être étudié avec une plus grande clarté. Ces outils pourraient également être intéressants pour comprendre la dynamique du processus de mouillage afin de disposer d'éléments objectifs de décision pour l'optimisation du processus, tels que les stratégies de nettoyage et de démouillage en distillation membranaire.

En utilisant l'outil optique in situ, les effets localisés des paramètres de fonctionnement (températures, débits, conditions hydrodynamiques locales, salinités d'alimentation, temps et membrane, etc.) sur le mouillage peuvent maintenant être évalués pendant toute la durée d'une expérience. Compte tenu des résultats obtenus à partir des effets des paramètres de fonctionnement, il est nécessaire de procéder à des tests supplémentaires, en considérant la pression de vide et la durée comme une variable permettant de meilleures stratégies de fonctionnement pour empêcher le mouillage en distillation membranaire sous vide. L'outil optique pourrait aider à comprendre la progression des mécanismes de mouillage et les effets de différentes stratégies de démouillage pourraient maintenant être évalués, ce qui constituerait une avancée importante vis-à-vis du vieillissement des membranes. Avec un développement expérimental plus poussé, les résultats obtenus avec cet outil pourraient être comparés aux différents modèles de mouillage.

References

[1] M. Rosegrant, X. Cai, S. Cline, N. Nakagawa, The role of rainfed agriculture in the future of global food production, Environ. Prod. Technol. Div. Discuss. Pap. 90 (2002).

[2] TechNavio, Global Desalination Market 2018-2022, Research and Markets, Dublin, Ireland, 2018. https://www.researchandmarkets.com/research/tbss7g/global?w=4 (accessed June 21, 2018).

[3] L.F. Greenlee, D.F. Lawler, B.D. Freeman, B. Marrot, P. Moulin, Reverse osmosis desalination: water sources, technology, and today's challenges, Water Res. 43 (2009) 2317–2348.

[4] J.-P. Mericq, S. Laborie, C. Cabassud, Vacuum membrane distillation of seawater reverse osmosis brines, Water Res. 44 (2010) 5260–5273. doi:10.1016/j.watres.2010.06.052.

[5] R.V. Linares, Z. Li, S. Sarp, S.S. Bucs, G. Amy, J.S. Vrouwenvelder, Forward osmosis niches in seawater desalination and wastewater reuse, Water Res. 66 (2014) 122–139.

[6] E. Drioli, A. Ali, F. Macedonio, Membrane distillation: Recent developments and perspectives, State--Art Rev. Desalination. 356 (2015) 56–84. doi:10.1016/j.desal.2014.10.028.

[7] J.-P. Mericq, S. Laborie, C. Cabassud, Vacuum membrane distillation for an integrated seawater desalination process, Desalination Water Treat. 9 (2009) 287–296.

[8] J.-P. Mericq, S. Laborie, C. Cabassud, Evaluation of systems coupling vacuum membrane distillation and solar energy for seawater desalination, Chem. Eng. J. 166 (2011) 596–606. doi:10.1016/j.cej.2010.11.030.

[9] E. Guillén-Burrieza, J. Blanco, G. Zaragoza, D.-C. Alarcón, P. Palenzuela, M. Ibarra, W. Gernjak, Experimental analysis of an air gap membrane distillation solar desalination pilot system, J. Membr. Sci. 379 (2011) 386–396.

[10] J.D. Gil, L. Roca, A. Ruiz-Aguirre, G. Zaragoza, M. Berenguel, Optimal Operation of a Solar Membrane Distillation Pilot Plant via Nonlinear Model Predictive Control, Comput. Chem. Eng. 109 (2018) 151–165.

[11] B. Ozbey-Unal, D.Y. Imer, B. Keskinler, I. Koyuncu, Boron removal from geothermal water by air gap membrane distillation, Desalination. 433 (2018) 141–150.

[12] J.-P. Mericq, S. Gosset, D. Bouyer, Vapor induced phase separation for super-hydrophobic polymeric membrane preparation, in: Congrès Société Fr. Génie Procédés SFGP 2017, Nancy, France, 2017.

[13] T. Eljaddi, D. Mejia, E. Favre, D. Roizard, 100% salt rejection for efficient distillation membranes: dream or reality?, in: Euromembrane, Valence, Spain, 2018.

[14] J.-P. Mericq, S. Gosset, D. Bouyer, Super-hydrophobic polymeric membrane preparation for membrane distillation by non-solvent induced phase separation, in: 10th World Congr. Chem. Eng., Barcelona, Spain, 2017.

[15] M. Gryta, Fouling in direct contact membrane distillation process, J. Membr. Sci. (2008). http://www.sciencedirect.com/science/article/pii/S0376738808007527.

[16] M.S. El-Bourawi, Z. Ding, R. Ma, M. Khayet, A framework for better understanding membrane distillation separation process, J. Membr. Sci. 285 (2006) 4–29. doi:10.1016/j.memsci.2006.08.002.

[17] M. Khayet, Membranes and theoretical modeling of membrane distillation: A review, Membr. Sep. Colloid Sci. 164 (2011) 56–88. doi:10.1016/j.cis.2010.09.005.

[18] M.R. Qtaishat, T. Matsuura, 13 - Modelling of pore wetting in membrane distillation compared with pervaporation A2 - Basile, Angelo, in: A.F. Khayet (Ed.), Pervaporation Vap. Permeat. Membr. Distill., Woodhead Publishing, Oxford, 2015: pp. 385–413. http://www.sciencedirect.com/science/article/pii/B9781782422464000131.

[19] M. Findley, Vaporization through porous membranes, Ind. Eng. Chem. Process Des. Dev. 6 (1967) 226–230.

[20] B.R. Bodell, Distillation of saline water using silicone rubber membrane, (1968).

[21] K.W. Lawson, D.R. Lloyd, Membrane distillation, J. Membr. Sci. 124 (1997) 1–25.

[22] A. Deshmukh, C. Boo, V. Karanikola, S. Lin, A.P. Straub, T. Tong, D.M. Warsinger, M. Elimelech, Membrane Distillation at the Water-Energy Nexus: Limits, Opportunities, and Challenges, Energy Environ. Sci. (2018).

[23] M. Khayet, T. Matsuura, Membrane Distillation: Principles and Applications, Elsevier, 2011. https://books.google.fr/books?id=5yzHdm8vOqMC.

[24] K. Smolders, A.C.M. Franken, Terminology for Membrane Distillation, Desalination. 72 (1989) 249–262. doi:10.1016/0011-9164(89)80010-4.

[25] V.V. Ugrozov, I.B. Elkina, V.N. Nikulin, L.I. Kataeva, Theoretical and experimental research of liquid-gap membrane distillation process in membrane module, Desalination Environ. Fresh Water All. 157 (2003) 325–331. doi:10.1016/S0011-9164(03)00412-0.

[26] C.A. Rivier, M.C. García-Payo, I.W. Marison, U. von Stockar, Separation of binary mixtures by thermostatic sweeping gas membrane distillation: I. Theory and simulations, J. Membr. Sci. 201 (2002) 1–16. doi:10.1016/S0376-7388(01)00648-2.

[27] D. Winter, Permeate Gap Membrane Distillation (PGMD), Encycl. Membr. (2016) 1–2.

[28] J. Swaminathan, H.W. Chung, D.M. Warsinger, F.A. AlMarzooqi, H.A. Arafat, J.H. Lienhard V, Energy efficiency of permeate gap and novel conductive gap membrane distillation, J. Membr. Sci. 502 (2016) 171–178. doi:10.1016/j.memsci.2015.12.017.

[29] L. Francis, N. Ghaffour, A.A. Alsaadi, G.L. Amy, Material gap membrane distillation: A new design for water vapor flux enhancement, J. Membr. Sci. 448 (2013) 240–247. doi:10.1016/j.memsci.2013.08.013.

[30] R. Bagger-Jørgensen, A.S. Meyer, C. Varming, G. Jonsson, Recovery of volatile aroma compounds from black currant juice by vacuum membrane distillation, J. Food Eng. 64 (2004) 23–31.

[31] Q.F. Alsalhy, S.S. Ibrahim, S.R. Khaleel, Performance of vacuum poly(propylene) membrane distillation (VMD) for saline water desalination, Chem. Eng. Process. Process Intensif. 120 (2017) 68–80. doi:10.1016/j.cep.2017.06.011.

[32] P.M. Duyen, P. Jacob, R. Rattanaoudom, C. Visvanathan, Feasibility of sweeping gas membrane distillation on concentrating triethylene glycol from waste streams, Chem. Eng. Process. Process Intensif. 110 (2016) 225–234.

[33] L.M. Dinh, P. Jacob, C. Visvanathan, Direct contact and sweeping gas membrane distillation for process intensification–a comparative study, Desalination Water Treat. 89 (2017) 53–64. doi:10.5004/dwt.2017.21371.

[34] E. Chabanon, D. Mangin, C. Charcosset, Membranes and crystallization processes: State of the art and prospects, J. Membr. Sci. 509 (2016) 57–67.

[35] T. Matsuura, Progress in membrane science and technology for seawater desalination—a review, Desalination. 134 (2001) 47–54.

[36] M. Gryta, The study of performance of polyethylene chlorinetrifluoroethylene membranes used for brine desalination by membrane distillation, Desalination. 398 (2016) 52–63. doi:10.1016/j.desal.2016.07.021.

[37] T.D. Dao, S. Laborie, C. Cabassud, Direct As(III) removal from brackish groundwater by vacuum membrane distillation: Effect of organic matter and salts on membrane fouling, Sep. Purif. Technol. 157 (2016) 35–44. doi:10.1016/j.seppur.2015.11.018.

[38] C. Boi, S. Bandini, G.C. Sarti, Pollutants removal from wastewaters through membrane distillation, Desalination. 183 (2005) 383–394.

[39] P. Jacob, P. Phungsai, K. Fukushi, C. Visvanathan, Direct contact membrane distillation for anaerobic effluent treatment, J. Membr. Sci. 475 (2015) 330–339.

[40] D. Rana, T. Matsuura, M. Kassim, A. Ismail, Radioactive decontamination of water by membrane processes—a review, Desalination. 321 (2013) 77–92.

[41] M. Monnot, G.D.M. Carvajal, S. Laborie, C. Cabassud, R. Lebrun, Integrated approach in eco-design strategy for small RO desalination plants powered by photovoltaic energy, Desalination. 435 (2018) 246–258.

[42] F. Macedonio, E. Curcio, E. Drioli, Integrated membrane systems for seawater desalination: energetic and exergetic analysis, economic evaluation, experimental study, Desalination. 203 (2007) 260–276.

[43] D. Woldemariam, A. Martin, M. Santarelli, Exergy analysis of air-gap membrane distillation systems for water purification applications, Appl. Sci. 7 (2017) 301.

[44] U.K. Kesieme, N. Milne, H. Aral, C.Y. Cheng, M. Duke, Economic analysis of desalination technologies in the context of carbon pricing, and opportunities for membrane distillation, Desalination. 323 (2013) 66–74.

[45] K. Zhao, W. Heinzl, M. Wenzel, S. Büttner, F. Bollen, G. Lange, S. Heinzl, N. Sarda, Experimental study of the memsys vacuum-multi-effect-membrane-distillation (V-MEMD) module, Desalination. 323 (2013) 150–160.

[46] E. Mendez, Sustainable desalination: Membrane distillation delivers greener clean water, Filtr. Sep. 49 (2012) 26–28.

[47] A. Ruiz-Aguirre, D.-C. Alarcón-Padilla, G. Zaragoza, Productivity analysis of two spiral-wound membrane distillation prototypes coupled with solar energy, Desalination Water Treat. 55 (2015) 2777–2785.

[48] K. Barr, G.J. Millar, I.D. Mackinnon, Desalination by a solar thermal membrane distillation process, in: 2013.

[49] M. Rommel, J. Koschikowski, M. Wieghaus, Solar driven desalination systems based on membrane distillation, in: Sol. Desalination 21st Century, Springer, 2007: pp. 247–257.

[50] S. Al-Obaidani, E. Curcio, F. Macedonio, G. Di Profio, H. Al-Hinai, E. Drioli, Potential of membrane distillation in seawater desalination: thermal efficiency, sensitivity study and cost estimation, J. Membr. Sci. 323 (2008) 85–98.

[51] Abdullah Alkhudhiri, Naif Darwish, Nidal Hilal, Membrane distillation: A comprehensive review, Membr. Distill. Compr. Rev. 287 (2011). doi:10.1016/j.desal.2011.08.027.

[52] E. Curcio, E. Drioli, Membrane distillation and related operations—a review, Sep. Purif. Rev. 34 (2005) 35–86.

[53] M. Khayet, J. Mengual, G. Zakrzewska-Trznadel, Direct contact membrane distillation for nuclear desalination. Part I: Review of membranes used in membrane distillation and methods for their characterisation, Int. J. Nucl. Desalination. 1 (2005) 435–449.

[54] C.K. Chiam, R. Sarbatly, Membranes and theoretical modelling of liquid-gas membrane separation for aromatic compounds removal from water: A review, Int. J. Glob. Environ. Issues. 12 (2012) 130–149. doi:10.1504/IJGENVI.2012.049376.

[55] S. Bandini, A. Saavedra, G.C. Sarti, Vacuum membrane distillation: experiments and modeling, AIChE J. 43 (1997) 398–408.

[56] C. Quist-Jensen, F. Macedonio, E. Drioli, Membrane crystallization for salts recovery from brine—an experimental and theoretical analysis, Desalination Water Treat. 57 (2016) 7593–7603.

[57] S. Bandini, G.C. Sarti, Heat and mass transport resistances in vacuum membrane distillation per drop, AIChE J. 45 (1999) 1422–1433.

[58] Eykens, K. De Sitter, C. Dotremont, L. Pinoy, B. Van der Bruggen, How to optimize the membrane properties for membrane distillation-A review, Ind. Eng. Chem. Res. (2016).

[59] B.K. Pramanik, K. Thangavadivel, L. Shu, V. Jegatheesan, A critical review of membrane crystallization for the purification of water and recovery of minerals, Rev. Environ. Sci. Biotechnol. 15 (2016) 411–439. doi:10.1007/s11157-016-9403-0.

[60] C. Charcosset, A review of membrane processes and renewable energies for desalination, Desalination. 245 (2009) 214–231.

[61] M. Khayet, Solar desalination by membrane distillation: Dispersion in energy consumption analysis and water production costs (a review), Desalination. 308 (2013) 89–101.

[62] E. Mathioulakis, V. Belessiotis, E. Delyannis, Desalination by using alternative energy: Review and state-of-the-art, Desalination. 203 (2007) 346–365.

[63] D. Eumine Suk, T. Matsuura, Membrane-based hybrid processes: a review, Sep. Sci. Technol. 41 (2006) 595–626.

[64] David M. Warsinger, Jaichander Swaminathan, Elena Guillen-Burrieza, Hassan A. Arafat, John H. Lienhard V, Scaling and fouling in membrane distillation for desalination applications: A review, Scaling Fouling Membr. Distill. Desalination Appl. Rev. 356 (2015) 294–313. doi:10.1016/j.desal.2014.06.031.

[65] G. Naidu, S. Jeong, S. Vigneswaran, T.-M. Hwang, Y.-J. Choi, S.-H. Kim, A review on fouling of membrane distillation, Desalination Water Treat. 57 (2016) 10052–10076. doi:10.1080/19443994.2015.1040271.

[66] L.D. Tijing, Y.C. Woo, J.S. Choi, S. Lee, S.H. Kim, H.K. Shon, Fouling and Its Control in Membrane Distillation-A Review, J Membr Sci. 475 (2015) 215.

[67] M. Rezaei, D.M. Warsinger, M. Duke, T. Matsuura, W.M. Samhaber, Wetting phenomenon in membrane distillation: mechanisms, reversal, and prevention, Water Res. (2018).

[68] M. Gryta, Influence of polypropylene membrane surface porosity on the performance of membrane distillation process, J. Membr. Sci. 287 (2007) 67–78.

[69] E. Guillen-Burrieza, A. Ruiz-Aguirre, G. Zaragoza, H.A. Arafat, Membrane fouling and cleaning in long term plant-scale membrane distillation operations, J. Membr. Sci. 468 (2014) 360–372.

[70] M. Gryta, Long-term performance of membrane distillation process, J. Membr. Sci. 265 (2005) 153–159.

[71] Pengtao Yue, Yuriko Renardy, Spontaneous penetration of a non-wetting drop into an exposed pore, Spontaneous Penetration Non-Wetting Drop Expo. Pore. 25 (2013) 52104. doi:10.1063/1.4804957.

[72] J. Ge, Y. Peng, Z. Li, P. Chen, S. Wang, Membrane fouling and wetting in a DCMD process for RO brine concentration, Desalination. 344 (2014) 97–107. doi:10.1016/j.desal.2014.03.017.

[73] A. Criscuoli, M. Carnevale, Desalination by vacuum membrane distillation: The role of cleaning on the permeate conductivity, Desalination. 365 (2015) 213–219.

[74] S. Velioğlu, L. Han, J.W. Chew, Understanding membrane pore-wetting in the membrane distillation of oil emulsions via molecular dynamics simulations, J. Membr. Sci. 551 (2018) 76–84.

[75] F.A. Banat, J. Simandl, Membrane distillation for propanone removal from aqueous streams, J. Chem. Technol. Biotechnol. 75 (2000) 168–178. doi:10.1002/(SICI)1097-4660(200002)75:2<168::AID-JCTB192>3.0.CO;2-X.

[76] F. Edwie, M.M. Teoh, T.-S. Chung, Effects of additives on dual-layer hydrophobic–hydrophilic PVDF hollow fiber membranes for membrane distillation and continuous performance, Chem. Eng. Sci. 68 (2012) 567–578. doi:10.1016/j.ces.2011.10.024.

[77] M. Qtaishat, M. Khayet, T. Matsuura, Novel porous composite hydrophobic/hydrophilic polysulfone membranes for desalination by direct contact membrane distillation, J. Membr. Sci. 341 (2009) 139–148.

[78] H. Julian, S. Meng, H. Li, Y. Ye, V. Chen, Effect of operation parameters on the mass transfer and fouling in submerged vacuum membrane distillation crystallization (VMDC) for inland brine water treatment, J. Membr. Sci. 520 (2016) 679–692. doi:10.1016/j.memsci.2016.08.032.

[79] L. Peña, J.M.O. de Zárate, J.I. Mengual, Steady states in membrane distillation: Influence of membrane wetting, J. Chem. Soc. Faraday Trans. 89 (1993) 4333–4338.

[80] Y.T. Chua, G. Ji, G. Birkett, C.X.C. Lin, F. Kleitz, S. Smart, Nanoporous organosilica membrane for water desalination: Theoretical study on the water transport, J. Membr. Sci. 482 (2015) 56–66. doi:10.1016/j.memsci.2015.01.060.

[81] S. Gruener, T. Hofmann, D. Wallacher, A.V. Kityk, P. Huber, Capillary rise of water in hydrophilic nanopores, Phys. Rev. E. 79 (2009) 067301.

[82] D. Dimitrov, A. Milchev, K. Binder, Capillary rise in nanopores: molecular dynamics evidence for the Lucas-Washburn equation, Phys. Rev. Lett. 99 (2007) 054501.

[83] T. Okada, T. Matsuura, A new transport model for pervaporation, J. Membr. Sci. 59 (1991) 133–149. doi:10.1016/S0376-7388(00)81179-5.

[84] D.Y. Cheng, S.J. Wiersma, Composite membrane for a membrane distillation system, (1983).

[85] A. Chanachai, K. Meksup, R. Jiraratananon, Coating of hydrophobic hollow fiber PVDF membrane with chitosan for protection against wetting and flavor loss in osmotic distillation process, Sep. Purif. Technol. 72 (2010) 217–224. doi:10.1016/j.seppur.2010.02.014.

[86] D.E. Suk, T. Matsuura, H.B. Park, Y.M. Lee, Development of novel surface modified phase inversion membranes having hydrophobic surface-modifying macromolecule (nSMM) for vacuum membrane distillation, Desalination. 261 (2010) 300–312.

[87] P. Ramon-Torregrosa, M. Rodríguez-Valverde, A. Amirfazli, M. Cabrerizo-Vílchez, Factors affecting the measurement of roughness factor of surfaces and its implications for wetting studies, Colloids Surf. Physicochem. Eng. Asp. 323 (2008) 83–93.

[88] L.M. Camacho, L. Dumée, J. Zhang, J. Li, M. Duke, J. Gomez, S. Gray, Advances in membrane distillation for water desalination and purification applications, Water. 5 (2013) 94–196.

[89] M. Callies, Y. Chen, F. Marty, A. Pépin, D. Quéré, Microfabricated textured surfaces for super-hydrophobicity investigations, Microelectron. Eng. 78 (2005) 100–105.

[90] D. Quéré, Rough ideas on wetting, Phys. Stat. Mech. Its Appl. 313 (2002) 32–46.

[91] M.M.A. Shirazi, A. Kargari, M. Tabatabaei, Evaluation of commercial PTFE membranes in desalination by direct contact membrane distillation, Chem. Eng. Process. Process Intensif. 76 (2014) 16–25. doi:10.1016/j.cep.2013.11.010.

[92] F. Edwie, T.-S. Chung, Development of simultaneous membrane distillation–crystallization (SMDC) technology for treatment of saturated brine, Chem. Eng. Sci. 98 (2013) 160–172.

[93] A.V. Pocius, D.A. Dillard, Adhesion science and engineering: surfaces, chemistry and applications, Elsevier, 2002.

[94] S. Ebnesajjad, C. Ebnesajjad, Surface treatment of materials for adhesive bonding, William Andrew, 2013.

[95] M. Essalhi, M. Khayet, 10 - Fundamentals of membrane distillation, in: Pervaporation Vap. Permeat. Membr. Distill., Woodhead Publishing, Oxford, 2015: pp. 277–316. http://www.sciencedirect.com/science/article/pii/B9781782422464000106.

[96] Eykens, K. De Sitter, C. Dotremont, L. Pinoy, B. Van der Bruggen, Characterization and performance evaluation of commercially available hydrophobic membranes for direct contact membrane distillation, Desalination. 392 (2016) 63–73.

[97] Z. Cui, N.T. Hassankiadeh, Y. Zhuang, E. Drioli, Y.M. Lee, Crystalline polymorphism in poly (vinylidenefluoride) membranes, Prog. Polym. Sci. 51 (2015) 94–126.

[98] M. Khayet, C. Cojocaru, Artificial neural network modeling and optimization of desalination by air gap membrane distillation, Sep. Purif. Technol. 86 (2012) 171–182.

[99] E. Drioli, A. Ali, S. Simone, F. Macedonio, S. Al-Jlil, F. Al Shabonah, H. Al-Romaih, O. Al-Harbi, A. Figoli, A. Criscuoli, Novel PVDF hollow fiber membranes for vacuum and direct contact membrane distillation applications, Sep. Purif. Technol. 115 (2013) 27–38.

[100] Y. Tang, N. Li, A. Liu, S. Ding, C. Yi, H. Liu, Effect of spinning conditions on the structure and performance of hydrophobic PVDF hollow fiber membranes for membrane distillation, Desalination. 287 (2012) 326–339.

[101] M. Khayet, A. Imdakm, T. Matsuura, Monte Carlo simulation and experimental heat and mass transfer in direct contact membrane distillation, Int. J. Heat Mass Transf. 53 (2010) 1249–1259.

[102] R.B. Saffarini, B. Mansoor, R. Thomas, H.A. Arafat, Effect of temperature-dependent microstructure evolution on pore wetting in PTFE membranes under membrane distillation conditions, J. Membr. Sci. 429 (2013) 282–294. doi:10.1016/j.memsci.2012.11.049.

[103] E. Guillen-Burrieza, M.O. Mavukkandy, M.R. Bilad, H.A. Arafat, Understanding wetting phenomena in membrane distillation and how operational parameters can affect it, J. Membr. Sci. 515 (2016) 163–174. doi:10.1016/j.memsci.2016.05.051.

[104] F. Banat, N. Jwaied, M. Rommel, J. Koschikowski, M. Wieghaus, Desalination by a "compact SMADES" autonomous solarpowered membrane distillation unit, Desalination. 217 (2007) 29–37.

[105] F. Banat, N. Jwaied, M. Rommel, J. Koschikowski, M. Wieghaus, Performance evaluation of the "large SMADES" autonomous desalination solar-driven membrane distillation plant in Aqaba, Jordan, Desalination. 217 (2007) 17–28.

[106] Y. Peng, J. Ge, S. Wang, Z. Li, Occurrence of salt breakthrough and air-vapor pocket in a direct-contact membrane distillation, Desalination. 402 (2017) 42–49. doi:10.1016/j.desal.2016.09.033.

[107] M. Gryta, The influence of the hydrodynamic conditions on the performance of membrane distillation, in: Hydrodyn.-Optim. Methods Tools, InTech, 2011.

[108] D. Winter, J. Koschikowski, D. Düver, P. Hertel, U. Beuscher, Evaluation of MD process performance: Effect of backing structures and membrane properties under different operating conditions, Membr. Distill. Relat. Membr. Syst. 323 (2013) 120–133. doi:10.1016/j.desal.2013.04.007.

[109] M. El Fray, M. Gryta, Environmental fracture of polypropylene membranes used in membrane distillation process, Polimery. 53 (2008) 865–870.

[110] C.-M. Bell, Comparison of polyelectrolyte coated PVDF membranes in thermopervaporation with porous hydrophobic membranes in membrane distillation using plate-and-frame modules, Chem. Eng. Process. Process Intensif. 104 (2016) 58–65. doi:10.1016/j.cep.2016.02.013.

[111] A. Cipollina, G. Micale, L. Rizzuti, Seawater desalination: conventional and renewable energy processes, Springer Science & Business Media, 2009.

[112] R.G. Raluy, R. Schwantes, V.J. Subiela, B. Peñate, G. Melián, J.R. Betancort, Operational experience of a solar membrane distillation demonstration plant in Pozo Izquierdo-Gran Canaria Island (Spain), Desalination. 290 (2012) 1–13. doi:10.1016/j.desal.2012.01.003.

[113] Y. Wang, Z. Xu, N. Lior, H. Zeng, An experimental study of solar thermal vacuum membrane distillation desalination, Desalination Water Treat. 53 (2015) 887–897. doi:10.1080/19443994.2014.927187.

[114] J. Koschikowski, M. Wieghaus, M. Rommel, V.S. Ortin, B.P. Suarez, J.R.B. Rodríguez, Experimental investigations on solar driven stand-alone membrane distillation systems for remote areas, Desalination. 248 (2009) 125–131.

[115] E. Guillen-Burrieza, R. Thomas, B. Mansoor, D. Johnson, N. Hilal, H. Arafat, Effect of dry-out on the fouling of PVDF and PTFE membranes under conditions simulating intermittent seawater membrane distillation (SWMD), J. Membr. Sci. 438 (2013) 126–139.

[116] F.A. Banat, J. Simandl, Theoretical and experimental study in membrane distillation, Desalination. 95 (1994) 39–52.

[117] M. Gryta, Degradation of Polypropylene Membranes Applied in Membrane Distillation Crystallizer, Crystals. 6 (2016) 33.

[118] M. Gryta, J. Grzechulska-Damszel, A. Markowska, K. Karakulski, The influence of polypropylene degradation on the membrane wettability during membrane distillation, J. Membr. Sci. 326 (2009) 493–502. doi:10.1016/j.memsci.2008.10.022.

[119] A. Hagedorn, G. Fieg, J. Koschikowski, T. Mann, Long-term experiences with field experiments on seawater desalination using membrane distillation, in: IDA World Congress, San Diego, USA, 2015.

[120] A.C.M. Franken, J.A.M. Nolten, M.H.V. Mulder, D. Bargeman, C.A. Smolders, Wetting criteria for the applicability of membrane distillation, J. Membr. Sci. 33 (1987) 315–328. doi:http://dx.doi.org/10.1016/S0376-7388(00)80288-4.

[121] L. Han, Y.Z. Tan, T. Netke, A.G. Fane, J.W. Chew, Understanding oily wastewater treatment via membrane distillation, J. Membr. Sci. 539 (2017) 284–294. doi:10.1016/j.memsci.2017.06.012.

[122] M. Gryta, The influence of magnetic water treatment on CaCO 3 scale formation in membrane distillation process, Sep. Purif. Technol. 80 (2011) 293–299.

[123] A. Marmur, C. Della Volpe, S. Siboni, A. Amirfazli, J.W. Drelich, Contact angles and wettability: Towards common and accurate terminology, Surf. Innov. 5 (2017) 3–8.

[124] M. Gryta, M. Barancewicz, Influence of morphology of PVDF capillary membranes on the performance of direct contact membrane distillation, J. Membr. Sci. 358 (2010) 158–167. doi:10.1016/j.memsci.2010.04.044.

[125] M.A. Al-Obaidli, An Investigation into Hydrophobic Membrane Fouling in Desalination Using Membrane Distillation Technology, in: HBKU Press Qatar, 2016: p. EEPP3310.

[126] L.D. Nghiem, F. Hildinger, F.I. Hai, T. Cath, Treatment of saline aqueous solutions using direct contact membrane distillation, Desalination Water Treat. 32 (2011) 234–241.

[127] B. Zhang, L. Liu, S. Xie, F. Shen, H. Yan, H. Wu, Y. Wan, M. Yu, H. Ma, L. Li, J. Li, Built-up superhydrophobic composite membrane with carbon nanotubes for water desalination, RSC Adv. 4 (2014) 16561–16566. doi:10.1039/C3RA47436D.

[128] M. Izquierdo-Gil, M. Garcıa-Payo, C. Fernández-Pineda, Air gap membrane distillation of sucrose aqueous solutions, J. Membr. Sci. 155 (1999) 291–307.

[129] T. Young, A Course of Lectures on Natural Philosophy and the Mechanical Arts: In Two Volumes, Johnson, 1807.

[130] L.R. Fisher, P.D. Lark, An experimental study of the Washburn equation for liquid flow in very fine capillaries, J. Colloid Interface Sci. 69 (1979) 486–492.

[131] E.W. Washburn, The dynamics of capillary flow, Phys. Rev. 17 (1921) 273.

[132] A. Kayvani Fard, Y.M. Manawi, T. Rhadfi, K. Mahmoud, M. Khraisheh, F. Benyahia, Synoptic analysis of direct contact membrane distillation performance in Qatar, Desalination. 360 (2015) 97–107.

[133] B.S. Lalia, E. Guillen, H.A. Arafat, R. Hashaikeh, Nanocrystalline cellulose reinforced PVDF-HFP membranes for membrane distillation application, Desalination. 332 (2014) 134–141.

[134] B.S. Kim, P. Harriott, Critical entry pressure for liquids in hydrophobic membranes, J. Colloid Interface Sci. (1987). http://www.sciencedirect.com/science/article/pii/0021979787900026.

[135] W. Purcell, Interpretation of capillary pressure data, J. Pet. Technol. 2 (1950) 11–12.

[136] W.R. Purcell, Capillary Pressures - Their Measurement Using Mercury and the Calculation of Permeability Therefrom, SPE-949039-G. (1949). doi:10.2118/949039-G.

[137] F.F. Zha, A.G. Fane, C.J.D. Fell, R.W. Schofield, Critical displacement pressure of a supported liquid membrane, J. Membr. Sci. 75 (1992) 69–80. doi:10.1016/0376-7388(92)80007-7.

[138] D.S. Antao, S. Adera, Y. Zhu, E. Farias, R. Raj, E.N. Wang, Dynamic Evolution of the Evaporating Liquid–Vapor Interface in Micropillar Arrays, Langmuir. 32 (2016) 519–526. doi:10.1021/acs.langmuir.5b03916.

[139] M.C. García-Payo, M.A. Izquierdo-Gil, C. Fernández-Pineda, Wetting Study of Hydrophobic Membranes via Liquid Entry Pressure Measurements with Aqueous Alcohol Solutions, J. Colloid Interface Sci. 230 (2000) 420–431. doi:http://dx.doi.org/10.1006/jcis.2000.7106.

[140] E. Guillen-Burrieza, A. Servi, B.S. Lalia, H.A. Arafat, Membrane structure and surface morphology impact on the wetting of MD membranes, J. Membr. Sci. 483 (2015) 94–103. doi:10.1016/j.memsci.2015.02.024.

[141] A.M. Rijke, The water repellency and feather structure of cormorants, Phalacrocoracidae, J. Exp. Biol. 48 (1968) 185–189.

[142] A. Elowson, Spread-wing postures and the water repellency of feathers: a test of Rijke's hypothesis, The Auk. (1984) 371–383.

[143] A.T. Servi, J. Kharraz, D. Klee, K. Notarangelo, B. Eyob, E. Guillen-Burrieza, A. Liu, H.A. Arafat, K.K. Gleason, A systematic study of the impact of hydrophobicity on the wetting of MD membranes, J. Membr. Sci. 520 (2016) 850–859. doi:10.1016/j.memsci.2016.08.021.

[144] P. Yazgan-Birgi, M.I. Hassan Ali, H.A. Arafat, Estimation of liquid entry pressure in hydrophobic membranes using CFD tools, J. Membr. Sci. 552 (2018) 68–76. doi:10.1016/j.memsci.2018.01.061.

[145] Z. Yan, H. Yang, H. Yu, F. Qu, H. Liang, B. Van der Bruggen, G. Li, Reverse osmosis brine treatment using direct contact membrane distillation (DCMD): Effect of membrane characteristics on desalination performance and wetting phenomenon, Environ. Sci. Water Res. Technol. (2018).

[146] J. Goldstein, D.E. Newbury, D.C. Joy, C.E. Lyman, P. Echlin, E. Lifshin, L. Sawyer, J.R. Michael, Scanning Electron Microscopy and X-ray Microanalysis: Third Edition, Springer US, 2013. https://books.google.fr/books?id=qpN0ngEACAAJ.

[147] S. Shukla, J.P. Méricq, M.P. Belleville, N. Hengl, N.E. Benes, I. Vankelecom, J. Sanchez Marcano, Process intensification by coupling the Joule effect with pervaporation and sweeping gas membrane distillation, J. Membr. Sci. 545 (2018) 150–157. doi:10.1016/j.memsci.2017.09.061.

[148] D. Amaya-Vías, E. Nebot, J.A. López-Ramírez, Comparative studies of different membrane distillation configurations and membranes for potential use on board cruise vessels, Desalination. 429 (2018) 44–51. doi:10.1016/j.desal.2017.12.008.

[149] J.-G. Lee, Y. Jang, L. Fortunato, S. Jeong, S. Lee, T. Leiknes, N. Ghaffour, An advanced online monitoring approach to study the scaling behavior in direct contact membrane distillation, J. Membr. Sci. 546 (2018) 50–60. doi:10.1016/j.memsci.2017.10.009.

[150] S.A. Hashemifard, T. Matsuura, A.F. Ismail, M. Rezaei Dasht Arzhandi, D. Rana, G. Bakeri, Characterization of partial pore wetting in hollow fiber gas absorption membrane contactors: An EDX analysis approach, Chem. Eng. J. 281 (2015) 970–980. doi:10.1016/j.cej.2015.07.036.

[151] K.W. Lawson, D.R. Lloyd, Membrane distillation. I. Module design and performance evaluation using vacuum membrane distillation, J. Membr. Sci. 120 (1996) 111–121.

[152] F.E. Ahmed, B.S. Lalia, R. Hashaikeh, Membrane-based detection of wetting phenomenon in direct contact membrane distillation, J. Membr. Sci. (2017). doi:10.1016/j.memsci.2017.04.035.

[153] Y. Chen, Z. Wang, G.K. Jennings, S. Lin, Probing Pore Wetting in Membrane Distillation Using Impedance: Early Detection and Mechanism of Surfactant-Induced Wetting, Environ. Sci. Technol. Lett. (2017). doi:10.1021/acs.estlett.7b00372.

[154] J. Hou, M.Y. Zulkifli, M. Mohammad, Y. Zhang, A. Razmjou, V. Chen, Biocatalytic gas-liquid membrane contactors for CO 2 hydration with immobilized carbonic anhydrase, J. Membr. Sci. 520 (2016) 303–313.

[155] A. McLeod, B. Jefferson, E.J. McAdam, Toward gas-phase controlled mass transfer in micro-porous membrane contactors for recovery and concentration of dissolved methane in the gas phase, J. Membr. Sci. 510 (2016) 466–471.

[156] S.-H. Yeon, K.-S. Lee, B. Sea, Y.-I. Park, K.-H. Lee, Application of pilot-scale membrane contactor hybrid system for removal of carbon dioxide from flue gas, J. Membr. Sci. 257 (2005) 156–160.

[157] E. Drioli, Y. Wu, Membrane distillation : An experimental study, Proc. Symp. Membr. Technol. 53 (1985) 339–346. doi:10.1016/0011-9164(85)85071-2.

[158] M. Gryta, Direct contact membrane distillation with crystallization applied to NaCl solutions, Chem. Pap.-SLOVAK Acad. Sci. 56 (2002) 14–19.

[159] G. Rácz, S. Kerker, Z. Kovács, G. Vatai, M. Ebrahimi, P. Czermak, Theoretical and experimental approaches of liquid entry pressure determination in membrane distillation processes, Period. Polytech. Chem. Eng. 58 (2014) 81–91. doi:10.3311/PPch.2179.

[160] J. Wang, X. Sun, Y. Yuan, H. Chen, H. Wang, D. Hou, A novel microwave assisted photo-catalytic membrane distillation process for treating the organic wastewater containing inorganic ions, J. Water Process Eng. 9 (2016) 1–8. doi:10.1016/j.jwpe.2015.11.004.

[161] D.M. Warsinger, A. Servi, G.B. Connors, M.O. Mavukkandy, H.A. Arafat, K.K. Gleason, Reversing membrane wetting in membrane distillation: comparing dryout to backwashing with pressurized air, Environ. Sci. Water Res. Technol. 3 (2017) 930–939.

[162] J.A. Sanmartino, M. Khayet, M.C. García-Payo, Reuse of discarded membrane distillation membranes in microfiltration technology, J. Membr. Sci. 539 (2017) 273–283. doi:10.1016/j.memsci.2017.06.003.

[163] N. Ghaffour, The challenge of capacity-building strategies and perspectives for desalination for sustainable water use in MENA, Desalination Water Treat. 5 (2009) 48–53.

[164] M. El-Bourawi, Z. Ding, R. Ma, M. Khayet, A framework for better understanding membrane distillation separation process, J. Membr. Sci. 285 (2006) 4–29.

[165] A.I. Stankiewicz, J.A. Moulijn, Process intensification: transforming chemical engineering, Chem. Eng. Prog. 96 (2000) 22–34.

[166] E. Chabanon, D. Roizard, E. Favre, Membrane contactors for postcombustion carbon dioxide capture: a comparative study of wetting resistance on long time scales, Ind. Eng. Chem. Res. 50 (2011) 8237–8244.

[167] W. Zhong, J. Hou, H.-C. Yang, V. Chen, Superhydrophobic membranes via facile bio-inspired mineralization for vacuum membrane distillation, J. Membr. Sci. 540 (2017) 98–107. doi:10.1016/j.memsci.2017.06.033.

[168] Z. Wang, J. Jin, D. Hou, S. Lin, Tailoring surface charge and wetting property for robust oil-fouling mitigation in membrane distillation, J. Membr. Sci. 516 (2016) 113–122. doi:10.1016/j.memsci.2016.06.011.

[169] Y. Shin, J. Choi, T. Lee, J. Sohn, S. Lee, Optimization of dewetting conditions for hollow fiber membranes in vacuum membrane distillation, Desalination Water Treat. 57 (2016) 7582–7592.

[170] W. Koros, Y. Ma, T. Shimidzu, Terminology for membranes and membrane processes, J Membr Sci. 120 (1996) 149–159.

[171] M. Khayet, M. Godino, J. Mengual, Theoretical and experimental studies on desalination using the sweeping gas membrane distillation method, Desalination. 157 (2003) 297–305.

[172] T.D. Dao, J.-P. Mericq, S. Laborie, C. Cabassud, A new method for permeability measurement of hydrophobic membranes in Vacuum Membrane Distillation process, Water Res. 47 (2013) 2096–2104. doi:10.1016/j.watres.2013.01.040.

[173] A.E. Allegrezza, E.T. Burke, Composite ultrafiltration membranes, US 06/864,074, 1989. https://www.google.com/patents/US4824568.

[174] J. Drelich, Guidelines to measurements of reproducible contact angles using a sessile-drop technique, Surf. Innov. 1 (2013) 248–254.

[175] S. Nejati, C. Boo, C.O. Osuji, M. Elimelech, Engineering flat sheet microporous PVDF films for membrane distillation, J. Membr. Sci. 492 (2015) 355–363.

[176] P. Jacob, S. Laborie, C. Cabassud, Visualizing and evaluating wetting in membrane distillation: New methodology and indicators based on Detection of Dissolved Tracer Intrusion (DDTI), Desalination. 443 (2018) 307–322. doi:10.1016/j.desal.2018.06.006.

[177] G.E.P. Box, D.W. Behnken, Simplex-Sum Designs: A Class of Second Order Rotatable Designs Derivable From Those of First Order, Ann Math Stat. (1960) 838–864. doi:10.1214/aoms/1177705661.

[178] M. Khayet, C. Cojocaru, C. García-Payo, Application of Response Surface Methodology and Experimental Design in Direct Contact Membrane Distillation, Ind. Eng. Chem. Res. 46 (2007) 5673–5685. doi:10.1021/ie070446p.

[179] P. Onsekizoglu, K. Savas Bahceci, J. Acar, The use of factorial design for modeling membrane distillation, J. Membr. Sci. 349 (2010) 225–230. doi:10.1016/j.memsci.2009.11.049.

[180] M. Khayet, C. Cojocaru, A. Baroudi, Modeling and optimization of sweeping gas membrane distillation, Spec. Issue Honour Profr. Takeshi Matsuura His 75th Birthd. 287 (2012) 159–166. doi:10.1016/j.desal.2011.04.070.

[181] M. Khayet, C. Cojocaru, Air gap membrane distillation: Desalination, modeling and optimization, Spec. Issue Honour Profr. Takeshi Matsuura His 75th Birthd. 287 (2012) 138–145. doi:10.1016/j.desal.2011.09.017.

[182] Y.Z. Tan, L. Han, W.H. Chow, A.G. Fane, J.W. Chew, Influence of module orientation and geometry in the membrane distillation of oily seawater, Desalination. 423 (2017) 111–123. doi:10.1016/j.desal.2017.09.019.

[183] M. Monnot, S. Laborie, C. Cabassud, Granular activated carbon filtration plus ultrafiltration as a pretreatment to seawater desalination lines: Impact on water quality and UF fouling, Desalination. 383 (2016) 1–11. doi:10.1016/j.desal.2015.12.010.

[184] W.M. Haynes, CRC Handbook of Chemistry and Physics, CRC press, 2014.

[185] J. Zolgharnein, A. Shahmoradi, J.B. Ghasemi, Comparative study of Box–Behnken, central composite, and Doehlert matrix for multivariate optimization of Pb (II) adsorption onto Robinia tree leaves, J. Chemom. 27 (2013) 12–20.

[186] M. Gryta, Concentration of NaCl solution by membrane distillation integrated with crystallization, Sep. Sci. Technol. 37 (2002) 3535–3558. doi:10.1081/SS-120014442.

[187] V. Chen, H. Li, A.. Fane, Non-invasive observation of synthetic membrane processes – a review of methods, J. Membr. Sci. 241 (2004) 23–44. doi:10.1016/j.memsci.2004.04.029.

[188] C. Duan, W.-N. Mei, W.-G. Yin, J. Liu, J. Hardy, M. Bai, S. Ducharme, Theoretical study on the optical properties of polyvinylidene fluoride crystal, J. Phys. Condens. Matter. 15 (2003) 3805.

[189] A. Siddiqui, N. Farhat, S.S. Bucs, R.V. Linares, C. Picioreanu, J.C. Kruithof, M.C. van Loosdrecht, J. Kidwell, J.S. Vrouwenvelder, Development and characterization of 3D-printed feed spacers for spiral wound membrane systems, Water Res. 91 (2016) 55–67.

[190] N. Sreedhar, N. Thomas, O. Al-Ketan, R. Rowshan, H. Hernandez, R.K. Abu Al-Rub, H.A. Arafat, 3D printed feed spacers based on triply periodic minimal surfaces for flux enhancement and biofouling mitigation in RO and UF, Desalination. 425 (2018) 12–21. doi:10.1016/j.desal.2017.10.010.

[191] N. Thomas, N. Sreedhar, O. Al-Ketan, R. Rowshan, R.K. Abu Al-Rub, H. Arafat, 3D printed triply periodic minimal surfaces as spacers for enhanced heat and mass transfer in membrane distillation, Desalination. 443 (2018) 256–271. doi:10.1016/j.desal.2018.06.009.

[192] M. Monnot, H.T.K. Nguyên, S. Laborie, C. Cabassud, Seawater reverse osmosis desalination plant at community-scale: Role of an innovative pretreatment on process performances and intensification, EPIC2015. 113 (2017) 42–55. doi:10.1016/j.cep.2016.09.020.

[193] Z. Wang, Y. Chen, X. Sun, R. Duddu, S. Lin, Mechanism of pore wetting in membrane distillation with alcohol vs. surfactant, J. Membr. Sci. 559 (2018) 183–195. doi:10.1016/j.memsci.2018.04.045.

[194] C.A. Schneider, W.S. Rasband, K.W. Eliceiri, NIH Image to ImageJ: 25 years of image analysis, Nat. Methods. 9 (2012) 671.

[195] L. Martínez-Díez, M.I. Vázquez-González, F.J. Florido-Díaz, Study of membrane distillation using channel spacers, J. Membr. Sci. 144 (1998) 45–56. doi:10.1016/S0376-7388(98)00024-6.

[196] Z. Lei, B. Chen, Z. Ding, Special distillation processes, Elsevier, 2005.

[197] T.D. Dao, Procédés membranaires pour l'élimination des métaux lourds: application de la distillation membranaire à l'élimination de l'Arsenic contenu dans les eaux, (2013).

[198] J.-P. Mericq, Approche intégrée du dessalement d'eau de mer: Distillation membranaire sous vide pour la réduction des rejets salins et possibilités de couplage avec l'énergie solaire, (2009).

[199] A. Hagedorn, G. Fieg, D. Winter, J. Koschikowski, A. Grabowski, T. Mann, Membrane and spacer evaluation with respect to future module design in membrane distillation, Desalination. 413 (2017) 154–167. doi:10.1016/j.desal.2017.03.016.

Appendixes

Chapter 2 Supplementary data

Membrane surface area

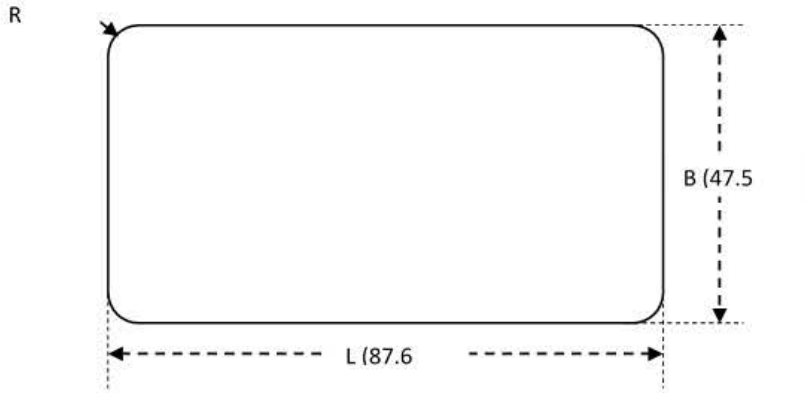

Figure C2.1 Dimensions of the membrane active layer

Area of the active layer (m^2)

$$A = L.W - 4r^2 + \pi r^2$$

Where, L= 87.6 mm, B= 47.5mm, r= 8mm

Thus, A= 0.0041060619 m^2 | 4.16E-03 m^2

Generalized flowchart of wetting detection using DDTI method

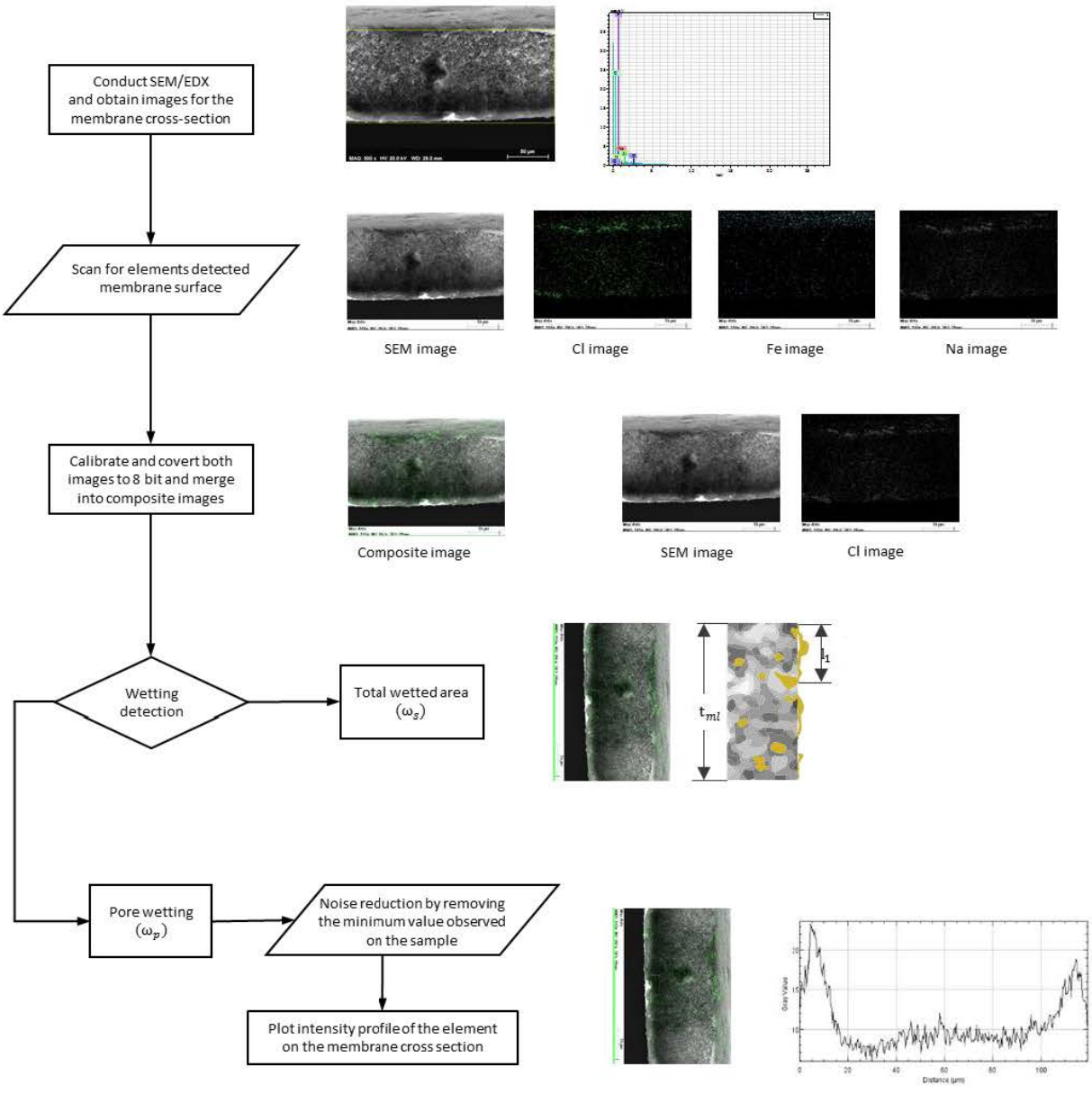

Figure C2.2: Protocol for image processing for wetting detection using salt intrusion as the detection technique under SEM/EDX

Data on flow simulation

Fluid flow simulations were conducted on the feed channel at operating conditions (T_f 42.5°C, Re 2191 without filtration) using pure water to identify the potential places on the membrane surface to detect wetting. The boundary conditions were, 1.77 m/s at the feed entrance, fluid (water) temperature 42.5°C and gauge pressure at feed outlet of the membrane cell. Below is a mesh used for conducting the fluid flow simulation.

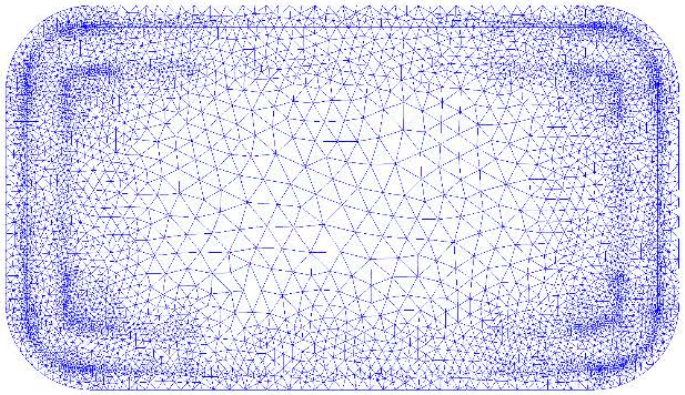

Figure C2.3 Meshing used for CFD

- **Boundary conditions**

Velocity Normal (1.77 m/s), Temperature (42.5 °C), Fluid: Water

- **Mesh**

Resolution factor 1.0, Edge growth rate 1.1, Minimum points on edge 2, Points on longest edge 10, Surface limiting aspect ratio 20, Mesh enhancement 1, Enhancement blending 1, Number of layers 10, Layer factor 0.6, Layer gradation 1.25

- **Meshed model**

Number of Nodes 387,743, Number of Elements 1,743,448

- **Physics**

Flow On, Incompressible fluid, Heat Transfer On, Auto Forced Convection On, Turbulence On

- **Solver settings**

Solution mode Steady State, Advection scheme ADV 5, Turbulence model SST k-omega DES

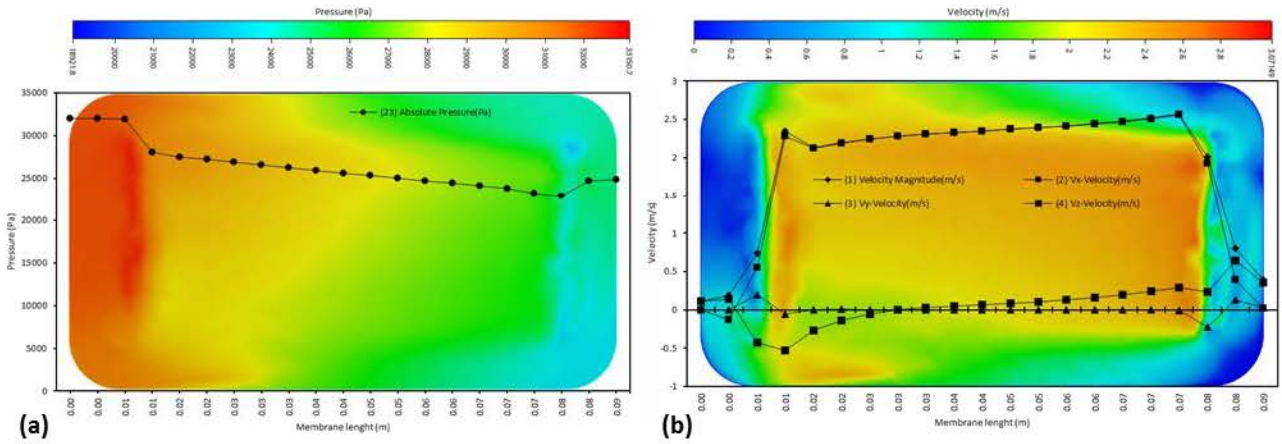

Figure C2.4: Fluid flow simulation with profile data for membrane cell (T_f 42.5°C and Re 2191) for (a) Absolute pressure (Pa) experienced by the membrane surface and (b) fluid flow in x,y,z with overall velocity magnitude (m/s) experienced by the membrane surface

The above **Figure** C3.3 presents the absolute pressure and velocity profile across the membrane surface from the feed side. It can be noted that as the membrane cell is designed like conventional MF/UF flat sheet membrane cells; the feed inlet and outlet ports on the feed side of the membrane module are located directly under the membrane surface at each end, which creates additional pressure at the inlet and some dead velocity zones on the edge of the membrane. It can be noted that at the membrane surface just above the inlet port; the absolute pressure is 33.15 kPa while the membrane surface at the outlet port experiences 22.88 kPa of pressure. This is additional to the 6 kPa being applied on the membrane by the vacuum. Thus, overall a high-pressure zone is created at localized points where LEP could be compromised during operation. Similarly, in the dead zones (w.r.t velocity magnitude) salt can start to form crystals and change the surface properties (like SFE and CA) resulting in wetting. Thus, to identify localized wetting, samples from potential problematic areas were taken and analyzed under SEM/EDS and later reduced to sampling locations presented in the chapter 3 and chapter 4

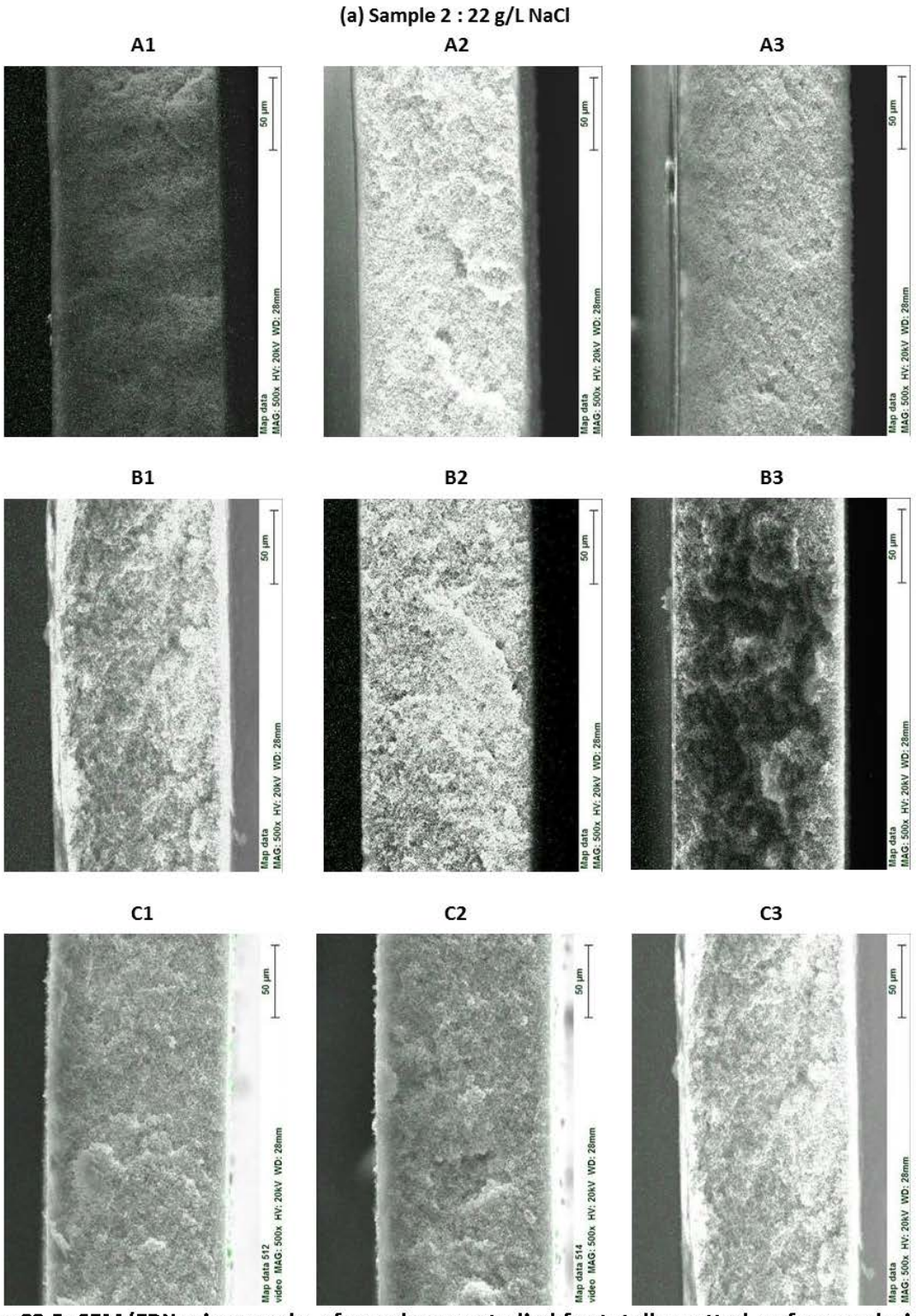

Figures C2.5: SEM/EDX micrographs of membranes studied for totally wetted surface analysis at 22g/L NaCl solution (to be viewed in color)

(a) Sample 3 : 166 g/L NaCl

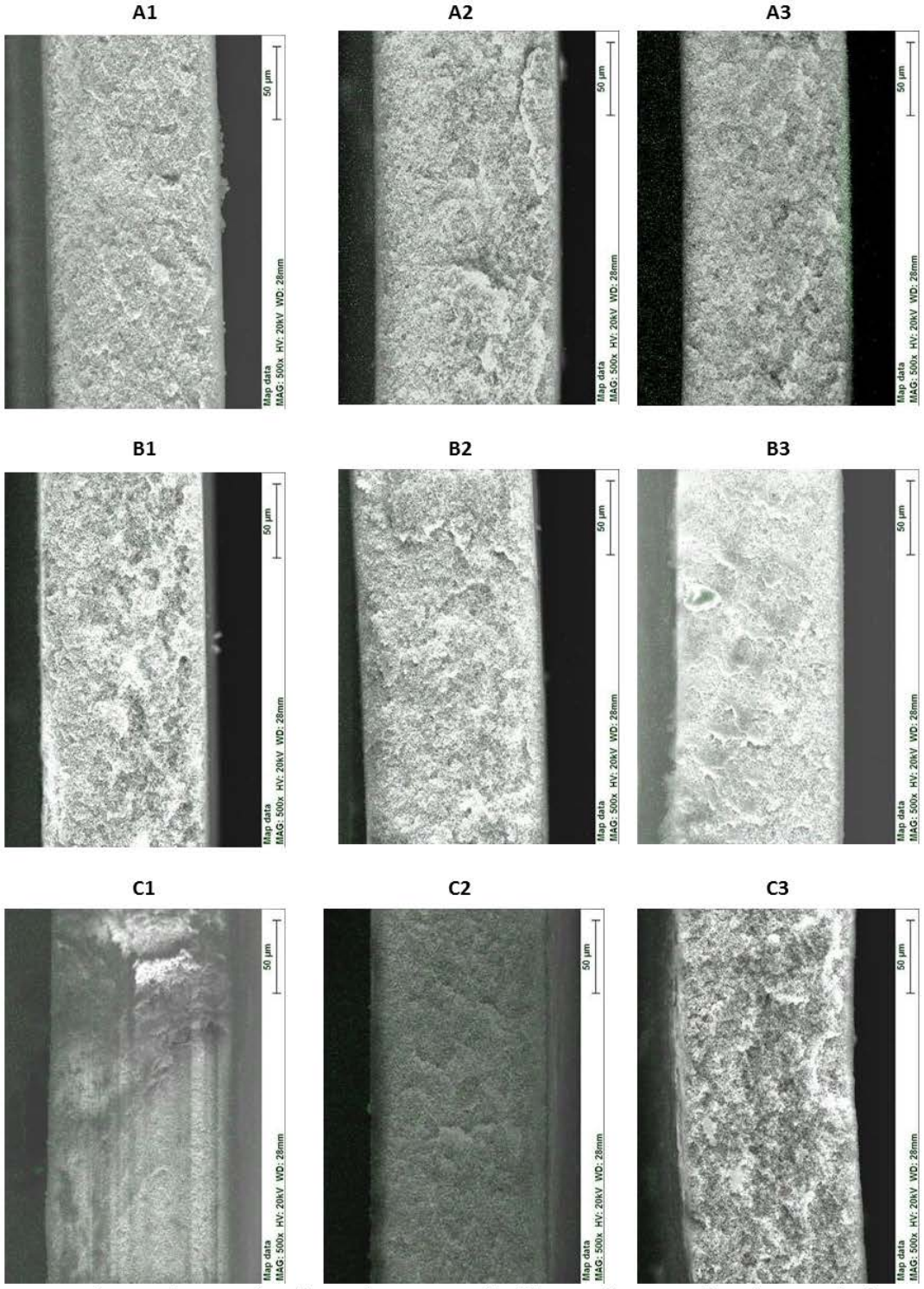

Figures C2.6: SEM/EDX micrographs of membranes studied for totally wetted surface analysis at 166 g/L NaCl solution (to be viewed in color)

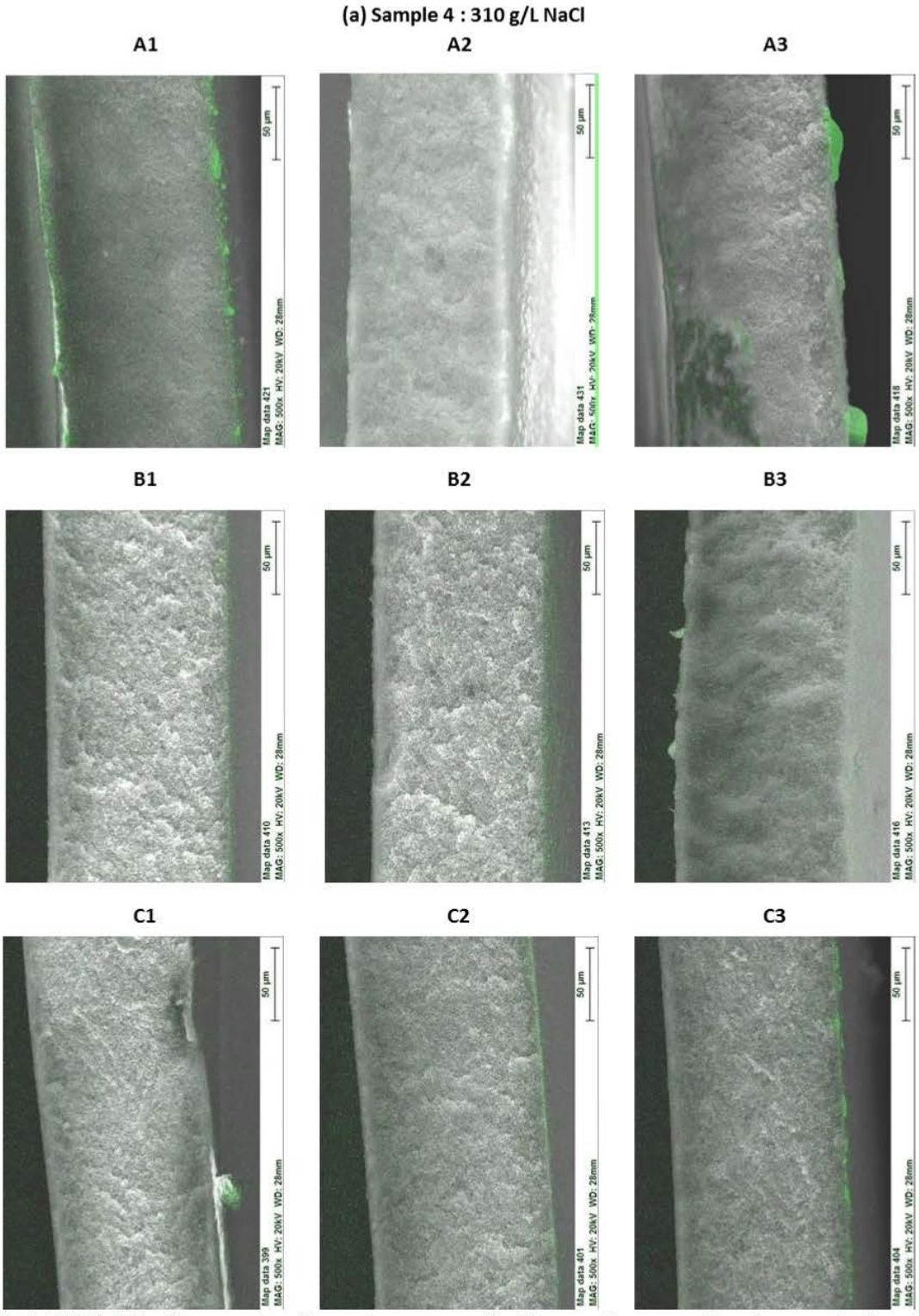

Figures C2.7: SEM/EDX micrographs of membranes studied for totally wetted surface analysis at 310 g/L NaCl solution (to be viewed in color)

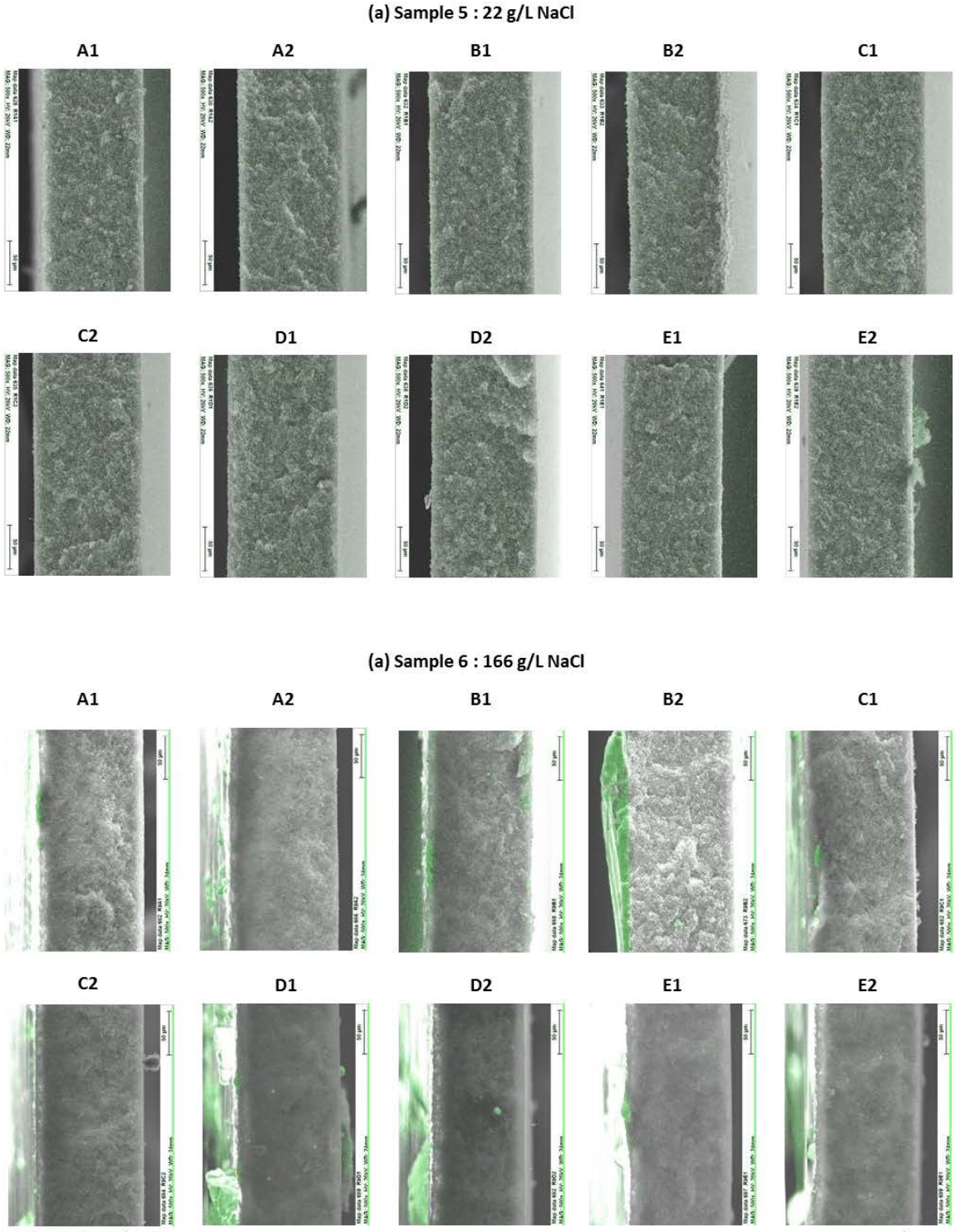

Figure C2.8: SEM/EDX micrographs on membranes studied for pore wetting analysis at (a) 22 g/L (b) 166 g/L NaCl solution

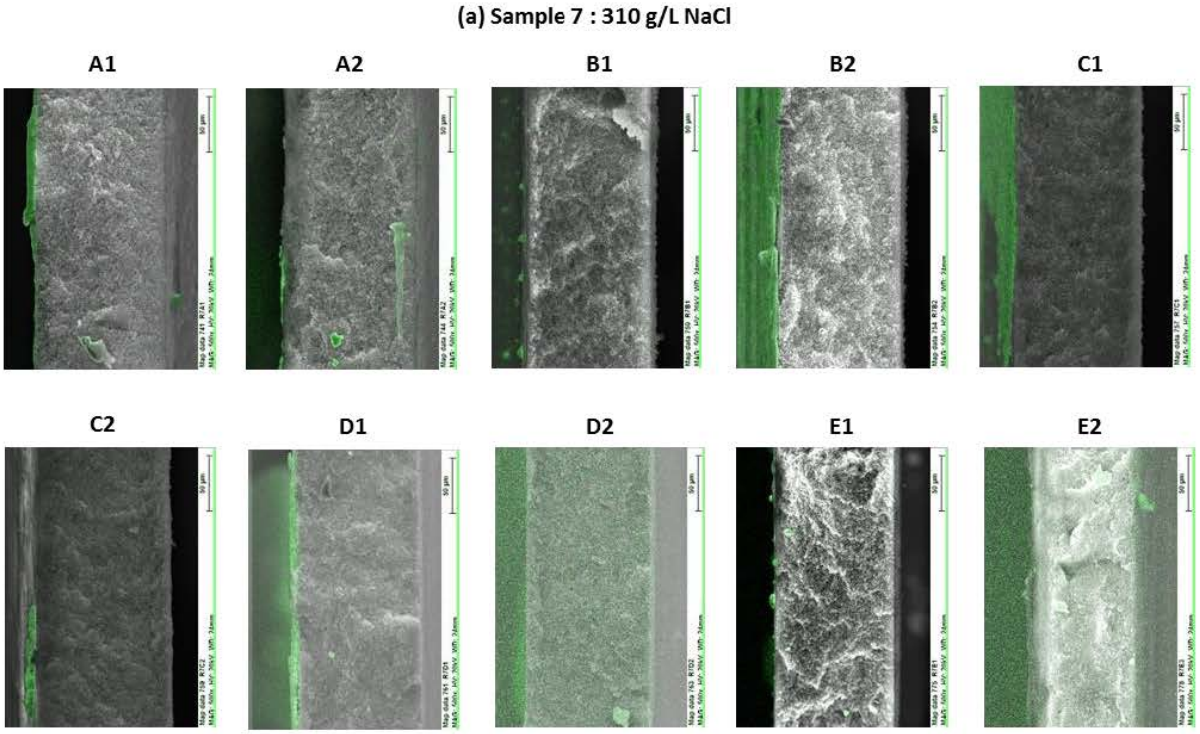

Figure C2.9: SEM/EDX micrographs on membranes studied for pore wetting analysis at 310 g/L NaCl solution

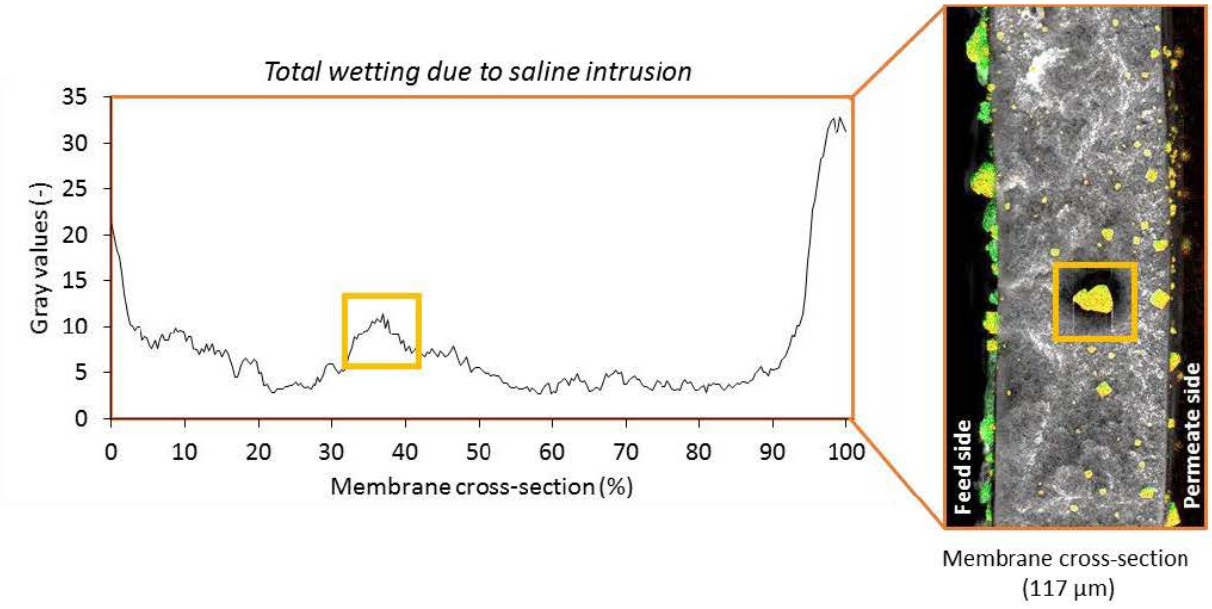

Figure C2.10: Example of pore wetting analysis on the studied membrane

Chapter 3 Supplementary data

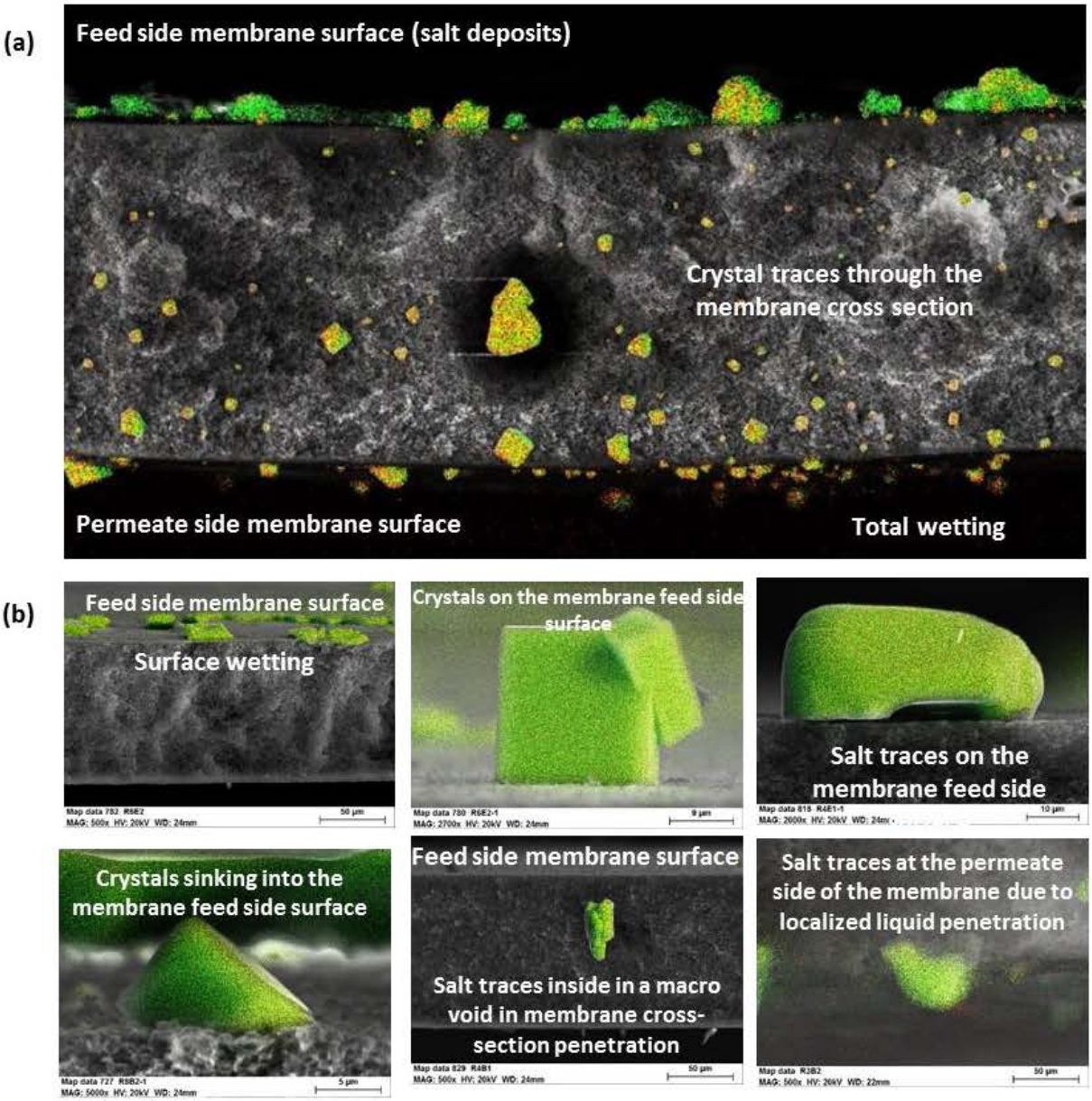

C3.1 EM/EDX micrographs of the membrane cross-section with different stages of wetting

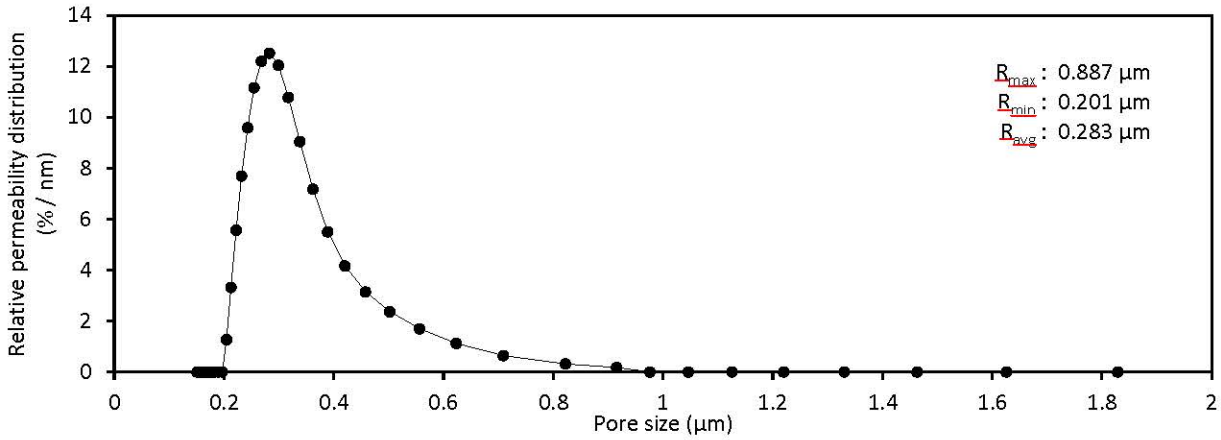

C3.2: Pore size distribution for durapore membranes

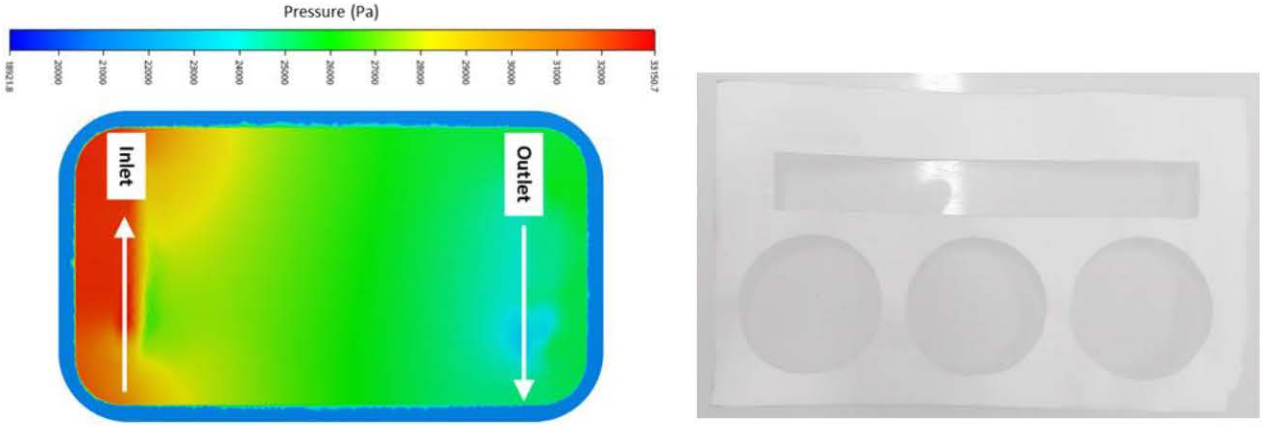

Figure C3.3 (a) Selection of sampling locations based on CFD simulations and (b) image of a membrane samples after subjection to operating conditions and cut using laser for SEM/EDX analysis and LEPw experiments (to be viewed in color)

Table C3.1: Chemical and physical properties of NaCl feed solution used in Part 1 of of Chapter 3

Sr. No	Temp. (°C)	NaCl (g/L)	Molarity (Na)	Molality (Cl)	pH	pe	Specific Conductance (µS/cm, @ Temp°C)	Density (g/cm^3)	Volume (L)	Activity of water	Ionic strength (mol/kgw)	Total alkalinity (eq/kg)
1	35	22	0.49	0.32	7	4	47493	1.01	1.01	0.986	0.40	1.90E-07
2	35	166	4.33	2.81	7	4	361077	1.13	1.07	0.879	3.57	2.33E-07
3	35	310	9.77	6.34	7	4	768412	1.26	1.15	0.726	8.05	1.92E-07
4	42.5	22	0.49	0.32	7	4	54629	1.01	1.01	0.986	0.40	3.99E-07
5	42.5	166	4.33	2.81	7	4	415099	1.12	1.07	0.879	3.57	4.79E-07
6	42.5	310	9.77	6.34	7	4	882197	1.25	1.16	0.726	8.05	4.14E-07
7	50	22	0.49	0.32	7	4	62064	1.00	1.02	0.986	0.40	7.15E-07
8	50	166	2.81	4.33	7	4	471334	1.12	1.07	0.879	3.57	8.53E-07
9	50	310	9.77	6.34	7	4	1000346	1.25	1.16	0.726	8.05	7.50E-07

Table C3.2: Chemical and physical properties of NaCl feed solution used in Part 2 of Chapter 3

Sr. No	Temp. (°C)	NaCl (g/L)	Molarity (Na)	Molality (Cl)	pH	pe	Conductivity (µS/cm, @ Temp °C)	Density (g/cm^3)	Volume (L)	Water activity	Ionic strength (mol/kgw)	Total alkalinity (eq/kg)
1	42.5	22	0.49	0.32	7	4	54629	1.01	1.01	0.986	0.40	3.99E-07
2	42.5	35	0.79	0.51	7	4	80749	1.02	1.02	0.978	0.65	4.25E-07
3	42.5	60	1.39	0.90	7	4	126884	1.04	1.03	0.961	1.14	4.54E-07
4	42.5	100	2.42	1.57	7	4	205648	1.07	1.04	0.932	1.99	4.76E-07
5	42.5	130	3.25	2.11	7	4	284374	1.09	1.05	0.909	2.68	4.81E-07
6	42.5	166	4.33	2.81	7	4	415099	1.12	1.07	0.879	3.57	4.79E-07
7	42.5	200	5.44	3.53	7	4	508386	1.15	1.09	0.848	4.48	4.72E-07
8	42.5	250	7.25	4.70	7	4	661696	1.20	1.12	0.797	5.98	4.51E-07
9	42.5	310	9.77	6.34	7	4	882197	1.25	1.16	0.726	8.05	4.14E-07

Data for Part 1 (Box Behnken design)

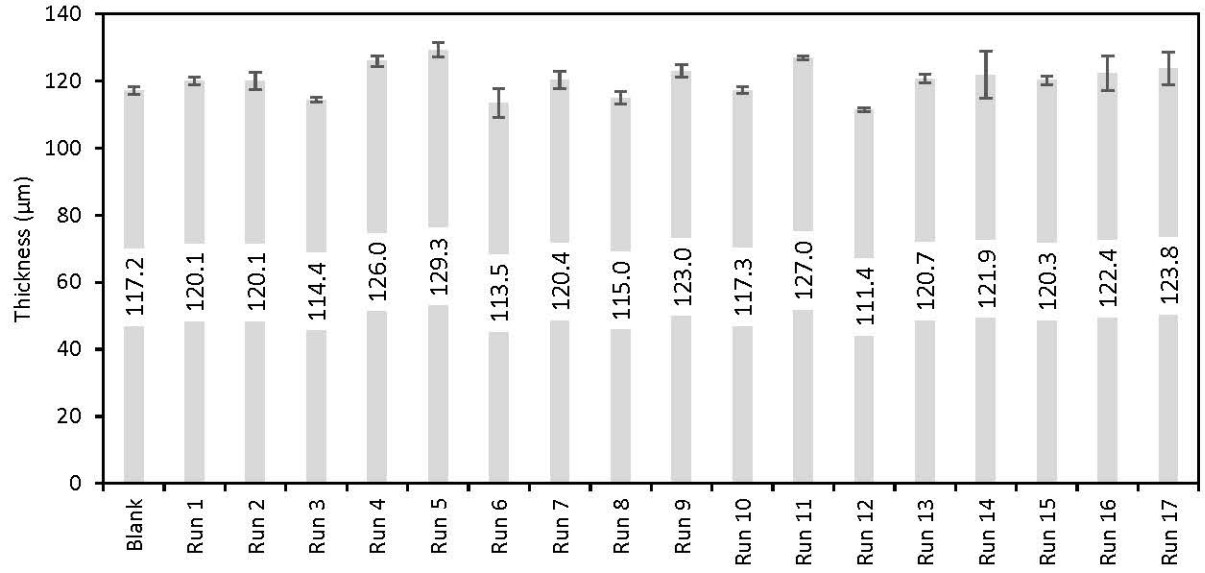

Figure C3.4 Variation of thickness in the membrane sample as compared to the blank membrane in part 1 of Chapter 3

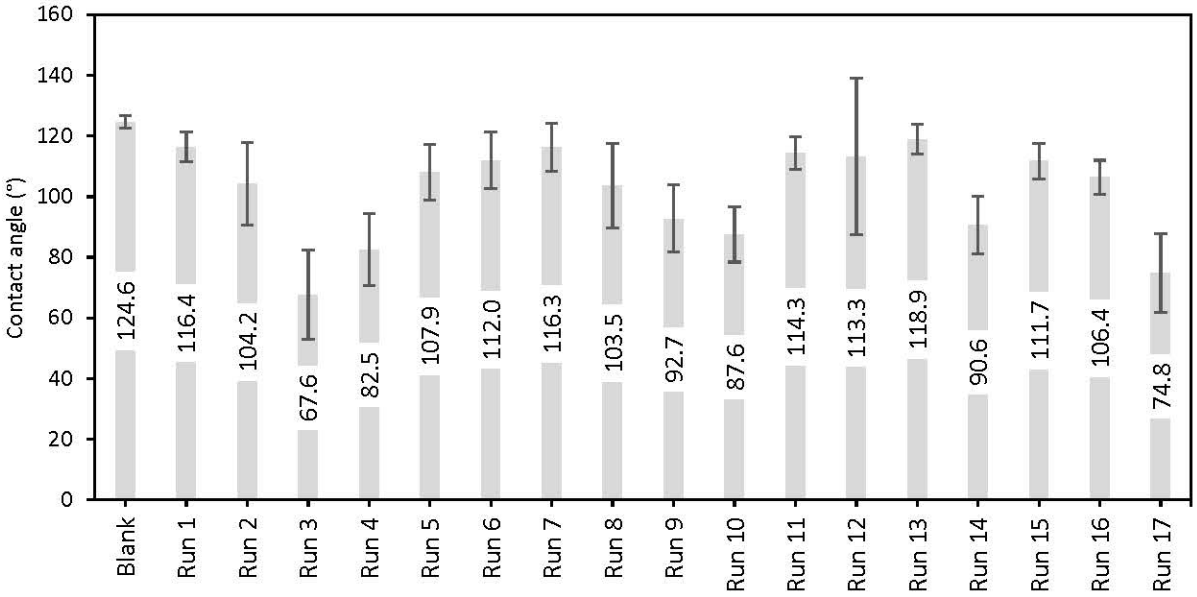

Figure C3.5 Contact angle of the membrane with stanadrd deviation for Part 1 of Chapter 3

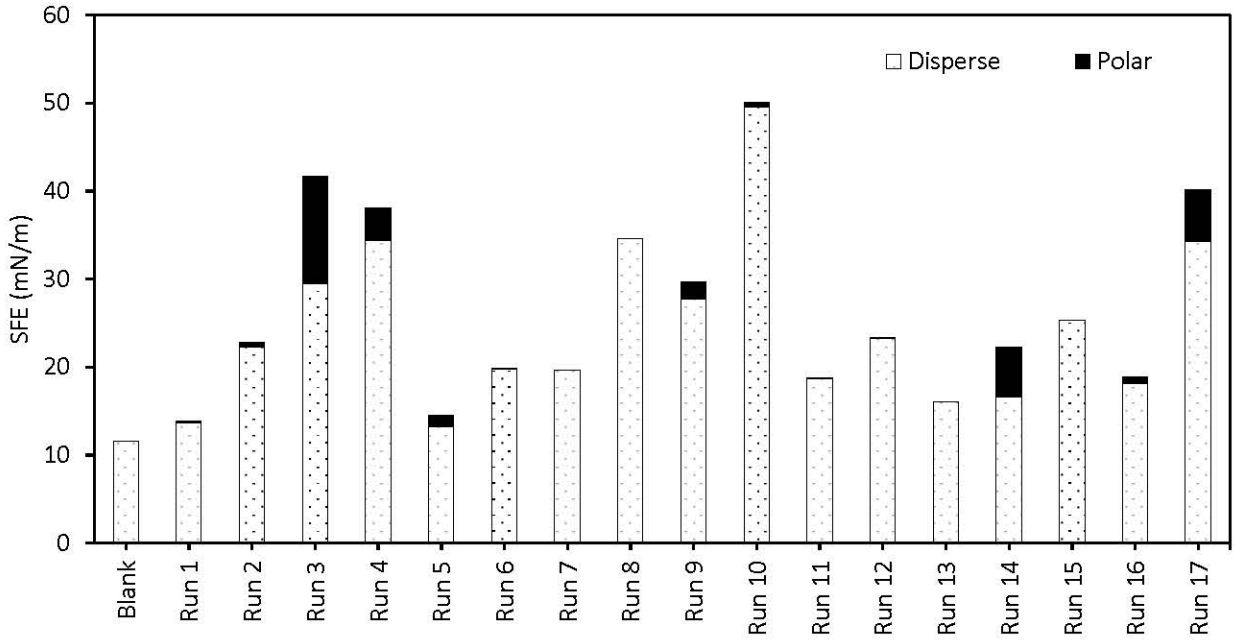

Figure C3.6 Surface free energy with contributions of polar and disperse energies for Part 1 of Chapter 3

Data for Part 2

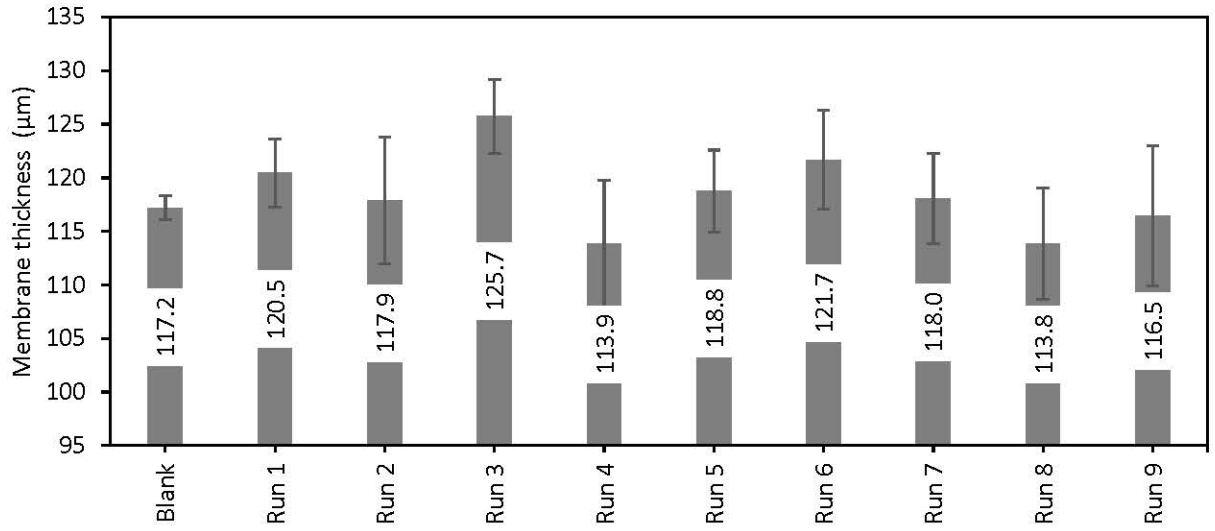

Figure C4.7 Variation of thickness in the membrane sample as compared to the blank membrane for Part 2 of Chapter 3

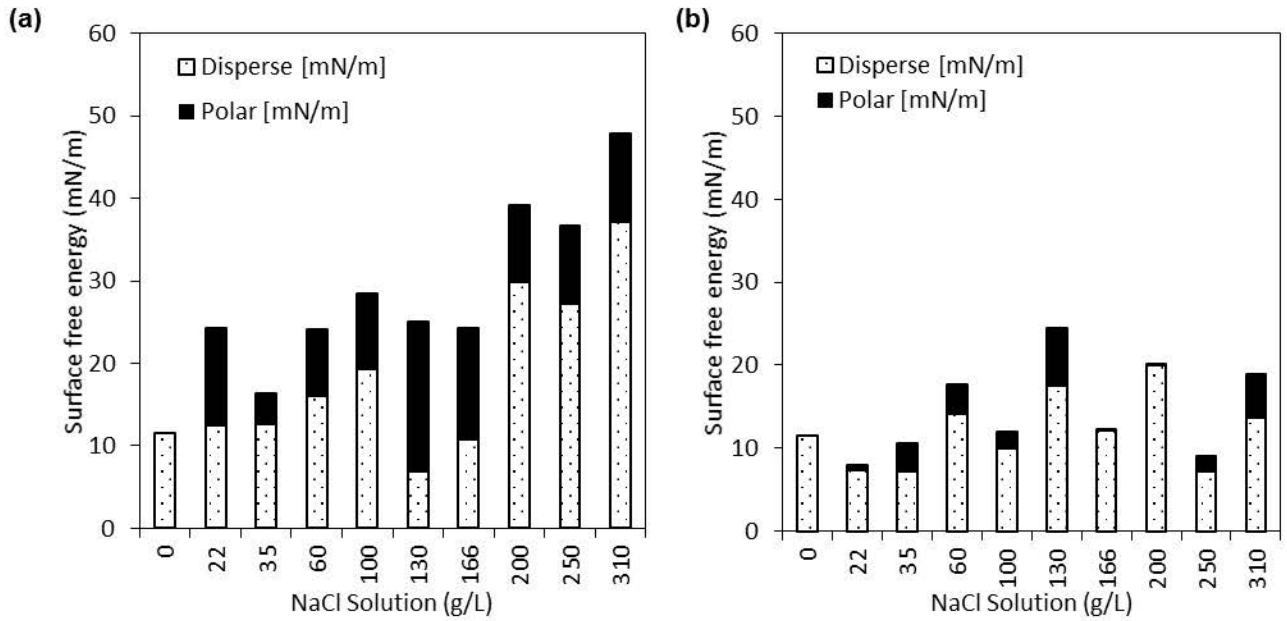

Figure C3.8 Surface free energy with contributions of polar and disperse energies of the studied membrane (a) before washing (b) after washing for Part 2 of Chapter 3

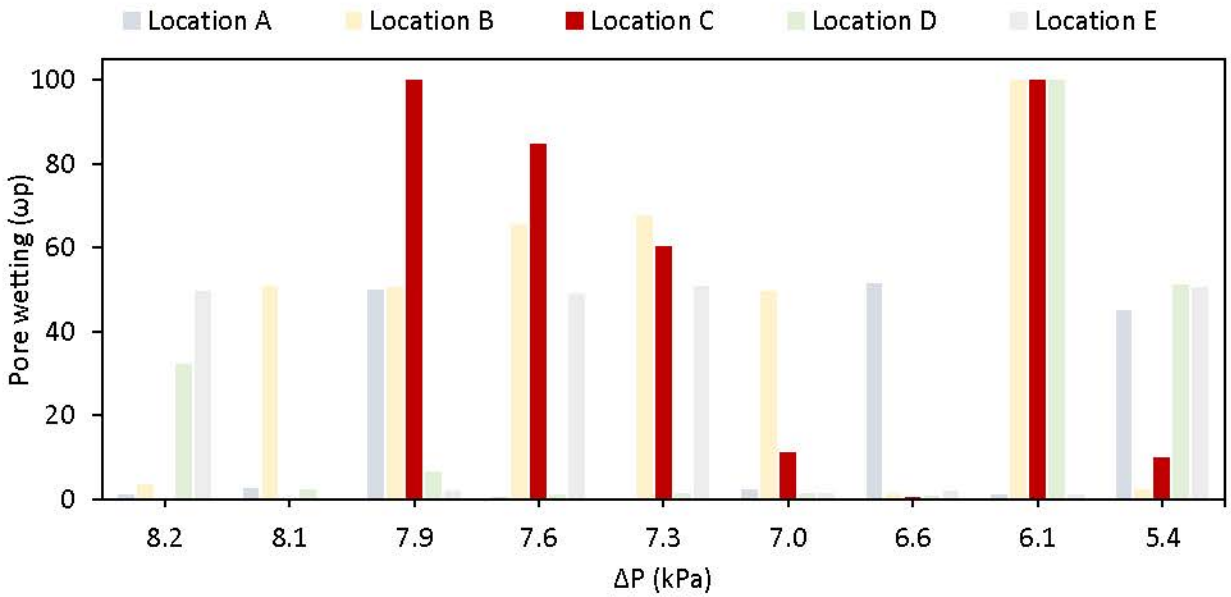

Figure C3.9 Influence of partial pressure on all sampling location for pore wetting ratio in Part 2 of Chapter 3

Table C3.3 Summary of results for the part 2 of Chapter 3

Sr. No	NaCl	Time	Permeate Pressure	Flux						Permeate	Feed Cond.	Permeate Cond.	Rejection
				Lowest	@ Temp	Highest	@ Temp	Median Flux	@ Temp	water collected	Average	Average	
	g/L	min	mbar	Kg/m².h	°C	Kg/m².h	°C	Kg/m².h	°C	g	µs/cm	µs/cm	%
Run 1	22	574.0	60.09	4.41	42.26	6.04	42.96	5.70	42.67	225.47	41076.97	2.34	99.994
Run 2	35	580.2	60.19	3.59	42.02	6.10	43.08	5.65	42.75	225.75	63621.95	1.42	99.998
Run 3	60	524.3	60.18	0.00	42.38	9.67	42.82	6.39	42.63	225.82	100715.62	1.84	99.998
Run 4	100	684.4	60.30	1.38	42.24	5.40	42.79	4.80	42.55	225.47	148372.29	3.31	99.998
Run 5	130	915.0	60.17	0.00	41.81	10.85	42.74	4.36	42.38	218.33	184220.70	2.19	99.999
Run 6	166	603.0	60.32	0.00	42.17	8.45	42.64	5.40	42.47	225.98	215177.54	1.84	99.999
Run 7	200	764.0	60.12	1.99	42.79	4.74	43.25	4.27	43.01	225.08	236368.81	4.70	99.998
Run 8	250	933.8	60.00	2.98	42.48	3.98	43.12	3.48	42.78	225.77	263130.73	4.91	99.998
Run 9	310	1440.8	60.00	1.94	42.17	2.86	42.92	2.28	42.61	225.58	290849.67	1.46	99.999

Table C3.4: Summary of LEP, CA and SFE (including polar and disperse energy) before and after washing the membrane samples in part 2 of Chapter 3

	Before washing								After washing									
	CA (°)	S.D.	SFE (mN/m)	S.D.	Disperse (mN/m)	S.D.	Polar (mN/m)	S.D.	CA	S.D.	SFE (mN/m)	S.D.	Disperse (mN/m)	S.D.	Polar (mN/m)	S.D.	LEP (bar)	S.D.
Blank	124.6	2.13	11.55	3.8	11.55	3.8	0.00	0.01	2.05	0.09	11.55	3.8	11.55	3.8	0.00	0.01	2.05	0.09
Run 1	90.57	5.68	24.32	7.85	12.45	2.5	11.87	5.4	120.2	5.81	7.89	3.1	7.3	2.3	0.59	0.8	1.67	0.32
Run 2	99.71	9.45	16.29	4.46	12.63	1.3	3.66	3.2	107	6.88	10.64	4.5	7.2	2.1	3.43	2.4	2.07	0.15
Run 3	86.95	2.49	24.11	5.3	16.03	3.3	8.08	2.1	98.66	8.65	17.63	6	14.12	3	3.51	3	1.87	0.40
Run 4	81.17	7.85	28.39	6.58	19.38	2.3	9.01	4.3	108.8	9.73	11.93	3.5	10.02	1.2	1.92	2.3	2.10	0.10
Run 5	80.01	5.2	25.08	10.7	6.88	4.5	18.2	6.2	86.81	7.38	24.52	4.9	17.54	1.4	6.98	3.5	1.93	0.29
Run 6	81.8	3.34	24.28	4.77	10.7	2.1	13.58	2.7	119.4	10.4	12.3	3.7	12.2	3.1	0.1	0.5	1.83	0.47
Run 7	72.68	6.6	39.12	5.52	29.86	2	9.25	3.5	110.5	6.51	20.18	2.8	20.03	2.3	0.15	0.4	1.87	0.06
Run 8	74.21	3.82	36.63	4.17	27.17	2	9.46	2.2	113	2.75	8.97	3.7	7.14	2.6	1.84	1.1	2.10	0.10
Run 9	63.16	10.7	47.89	9.22	37.19	3.3	10.7	5.9	94.39	4.87	18.93	6.7	13.7	4.1	5.23	2.6	1.97	0.06

Chapter 4 Supplementary data

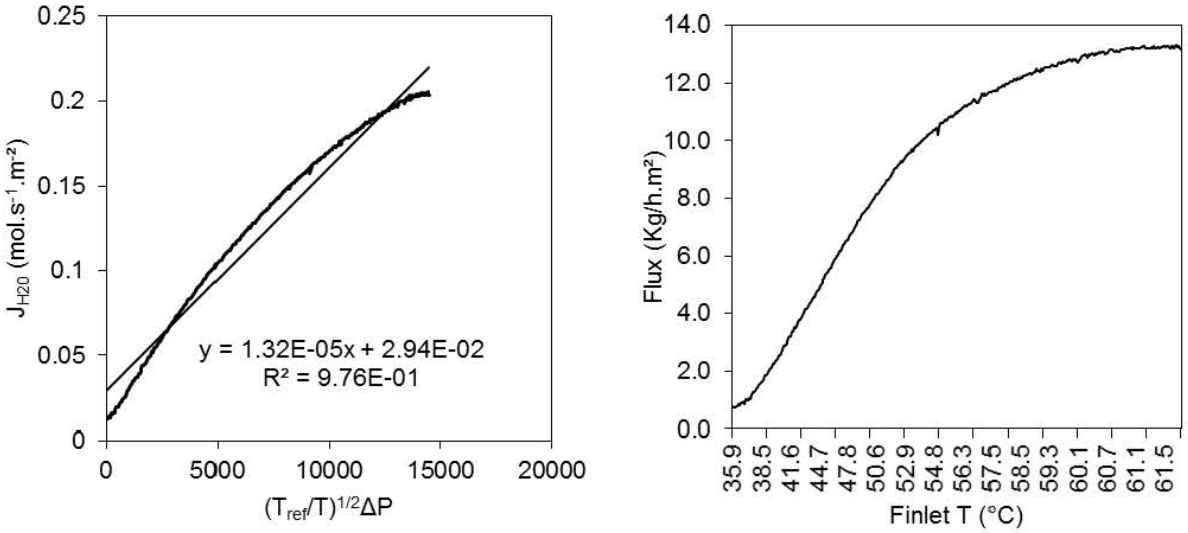

Figure C4.1 Permeability measurement (in laminar flow) using temperature variation (35 – 61 °C) method at 6kPa vacuum pressure and pure water flux in the newly developed membrane cell

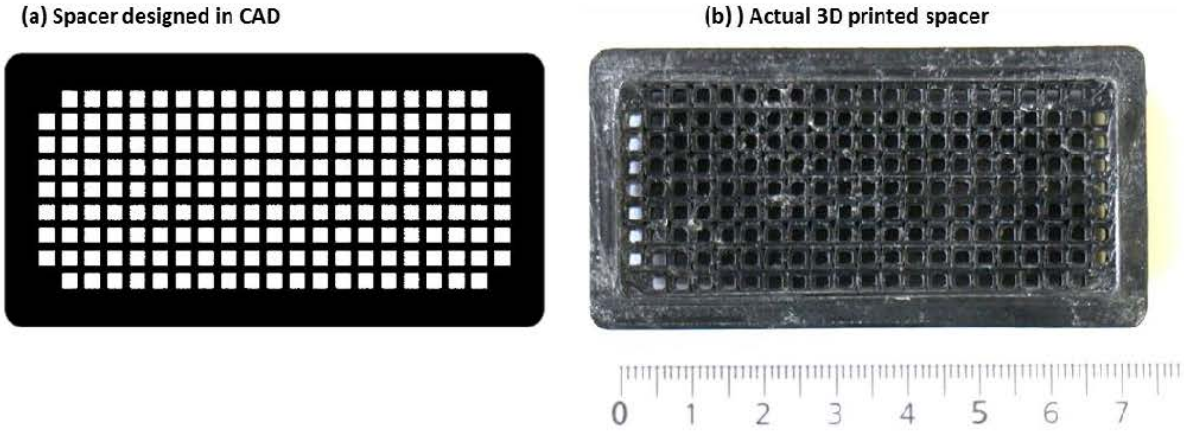

Figure C4.2 3D printed spacer used in the membrane cell in the newly developed membrane cell

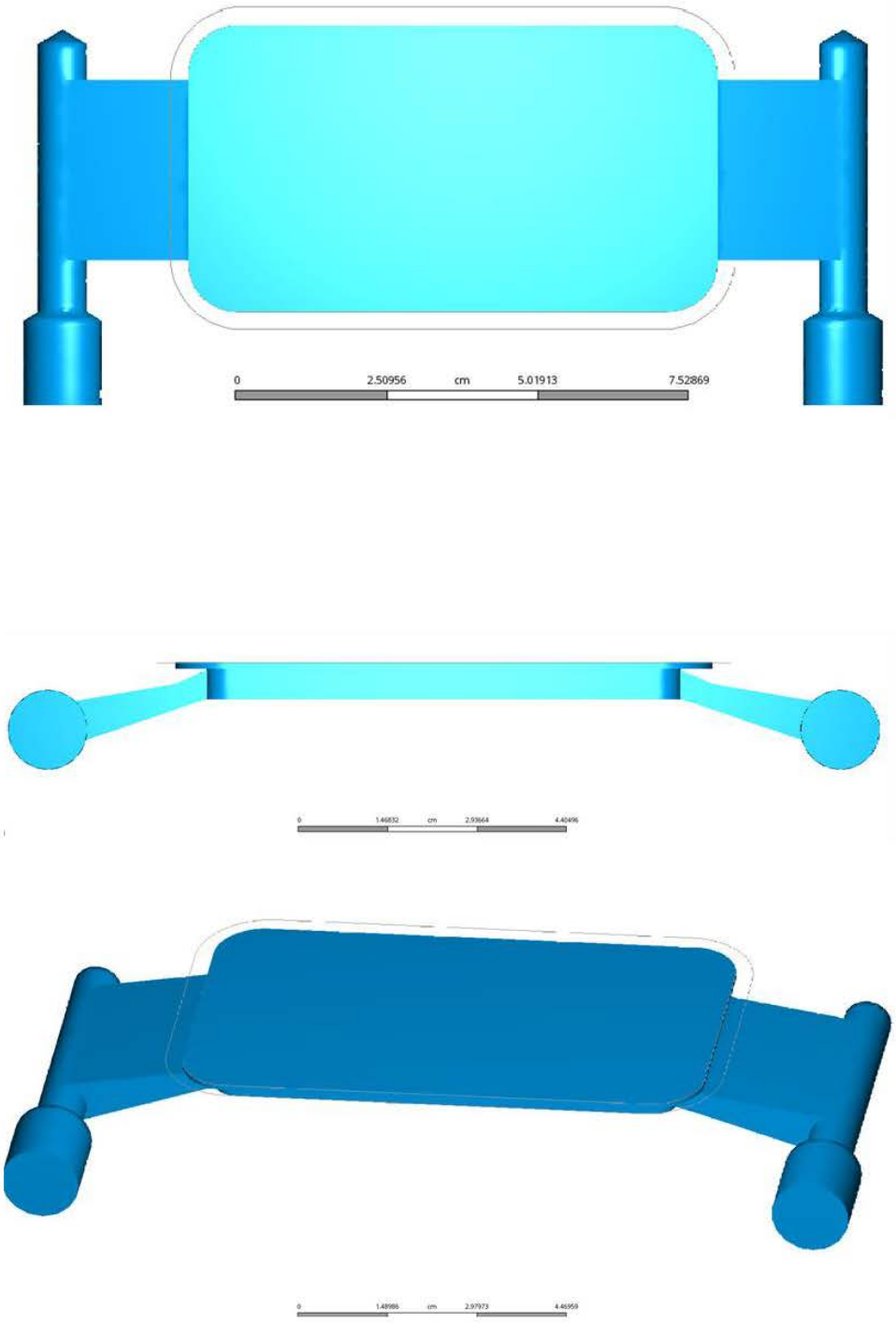

Figure C4.3 Feed side membrane geometry (to be viewed in color)

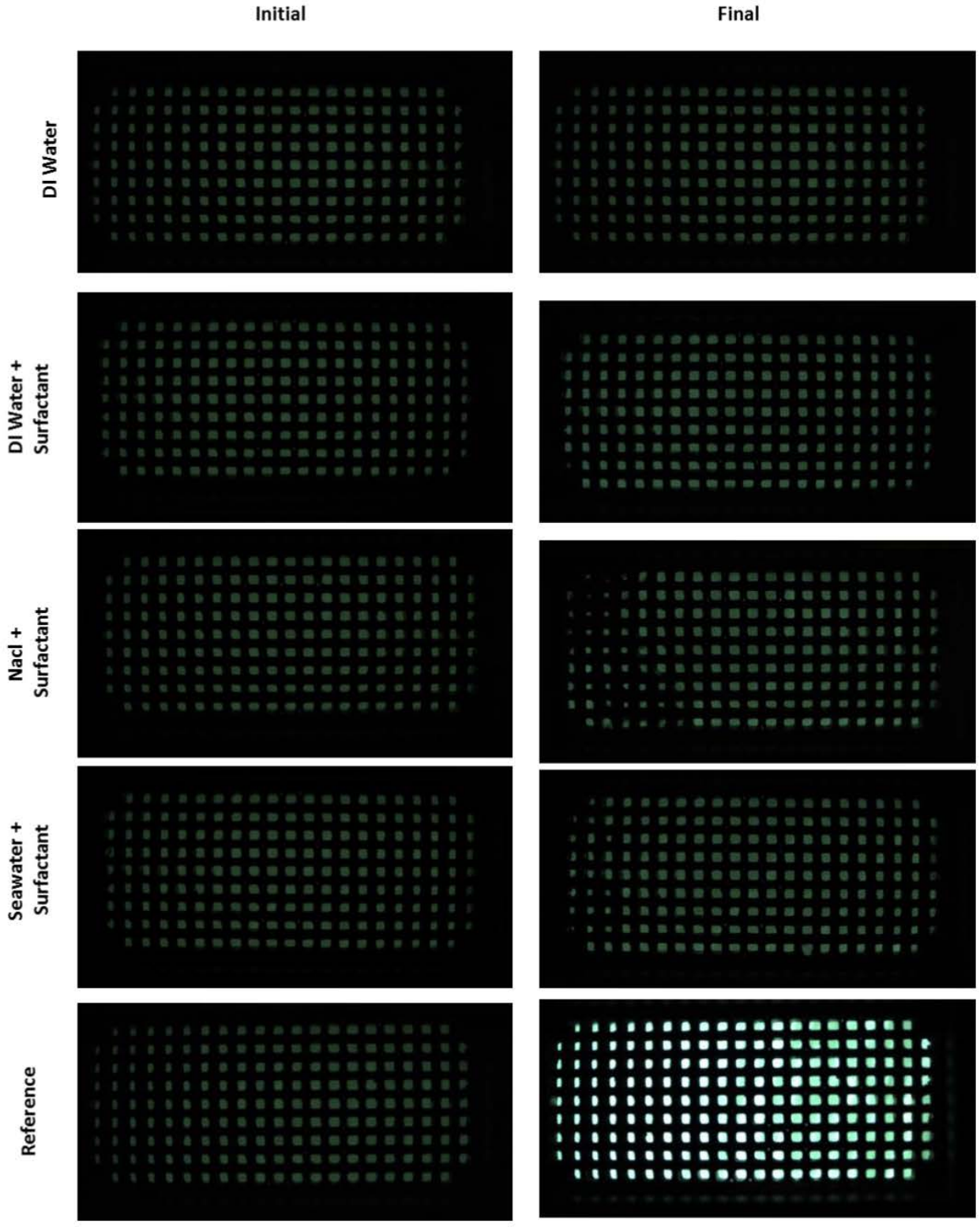

Figure C4.4 Membrane before (Initial) and after(final) wetting with surfactant for different solutions (to be viewed in color)

Figure C4.5 Membrane surface after wetting induced by surfactant

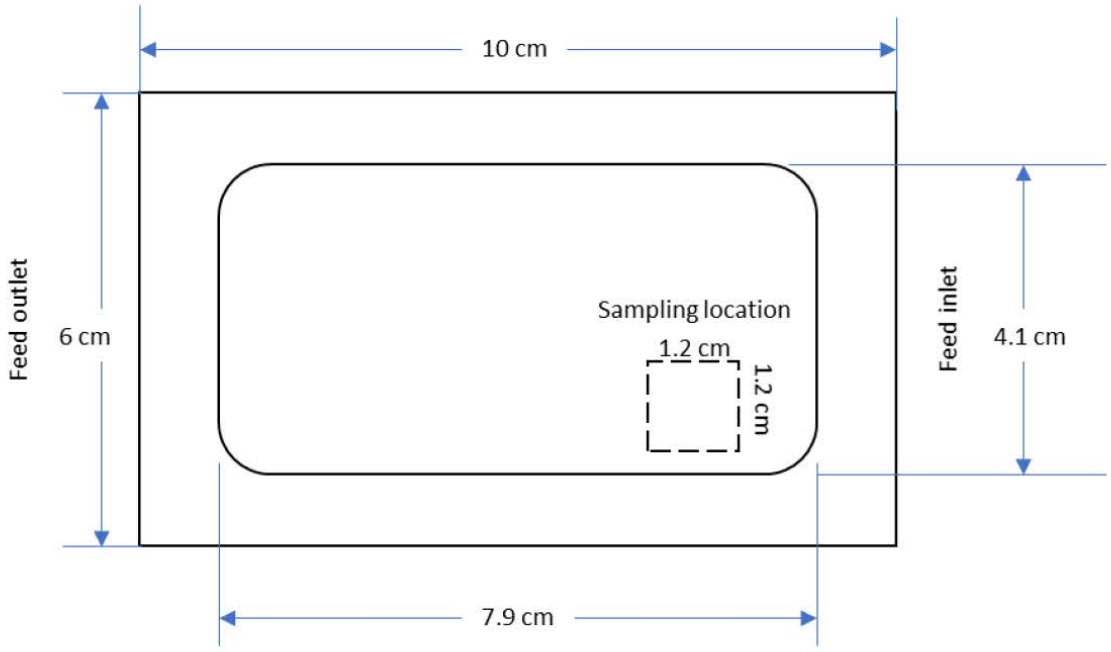

Figure C4.5 Membrane sampling location for SEM/EDX analysis

Chapter 5 Supplementary data

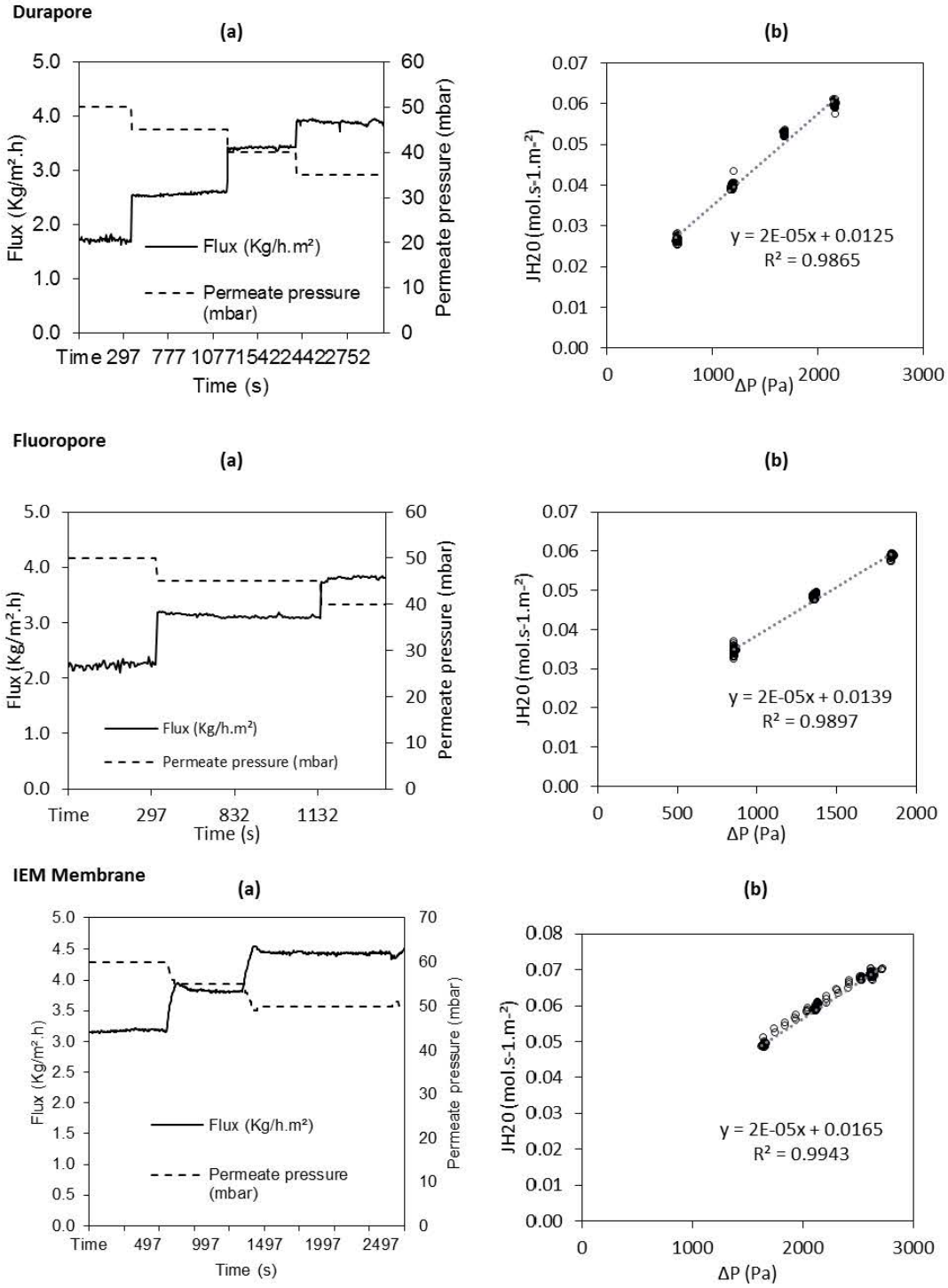

Figure C2.1:Example of (a) flux response (b) permeability measurement(K_k slope) by pressure variation method (for Durapore, Fluoropore and IEM M16 membranes ; Feed temperature 35°C, Re 2199, Pp (2 – 4.7 kPa)

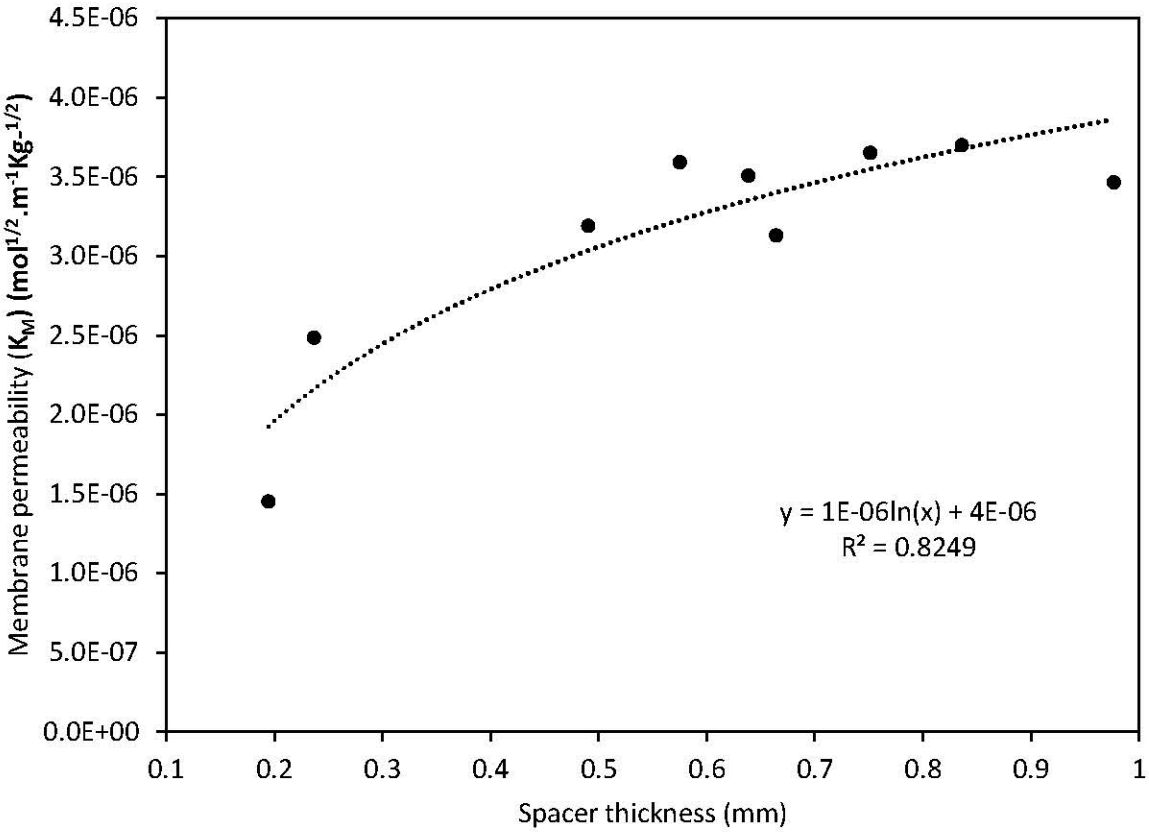

C5.1 The effect on membrane permeability (Durapore membrane 0.22 µm) as a function of spacer thickness

Nomenclature

Acronym	Description	Unit
A	Membrane area	m^2
ACA	Advancing contact angle	°
AGMD	Air gap membrane distillation	
ANOVA	Analysis of variance	
B	Membrane permeability	
BBD	Box-Behnken design	
b_p	Boiling point	°C or K
BP	Bubble point	
C	Salt concentration	g/L
$C_{i,f}$	Concentration of component i in feed	
$C_{i,p}$	Concentration of component i in permeate	
C_i	Concentration of the component i	
CA	Contact angle, reported in Θ but Rad used in equation	
CA	Contact angle	°
CCD	Central composite design	
C_f	Salinity	g/L
cf.	Confer/conferatur	
C_o	Number of central points	
D^*	Dimensionless spacing ratio	
D.I. water	De-ionized water	
D_i	Diffusion co-efficient	
DCMD	Direct contact membrane distillation	
DoE	Design of experiments	
EDX	Energy-dispersive X-ray spectroscopy	
EIC	Electrochemical impedance spectroscopy	
F	Flow rate	m/s or L/h
FS	Flat sheet	

Acronym	Description	Unit
FTIR	Fourier transform infrared spectroscopy	
HF	Hollow fiber	
i.e.	That is	
J	Flux	
J	Flux	$Kg/m^2.h$
K	Thermal conductivity	W/m.K
K	Number of factors	
K_M	Membrane permeability in VMD	
LEP	Liquid entry pressure	bar
LEP_w	Liquid entry pressure with pure water	Pa / bar
MD	Membrane distillation	
MDCr	Membrane distillation crystallizers	
MED	Multiple-effect distillation	
mp	Melting point	°C or K
MPS	Mean pore size	
MSF	Multi stage flash	
MW	Molecular weight	
N	Number of experiments	
N_l	Weight flow rate	Kg/s
ND	Refractive index	
Θ_{eff}	Effective contact angle	
P	Pressure	bar or kPa
$p_{i,m}$	Partial pressure of the component i on the membrane surface on the feed side	
$p_{i,p}$	Partial pressure of the component i on the membrane surface on the feed side and downstream	
p_0	Vapor pressure of flat liquid vapor interface	
$p_{i,f}$	Vapor pressure of feed	
$p_{i,p}$	Vapor pressure of permeate	

Acronym	Description	Unit
P3FEt/PTrFE	Polytrifluoroethylene	
pc	Capillary pressure	
PC	Polycarbonate	
PDMS	Polydimethylsiloxane	
PHMA	Polyhexylmethacrylate	
PP	Polypropylene-isotactic	
P_p	Partial pressure of water	
PTFE / Teflon	Polytetrafluoroethylene	
PV	Pervaporation	
PVA	Polyvinylacetate	
PVDF	Polyvinylidene fluoride	
r avg	Average pore radius	µm or m
r max	Pore radius maximum	µm or m
Re	Reynolds number	
r_h	Hydraulic radius	
RO	Reverse osmosis	
ROI	Region of interest	
RSM	Response surface methodology	
S_i	Solubility co-efficient	
SDG	Sustainable development goal	
SEM	Scanning electron microscopy	
SFE	Surface free energy	mN/m
SGMD	Sweeping gas membrane distillation	
SR	Salt rejection	
ST	Surface tension	mN/m
STP	Standard pressure and temperature	
T	Temperature	°C or K
T_f	Feed temperature	°C
TDS	Total dissolved solids	mg/L

Acronym	Description	Unit
TSGMD	Thermostatic sweeping gas membrane distillation	
UN	United nations	
V_m	Molar volume	
VMD	Vacuum membrane distillation	
w.r.t	With respect to	
x	Distance from the liquid/membrane interface	
α	Structural angle	
δ	Membrane thickness	µm or m
δ_l	Distance the liquid had penetrated into the membrane pores	µm or m
δ_m	Total membrane cross-section thickness	µm
ΔP	Transmembrane pressure difference	
ΔT	Transmembrane temperature difference	°C or K
ε	Porosity	
H	Viscosity of the liquid	Pa. s
P	Density	kg/m^3
T	Tortuosity	
Υ	Surface tension	mN/m
ω_p	Pore wetting ratio	
ω_s	Totally-wetted surface ratio	